DEAD-END AND CROSSFLOW MICROFILTRATION OF YEAST AND BENTONITE SUSPENSIONS: EXPERIMENTAL AND MODELLING STUDIES INCORPORATING THE USE OF ARTIFICIAL NEURAL NETWORKS

Submitted by: Jenny Ní Mhurchú BE

For the qualification of PhD

At Dublin City University,
School of Biotechnology

Under the Supervision of

Dr. Greg Foley

July 2008

I hereby certify that this material, which I now submit for assessment on the programme of study leading to the award of PhD (Biotechnology) is entirely my own work and has not been taken from the work of others save and to the extent that such work has been cited and acknowledged within the text of my work.

Signed: _____   ID No.: _____
             Candidate

Date: _____

Papers related to the work in this thesis:

Ní Mhurchú, J. and G. Foley (2006)

Dead-end filtration of yeast suspensions: Correlating specific resistance and flux data using artificial neural networks.

Journal of Membrane Science 281(1-2): 325-333.

Ní Mhurchú, J., Havel, J., Foley, G.

Dynamic modelling of stirred cell microfiltration using a computationally efficient neural network

Separation and Purification Technology (Submitted 2008)

TABLE OF CONTENTS

APPLICATION OF ARTIFICIAL NEURAL NETWORKS AND SEMI-EMPIRICAL MODELLING TECHNIQUES TO MEMBRANE FILTRATION PROCESSES

ABSTRACT

The applicability of artificial neural networks (ANNs) and semi-empirical modelling techniques for correlation and prediction of the filtration characteristics of microfiltration systems was assessed.

ANNs were developed to correlate specific cake resistance and steady state flux of dried yeast suspensions in dead-end microfiltration for a range of operating parameters. Trained networks were used in predicting filtration characteristics of previously unseen data, with excellent agreement. Network weights were interpreted for both the specific resistance and flux networks with the effective contribution of each input parameter showing trends that were as expected.

A novel neural network technique was developed for the prediction of dynamic flux data in batch stirred microfiltration of bentonite (a clay which forms an aqueous suspension with non-Newtonian rheology), based on eliminating the use of the time series explicitly as an input to the network. This approach reduces the size and complexity of network necessary for correlation and prediction of time series data, thus reducing processing times required, while achieving excellent R^2 values for prediction of previously unseen data. This novel approach was also

used in the correlation and prediction of batch crossflow microfiltration of bentonite.

Drawbacks of the artificial neural network approach include the lack of information obtainable about the physical characteristics of a given system, and the models obtained in this manner are empirical in nature. Although a legitimate approach especially in the modelling of complex systems, the development of physical models to describe these systems is a more fundamental chemical engineering approach to the problem. The use of physical modelling especially in batch systems where the concentration in the system is changing as a function of time is an interesting problem and gives more qualitative insight into what is happening in the system. Semi-empirical models based on the idea of simultaneous particle deposition and cake removal were developed to describe stirred microfiltration, batch crossflow and continuous crossflow of bentonite suspensions.

The basic model incorporating a cake removal rate constant k was found to fit qualitatively to stirred filtration data, however the predicted specific cake resistance was over-estimated when compared with experimentally determined values. The basic model was modified by the introduction of two extra terms - a critical flux, J^*, below which cake removal by shearing does not take place, and an instantaneous membrane fouling constant, b.

The modified model was found to give reasonable approximations to the experimentally determined specific cake resistance for the stirred system, including accurate prediction of the effect of increasing crossflow velocity leading

to a decrease in specific cake resistance. Reasonable trends in the model parameters were seen in some but not all cases for the stirred system.

On application of this model to batch crossflow filtration data the specific cake resistance was largely overestimated, and this and the model parameters were not found to follow consistent trends. This finding was attributed in part to changing flow regimes in the system due to increases in concentration and crossflow velocity.

The modified model incorporating irreversibility was applied to continuous laminar crossflow filtration, and crossflow experiments were extended by flushing of the membrane after filtration to investigate the irreversibility of cake formation in the system. The model was found to fit well to flux decline data, with sensible trends in the specific cake resistance and the model parameters; however, the cake removal by the flushing phase was not well represented by the model.

ACKNOWLEDGEMENTS

First and foremost I offer my sincerest thanks to Greg Foley, who consistently made himself available for support and guidance. I always felt great confidence in my work and newly motivated after each meeting - which must be the mark of a great supervisor! One simply could not wish for a better or friendlier supervisor, and I think I may have been the envy of the entire department, especially when the pressure was on and Greg was returning corrected drafts of the thesis within a matter of days rather than weeks.

I would like to express my gratitude to the Orla Benson Trust, for providing me with the opportunity to travel to the Czech Republic, where the mentoring of Professor Josef Havel was gratefully received, and to whom thanks is due for taking such good care of me during my stay at Masaryk University.

A huge thank you to Brian Freeland – without whom I would be sitting on the floor of a flooded lab, surrounded by the wrong size spanners and tangled up in a mile of PTFE tape, with pressure gauges exploding around my head!

Thanks to all of the post grads throughout the years for providing much needed relief from PhD work in the form of seemingly endless cups of tea. Special thanks to Sue Townsend and Eva Campion for always being there for me, and of course for dressing up with me for the BRS Christmas Parties!

Thank you to my family, for always looking after me so well. Thanks Mum and Dad for always knowing when I needed a pick-me up, usually in the form of being brought out for lunch! Thanks Stephen and Richard for being great brothers.

Thanks Christina for all the hugs. Thank you to all of you for never complaining (much) when I made completely unreasonable demands for silence! You guys are the best family anyone could ask for.

A huge thank you to Darragh Lawler, who managed to put up with me for the entire duration of my PhD, no mean feat considering he was one I usually took all of my stresses out on! Thanks Darragh, I hope we'll always be there for each other the way we have been for the last few years. Thanks also for all of the wacky ideas you had relating to my research… sometimes trying to convince you of why they were completely insane gave me some genuinely decent ideas!

This thesis is dedicated to my family, Darragh and my close friends (you know who you are!) for keeping me grounded and in touch with real life. May you all continue to be wonderful, positive influences in my life.

NOMENCLATURE

Symbol	Meaning	Units
a	Constant in Equation 2-1	-
A	Membrane area	m^2
A	Constant in Equations 3-4 and 3-5	-
a,b	Constants in Equation 1-16	-
a,b,c,d,e,f	Constants in Equation 3-5	various
b	Instantaneous membrane fouling constant	-
c	Mass of solids per unit volume of filtrate	g/L
C	Concentration	g/L
C_0	Initial Concentration	g/L
D	Pipe diameter in Equation 5-29	m
d_p	Particle diameter	m
F_f	Frictional force	N
F_N	Normal force	N
F_t	Tangential hydrodynamic force	N
g	Activation function in Equation 1-12	-
g,h,i,j,k,l	Constants in Equation 3-6	various
J	Filtrate flux	m/s
J^*	Critical Flux	m/s
J_0	Initial Flux	m/s
K	Kozeny constant in Equation 1-7	-
K	Fluid consistency index in Equation 5-28	$(g/L)^n$
k	Cake removal rate Chapters 5 and 6	s^{-1}
k	Constant in Hermia Blocking Laws (Equation 1-10)	-
k_c	Particle compressibility parameter in Equation 1-8	Pa^{-1}
L_m	Membrane thickness in Equation 5-14	m
m	Mass of particles per unit membrane area	kg/m^2
n	Constant in Hermia Blocking Laws (Equation 1-10)	-
n	Compressibility index in Equation 2-1	Pa^{-1}
n	Constant in Equations 3-4 and 3-6	-
N	Impeller rotational speed	RPM
N	Number of data points in Equation 3-2	-

n_h	Number of neurons in hidden layer in Garson Equation	-
n_v	Number of input variables in Garson Equation	-
O_j	Absolute value of the weight from the jth neuron in hidden layer in Garson Equation	-
p	Constant in Equation 1-9	-
R	Total number of batch runs in Equation 3-8	-
R_c	Cake resistance	m^{-1}
R_m	Membrane resistance	m^{-1}
R_{m0}	Initial clean membrane resistance	m^{-1}
R_T	Total resistance to flow	m^{-1}
s	Steepness parameter in Equation 1-13	-
S_v	Mean particle surface area per unit volume in Equation 1-7	m^2/m^3
t	Time	s
t	Constant in Equation 1-13	
u	Crossflow velocity or Impeller Tip Speed	m/s
V	Filtrate volume	m^3
V	Volume in Stirred Cell in Figure 5-1	m^3
v	Relative effect of input variable	-
V_0	Initial volume	m^3
V_R	Feed reservoir volume	m^3
w_{kj}	Absolute value of weight from k^{th} input to the jth hidden neuron	-
w_{vj}	Absolute value of weight from the input of interest to the jth hidden neuron	-
x_i	Data point to be normalised in Equation 1-16	-
x_i^*	Normalised data value in Equation 1-16	-
x_{max}	Maximum value of data point	-
x_{min}	Minimum value of data point	-
y	Dependent variable in Equation 3-3	-
$y(x)$	Output from neuron x in Equation 1-12	-
$\hat{y}_r$	Predicted output in Equation 3-8	-

Symbol	Meaning	Units
α	Specific cake resistance	m/kg
α_0	Zero pressure specific cake resistance in Equation 1-8	m/kg
β	Constant in Equation 5-14	-
δ	Cake thickness in Equation 5-15	m
ε	Cake porosity	-
ϕ_p	Particle volume fraction in cake (Equation 5-18)	-
η_f	Coefficient of friction in Equation 5-16	-
κ	Membrane permeability in Equation 5-14	-
μ	Filtrate viscosity	Pa s
ΔP	Applied pressure	Pa
ΔP_c	Cake pressure drop	Pa
ρ_c	Particle density	kg/m^3
ΔP_{tm}	Transmembrane pressure drop	Pa
θ	Variables in Equation 3-3	-
σ	Standard deviation	-
τ_w	Wall shear stress	Nm^{-2}
τ_{xi}	Relative importance of parameter in Equation 3-8	-

Abbreviation	Meaning
ANN	Artificial Neural Network
BP	Backpropagation
BSA	Bovine Serum Albumin
CB	Complete Blocking in Hermia Blocking Laws
CF	Cake Filtration in Hermia Blocking Laws
CFMF	Crossflow microfiltration
CFUF	Crossflow ultrafiltration
IB	Intermediate Blocking in Hermia Blocking Laws
IS	Ionic strength
MF	Microfiltration
MSE	Maximum squared error
NF	Nanofiltration
PES	Polyethersulphone
PS	Particle size
RB	Radial Basis Network
RK	Runge-Kutta
RO	Reverse Osmosis
SB	Standard Blocking in Hermia Blocking Laws
SEM	Scanning electron microscopy
UF	Ultrafiltration

LIST OF FIGURES

LIST OF TABLES

CHAPTER 1: Membrane Filtration Processes and Modelling Techniques

1.1   Introduction

Filtration involves the separation of particles from a particle/fluid mixture. During filtration, particles that are larger than the pore size of the membrane deposit to form a filter cake on the upstream side of the membrane. Microfiltration refers to the separation of particles in the range $0.1 - 10$ μm. The driving force for microfiltration is a pressure difference across the membrane and its associated filter cake, which forces filtrate through the filter cake and membrane. The necessary pressure difference is achieved either by applying pressure in a sealed environment by a compressed gas, piston or pump on the upstream side of the membrane, or by applying a vacuum to the filtrate side of the membrane.

Microfiltration is characterised by operation at low pressures, (typically less than 3.5 bar) and by high permeation fluxes. One of the major limitations of microfiltration is the fouling of the membrane caused by the deposition and adsorption of solute or of suspended particles. The advantages of using membrane separation processes such as microfiltration are their operation without phase change, relatively low energy consumption, and the ability to operate at ambient temperature. Microfiltration may be performed in three main configurations; dead-end, stirred and crossflow.

Some applications of microfiltration include the treatment of wastewaters (Cheryan 1986; Kang and Choo 2003); clarification of beverages, for example fruit juices (de Barros *et al.* 2003; Youn *et al.* 2004); wine and beer (Blanpain *et*

al. 1993; Czekaj *et al.* 2000a, 2001); continuous product removal and cell recycle during fermentation and downstream processing of fermentation broths (Nagata *et al.* 1989; Li *et al.* 1996) and plasmapheresis (continuous separation of blood from plasma cells) (Sakai *et al.* 1989).. One of the key measures of the performance of microfiltration processes is the filtrate (or permeate) flux, defined as filtrate flowrate per unit membrane area. Extensive research has shown that this parameter is a complex function of operating conditions (pressure, crossflow velocity), membrane properties, module geometry and feed properties (concentration, pH etc.). While there have been a large number of theoretical models developed for the various membrane processes, few of these are accurate except for with the simplest of model systems. These models are generally unable to predict membrane performance when the feed is a complex (and poorly characterised) mixture and when membrane fouling, (as distinct from cake formation), is a major contributor to flux decline.

In this chapter, a brief introduction is first given into the principles of operation of dead-end and crossflow microfiltration.

There is a wealth of published experimental studies examining the behaviour of flux decline and filtration characteristics for different systems. The focus of this introduction will be on research pertaining to the systems examined in this thesis, namely the dead-end microfiltration of microbial suspensions (in this case re-suspended dried yeast cells), and the stirred and crossflow microfiltration of a non-Newtonian colloidal suspension of bentonite clay. The rheology of bentonite and its effect on the filtration characteristics is given some consideration.

The focus of the second part of this chapter is the application of theoretical and empirical models to microfiltration, including an in-depth introduction to artificial neural networks (ANNs). ANNs are computational devices that have been little applied to filtration problems, and as such will require more introduction than traditional modelling techniques based on first principles analyses.

The overall aim of the work presented in this thesis is to explore the use of more empirical, yet accurate, models for membrane processes. While the focus of this work is microfiltration processes, the techniques used are applicable to any membrane separation process.

1.2   Classification of Membrane Filtration Techniques

Microfiltration techniques are generally classified on the basis of the direction of the flow of the feed suspension that is being processed. In theory, all components in a suspension that are smaller than the pore size of the membrane will pass through the membrane, and particles larger than the pores will be retained on the upstream side of the membrane. The mode of operation chosen is based on the nature of the feed solution. Dead-end filtration systems are usually of a simpler configuration than crossflow systems and require less capital outlay and maintenance costs, however, filtration performance is often poor in dead-end mode due to the high resistance to filtrate flow by rejected material. Thus the dead-end configuration is a viable option only when the particle loading in the feed is low, for example in the purification of gases or in clarification of filtration media. Crossflow filtration is preferred for higher solids loading and when performance in dead-end mode is poor.

1.2.1 Dead-End Filtration

In dead-end microfiltration, the feed suspension flows perpendicularly to the membrane (Figure 1-1). Any solids in the feed that are larger than the pore size of the membrane are deposited on the membrane surface, forming a cake of solids. The liquid that passes through the membrane is called the filtrate.
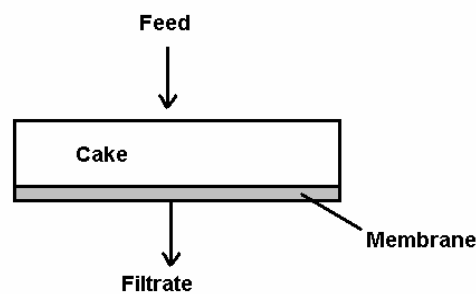
Figure 1-1: Dead-End Microfiltration

Most dead-end filtration processes are carried out in batch mode and therefore the mass of the filter cake grows until all the particles are deposited, or until the capacity of the filter has been reached, in which case further filtration is not possible. The filtration rate decreases with filtration time due to the hydraulic resistance of the filter cake.

Laboratory scale dead-end filtration is often carried out in a filtration cell which is simply a cylindrical vessel, usually made of stainless steel, fitted with a porous support onto which is placed the membrane. An exit port is provided for the filtrate which is collected and weighed on a digital balance. For accurate measurements and efficient data collection, the balance can be connected to a personal computer. The flux is calculated by measuring the mass (and hence the

4

volume if the density is known) of filtrate collected in a known time. The pressure is kept constant by connecting the cell to a compressed air (or nitrogen) source.

1.2.2 Stirred Microfiltration

In stirred microfiltration the filtration is nominally perpendicular to the membrane, as in dead-end microfiltration. However the filter cell is equipped with a stirrer or impeller. The fluid between the rotating impeller and the membrane flows tangential to the membrane and therefore some of the particles in the permeating liquid are kept suspended in the bulk liquid and do not deposit on the membrane surface (Figure 1-2). Therefore, stirred filtration may be expected to have higher permeation fluxes over a longer period of time than dead-end filtration, in which all of the solids in the feed deposit on the membrane.
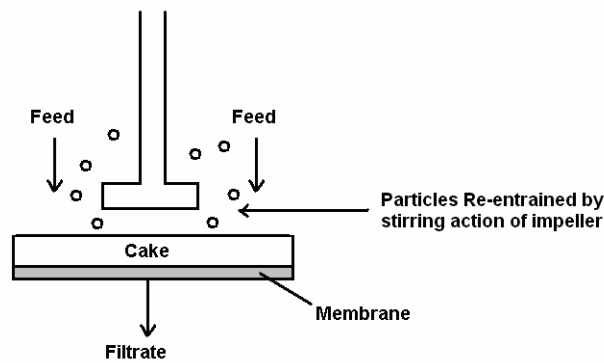
Figure 1-2: Stirred Microfiltration

However, significant initial permeate flux decline cannot be avoided due to the hydraulic resistance of the accumulating particle (cake) layer. Initially, cake formation in stirred filtration occurs in a similar manner to dead-end filtration

5

(Tanaka *et al.* 1993). The observed decline in permeate flux during stirred filtration is typically rapid at the start of the filtration process and then gradually diminishes until a steady-state (or pseudo-steady state) flux is attained. The growth of the cake stops, or approaches pseudo steady state, until such a time as the liquid level in the cell drops to levels too low to sustain the steady state flux.

Stirred microfilters have been used as a method to approximate true crossflow systems operating at the same pressure and similar tangential velocity as that of the crossflow system (Kim *et al.* 2001; Nuengjamnong *et al.* 2005).

1.2.3   Crossflow Microfiltration

In crossflow microfiltration, (CFMF), the feed suspension flows tangentially to the membrane surface. CFMF is operated with two effluent streams: a permeate stream (or filtrate stream) and a retentate stream. Only a part of the feed suspension passes through the medium as recovered product (permeate), and the other part flows tangentially along the membrane surface (retentate).
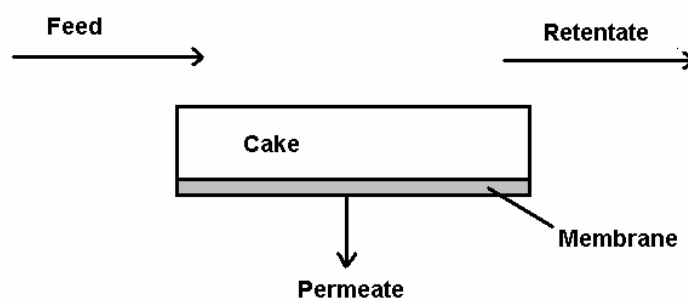
Figure 1-3: Crossflow Microfiltration

Crossflow microfiltration is usually carried out using stacked sheet, hollow fibre, or tubular membrane configurations. Hollow fibre and tubular modules have a shell-and-tube type configuration, the differences being that hollow fibre modules usually consist of a greater number of tubes with a smaller diameter than the tubes used in tubular modules. Stacked sheet modules may have flat sheet or spirally wound configurations. Fluid flow in stacked sheet and hollow fibre modules is nominally laminar, an issue which becomes of importance when filtering shear-sensitive cells. However, care must be taken, as the presence of spacer screens in these systems can act as turbulence promoters. Flow is usually turbulent in tubular flow modules, which can result in improved fluxes but the small membrane area per unit volume in these system can offset this advantage.

In small scale research studies, crossflow systems are usually run with a feed pump only and are thus operated without a recycle loop. Experiments are operated in either batch or total recycle mode. In batch mode, the retentate only is recycled to the feed reservoir, thus causing the feed concentration to increase over time. In total recycle mode, the retentate and filtrate are both returned to the feed tank, thus simulating a true continuous (single-pass) system. In Chapter 3 of this thesis, an atypical experimental set-up is described which is neither truly batch nor truly continuous.

1.2.4 Membranes

Microfiltration membranes generally have pore sizes in the range $0.1 - 1$ μm. Membrane structure will depend on the material and method of construction. The most common materials used for microfiltration membranes are polymer based

materials such as cellulose, polysulphone or polycarbonate; or ceramic membranes made from materials such as alumina or zirconia. Microfiltration membranes are generally symmetric i.e., they consist of approximately the same structure throughout the membrane. In contrast, ultrafiltration membranes are normally asymmetric, consisting of a thick porous layer covered with a thin layer of low porosity (Bowen 1993).

The membrane type plays an important role in the rejection of particles from the feed particularly at early filtration times. However, in microfiltration operations, the deposited cake layer is usually the limiting resistance and the membrane type after low filtration times may be of little significance.

1.2.5   Applications of Microfiltration

Microfiltration is an attractive separation process when other techniques such as centrifugation or sedimentation are unfeasible. This may occur when the particles to be separated are small in size or the density difference between particle and fluid phases is small.

Applications of microfiltration are many and varied and include bacterial (Nagata *et al.* 1989; Shimuzu *et al.* 1993), yeast (Rushton and Khoo 1977; Hughes and Field 2006) and mammalian cell harvesting (Maiorella *et al.* 1991); and separation of antibiotics and viral containing solutions (Madaeni *et al.* 1995). In the food industry microfiltration is widely used in the clarification of wine (Czekaj *et al.* 2001), beer (Blanpain *et al.* 1993) and juices (Youn *et al.* 2004). It is widely used in other industries such as filtering of colloidal or latex based paints (Doneva *et al.* 1998), separation of colloidal oxides and hydroxides for metal recovery, in

wastewater treatment (Kang and Choo 2003), and in plasma separation from blood for therapeutic and commercial uses (Sakai *et al.* 1989).

Membrane bioreactors have been the subject of much research and have found increased use industrially (especially in wastewater treatment) in recent years. Two membrane bioreactor configurations exist: an external/sidestream configuration and an internal configuration. In the external configuration, a membrane module is attached externally to a reactor or fermenter and the suspension is pumped to the filtration module with the retentate being returned to the reactor. Fresh medium may be added as the filtrate is removed from the system, allowing simultaneous product formation and recovery (Choo and Lee 1998; Park *et al.* 1999; Kim *et al.* 2001; Ognier *et al.* 2002). In the case of the internal configuration (commonly known as a submerged membrane system), the membrane is immersed in the reactor (Chang and Fane 2001; Sridang *et al.* 2008).

1.3 Flux Decline in Filtration

Filtration performance is generally expressed in terms of the filtrate flux, J, the volume of filtrate that passes through unit membrane area in unit time. The Darcy equation describing fluid flow in packed beds is used extensively in filtration theory:

$$J = \frac{\Delta P}{\mu R_T} \qquad\qquad\qquad [1\text{-}1]$$

where R_T is the total resistance to flow, ΔP is the applied (trans-membrane) pressure and μ is the filtrate viscosity.

There are many factors that cause the filtrate flux to decline. The formation of a cake layer is usually the cause of the steep decline in filtrate flux, however other phenomena such as the plugging of the membrane pores by particles, infiltration of fines into the filter cake (Tanaka *et al.* 1994) or membrane fouling by macrosolutes can also contribute to flux decline. These phenomena are referred to as fouling, where fouling is any phenomenon, other than pure cake formation, that contributes to flux decline.

1.3.1   Dead-End Microfiltration of Microbial Suspensions

For dead-end microfiltration, if the cake resistance is dominant and membrane fouling can usually be assumed to be negligible, the Darcy Equation (Equation 1-1) can be written

$$J = \frac{\Delta P}{\mu(R_m + \alpha m)} \qquad\qquad [1\text{-}2]$$

where J is the filtrate flux, ΔP is the applied (trans-membrane) pressure, μ is the filtrate viscosity, R_m is the membrane resistance, α is the specific cake resistance and m is the cake mass per unit membrane area. In dead-end filtration, m can be related to the filtrate volume, V, by the expression

$$m = \frac{cV}{A} \qquad\qquad [1\text{-}3]$$

where A is the membrane area and for microbial filtration, c is the wet mass of cells per unit filtrate volume.

1.3.1.1 The Specific Cake Resistance

The specific cake resistance α is a measure of the 'filterability' of the suspension because it is the value of this parameter, and its dependence on pressure, that determines how quickly a filtration can be performed. In most dead-end filtration processes, the resistance of the cake layer is dominant and therefore, it is essential that α be measured easily and that the factors affecting α are understood.

The classic method for determining the specific cake resistance is to measure the volume, V, of filtrate as a function of time, t, during a batch filtration at constant pressure. In this way, the specific cake resistance can be measured (or process performance calculated) from the well-known expression, derived using Equation 1-1 and Equation 1-2 and valid for constant pressure filtration (Rushton *et al.* 1996), namely

$$\frac{t}{V} = \frac{\mu R_m}{A \Delta P} + \frac{\alpha \mu c}{2 A^2 \Delta P} V \qquad\qquad [1\text{-}4]$$

where A is the membrane area and c is wet cell mass per unit volume of filtrate. Therefore, α can be determined from the slope of a plot of t/V versus V. As mentioned previously, the value of α determines to a large extent the efficiency of a process. However, while filtration equations are simple in form, much complexity is concealed because the specific resistance is dependent on many other variables. Traditionally, the main factor assumed to affect the specific resistance is the pressure drop across the filter cake, ΔP_c, where this quantity is defined by the expression

$$\Delta P_c = \Delta P - \mu R_m J \qquad\qquad [1\text{-}5]$$

11

Although α is technically dependent on cake pressure drop, most authors correlate dead-end specific resistance data in terms of the total applied pressure, ΔP, an approach that is reasonable as long as the cake resistance is dominant throughout the filtration.

The wet cell concentration, c is a difficult parameter to measure, as reporting the concentration based on a wet *pellet* mass from a centrifuged sample is not sufficient, as it contains intercellular water. There are a number of methods that have been developed to measure the true wet cell concentration, including measurement of the dextran uptake of the void volume of the cell pellet (McCarthy *et al.* 1998b; Chandler and Zydney 2004); measurement of the dry cell concentration with an assumption of typical cellular moisture content of 70 % (Shimuzu *et al.* 1993); replacement of interstitial water of a wet filter cake with ethanol with subsequent evaporation of the ethanol allowing the cake to be weighed to find the wet cell mass (Oolman and Liu 1991) and compression of filter cake overnight with subsequent weighing, assuming that the intercellular moisture drains from the cake over this period (Okamoto *et al.* 2001). These experimental techniques are not trivial and there is no easy way to measure accurately the wet cell concentration.

Definition of the specific cake resistance on the basis of the dry cell weight has been used in previous studies (Hodgson *et al.* 1993; Ohmori and Glatz 1999) and it is this approach that is used in this work due to ease of use.

1.3.1.2 The Steady State Method

A commonly used way of measuring the specific cake resistance over a range of pressures in a single experiment is to use the so called steady state method (Nakanishi *et al.* 1987). This involves filtering a volume, *V*, of suspension of known concentration (mass particles per unit volume of suspension), *C*, at a low pressure. The filtrate is collected, returned to the cell and passed through the filter cake at the same low pressure as before. The flux is recorded and the pressure then increased in a step-wise fashion with the flux monitored continuously. As each new pressure is set, the flux will rapidly approach a steady value. The cake mass per unit area is the same at all pressures as outlined in Equation 1-2. Thus the specific cake resistance can be evaluated at each pressure from the expression

$$\alpha = \frac{\Delta P / \mu J - R_m}{CV / A} \qquad\qquad [1\text{-}6]$$

where *J* is the steady flux recorded at each pressure. Assuming no membrane fouling, the membrane resistance, R_m, can be evaluated by measuring the flux of pure water through a clean membrane.

There is some doubt about the theoretical correctness of this method (Tien and Ramarao 2008). These authors regard the steady state method as compression of an existing cake rather than cake filtration, and also call into question the fact that the concentration profile in the cake is not taken into account. However, for the purposes of this research, a more detailed analysis of specific cake resistance is unnecessary as the specific resistance values are of interest only as data for analysis using Artificial Neural Networks.

1.3.1.3   The Carman-Kozeny Equation

The Carman-Kozeny equation is often used to relate specific cake resistance to particle size and may be written

$$\alpha = \frac{KS_v^2}{\rho_c}\frac{1-\varepsilon}{\varepsilon^3}$$

[1-7]

where K is the Kozeny constant, ρ_c is the particle density, S_v^2 is the mean particle surface area per unit volume and ε is the cake porosity.

If all of the particles in the suspension are spherical and of the same diameter, d_p, this expression may be simplified to

$$\alpha = \frac{36K}{\rho_c d_p^2}\frac{1-\varepsilon}{\varepsilon^3}$$

[1-7b]

The d_p^{-2} dependence of α has been shown to be quite accurate experimentally (McCarthy 2001) however the use of this equation for predicting the specific cake resistance is limited as it requires the measurement of the cake porosity. Furthermore, it is necessary to assign a value to the Kozeny constant, which varies with the type of suspension (McCarthy *et al.* 1998b).

Particle size and size distribution effects have been shown to affect microfiltration resistances. For the case of inorganic suspensions, increasing particle size has been shown to cause a reduction in the resistance to filtrate flow for filtration of spherical latex particles (Ogden and Davis 1990) and glass and silica particles (Chellam and Weisner 1998). For yeast cells, it has been shown that specific cake resistance is increased when particle size is reduced by cell breakage (Shimuzu *et*

al. 1994) and for microbial suspensions, increasing the surface area per unit volume S_v (i.e. reduction in particle size) was shown to lead to an increase in specific cake resistance (Nakanishi *et al.* 1987). The size distribution of the suspension also affects the filtration characteristics, as smaller particles fill the gaps in the cake between larger particles, thus reducing cake voidage and increasing the specific cake resistance (Wakeman 1975; Free *et al.* 1998).

1.3.1.4   Experimental Observations

Experimental investigations into dead-end microfiltration have not been widely published, and most studies in fact form the initial investigations leading into crossflow studies.

Flux decline in dead-end filtration of microbial cells such as yeasts has been shown to be affected by many different cell and suspension properties.

Increasing the applied pressure generally increases the filtrate flux as it is the transmembrane pressure that is the driving force for filtration. Cell-based filter cakes are usually compressible. A linear relationship rather than the standard power law equation used to correlate specific resistance and applied pressure has been shown to be more applicable in microfiltration of microbial suspensions (McCarthy *et al.* 1998a). A number of correlations have been developed based on this linear relationship for different cell suspensions (Reismeier *et al.* 1989; Rushton *et al.* 1995; Tanaka *et al.* 1997) and for resuspended dried yeast cells of the type employed in this work, the following equation has been used to correlate specific cake resistances over a wide range of pressures (McCarthy *et al.* 1998a; 1998b; 1999; 2002a):

15

$$\alpha = \alpha_0\left(1 + k_c \Delta P_c\right) \qquad\qquad\qquad [1\text{-}8]$$

Where α_0 is the zero pressure specific cake resistance and k_c is a parameter reflecting the particle compressibility.

An increase in suspension concentration leads to a corresponding decrease in filtrate flux. Scant evidence has been reported of the specific resistance of yeast suspensions increasing with suspension concentration (Mota *et al.* 2004), a finding that is supported in recent work on the ultrafiltration of silica suspensions (Zaidi and Kumar 2005). These findings are atypical as most authors would consider the specific resistance to be independent of concentration.

Cell morphology has been shown to play a part in the specific cake resistance, with rod-like cells tending to have a greater compressibility than ellipsoidal cells (McCarthy *et al.* 1998b; 2002a). Specific resistances for microbial cells have also been shown to be dependent on the cell surface properties such as the extracellular matrix (Hodgson *et al.* 1993; Ohmori and Glatz 2000). Extracellular matrices on the surface of cells have been shown to lead to a large increase in the specific resistance of *C. glutamicum* grown in a complex medium (Ohmori and Glatz 2000).

Liquid properties such as pH and ionic strength have been shown to play a role in the specific resistance of microbial suspensions. Increase in specific resistance with increasing pH has been shown to be due to increased cell surface charge leading to a more resistant cake with fewer macropores due to cell aggregation for cakes of *S. griseus* (Shirato and Esumi 1963) and *C. glutamicum* (Ohmori and

Glatz 1999). Decline in specific resistance with increasing ionic strength at fixed pH has been observed for *C. glutamicum* (Ohmori and Glatz 1999).

Medium components have also been shown to influence the specific cake resistances of microbial suspensions. Amino acid addition leading to aggregation of cells and increased specific resistance has been observed (Ohmori and Iritani 2004a) while addition of ammonium chloride has been seen to lead to decreased specific resistance, tying in with the effects of ionic strength observed above (Ohmori *et al.* 2004). Addition of protein (BSA) to suspensions of *C. glutamicum* has been shown to increase the specific resistance in ultrafiltration due to increased aggregation of cells by BSA and formation of a gel layer of BSA on the membrane surface (Ohmori and Iritani 2004b).

Although cake formation is usually the dominant resistance in dead-end microfiltration of microbial suspensions, membrane fouling effects have been found to have an influence in many cases. Fouling may be caused by macrosolutes absorbing or depositing within the membrane pores or on the membrane surface, or by plugging of the membrane pores by particles in the feed suspension (Tracey and Davis 1994). In the filtration of biological suspensions, proteins, polysaccharides or lipids may all contribute to membrane fouling, and fouling can be affected by many factors such as the pH, ionic strength, protein structure, degree of hydration of the protein, membrane surface chemistry, membrane surface charge and applied pressure (Bowen 1993; Bowen and Cao 1998).

1.3.2 Crossflow Filtration of Colloids

In CFMF, some of the particles in the permeating liquid may be carried away by the tangential flow (crossflow) and thus will not deposit on the membrane surface. Therefore, crossflow filtration may be expected to have higher permeation fluxes over a longer period of time than dead-end filtration, in which all of the solids in the feed deposit on the membrane. However, significant initial permeate flux decline cannot be avoided due to the hydraulic resistance of the accumulating particle (cake) layer. The observed decline in permeate flux during crossflow filtration is typically rapid at the start of the filtration process and then gradually diminishes until a steady-state (or pseudo-steady state) flux is attained. Although the thickness of the filter cake can be limited in crossflow filtration and, in theory, filtration performance should be superior to that in dead-end filtration, the properties of the cake layer can be substantially different to that in dead-end filtration. Average specific cake resistances have been shown in some cases to be greater than that in dead-end filtration (Foley 1994).

Crossflow filtration has been shown to be advantageous in the separation of dispersions of colloids and fine particles as many of these suspensions are compressible, have a density close to that of the liquid phase, have a high viscosity, or are gelatinous (Bowen and Jenner 1995).

1.3.2.1 Experimental Observations

Experimental investigations have shown that many factors affect filtration performance in crossflow filtration, including the feed concentration, transmembrane pressure drop, crossflow velocity and feed suspension properties.

In practice, the cake mass is generally seen to increase with the transmembrane pressure, feed particle concentration and membrane pore size, and to decrease with crossflow velocity (McCarthy *et al.* 2002b).

Flux dynamics during microfiltration have been described by Belfort *et al.* (1994) as following the sequence: (i) Fast internal sorption of macromolecules, in which the macromolecules such as proteins adsorb onto the membrane surface or pores; and (ii) the build-up of sublayers and layers of particles on the membrane. If the module is being operated in batch mode, the crossflow fluid can become so viscous that previously turbulent flow may become laminar leading to a further reduction in flux (Pritchard *et al.* 1995).

Numerous experimental observations of crossflow microfiltration of colloidal suspensions have shown that the flux declines rapidly as a layer of rejected particles deposit on the membrane surface. Increased concentration has shown to lead to a greater flux decline (Bowen and Jenner 1995; Chen *et al.* 1997). This period of initial flux decline is followed by a more gradual flux decline followed by the establishment of a pseudo steady state flux (Hong *et al.* 1997).

The transmembrane pressure is the driving force for microfiltration, and hence an increase in ΔP_{tm} should increase filtrate fluxes. However, this also increases the cake layer thickness, causing an increase in cake resistance. The issue of filter cake compressibility, which is affected by ΔP_{tm}, will also have an effect on the filtration characteristics. An increase in the transmembrane pressure will result in higher initial fluxes, however it will also lead to a more rapid flux decline (Field *et al.* 1995). In many cases for highly compressible colloidal cakes such as those formed with bentonite suspensions, the applied pressure is shown to have a small

effect on the flux after early filtration times (Fordham and Ladva 1989; 1992). For suspensions of incompressible particles such as silica, increase in the applied pressure is shown to lead to increased fluxes (Hong *et al.* 1997).

The temperature of the feed suspension affects the viscosity, and hence the filtration characteristics. The temperature will also affect the retentate viscosity, which can affect the cake formation by affecting shear forces acting on the cake. The effect of temperature is complex as the effect of viscosity is complex. The Darcy equation predicts that reducing the filtrate viscosity (by increasing the temperature) should lead to an increase in flux. However, the increase in flux leads to a greater deposition of particles – i.e. the *m* in the Darcy equation increases as the viscosity is decreased. An increase in feed suspension viscosity leads to an increase in wall shear stress τ_w, leading to a tendency for the cake mass to decrease (Pritchard *et al.* 1995), as the increased shear stress can result in increased particle removal from the cake. This results in the cake thickness being limited, and the filtrate flux is normally increased.

A power law relationship is generally used in relating the crossflow velocity to the filtrate flux (Porter 1990):

$$J \propto u^p \hspace{4cm} [1\text{-}9]$$

where u is the crossflow velocity, and *p* is a constant that depends on the process parameters and the crossflow module used.

At the initial stages of colloid crossflow filtration, the permeate flux has been shown to be independent of crossflow velocity (Hong *et al.* 1997) and flux decline mimics that of dead-end filtration (Fordham and Ladva 1989).

Smaller particles sizes have been shown to lead to more rapid initial flux decline (Hong *et al.* 1997) and the slope of the initial flux decline rate has been shown to be inversely proportional to the square of the particle radius, which ties in with the d_p^{-2} dependence of specific resistance reported for dead-end filtration (McCarthy 2001).

Fouling of the membrane causes a decrease in filtration efficiency and can result in loss of product. Fouling may be caused by plugging of membrane pores by particles in the feed suspension, or by adsorption of macromolecules within the pores of the membrane. Fouling is influenced by the suspension properties, such as pH and ionic strength, and also on the membrane properties (material of construction, charge) as well as on the pore size (Bowen and Cao 1998).

Much research has been devoted to the reduction of flux decline phenomena in crossflow microfiltration, in order to render the process more industrially viable and less costly. Several practical approaches have been used, including modifying the surface chemistry of the membrane to increase the repulsive forces between the membrane and the solute, and methods focused on increasing the back-transport of solutes away from the membrane. Modifications to the basic filter configurations have also been used in an attempt to improve filtrate flux, by improving mass transfer at the membrane surface and the back migration of retained species away from the membrane-solution interface. Physical methods have also been employed, such as the addition of seed particles to attract dissolved macromolecules away from the membrane, and the use of electric fields to move charged molecules away from the membrane.

The surface chemistry of the membrane may be modified in order to reduce the attractive forces or increase the repulsive forces between the membrane and the solute. A range of techniques have been employed experimentally to this end, including adsorption of hydrophilic polymers (Kim *et al.* 1988), irradiation methods (Nyström and Jarvinen 1991) and low temperature plasma activation (Kramer *et al.* 1989).

Modules have been designed to include turbulent flow and enhanced mixing to improve filtrate flux. Baffles may be inserted in the filtration modules to generate turbulence and lessen the rate of flux decline (Field *et al.* 1995). Membranes may be pleated or curved (Moulin *et al.* 1996). Composite modules which incorporate both dead-end and crossflow filtration have been used (Bai and Leow 2002).

Many techniques focus on reducing the cake layer thickness, such as when the direction of tangential flow is periodically reversed (Howell *et al.* 1993) or the direction of filtrate flow may be reversed, known as backflushing, or backpulsing (Tanaka *et al.* 1995; Redkar *et al.* 1996). Other hydrodynamic modifications have been used to improve filtrate flux such as pulsation of the feed stream and the production of centrifugal instabilities such as Dean and Taylor vortices (Moulin *et al.* 1996; Kluge *et al.* 1999; Moll *et al.* 2007). Vibrating modules have been used (Al Akoum *et al.* 2002) and shear enhancement using vibrations has been found to cause an increase in the permeate flux. Infrasonic pulsing has been investigated as a method of removing foulant and improving filtrate flux (Czekaj *et al.* 2000b).

Much research has focused on the manipulation of the suspension properties in order to reduce fouling and improve the filtrate flux. On the basis of the idea that a particle size that is too small will plug the pores of a membrane, and that a

particle size that is too large will block the lumen of a hollow fibre filtration module, Wickramasinghe *et al.* (2002) investigated the effect of molecular weight and charge density of cationic polyelectrolytes on the permeate flux of bakers yeast cell suspension. These polyelectrolytes serve as flocculants, which led to an improvement in the permeate flux.

Constant flux filtration is a mode of operation which has been used in research into fouling reduction (Foley *et al.* 1995a). In constant flux filtration, the transmembrane pressure increases during normal operation to keep the flux constant, thus overcoming any fouling resistance that builds up on the membrane. It has been shown that a low initial transmembrane pressure followed by a gentle increase, leads to a low rate of fouling and reduced the degree of irreversible fouling (Field *et al.* 1995). For constant flux filtration, the transmembrane pressure is monitored as a function of time for a constant filtrate flux, in order to characterise the filtration performance.

1.3.3 Bentonite

Bentonite is a clay consisting predominantly of sodium montmorillonite. Montmorillonite is a di-octahedral smectite mineral with a layered crystal structure with negative surface electrical charges arising from isomorphic substitutions of magnesium for aluminium in the crystal sheets. The clay swells in water by taking up inter-layer water, eventually leading to complete dispersion. The size of a montmorillonite particle is thus not very well-defined, but they may be regarded as flat plate-like particles of lateral dimensions of order 1 µm and thickness of the order of 10 nm (Fordham and Ladva 1989).

1.3.3.1 Bentonite Rheology and Filtration Characteristics

Bentonite clays have been reported as generally having complex rheological characteristics (Benna *et al.* 1999; Güngör 2000; Mahto and Sharma 2004). In an aqueous dispersion, water can penetrate into the interlayer space and cause swelling of bentonite. Bentonite exists as small plates as described previously, which, when hydrated, separate to form a colloidal suspension with enormous surface area made up of small platelets separated by a layer of water molecules. Plate surfaces are positively charged, while platelet edges are negatively charged. Swelling indices of bentonite are generally in the range 3 – 4 (Mahto and Sharma 2004). Measurement of the swelling index is described by Mishra *et al.* (1985). During hydration, the charged platelets repel each and move apart, and so swelling begins. Water molecules partially neutralise the exposed surfaces holding them apart, thus exposing the large reactive surfaces (Figure 1-4).
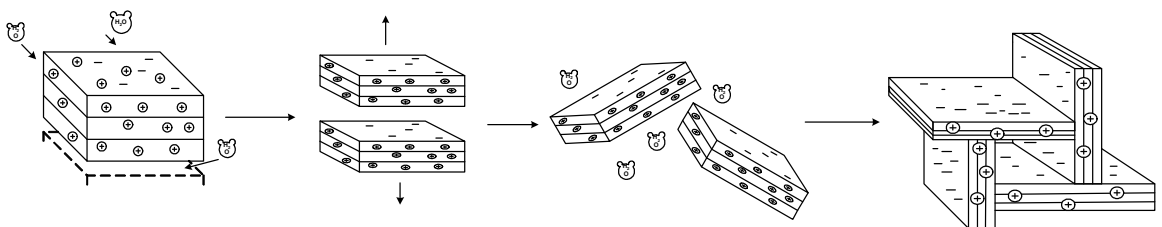
Figure 1-4: Structure of Aqueous Bentonite Suspensions (Zoecklein 1988)

Aqueous suspensions of bentonite have been shown to exhibit Bingham Plastic properties for dilute (Alemdar *et al.* 2005) and concentrated (Güngör 2000) suspensions. At low shear rates, systems exhibit non-Newtonian flow, which is characterized by a progressive decline in viscosity as shear rate increases. Above a certain value of shear rate, the flow curve becomes linear. According to the Bingham model, the slope of the linear part of the flow curve is referred to as the

plastic viscosity, the intercept of the linear portion of the curve with the stress axis is referred to as the Bingham yield (stress) value.

The rheology of bentonite suspensions has been found to be time-dependent (Benna *et al.* 1999). Experimental analysis of the suspensions used in this research found them to be mildly thixotropic (i.e., at a constant shear rate, apparent viscosity values dropped over time). However over the time course of interest in this research, thixotropic effects can be considered negligible up to a concentration of 10 g/L.

The suspension pH has been found to have a strong affect on the rheological properties of purified sodium bentonite suspensions (Benna *et al.* 1999). It was found that when the pH values became more basic, the yield stress decreased. This reached a minimum before increasing sharply, for a very basic medium. In an acidic suspension, the yield stress increased and reached a maximum for pH in a weakly acidic suspension before decreasing again at lower pHs. It is probable that in a very acidic medium the structure of the clay itself is attacked, leading to the decrease in yield stress.

The non-Newtonian rheological nature of bentonite suspensions can be expected to have a pronounced effect on the filtration characteristics. Tying in with the Bingham plastic model, shear thinning behaviour may be expected at lower shear rates while at higher shear rates rheological behaviour should approach Newtonian characteristics. This is supported by the work of Doneva *et al.* (1997) in crossflow filtration of aqueous bentonite suspensions. Benna *et al.* (2001) investigated the effect of clay content on the static (dead-end) filtration of purified sodium bentonite clay suspensions at two different pressures (1.5×10^5 and 5.7×10^5

Pa). They found that as the concentration increases, the thickness of the obtained cake increases, leading to the decrease of filtrate flux. This effect was found to be more marked at lower applied pressures. Hamachi *et al.* (1999) investigated the cake characteristics in crossflow microfiltration of bentonite suspensions as a function of the operating conditions. In a previous paper (Hamachi and Mietton Peuchot 1996) they designed a method of measuring the deposit thickness on the membrane using a He-Ne laser beam and a photomultiplier. This analysis was extended by investigating the cross-flow microfiltration of bentonite suspensions, analysing the deposit thickness as a means of explaining filtration behaviour (Hamachi and Mietton Peuchot 2002). They found that at the start of filtration, the crossflow velocity has little effect on the deposit build-up and that an increase in transmembrane pressure offsets the deposit growth for the same permeate flux. They conclude that for the filtration of compressible cakes such as bentonite, improvement of the filtrate flux must be addressed by manipulation of the crossflow velocity rather than the transmembrane pressure.

1.4   Theoretical and Empirical Modelling of Filtration Processes

A focus of the work in this thesis is the development of correlations based on experimental data. A number of approaches are used, including non-linear regression, artificial neural networks and semi-empirical modelling.

In this section, theoretical analyses of microfiltration are outlined followed by a summary of empirical modelling techniques. The following section is a comprehensive introduction to artificial neural networks and their application to membrane filtration problems.

1.4.1 Resistance Models

Hermia (1982) developed four distinct models based on the Darcy equation (Equation 1-1) to describe dead-end filtration behaviour. These models form the basis of many attempts at modelling filtration processes. The relationships described were the complete blocking model, which assumes that each particle that deposits on the membrane will seal a membrane pore; the intermediate blocking model which assumes that only a portion of the deposited particles will seal a pore; the standard blocking model, which assumes that the pore volume will decrease proportionally to the filtrate volume by deposition of solids on the pore walls; and the cake filtration model, which assumes that the cake resistance is proportional to the filtrate volume. Resistance models were developed for dead-end microfiltration and must be adapted for application to crossflow filtration, and in general, differ on the basis of the mechanism of fouling, whether internal or external.

The constant pressure filtration law from which these models were derived may be written as follows:

$$\frac{d^2t}{dV^2} = k\left(\frac{dt}{dV}\right)^n \qquad\qquad [1\text{-}10]$$

The values of k and n depend on the blocking model applicable. For the complete blocking model $n = 2$; for intermediate blocking $n = 1$; for standard blocking $n = {}^3/_2$; and for cake filtration $n = 0$.

Integration of Equation 1-10 incorporating these values of n leads to the Hermia models summarised in Table 1-1, where J_0 is the initial flux.

Table 1-1: Hermia Blocking Laws

Law	Equation	Description
Complete Blocking	$V = \dfrac{J_0}{k_{CB}}\left(1 - e^{-k_{CB}t}\right)$	Particles do not accumulate on each other and particles arriving at the membrane will seal pores ($d_{particle} = d_{pore}$)
Intermediate Blocking	$V = \dfrac{J_0}{k_{IB}}\ln(1 + k_{IB}t)$	Particles do accumulate on each other and seal membrane pores ($d_{particle} = d_{pore}$)
Standard Blocking	$\dfrac{t}{V} = \dfrac{1}{J_0} + \dfrac{k_{SB}}{J_0}t$	Particles deposit on the pore walls, decreasing the internal pore diameter ($d_{particle} \ll d_{pore}$)
Cake Filtration	$\dfrac{t}{V} = \dfrac{k_{CF}}{4J_0^2}V + \dfrac{1}{J_0}$	Particles are retained due to sieving and form a cake on the membrane surface ($d_{particle} \gg d_{pore}$)

In the standard blocking model, it is assumed that only internal fouling occurs – i.e. that the pore volume decreases proportionally to the filtrate volume. When the standard blocking model holds for a system, a plot of t/V against t is linear, where t is time and V is permeate volume.

The cake formation model assumes that only external fouling of the membrane occurs, with particles building up in a cake on the surface of the membrane. Permeate flux decreases as the cake thickness increases. For the cake formation model, a plot of t/V versus V is linear.

Leading on from the constant flux work of Field *et al.* (1995), the critical flux concept was introduced. The critical flux hypothesis is that on start-up of a crossflow filtration run, there exists a flux below which a decline of flux with time

does not occur. A manipulation of the blocking laws of Hermia (1982) led to a unifying equation for CFMF:

$$-\frac{dJ}{dt}J^{n-2} = k\left(J - J^*\right)$$ [1-11]

where J is the permeate flux, and n and k are constants depending on the mechanism of fouling in the same manner as the original Hermia laws. For cake filtration, $n = 0$, for complete blocking $n = 2$ and for intermediate blocking $n = 1$. J^* in all cases can be considered to be a critical flux which should not be exceeded if fouling is to be avoided.

Different mechanisms based on transport along or away from the membrane have been proposed based on the failure of the simple ultrafiltration concentration polarisation theory to account for the behaviour of crossflow microfiltration of colloidal suspensions, known as the flux paradox (Green and Belfort 1980).

Particle back-transport models have been developed to describe the deposition of particles being balanced by the diffusion of particles away from the cake. This type of model includes those governed by Brownian diffusion (Einstein 1956), inertial lift (Forstrom *et al.* 1975) and shear induced diffusion (Zydney and Colton 1986). Brownian diffusion coefficients caused under-prediction of the flux by one to two orders of magnitude, with the higher than expected fluxes attributed to shear forces caused by the tangential flow. Thus the shear-induced models were developed, using experimentally determined shear-induced diffusion coefficients to predict cake formation and flux behaviour, with shear-induced diffusion coefficients being a function of shear rate, particle concentration and particle size (Leighton and Acrivos 1987). However studies incorporating in-situ observation

of the behaviour of particles in such systems have not found evidence of diffusion away from the membrane or cake surface (Mackley and Sherman 1992; Wakeman 1994; Li *et al.* 1998) and particle polydispersity effects have been shown to be inadequately described by models of this type (Chellam and Weisner 1998).

With flowing cake or convective models, the deposition of particles on the membrane is balanced by the flow of particles tangential to the membrane (Davis and Birdsell 1987) and the flowing cake theory (Leonard and Vassilieff 1984) assumes that particles carried to the membrane or cake surface roll or slide along the surface due to the crossflow.

This type of model has been combined with the resistance in series model to develop relationships describing the thickness and resistance of the cake (Dharmappa *et al.* 1992; Piron *et al.* 1995; Vyas *et al.* 2001).

Force balance models have been developed which analyse the forces exerted on an isolated particle depositing on the filter cake (Wang *et al.* 1995; Vyas *et al.* 2001; Cheng *et al.* 2008). Particles will stop depositing on the cake layer when the tangential forces are sufficient to overcome the normal drag forces caused by the permeate flow. Therefore, larger particles are more likely to escape in the retentate due to their larger tangential forces. Models of this kind can be used to describe preferential deposition of smaller particles found in polydisperse suspensions (Foley *et al.* 1995b).

Empirical models are generally based on the Darcy Equation where the cake resistance is related to process parameters by some empirical correlation (Riesmeier *et al.* 1989; Knoell *et al.* 1999). The predictive capabilities of

empirical models are limited to the suspensions and system configurations studied and cannot shed any light on the fundamental mechanisms of crossflow microfiltration.

Many complexities exist due to the interaction of various parameters that affect filtration performance, (such as particle properties like size, shape and charge, solution properties such as ionic strength and pH, and membrane properties), and as yet, no generalized model or method for modelling crossflow microfiltration has been developed. The use of this models previously developed are restricted by constraints such as assumptions of no irreversible fouling, or pore blocking, and that the particles should not aggregate. Thus attention has turned to alternative methods, such as the use of artificial neural networks.

1.5   Artificial Neural Networks

An artificial neural network (ANN) is an assembly of interconnected simple processing elements known as units or 'nodes', the operation of which is loosely based on the brain. The ability of a neural net to map data and make predictions is based on the inter-unit connection strengths, known as 'weights', which are obtained through a set of training data by a process of adaptation called 'supervised learning' (Callan 1999). The advantages of the use of ANNs over traditional first principles modelling or other empirical approaches are that the ANN can be highly non-linear, the structure can be more complex (and hence more representative of the system), the structure does not have to be pre-specified, and the models are quite flexible (Demuth and Beale 2004).

The artificial neural network operates on a similar principle to that of a biological neural network where each node represents a biological neuron. The incoming synapse of a biological neuron has a weight associated with it. The weight of each synapse, times its input, is summed for all incoming synapses and the neuron then fires, sending a value to another neuron in the network. This same principle is applied in an ANN. Each node in the ANN has a set of input lines (analogous to the synapses in a biological neuron). Each node also has an 'activation function', or 'transfer function', which tells the node when to send a value to another node in the network.

A single neuron may be represented mathematically as

$$y(x) = g\left(\sum_{i=0}^{n} w_i x_i \right)$$
[1-12]

where x is a neuron with n inputs and one output $y(x)$, and w_i are weights determining how much each input should be weighted. g is an activation function that weights how powerful the output (if any) should be from the neuron, based on the sum of the input.

In order to introduce non-linearity to the neural network, the appropriate transfer or activation function must be chosen. Activation functions range from simple threshold functions to sigmoid or hyperbolic tangent functions. It is necessary to introduce non-linearity to the ANN as this is what gives the network its computational power – without non-linearity, the network becomes a basic matrix multiplication operation. It is common to introduce non-linearity by using the sigmoid transfer function on the hidden layer neurons while simplifying the

network by using a linear transfer function on the output neurons. However a complex system will require the use of non-linear transfer functions on all neurons in order to accurately capture the system relationships.

The sigmoid transfer function takes the input, which may have any value between plus and minus infinity, and gives an output in the range 0 to 1. The form of the sigmoid function may be written as:

$$f(x) = \frac{1}{1 + e^{-2s(x+t)}} \qquad\qquad [1\text{-}13]$$

where t is the value that pushes the centre of the activation function away from zero and s is a steepness parameter.

This transfer function is commonly used in backpropagation networks of the type used in this study due to its differentiability (Bowen *et al.* 1998).

The t parameter, along with the weights, is adjusted as the neuron learns. In order to lead to a less complicated system; with only one parameter being adjusted (the weights) a bias term is introduced. The bias neuron lies in one layer, is connected to all of the neurons in the next layer, but none in the previous layer, and always emits 1. Since the bias neuron emits 1, the weights, connected to the bias neuron, are added directly to the combined sum of the other weights, just like the t value in an activation function. The equation for a neuron incorporating a bias term may be written as

$$y(x) = g\left(w_{n+1} \sum_{i=0}^{n} w_i x_i \right) \qquad\qquad [1\text{-}14]$$

where the weight for the bias neuron is represented as w_{n+1}.

Addition of the bias neuron allows the removal of the t term from the activation function. The sigmoid activation function may then be written

$$g(x) = \frac{1}{1 + e^{-x}}$$

[1-15]

where the $2s$ is absorbed into the weight term. Thus only the weights need to be adjusted during training of the ANN (Drakos and Moore 1993).

In an ANN the nodes are arranged in layers. Each of the nodes in a given layer is connected to nodes in another layer. Typically, there are three types of layers to an ANN – an input layer, one or more hidden layers, and an output layer. Figure 1-5 shows a 3-4-1 network, where there are three inputs, four neurons in the hidden layer, and one output. Thus training of this network consists of specifying a total of [(3 + 1) x 4 + 5 = 21] weights.
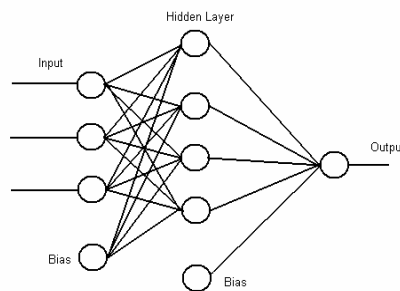
Figure 1-5: Neural Network Architecture

The hidden units are so called because they do not take direct input from the environment or send information directly out into the environment. The input layer is where the data vector is fed into the network. This feeds into the hidden

layer, which in turn feeds into the output layer. The processing of the network occurs in the nodes of the hidden layer and the output layer.

The weights and the biases in the neural network are initialised to small random values between +0.1 and -0.1 at the start of the training phase. The training process involves feeding the ANN known inputs and outputs which gradually modify the connection weights. The back-propagation learning algorithm is implemented to modify estimates of the values of the weights and establish the network structure (Demuth and Beale 2004). The weights eventually converge to values which allow them to be used in predicting an unknown output.

1.5.1 Training, Validation and Testing

In order to use a neural network as a predictive tool, the available data is divided into three subsets, for training, validation and testing (Bowen *et al.* 1998b). To avoid over fitting (where the network is unable to generalise due to being over trained) an early stopping mechanism is incorporated into the ANN. As the weights and biases of the network are updated continuously to minimise the MSE (Mean Squared Error) of the training data, the error of the validation data is also calculated, and if the MSE of the validation data starts to increase, training is stopped. This is known as 'cross-validation' (Maier and Dandy 2000). After the training phase, the ANN is used to simulate the output of a set of test data. If the ANN returns values of the output for the test data within an acceptable margin, then the ANN can be said to be successfully trained, and may be used as a predictive tool. It has been shown that the size of the validation dataset may be very small compared to the training and test datasets (Amari *et al.* 1997).

1.5.2 The BackPropagation Neural Network

The back-propagation neural network (Rumelhart *et al.* 1986) is the most representative learning model for the ANN (Aydiner *et al.* 2005). Back-propagation involves working backward from the output layer to adjust the weights accordingly, and reduce the average error across all layers. This process is repeated until the weights reach their optimal values and the error in the output is minimised. The basic backpropagation algorithm adjusts the weights in the steepest descent direction. This is the direction in which the performance function is decreasing most rapidly.

The network training consists of three stages: (i) feed-forward of the input training pattern; (ii) calculation and back-propagation of the associated error; and (iii) the adjustment of the weights (Chellam 2005). The ANN output corresponding to the input patterns is then compared with the target values and the weights were adjusted to reduce the maximum squared error. For a back-propagation artificial neural network (BP-ANN) using the sigmoid transfer function, the output is a real number in the range [0, 1]. Although it is possible for the input data to take any values between minus and plus infinity, convergence is more readily achieved through normalisation of the input and output data (Fu *et al.* 2005). This is due to the fact that the normalisation of the data minimises the chances of convergence to a local minimum on the error surface. The linear normalisation method is employed in this study, i.e.

$$x_i^{'} = a\frac{x_i - x_{\min}}{x_{\max} - x_{\min}} + b \qquad\qquad [1\text{-}16]$$

where x_i' is the normalised value, x_i the original data point, x_{max} and x_{min}, respectively, the maximum and minimum values for x, and a and b are the positive constants allowing to fix the limits of the interval for the scale values. In many cases, a and b are set as 0.6 and 0.2, thus the range of the data after normalisation is [0.2, 0.8]. The scale of the sigmoid transfer function is [0, 1], so training the network in the range 0.2 – 0.8 allows a margin for extrapolation outside the range of the training data.

Two different ANN programs were used in this study, Matlab (© The Mathworks) and Trajan (© Statsoft). The Matlab software used initially was an excellent package for use initially as it required an in-depth knowledge of the workings of neural networks. Also as Matlab requires coding of the network particulars, greater flexibility is possible in network design and operation. However, Trajan software was found to be more user friendly, and enabled the weight matrices to be saved as a file in order to use the trained network as a predictive tool. Trajan software did not require pre-normalisation of the input data, incorporating this step into the software, whereas Matlab required the user to normalise the inputs before use.

Performance criteria for ANNs generally include one or more of the following: prediction accuracy, training speed and the time delay between the presentation of inputs and the reception of outputs for a trained network (Maier and Dandy 2000).

1.5.3 Neural Networks and 'Black Box' Models

The use of ANNs as a modelling or predictive tool has been called a 'black box' approach previously, a view that stems from the fact that the contribution of the

37

input variables to the final output variables is difficult to elucidate from the network (Piron *et al.* 1997). This view stems from the fact that the contribution of the input variables in predicting the value of the output is difficult to establish. Consequently, input variables are often entered into the network and an output value is generated without gaining any understanding of the inter-relationships between the variables, and therefore, providing no explanatory insight into the underlying mechanisms being modelled by the network (Olden and Jackson 2002). The 'black box' nature of ANNs is viewed as a major weakness compared to traditional statistical approaches that can readily quantify the influence of the independent variables in the modelling process.

The size of the training datasets necessary for meaningful predictions from an ANN must be determined by a trial and error procedure and is system specific. There is also a level of uncertainty associated with the network weights once they have been determined, as there may be a tendency for a trained network to converge to a local minimum rather than the global minimum for the system. The use of principle component analysis on the network inputs may be useful in identifying the relevant inputs for a network.

Despite the 'black-box model' theory, some techniques have been established that allow for examination of the network weights and structure in order to elucidate some information about the relative contributions of the input variables on the network output, including a weight partitioning method referred to here as the Garson Equation (Garson 1991) used for crossflow microfiltration previously by Chellam (2005) and for prediction of microbial grown (Hajmeer *et al.* 1997), fish abundance (Mastrorillo *et al.* 1997; Brosse *et al.* 1999; Gozlan *et al.* 1999) and

ammonia emissions (Lim *et al.* 2007). A technique for assessing the individual and interactive effects of the input variables in the network prediction process was also developed by Olden and Jackson (2002) by use of randomisation protocols to partition the importance of the network weights. Cheng *et al.* (2008) develop a method of evaluating the contribution of input parameters based on the change in the output (the flux) around the time points along the flux-time curve for CFMF of colloidal suspensions. They use the following equation:

$$\tau_{x_i}(t) = \frac{1}{R} \sum_{r=1}^{R} \frac{\partial \hat{y}_r}{\partial x_i}, \quad x_i = IS, pH, PS, \Delta P \qquad \text{[1-17]}$$

where τ_{xi} is the relative importance and the operating parameters of interest are the ionic strength (IS), pH, particle size (PS) and transmembrane pressure ΔP, and R is the total number of batch microfiltration runs. ($\hat{y}_r$ is the predicted output for the run being evaluated, in this case the flux). This equation must be computed by evaluating the effect of each individual operating condition while the other variables are kept constant. While this approach is valid, the computational effort involved is large as each input variable must be evaluated separately and must be evaluated for each data point in the system.

An excellent review of the issues associated with analysis of the effect of the inputs to a network on the outputs is given by Sarle (1997).

1.5.4 Application of ANNs to Membrane Filtration Processes

Artificial neural networks have been used successfully in modelling and prediction of various different membrane filtration processes.

In ultrafiltration, ANNs have been applied to processing of proteins (Bowen *et al.* 1998a; Curcio *et al.* 2005), milk (Razavi *et al.* 2003a; 2003b), colloids (Bowen *et al.* 1998b), juices (Rai *et al.* 2005) and in drinking water production (Delgrange *et al.* 1998; Delgrange-Vincent *et al.* 2000).

In the case of other membrane processes, ANNs have been used in correlation and prediction of nanofiltration data regarding salt rejection, membrane fouling and contaminant removal (Bowen *et al.* 2000; Shetty and Chellam 2003; Shetty *et al.* 2003).

In microfiltration, ANNs have been applied to modelling flux decline for many suspension types, including phosphates (Aydiner *et al.* 2005), bentonite (Hamachi *et al.* 1999) and yeast (Piron *et al.* 1997).

Application of ANNs to dynamic filtration data is discussed in further detail in Chapter 3, where a novel network architecture is developed.

1.6   Conclusions

In this chapter experimental observations and modelling techniques in dead-end and crossflow microfiltration of microbial and colloidal suspensions are discussed. However limited applicability of theoretical and empirical models describing flux decline in filtration systems has meant that no general model describing dead-end or crossflow microfiltration has been developed.

In Chapter 2, the dead-end microfiltration of resuspended dried yeast cells is investigated and the specific resistance data correlated using an artificial neural network. A weight partitioning method based on analysis of the network weights

is used to elucidate the relative importance of process parameters on the specific resistance.

Chapters 3 and 4 deal with stirred and batch crossflow microfiltration of aqueous bentonite suspensions. A novel artificial neural network architecture is developed allowing the evaluation of the evolution of the relative importance of the input parameters as filtration time progresses.

Although ANNs are shown to be used with good accuracy in prediction of microfiltration data in Chapters 2 – 4, a semi-empirical modelling approach based on the concept of simultaneous particle deposition and cake removal is developed in Chapters 5 and 6 for stirred, batch and continuous crossflow microfiltration of bentonite suspensions, in order to attempt to gain a more fundamental understanding of the physical mechanisms governing filtration of bentonite. Using force balance concepts, irreversible cake formation and membrane fouling are also incorporated into the basic model.

CHAPTER 2: DEAD END MICROFILTRATION OF YEAST SUSPENSIONS: MODELLING OF SPECIFIC CAKE RESISTANCE AND STEADY STATE FLUX USING ARTIFICIAL NEURAL NETWORKS

2.1   Introduction

Dead-end filtration is a useful tool employed in the separation of cells from a fermentation broth, a critical step in the recovery of many chemicals of biological origin as described in Chapter 1. Despite its relative maturity, many aspects of the fundamental mechanisms of dead-end filtration remain poorly understood. Dead-end filtration of microbial suspensions has not received a great deal of attention in the literature. Indeed, much dead-end filtration data is to be found as preliminary work in papers devoted to crossflow filtration. The equations used to correlate specific resistance data are varied but most authors use the classic power-law equation (Nakanishi *et al.* 1987; Oolman and Liu 1991; Shimuzu *et al.* 1993)

$$\alpha = a\Delta P^{n} \qquad\qquad\qquad [2\text{-}1]$$

where *a* is a constant and *n* is the referred to as the compressibility index. A value of zero for *n* represents an incompressible filter cake and increasing values of *n* represents increasing filter cake compressibility. In the filtration studies of non-microbial suspensions, Equation 2-1 has generally been found to accurately represent the pressure dependence of the specific resistance at high pressures (Rushton *et al.* 1996). The use of Equation 2-1 in microbial filtration has proved to be more problematic and in some cases a linear relationship between specific

resistance and pressure is employed (Reismeier *et al.* 1989; Tanaka *et al.* 1997; McCarthy *et al.* 1998a; McCarthy *et al.* 2002a).

The specific cake resistance is dependent on many parameters other than pressure. A comprehensive review of the factors affecting specific resistance in dead-end microfiltration of microbial suspensions is given by Foley (2006). The combined effects of ionic strength and pH are well known to influence specific resistance in a complex manner that is very system specific (Shirato and Esumi 1963; Ohmori and Glatz 1999; Ohmori *et al.* 2004). In addition to the effects of pH and ionic strength, microbial filtration is complicated by subtleties that arise due to the biological nature of the suspensions. Hodgson *et al.* (1993) demonstrated the importance of cell surface properties on filtration behaviour. Very often these properties are affected by, and related to, conditions such as the type of growth medium used to produce the cells (Ohmori and Glatz 2000; Ohmori and Iritani 2004a), the stage of the growth cycle at which the cells are harvested for filtration and the possibility of cell aging between halting the fermentation and performing the filtration (Okamoto *et al.* 2001; Meireles *et al.* 2003).

As well as causing changes in cell surface properties, medium components may also provide additional resistance to flow. Solid medium components may cause cake clogging (Tanaka *et al.* 1994) while concentration polarisation of soluble components may also be significant if solute rejection occurs (Ohmori and Iritani 2004b). Both of these phenomena may increase the effective specific cake resistance.

Further complications have been suggested by Mota *et al.* (2004), who have found evidence that the specific resistance of yeast suspensions increases with increasing

suspension concentration, a finding that is supported in recent work on the ultrafiltration of silica suspensions (Zaidi and Kumar 2005). These findings are atypical as most authors would consider the specific resistance to be independent of concentration.

Given the number of factors affecting the specific cake resistance, prediction of this parameter becomes problematic. While conventional non-linear regression approaches could be used to derive experimental correlations, the complexity of the problem, especially the dependence of specific resistance on pH and ionic strength, makes such an approach difficult and likely to lead to very complex and unwieldy empirical equations. In this context, artificial neural networks (ANNs) may provide a promising avenue of research. The aim of an approach based on ANNs is not unlike that of conventional non-linear regression in that experimental data can be used to develop computational algorithms that will allow a given quantity to be predicted for any set of process variables within the range of the original experimental data (Fu *et al.* 2005). While the network architecture must be chosen after some numerical experimentation, no assumptions about the functional relationship between the independent (input) variables and the dependent variables (output) are required. Furthermore, even quite simple network architectures can reproduce highly complex non-linear behaviour.

The aim of this chapter is to develop artificial neural networks for use as a predictive tool for the specific resistance and steady flux through cakes formed by bakers yeast suspensions over a range of pressures, pHs, ionic strengths, cell concentrations and membrane resistances. ANNs are constructed, trained and validated and found to perform well in the correlation and prediction of specific

resistance and filtrate flux. Furthermore, an attempt is made to interpret the relative effects of the network inputs on the network output using a weight partitioning method.

2.2 Materials and Methods

2.2.1 Yeast Suspensions

Experiments were conducted with suspensions of dried 'Fermipan' bakers yeast (DSM Bakeries, Holland) resuspended in distilled water and freshly prepared before use. Suspensions were washed twice with a 0.5 M NaOH solution and then 3 times with distilled water. The washing step involved suspension of 1.5 g of cells in 15 ml of either NaOH or distilled water, followed by centrifugation for 3 minutes at 3500 rpm, and the supernatant removed. Cells were washed in caustic solution because washing in pure water alone resulted in protein that had leached from the cells remaining in the suspension. It is well established that proteins can cause fouling of microfiltration membranes and the presence of this protein would have affected the specific cake resistance measurements. The dry mass of cells after the washing steps was found to be 50 % of the unwashed dry mass and it is this dry mass concentration that is reported throughout. The pH of each solution was adjusted to the desired value by adding either 0.5 M HCl or 0.5 M NaOH. The salt concentration (and therefore the ionic strength) was adjusted by adding NaCl.

2.2.2 Membranes

Experiments were performed using the following hydrophilic polyethersulphone membrane discs (47 mm diameter): (i) a Supor®-450 membrane filter from Pall Corporation with a nominal pore size of 0.45 μm and a thickness of 140 μm, and (ii) a Supor®-200 membrane filter from the same supplier with a nominal pore size of 0.2 μm and a thickness of 145 μm. The 0.45 μm membrane had a mean resistance to flow of 1.78×10^{10} m^{-1}, and the 0.2 μm membrane had a mean resistance to flow of 3.81×10^{10} m^{-1}. Slight variability (in the order of 10 % - 15 %) in the membrane resistances was noted. A clean membrane was used for each run, and the membrane resistance was experimentally determined before each run. The membranes were supported in the filtration cell with circumferential supports of width 1 mm and the effective filtration area was 1.59×10^{-3} m^{2}.

2.2.3 Filter Cell

Microfiltration experiments were carried out using a 150 ml, 47 mm diameter stainless steel dead-end filtration cell from Pall Corporation.
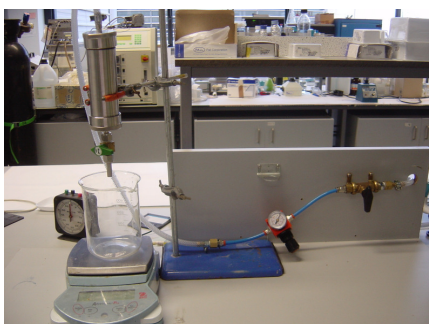
Figure 2-1: Dead-End Filtration Equipment

The cell was pressurised using compressed air and the pressure controlled using a regulator. All experiments were carried out at room temperature. Fresh yeast suspension and a new membrane were loaded into the apparatus for each experiment. The filtrate was collected in a reservoir placed on an electronic balance (Mettler Toledo BS3001) interfaced to a computer using Winwedge® software (TAL Technologies, Inc., PA, USA) to collect and record time and filtrate mass data at one second intervals. After each run, the apparatus was thoroughly cleaned using Teepol detergent, followed by a rinse of distilled water.

2.2.4   Filtration Method

2.2.4.1   Membrane Resistance R_m

The membrane resistances were determined by measuring the filtrate flux of distilled water through the membrane at a fixed pressure and applying Equation 1-2 with $m = 0$.

2.2.4.2   The Steady State Method

The steady state method (Nakanishi *et al.* 1987) described in Chapter 1 was employed to determine the specific resistance of the filter cake. Although this method for measuring specific resistance may be incorrect (Tien and Ramarao 2008), the purpose of this experimental study is the generation of data for use in evaluation of modelling using ANNs rather than an in-depth analysis into the specific resistance of cakes of yeast cells, and as such the steady state method is deemed accurate enough.

In this method, a given volume of yeast suspension (typically 100 mL), containing a known dry mass of yeast, was filtered at a pressure of 0.2 bar. Once the initial (dynamic) filtration was complete, the pressure was released. The filtrate was carefully returned to the filtration module, ensuring that the cake of cells was not disturbed. The cell was re-pressurised to the pressure employed to form the filter cake (0.2 bar) and filtration recommenced. The filtrate flux was allowed to reach steady state before the transmembrane pressure was incremented to the next pressure, and recorded at 5 different pressures between 0.2 and 2 bar. The filtrate mass was monitored continuously through the experiment and the steady state flux was determined from this measurement for each pressure. The specific resistance α was then calculated by applying Equation 1-2. It should be noted that it is generally found that the specific resistance of a microbial cake at a given pressure is independent of whether or not the cake has been exposed previously to different pressures (McCarthy *et al.* 1999) and hence the approach of incrementing the pressures in the way described above is valid.

2.2.4.3   Membrane Fouling

The membrane was examined for evidence of irreversible fouling after each experiment. This was achieved by washing the membrane with distilled water and then measuring the flux of distilled water through the washed membrane. Although there was some evidence of membrane fouling, the membrane resistance before and after filtration was of the order of $10^{10}\,\text{m}^{-1}$, whereas the cake resistance ranges between $10^{12}\,\text{m}^{-1}$ and $10^{13}\,\text{m}^{-1}$. Therefore, the increase in membrane resistance due to fouling does not affect the filtration characteristics and the cake resistance is the limiting resistance.

2.3 Experimental Observations

2.3.1 Filtration Behaviour

Preliminary experiments were carried out in order to characterise the filtration behaviour of the yeast cell suspension system, and to identify the key operating parameters prior to designing a set of experiments for use with an ANN to describe the steady filtrate flux and the specific cake resistance in terms of the operating parameters which affect them. In the absence of membrane fouling and/or cake clogging a plot of t/V versus V in dead-end filtration should lead a straight line with a slope that is proportional to the specific cake resistance. In experiments over a wide range of conditions, all t/V versus V plots obtained during the initial cake formation step were found to be linear suggesting that the performance of the filtration system employed in this study is dominated by the cake resistance (Figure 2-2).
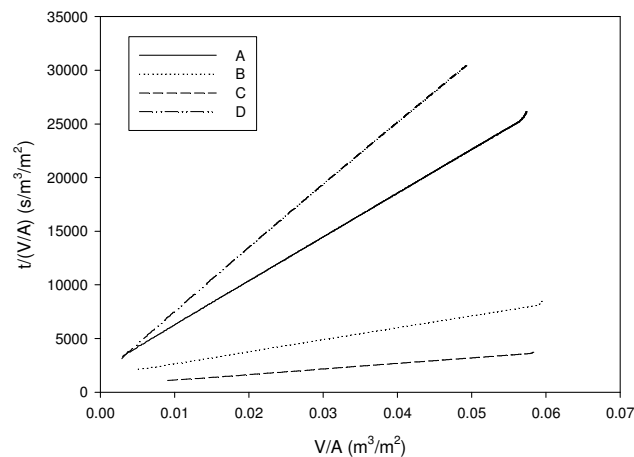
Figure 2-2: Ruth Plots ($t/_{(V/A)}$ versus $V/_A$)

A – Yeast Concentration = 7g/L, pH 8, Salt Concentration 2g/L, Pore Size 0.2μm;
B – Yeast Concentration = 3g/L, pH 2, Salt Concentration 5g/L, Pore Size 0.2μm;
C – Yeast Concentration = 0.75g/L, pH 4, Salt Concentration 4g/L, Pore Size 0.45μm;
D – Yeast Concentration = 11g/L, pH 9, Salt Concentration 1g/L, Pore Size 0.2μm

49

The process parameters that were identified for investigation in determining the specific cake resistance and filtrate flux were the applied pressure ΔP, yeast concentration C, pH, salt concentration and membrane resistance R_m.

2.3.1.1 Applied Pressure ΔP

Figure 2-3 shows plots of specific cake resistance, measured by the steady state method, as a function of pressure, at various pHs. The magnitudes of the specific resistance values are in agreement with other workers (Rushton and Khoo 1977; Piron *et al.* 1995), but higher than those of Nakanishi *et al.* (1987) and McCarthy *et al.* (1999). This is probably due to variations in the types of dried yeast employed in each study as well as differences in the various cell washing regimens used. It should be noted also that differences in specific resistance values can occur depending on the whether this parameter is defined in terms of a dry cell mass or a wet cell mass. In general, the specific resistance based on a dry cell mass will be larger than its wet cell equivalent.

In Figure 2-3, the dependence of specific resistance on pressure is shown to be linear in agreement with other workers (Tanaka *et al.* 1997; McCarthy *et al.* 1998b; McCarthy *et al.* 2002a) and there is a strong and complex dependence on pH of both the specific resistance at a given pressure and of the cake compressibility, where the latter is proportional to the slope of the α versus ΔP plot (McCarthy *et al.* 1998a). An increase in the applied transmembrane pressure serves to increase the steady filtrate flux (Figure 2-4).
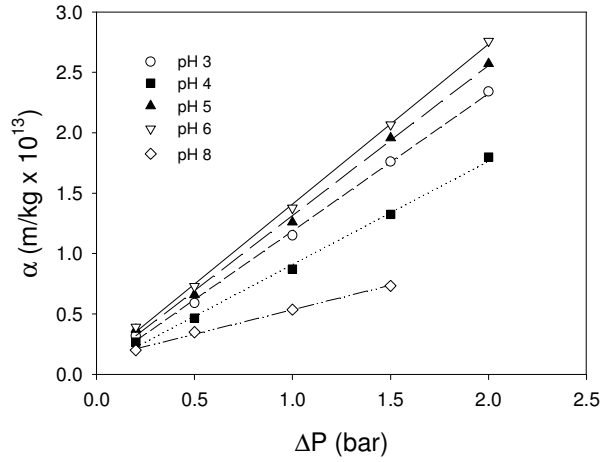
Figure 2-3: Effect of pressure and pH on α for = 5g/L and membrane pore size 0.45μm

2.3.1.2 Yeast Concentration *C*

The effect of increasing the yeast concentration was to decrease the steady flux attained (Figure 2-4, pH 9, Salt Concentration 4g/L and Pore Size 0.2 μm). This is as expected as the mass of cake on the membrane increases with increasing yeast concentration, thus increasing the resistance to flow and decreasing the steady state filtrate flux.
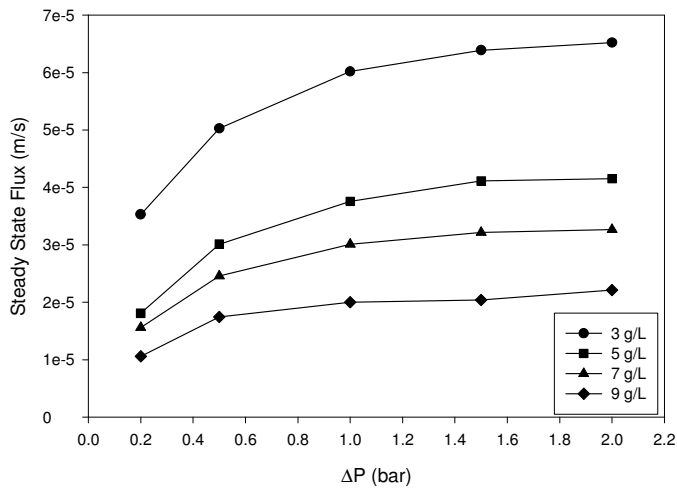
Figure 2-4: Effect of ΔP and *C* on Steady State Flux

In the case of the specific resistance, the expectation would normally be that the effect of concentration should be negligible; however some studies show that the specific cake resistance may show a dependence on suspension concentration. Mota *et al.* (2004) found that the specific resistance increased with increasing concentration of yeast cells, while Zaidi and Kumar (2005) found a similar effect with silica suspensions. In the work of Mota *et al.* (2004), the specific resistance approximately doubled as the dry weight cell concentration increased from about 4 g/L to 40 g/L, at pressures of 40 kPa and 80 kPa. Zaidi and Kumar (2005) found that the specific resistance of silica suspensions increased by a factor of approximately three as the concentration increased from about 3 g/L to 28 g/L. These results were obtained at pressures of 135 kPa, 270 kPa and 405 kPa. However, using linear regression on the data in this study, it was found that the slopes of plots of specific resistance versus yeast concentration were insignificantly different from zero at the 95 % confidence level and thus it can be concluded that concentration has no apparent effect on specific resistance (Figure 2-5, pH 9, Salt concentration 4 g/L, Membrane Pore Size 0.45 μm).
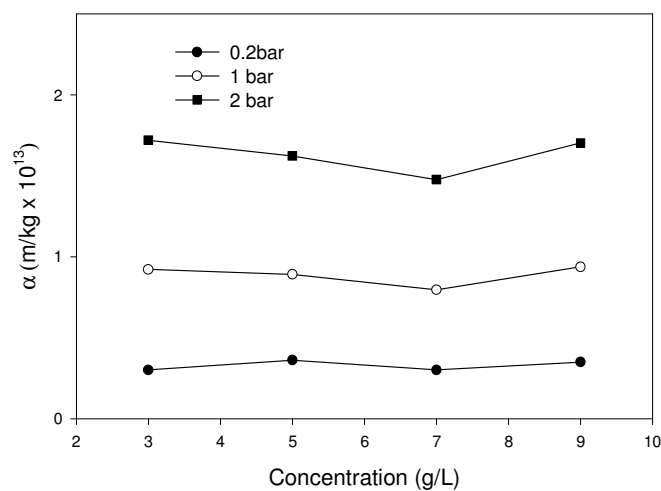
Figure 2-5: Effect of concentration on α at various pressures

2.3.1.3 pH and Salt Concentration

The effect of pH and Salt Concentration on the steady state flux and the specific resistance proved complex. The ionic character of the suspension was varied by the addition of NaCl and the pH was varied by addition of NaOH or HCl. There was a non-linear relationship between pH and α as may be seen from Figure 2-3 and Figure 2-6. There may also be an interaction between the effects of the salt concentration and the pH as these would be linked in the ionic character of the suspension (Figure 2-6 and Figure 2-7, at yeast concentration 5 g/L and membrane pore size 0.45 μm). The apparent complexity of the behaviour means that a conventional non-linear regression approach to developing a correlation of specific resistance will prove problematic because in that approach some functional relationship between specific resistance and the various parameters affecting it must be assumed. This relationship is likely to be quite complicated and unwieldy in form. These complex interactions make modelling of this process in physical terms very difficult, supporting the use of ANNs to model the system.
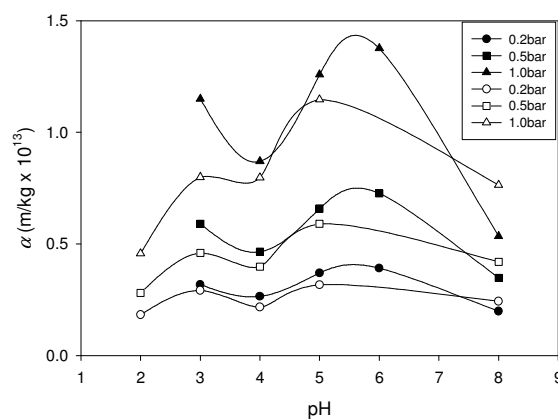
Figure 2-6: Effect of salt concentration on α at various pressures and pHs
Closed Symbols 2 g/L NaCl, Open Symbols 6 g/L NaCl.

53
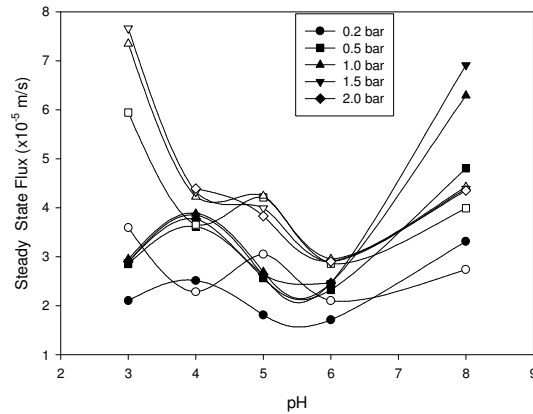
**Figure 2-7: Effect of pH and Salt Concentration at a range of pressures on Steady State Flux
Closed Symbols 2 g/L NaCl, Open Symbols 6 g/L NaCl**

2.3.2 Experimental Design

The experimental data in this chapter was collected for the purpose of developing
a neural-network based correlation for the specific resistance and filtrate flux in
dead-end microfiltration. As described in Section 2.3, the process parameters that
are assumed to affect the filtrate flux were the applied transmembrane pressure
ΔP, the yeast concentration C, the pH, the ionic strength and the membrane
resistance R_m. One would expect the effect of membrane resistance on the flux to
be small, as the membrane resistance is much smaller than the resistance to flow
provided by the cake of cells. Furthermore, the effect of R_m on α should be small
as R_m affects α indirectly through its effect on cake pressure drop ΔP_c. When the
cake resistance is dominant, the cake pressure drop is essentially independent of
R_m. However it was decided to include the cell concentration and membrane
resistance in the neural network work, in order to ascertain whether the
predictions of the Garson equation (Equation 2-3), which attempts to give some

54

insight into the underlying physical phenomena in the system using a weight partitioning method, agree with these findings.

The experimental population was devised using a range of possible combinations of the process parameters that were deemed of importance in the dead-end filtration of the yeast suspensions employed in this study. These were set to the values outlined in Table 2-1.

Table 2-1: Possible Parameter values in Dead End Microfiltration of Yeast Cells

Yeast Conc. (g/L)	pH	NaCl Conc. (g/L)	Pore Size (μm)	ΔP (bar)
3	2	0	0.45	0.2
5	3	1	0.2	0.5
7	4	2		1.0
9	5	3		1.5
11	6	4		2.0
13	7	5		
15	8	6		

All of the possible combinations of the values of the parameters of the first four columns of Table 2-1 were numbered and using a random number generator (in Excel), 30 experiments were chosen at random. The reason for choosing a random sample of experiments is to illustrate the applicability of the neural network approach to a process in which interactions between parameters are not necessarily understood. This lack of understanding would make impossible the use of a partial factorial design, for example. Choosing the experiments randomly needs no prior knowledge of the effect of the process parameters or their interactions on the experimental outcome.

Each combination of process parameters was performed at 5 different pressures, so a sample of 150 experiments was thus performed from all of the possible combinations of the process parameters. The specific resistance and steady state flux were experimentally determined for each parameter combination selected.

Table 2-2: Experimental Combinations and Choice of Training, Validation and Testing Data

Yeast Conc. (g/L)	pH	Salt Conc. (g/L)	Pore Size (mm)	Training (T), Validation (V), Test (X)[a]
3	2	7	0.2	T,T,T,T,T
3	2	2	0.2	T,V,T,T,T
3	7	2	0.45	T,V,T,T,T
3	9	4	0.2	T,X,T,T,X
5	4	0	0.45	T,T,T,X,X
5	5	5	0.45	T,V,T,T,T
5	9	4	0.2	T,X,V,X,X
7	2	1	0.45	T,V,T,T,T
7	2	5	0.45	T,T,T,T,X
7	4	0	0.2	T,T,T,T,X
7	4	1	0.45	T,T,X,T,T
7	8	2	0.2	T,T,X,T,X
7	8	6	0.2	T,T,T,X,T
7	9	4	0.2	T,X,T,X,X
9	5	3	0.2	T,T,T,T,V
9	5	4	0.2	T,T,T,X,T
9	9	0	0.2	V,T,T,T,T
9	9	3	0.45	T,V,T,T,X
9	9	4	0.2	T,T,T,T,X
11	4	3	0.2	T,V,T,T,X
11	6	6	0.2	V,T,T,T,T
11	8	3	0.45	T,V,X,T,X
11	9	1	0.2	T,V,T,X,X
11	9	2	0.45	T,T,X,X,X
13	4	3	0.45	T,T,T,T,T
13	8	2	0.2	T,T,T,X,X
13	8	3	0.45	T,V,T,T,T
15	5	0	0.45	T,T,T,T,X
15	5	1	0.45	T,T,T,T,X
15	6	3	0.45	T,T,X,X,T

[a] Letters correspond to experimental pressures of 0.2, 0.5, 1, 1.5 and 2 bar respectively

2.4   Artificial Neural Networks

The principles of artificial neural networks and their application to membrane processes have been described in detail previously in Chapter 1 and here only the key features of the implementation of this approach are given. A feed-forward ANN employing the sigmoid transfer function and the Levenberg-Marquardt algorithm for training was constructed with the MATLAB 7.0 Neural Networks Toolbox (The MathWorks Ltd., UK). All network weights were assigned random initial values in the range [-0.1, +0.1], training was conducted in batch mode and the training rate was set at the Matlab default value. Input data were normalised in Excel prior to use according to Equation 2-2 used by Fu *et al.* (2005)

$$x_i^* = a \frac{x_i - x_{min}}{x_{max} - x_{min}} + b \qquad\qquad [2\text{-}2]$$

where x_i^* is the normalised value, x_i the original data point, x_{max} and x_{min}, respectively, the maximum and minimum values for x, and a and b are the positive constants allowing the limits of the interval for the scaled values to be fixed. In this study, a and b are set as 0.6 and 0.2, thus the range of the data after normalisation is [0.2, 0.8]. The scale of the sigmoid transfer function is [0, 1], so training the network in the range 0.2 – 0.8 allows a margin for extrapolation outside the range of the training data.

The data in this study was divided into three sub-sets; a training set, a validation set and a test set as described previously (Bowen *et al.* 1998a). Using a technique known as cross-validation, the validation set prevents over-training of the network

by stopping training early once the maximum error (MSE) in the validation set begins to increase (Maier and Dandy 2000). The number of training points was chosen arbitrarily to be 104 and training points were selected to ensure that extreme values of the output (specific cake resistance) were included in the training set, as shown later in Figure 2-10. The number of validation points was 13 and the number of test points was 33. It has been shown by Amari *et al.* (1997) that the number of data points used for cross-validation should be very small compared to the number of training points. Reduction in the number of training data points reduced the accuracy of the final network. Table 2-2 provides a summary of all the experimental conditions employed and shows which experiments were used for training, validation and testing.

2.4.1 Neural Network Design

The network architecture refers to the number of layers in the network and the number of neurons in each layer. It has been shown previously that just one hidden layer is generally sufficient to model most data sets in membrane separation processes (Chellam 2005). Training of the network is performed by updating the networks weights over a number of epochs, or iterations, until the maximum squared error (MSE) in the validation data set begins to increase as outlined previously. Optimisation of the network architecture, with the aim of minimising the MSE for the training data, was performed via a trial and error procedure. The number of neurons in the input layer should match the number of input parameters (in this case, five) and the number of neurons in the output layer matches the number of outputs. A network with 1 hidden layer and 9 neurons in that hidden layer is shown in Figure 2-8. The effect of number of neurons in the

hidden layer on the MSE of the training data for the specific resistance is examined in a trial and error procedure in order to determine the network architecture that can best represent the specific resistance data.
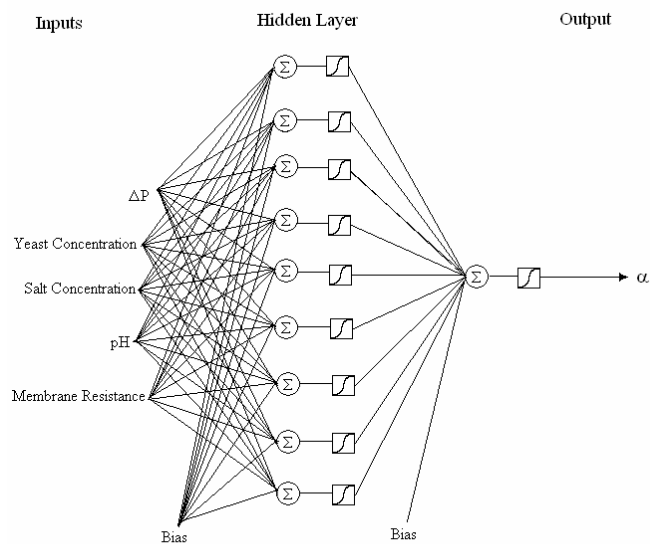
Figure 2-8: Network Architecture

The effect of the number of hidden neurons on the MSE for the specific resistance data is shown in Figure 2-9 (MSE for nine neurons = 9.85×10^{-8}) and, on that basis, a 5-9-1, fully connected architecture was chosen.
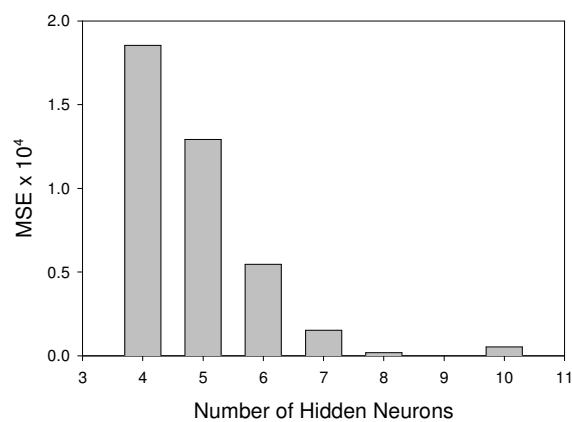
Figure 2-9: Optimisation of Network Architecture

59

2.4.2 Network Prediction

2.4.2.1 Specific Cake Resistance α

Figure 2-10 shows the fit of the optimised 5-9-1 network to the full set of specific resistance data, including those used in training, validation and testing. The network is found to correlate each dataset well.
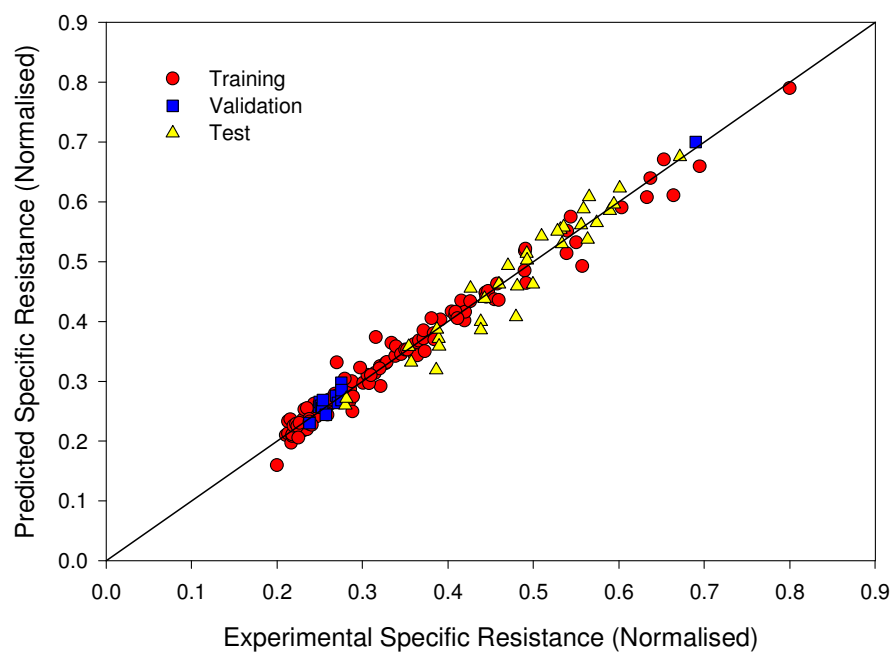
Figure 2-10: Fit of Optimised Network to Specific Resistance Data
Solid line denotes the y=x line

For the training dataset, the regression equation is y = 0.97x + 0.009 with an R^2 value of 0.98. 95 % confidence intervals for the slope and the intercept are [0.94, 1] and [-0.001, 0.02] respectively. For the validation dataset, the regression equation is y = 1.0143x + 7x10^{-4} with an R^2 value of 0.99. 95 % confidence limits for the slope and intercept are found to be [0.96, 1.07] and [-0.02, 0.02] respectively. For the test dataset, the regression equation is y = 1.12x – 0.06 with

an R^2 value of 0.94. 95 % confidence limits for the slope and intercept are [1.01, 1.22] and [-0.01, -9×10^{-3}] respectively.

Therefore, the neural network approach offers a potential alternative to more traditional regression techniques for correlating specific resistance behaviour, especially when factors in addition to pressure are included in the analysis. In combination with conventional filtration theory, the neural network could be used to form a hybrid model that calculates filtration performance over a wide range of suspension and process conditions.

2.4.2.2 Steady State Flux

While the focus of this study has been to develop an ANN to predict the specific resistance from which process characteristics can be calculated, the possibility of using the same ANN to predict the filtrate flux data directly has been investigated. The advantage of this approach is not so much its applicability to dead-end filtration, since the experimental set-up is somewhat artificial and does not reflect the true batch nature of industrial filtration processes, but because the ANN for predicting steady fluxes is easily extended to crossflow systems where specific resistance measurements are very difficult to obtain (McCarthy *et al.* 2002b). Figure 2-11 shows the fit of a 5-9-1 network obtained in the experiments described above. Exactly the same training, testing and validation sets as for the specific resistance network were used, although a superior fit may have been obtained if a new training set had been chosen specifically for the flux data and if the network architecture had been optimised using the flux data rather than specific resistance. As can be seen, the ANN for the flux correlates the data well and could form the basis of an ANN applied to predicting steady state fluxes in

61

crossflow systems once additional inputs such as crossflow velocity, and module geometry are included.
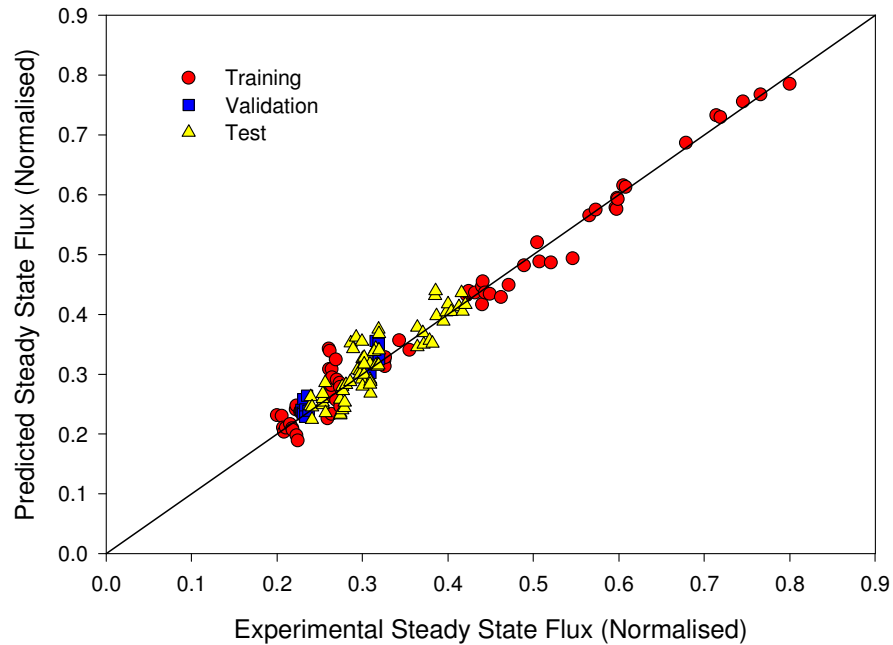
Figure 2-11: Fit of 5-9-1 Network to Steady State Flux Data
Solid line denotes the y=x line

For the training dataset, the regression equation is $y = 0.97x + 0.02$ with an R^2 value of 0.98. 95 % confidence limits for the slope and the intercept are found to be [0.93, 1] and [0.002, 0.03] respectively. For the validation dataset, the regression equation is $y = 1.06x - 0.05$ with an R^2 value of 0.91. 95 % confidence limits for the slope and intercept are found to be [0.86, 1.27] and [-0.06, 0.05] respectively. For the test dataset, the regression equation is $y = 1.03x - 0.007$ with an R^2 value of 0.8. 95 % confidence limits for the slope and intercept are [0.91, 1.16] and [-0.05, 0.03] respectively.

2.4.3   Interpretation of the Network Weights

In this chapter, it has been shown that an artificial neural network can be used to correlate dead-end specific resistance and flux data. However, previous researchers have shown that the network weights corresponding to an apparently best fitting network are not unique (Curry and Morgan 2006). Indeed, two networks with identical architecture, trained with the same data, may model that data with very similar accuracy and yet the final network weights obtained will almost certainly not be the same. The initial values of the weights (which are initialized here to random values between -0.1 and +0.1) have a strong effect on the final weights obtained for the trained network. This is because the initial weight vector determines the network starting point on the error hyper-space (Bowen *et al.* 2000). There is a tendency, when training, for the network to move into the closest local minimum to the starting point on the error surface, rather than to obtain the global minimum. The number of hidden neurons is directly proportional to the number of local minima in the error surface, and therefore adding more hidden neurons to the network will increase the risk of the network becoming trapped in a local minimum.

This variability in the weights obtained when training a network has implications for interpreting the networks weights. Traditionally, ANNs have been looked on as 'black-box' models, where an accurate description of the process is not required, relying merely on the ability of neural networks to approximately calculate the outputs of a system from knowledge of its inputs (Piron *et al.* 1997). However, some attempts have been made to assess the network connection weights in order to quantitatively derive some cause-effect information, using a

weight partitioning method. The equation used by Chellam (2005), developed by Garson (1991), can be written

$$v = \frac{\sum_{j=1}^{n_h}\left[\left(w_{vj}/\sum_{k=1}^{n_v}w_{kj}\right)O_j\right]}{\sum_{i=1}^{n_v}\left[\sum_{j=1}^{n_h}\left[\left(w_{vj}/\sum_{k=1}^{n_v}w_{kj}\right)O_j\right]\right]} \qquad [2\text{-}3]$$

where v represents the relative effect of the input variable, v, on the output, n_v is the number of input variables, n_h is the number of neurons in the hidden layer, w_{kj} represents the absolute value of the weight from the k-th input to the j-th neuron and O_j represents the absolute value of the weight from the j-th neuron. (A sample calculation illustrating the practical application for a simple network is shown in a short appendix at the end of this chapter.) However, since the network weights are variable, depending on the initial weights used in the training process, the computed effects of input parameters will also be variable. To investigate this phenomenon, the 5-9-1 specific resistance and flux networks are trained over a series of 20 runs with random initial weights in each case. While the effects of the inputs on the output were found to vary, this variation was small as shown later (Figure 2-12 and Figure 2-13), suggesting that the variability of network weights does not make their interpretation impossible.

2.4.3.1   Relative Effect of Input Parameters

From Figure 2-12, it is clear that the main parameters affecting the specific resistance are the pressure and the pH, as would have been expected from Figure 2-3 and Figure 2-6. The effects of the other parameters are lower but not insignificant. This analysis indicates that the relative importance of the salt

64

concentration, yeast concentration and membrane resistance are similar. However it was shown previously that the effect of yeast concentration on α is negligible using a standard regression analysis, whereas the salt concentration was shown to have a small effect on α in Figure 2-6. It is important to note, however, that this approach is only semi-quantitative and a non-zero value for the relative effect of a parameter does not imply a cause-effect relationship but simply shows that the experimental output was different for various values of a given input. This variation may have been due to normal experimental scatter rather than representing a true relationship. Error bars represent the standard error over 20 runs in Figures 2-11 and 2-12. Figure 2-13 gives the relative effects of the input parameters on the flux. The effect of yeast concentration on the flux is large, as would be expected from Equations 1-1 and 1-2, as concentration appears explicitly in mechanistic filtration theory. The other parameters that have the most effect are the pressure and the pH. This approach of calculating the relative effects of various input parameters on the system output would be most useful in complex systems where the underlying physics was not well understood and it was desired to identify key process parameters. However, its semi-quantitative nature means that it will only serve as a guide that may aid in reducing the amount of experimentation required but will not lead to a true physical understanding of the process.
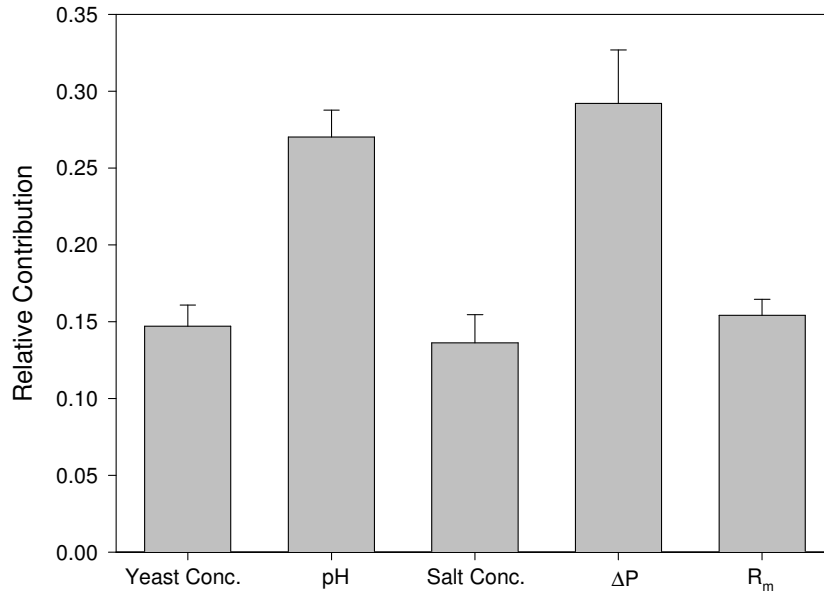
Figure 2-12: The (mean) relative importance of input parameters to the specific cake resistance
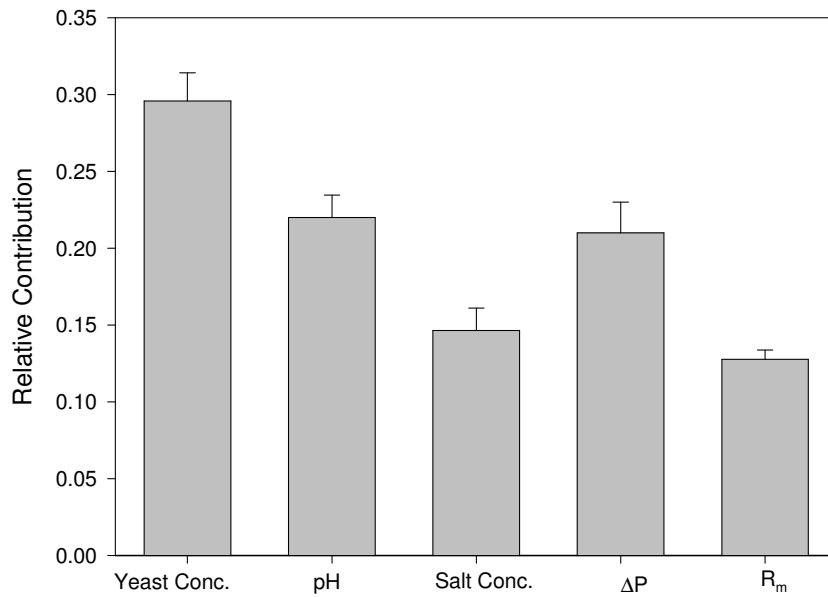
Figure 2-13: The (mean) relative importance of input parameters to the steady state flux.

It is possible that this analysis could be used in a similar manner to principal component analysis. The smallest inputs could be regarded in some cases as

insignificant (as for the case of specific resistance, where the concentration and membrane resistance are seen to have no effect). An interesting analysis could be the elimination of the inputs which have the smallest relative effect on the network outputs, allowing for more in-depth analysis of the more important effects.

2.5   Conclusions

This chapter focused on the correlation of specific cake resistance and flux data in dead-end filtration of yeast suspensions using artificial neural networks. The results obtained show that excellent agreement between experimental data and predicted values could be achieved over wide ranges of pressure, membrane resistance, yeast concentration, and suspension pH and ionic strength. The approach is easily extended to include the many other factors that affect the specific resistance. The neural network for the steady state flux would be easy to extend to encompass crossflow filtration by the addition of parameters such as the crossflow velocity and module configuration. The network weights were interpreted using the weight partitioning method suggested by Garson (1991) to evaluate the relative effect of the input parameters on the specific cake resistance and the steady state flux. This is an area that is worthy of further study as it is very desirable to be able to extract meaning from the weight matrix of neural networks.

As discussed previously, dead-end filtration is of limited applicability industrially. Chapters 3 and 4 will focus on the extension of this method to stirred and batch crossflow microfiltration systems, where prediction and optimisation of flux decline is a topic of much research.

This chapter has focused on the filtration of microbial cells; however, this approach should be applicable to more complex suspensions. In an attempt to test the accuracy of this method when applied to more complex systems, filtration experiments from this point forward will be carried out using a non-Newtonian, shear thinning, thixotropic suspension of bentonite clay.

2.6   Appendix - Matlab Code

Creation of an ANN in Matlab is made easy by the use of built-in functions in the Neural Network Toolbox. The code for the network used in prediction of specific resistance data may be seen in Code 2-1, where the importing of the data, the initialisation of the network (setting up the network architecture and the transfer functions to be used, and setting of the network training parameters), initialisation of the weight and bias matrices, training of the network, generation of a plot of the network performance (evolution of the error in the three datasets) and simulation of the training dataset are shown. It is important to note that the normalisation of the input and output data is performed in Excel prior to being imported to Matlab, although incorporation of code to perform this task in Matlab itself would be quite simple.

Code 2-1: Network Initialisation

```matlab
% Reading in the inputs and the target values for training
p=xlsread('alphainputs', 'training');
t=xlsread('alphatargets', 'training');

% reading in validation data
validationinputs=xlsread('alphainputs', 'validation');
validationtargets=xlsread('alphatargets', 'validation');
val.P=validationinputs; val.T=validationtargets;

%reading in test data
testinputs=xlsread('alphainputs', 'testing');
testtargets=xlsread('alphatargets', 'testing');
test.P=testinputs; test.T=testtargets;
ptr=p; ttr=t;

% Making the network using the logsig transfer function
no_hidden_neurons=9;
no_input_neurons=5; %fixed
no_output_neurons=1; %fixed
net=newff(minmax(ptr), [no_hidden_neurons no_output_neurons], {'logsig' 'logsig'}, 'trainlm');

% Setting the network parameters
net.trainParam.goal=1e-8;
net.trainParam.epochs=150;
net.trainParam.show=25;
net.trainParam.max_fail=20;

% Initialising the weight and bias matrix to random values between -0.1 and +0.1
a=-0.1;
b=+0.1;
h=(no_input_neurons*no_hidden_neurons+no_hidden_neurons+no_hidden_neurons*no_output_
neurons+no_output_neurons);
y=a + (b-a) * rand(h,1);

net=setx(net, y);

initialinputweights=net.iw{1,1};
initiallayerweights=net.lw{2,1};

% Training the network
[net, tr]=train(net, ptr, ttr, [], [], val, test);




% Plotting the performance of the network - the network stops training if the validation error starts
to increase
plot(tr.epoch, tr.perf, tr.epoch, tr.vperf, tr.epoch, tr.tperf);
legend('Training', 'Validation', 'Test', -1);
ylabel('Squared Error'); xlabel('Epoch');
% Simulating the network using the training dataset inputs
a=sim(net, p);
figure
% Performing linear regression on the network outputs and comparing with
% the targets
[m, b, r]=postreg(a, t);
```

The data is divided into three sections as mentioned previously, and the datasets are saved as excel spreadsheets. Two spreadsheets are generated, one containing the network inputs (named alphainputs.xls) and one containing the network targets (named alphatargets.xls). Each spreadsheet contains three worksheets, named 'training', 'validation' and 'testing'. The format for the input data may be seen in Table 2-3, where the experimental conditions for each run are contained in columns, and each experimental parameter occupies a row.

Table 2-3: Inputs to ANN

Yeast Conc.	0.40	0.70	0.30	…
pH	0.37	0.37	0.46	…
Salt Conc.	0.20	0.46	0.63	…
ΔP	0.20	0.20	0.20	…
R_m	0.64	0.32	0.29	…

The network targets are contained in a single row.

The network inputs and targets are read into Matlab using the function 'xlsread', and each dataset is named within the code. For example, the network inputs for the training dataset are imported and given the name 'p' using the code:

```
p=xlsread('alphainputs', 'training');
```

The number of input, output and hidden neurons are specified, and the network is initialised using the function 'newff', which creates a feedforward, backpropagation network.

```
net=newff(minmax(ptr), [no_hidden_neurons no_output_neurons], {'logsig' 'logsig'}, 'trainlm');
```

The arguments which must be included with the function 'newff' are:

- An Rx2 matrix of minimum and maximum values for R input elements (minmax(ptr))

- The number of hidden neurons and the number of output neurons

- The transfer functions used between each layer ('logsig' for both in this case, the sigmoidal transfer function)

- The training algorithm ('trainlm' – the Leverberg Marqhardt algorithm – a method for convergence using a variation on the steepest descent method)

The network training parameters are set using built-in functions.

```
net.trainParam.goal=1e-8;
net.trainParam.epochs=150;
net.trainParam.show=25;
net.trainParam.max_fail=20;
```

where net.trainParam.goal is the desired MSE, net.trainParam.epochs is the number of passes, net.trainParam.show specifies the number of iterations after which the progress of the network will be displayed in Matlab, and net.trainParam.max_fail is the number of epochs for which the validation error is allowed to increase before training is stopped.

The network performance is plotted as in Figure 2-14. This figure is automatically generated by Matlab when training a network. Although it seems that the error for the test dataset is initially small with a rapid increase followed by a decrease, this is likely to be an anomaly within the initialisation of the weights, where the network weights happen to fit well to the test dataset.

71
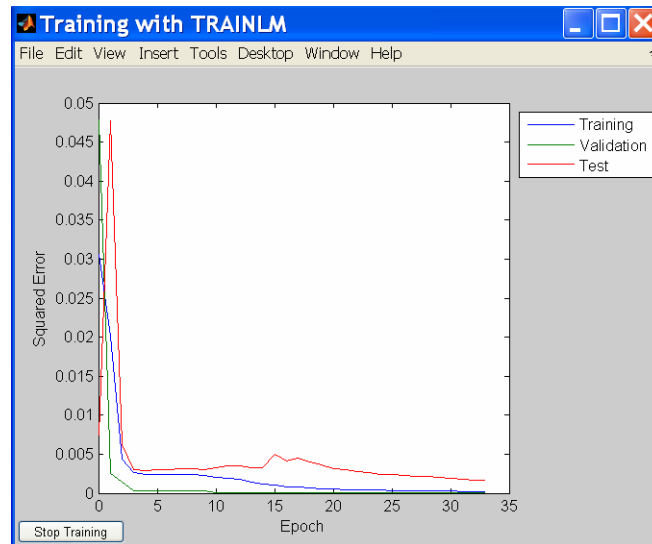
Figure 2-14: Network Performance

The training dataset is then simulated and using linear regression, the network output is compared to the target dataset.

```
a=sim(net, p);
figure
[m, b, r]=postreg(a, t);
```

This code generates the plot shown in Figure 2-15.
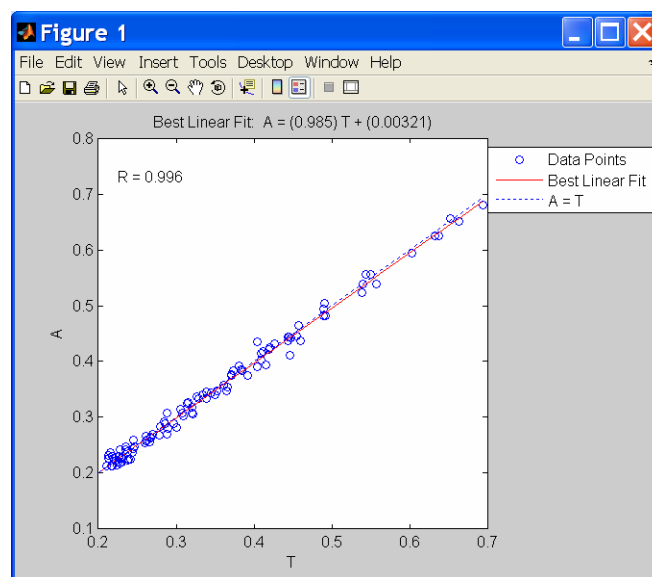
Figure 2-15: Comparison of Network Simulation of Test Data with Targets

72

The evaluation of the relative importance of the input parameters using the Garson Equation (Equation 2-3) as described previously is shown in Code 2-2 below. This code generates the relative importance as a proportion of 1. A sample calculation for the Garson Equation is also shown below (Section 2.6.1).

The network simulation of the training, validation and test datasets are plotted separately and altogether as one dataset and compared with the target data with Code 2-3.

Code 2-2: Garson Equation

```matlab
inputsize=size(p);
no_inputs=inputsize(1,1);
no_datapoints=inputsize(1, 2);

realinputweightmatrix=net.iw{1,1};
inputweights=abs(realinputweightmatrix);
reallayerweights=net.lw{2,1};
layerweights=abs(reallayerweights);
rowsumsinputs=sum(inputweights');

% Code to Work out the Garson Equation
%Top Line
k=1 % k is the variable of interest
while k<=no_inputs

    j=1;

    while j<=no_hidden_neurons
        wvj=inputweights(j,k);

        wkj=rowsumsinputs(1,j);

        oj=layerweights(1,j);
        top(j)=(wvj/wkj)*oj;
        j=j+1;
    end
    topline=sum(top');

    %Bottomline will always be the same, regardless of the variable you're
    %interested in. It's basically the sum of all the possible top lines you
    %could have.

    inputparameter=1;

    while inputparameter<=no_inputs
        hiddenneuron=1;
        while hiddenneuron<=no_hidden_neurons
            wvq=inputweights(hiddenneuron,inputparameter);

            wxq=rowsumsinputs(1,hiddenneuron);

            oq=layerweights(1,hiddenneuron);
            btop(hiddenneuron)=(wvq/wxq)*oq;
            hiddenneuron=hiddenneuron+1;
        end
        toplinesb(inputparameter)=sum(btop');
        inputparameter=inputparameter+1;
    end

    bottomline=sum(toplinesb');

    parameterinfluence=topline/bottomline

    k=k+1
end
```

Code 2-3: Generation of Plots for Training, Validation and Test Datasets

```matlab
% Plotting training set of data
j=ptr;
k=ttr;
atrain=sim(net,j);
figure
plot(k, atrain, 'ro', k, k);
u=k*.1+k;
v=k-.1*k;
hold on
plot(k, u, 'm-', k, v, 'c-');
location=2;
legend('Training Data', '100% Agreement', '10% Above', '10% Below', location);
title('Test of Network - Training Data');
ylabel('Network Output');
xlabel('Target Values');

% Checking with validation set of data
zz=val.P;
kk=val.T;
avalidation=sim(net,zz);
figure
plot(kk, avalidation, 'ro', kk, kk);
q=kk+.1*kk;
w=kk-.1*kk;
hold on
plot(kk, q, 'm-', kk, w, 'c-');
location=2;
legend('Validation Data', '100% Agreement', '10% Above', '10% Below', location);
title('Test of Network - Validation Data');
ylabel('Network Output');
xlabel('Target Values');

% Checking with test set of data
jj=test.P;
ll=test.T;
atest=sim(net,jj);
figure
plot(ll, atest, 'ro', ll, ll);
qq=ll+.1*ll;
ww=ll-.1*ll;
hold on
plot(ll, qq, 'm-', ll, ww, 'c-')
location=2;
legend('Test Data', '100% Agreement', '10% Above', '10% Below', location);
title('Test of Network - Test Data');
ylabel('Network Output');
xlabel('Target Values');
%

% Checking with entire set of data
totalinputs=xlsread('alphainputs', 'total');
totaltargets=xlsread('alphatargets', 'total');
wholetest=sim(net,totalinputs);
figure
plot(totaltargets, wholetest, 'ro', totaltargets, totaltargets);
rr=totaltargets+.1*totaltargets;
ee=totaltargets-.1*totaltargets;
hold on
plot(totaltargets, rr, 'm-', totaltargets, ee, 'c-')
location=2;
legend('Entire Data Set', '100% Agreement', '10% Above', '10% Below', location);
title('Test of Network - Entire Data Set');
ylabel('Network Output');
xlabel('Target Values');
```
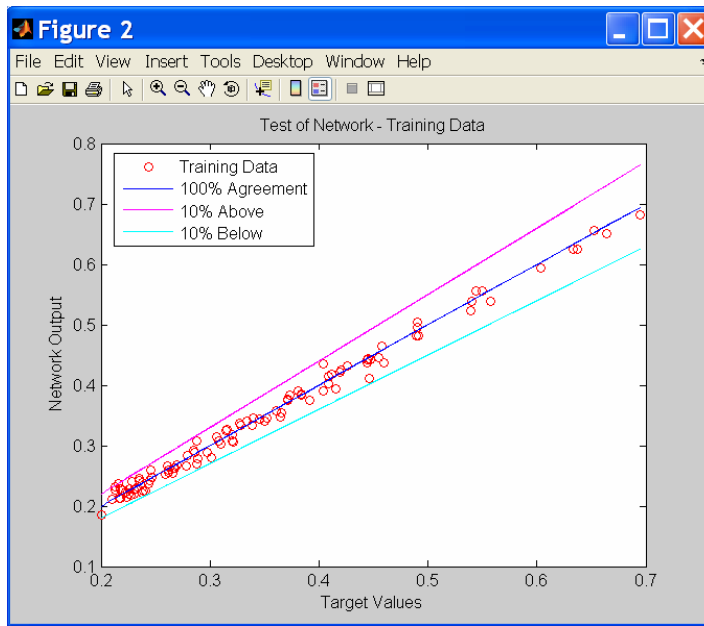
Figure 2-16: Training Dataset
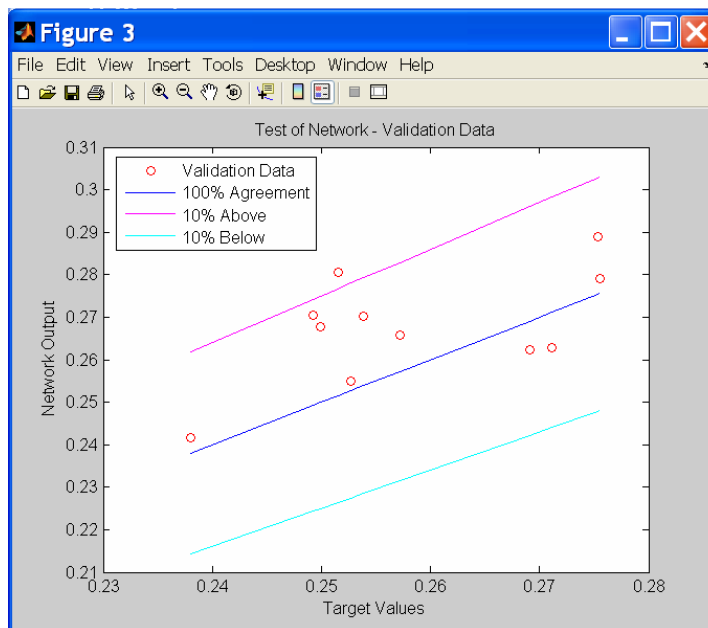
Figure 2-17: Validation Dataset
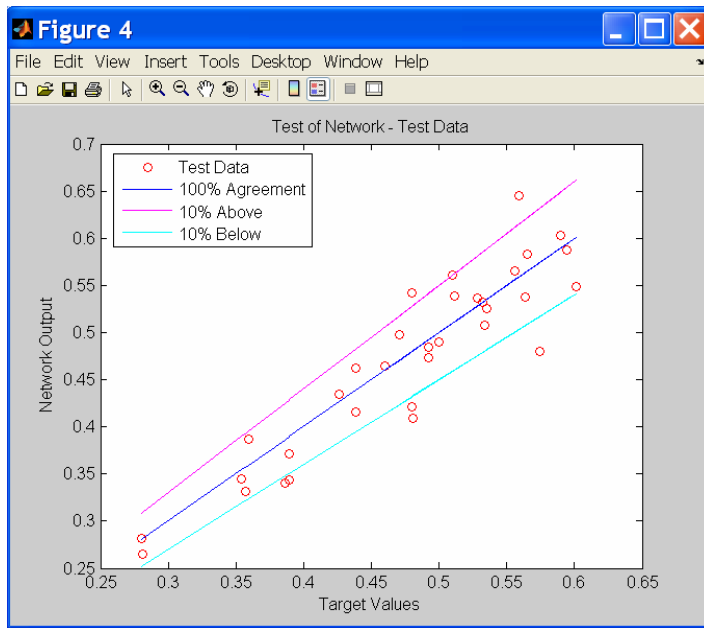
Figure 2-18: Test Dataset
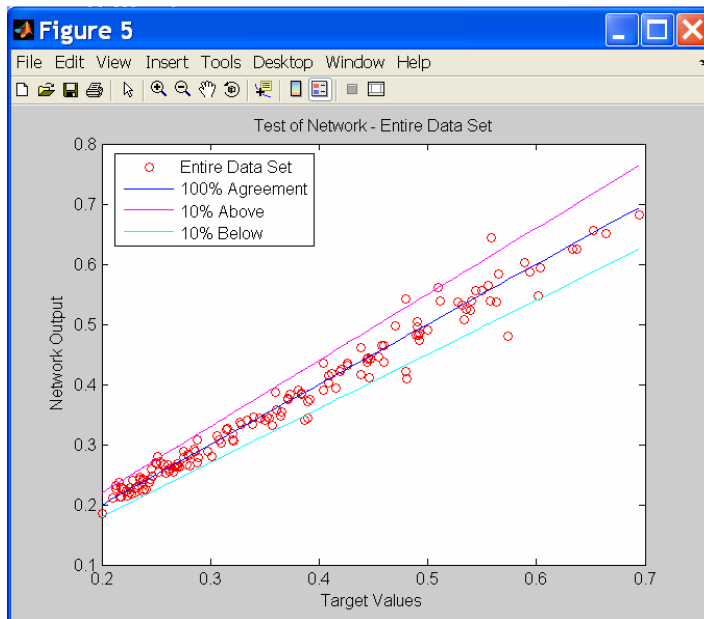
Figure 2-19: Entire Dataset

2.6.1 Sample Calculation of Relative Effect of Input Parameters Using the Garson Equation

Consider a neural network with two inputs, a single hidden layer with three neurons and a single output (Figure 2-20). After training of the network, the network weights are found to have the values given in Table 2-4.

Table 2-4: Network Weights for Garson Equation

From 1st Input to Hidden Layer		From 2nd Input to Hidden Layer		From Hidden Layer to Output	
$w_{1,1}$	0.517	$w_{2,1}$	0.649	O_1	0.981
$w_{1,2}$	0.162	$w_{2,2}$	0.132	O_2	0.461
$w_{1,3}$	0.488	$w_{2,3}$	0.584	O_3	0.641
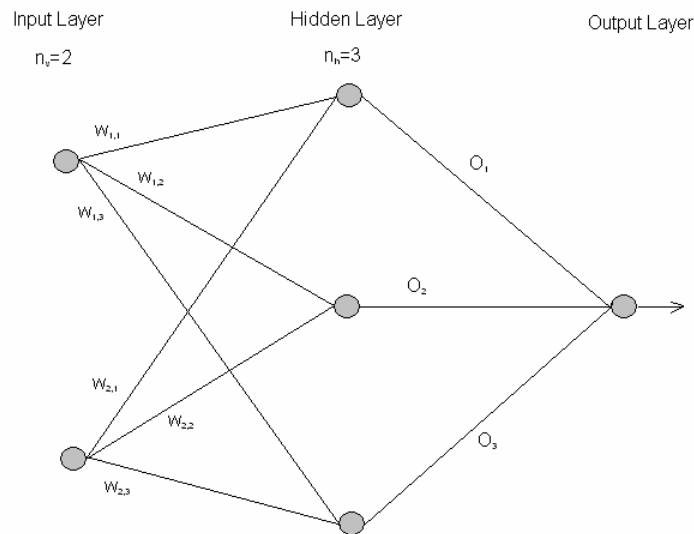
Figure 2-20: Sample Network for Garson Equation

The relative effect of the first input on the network output is given, according to the Garson Equation (Equation 2-3), by the expression

$$
v = \frac{\left(\dfrac{0.517}{0.517+0.649}\right)0.981 + \left(\dfrac{0.162}{0.162+0.132}\right)0.461 + \left(\dfrac{0.488}{0.488+0.584}\right)0.641}{X+Y}
$$

where

$$
X = \left(\frac{0.517}{0.517+0.649}\right)0.981 + \left(\frac{0.162}{0.162+0.132}\right)0.461 + \left(\frac{0.488}{0.488+0.584}\right)0.641
$$

and

$$
Y = \left(\frac{0.649}{0.517+0.649}\right)0.981 + \left(\frac{0.132}{0.162+0.132}\right)0.461 + \left(\frac{0.584}{0.488+0.584}\right)0.641
$$

Thus, the relative effect of the first input works out to be 0.5078.

CHAPTER 3: STIRRED CELL MICROFILTRATION OF BENTONITE SUSPENSIONS: DYNAMIC MODELLING USING A NOVEL NEURAL NETWORK METHOD

In stirred microfiltration the filtration is nominally perpendicular to the membrane, as in dead-end microfiltration. However the filter cell is equipped with a stirrer or impeller, and the shearing action provided by this keeps the solids in suspension and limits deposition on the membrane, mimicking crossflow microfiltration. It has been established that the process parameters that influence the filtration behaviour of this kind of system include the pressure, temperature, feed concentration, stirring speed, membrane morphology or resistance and initial solids concentration (Zokaee *et al.* 1999). Filtration characteristics for this type of system have been investigated for bacterial cells (Zokaee *et al.* 1999) natural organic matter in drinking water treatment (Fan *et al.* 2001; Cho *et al.* 2006), proteins (Ho and Zydney 2000), glass industry wastewater containing colloidal clay and glass particles (Kang and Choo 2003), and turbidity constituents of beer and wine (Czekaj *et al.* 2000a, 2001).

Few studies have been devoted to the modelling of this type of system and most of these focus on the stirred filtration of protein solutions. In many cases, fouling in stirred microfiltration of proteins has been found to be dominated by internal fouling mechanisms initially and later by a period of external fouling (Zokaee *et al.* 1999; Ho and Zydney 2000; Czekaj *et al.* 2001). Models used have been based on constant pressure blocking filtration laws, where the Standard Blocking Model has shown good agreement at low filtration times and for dilute solutions, and the

cake filtration model (in dead-end systems) has shown good agreement at higher filtration times (Zokaee *et al.* 1999). Ho and Zydney (2000) developed a model incorporating these phenomena into a single mathematical expression. These models prove to be rather limited, in that they could not be expected to work outside the confines of the particular experimental system. Also, complex interactions based on suspension characteristics such as pH and ionic strength are mostly neglected in the analyses. Thus, it is unlikely that they would work for highly complex systems such as fermentation broths or non-Newtonian suspensions. Further discussion of complexities in this type of system may be found in Chapter 1. For these reasons, the use of empirical modelling techniques based on neural networks is an attractive approach.

The objective of this chapter is to investigate the dynamic behaviour of the stirred system in the microfiltration of particulate suspensions and to explore the use of artificial neural networks in modelling these systems. Modelling of system dynamics is important in the context of industrial application of filtration processes (Bowen *et al.* 1998a; Aydiner *et al.* 2005). For example, in a typical process plant in which filtration plays a part, a simple model of flux dynamics would allow prediction of filtrate volume in a given time from the relationship

$$V = A \int_0^t J dt \qquad [3\text{-}1]$$

It is proposed, in this study, to perform exploratory work to determine if ANNs provide a good approach to modelling such a batch system.

The filtration of suspension of two types of solid is described: calcium carbonate and bentonite, the latter forming a highly non-Newtonian suspension. The data

obtained is used to show the difficulties involved in using non-linear regression approaches to data fitting and to evaluate the potential of the neural network approach.

3.1   Materials and Methods

3.1.1   Filter Cell and Reservoir

Experiments were performed using a stirred cell with capacity of 180ml and internal diameter 63mm (Figure 3-1, Amicon, Millipore).
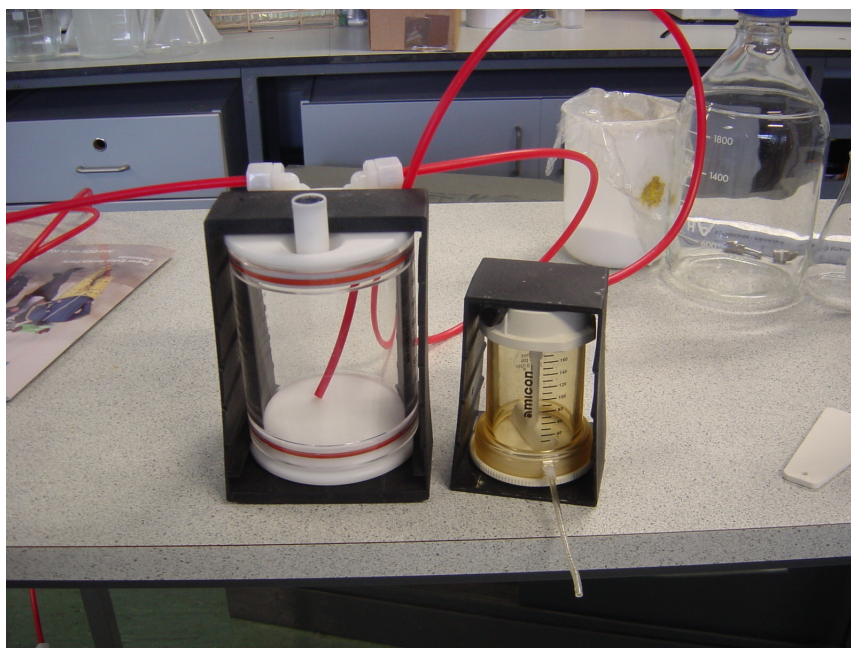
Figure 3-1: Stirred Cell and Reservoir

An o-ring of 1mm thickness was used to ensure a seal in the stirred cell. The cell is equipped with a stirrer of diameter 47 mm, the stirring speed of which was controlled using magnetic stirring plates (Stuart Scientific and IKA Labortechnik). The stirred cell was fed from a reservoir of capacity 800ml (Amicon, Millopore). The cell and reservoir were pressurised using compressed air (Figure 3-2). It is

important to note that this set-up is unusual in that is consists of a quasi-continuous two-compartment system. The feed is placed in the reservoir, and pressure is applied. Some of the feed moves from the reservoir into the stirred cell, with the volume in the stirred cell being dependent upon the applied pressure. For most of the run, the volume in the stirred cell is constant but the particle concentration is increasing due to the build-up of particles on the membrane surface as filtration proceeds, and this is followed by a final phase (when the reservoir has emptied) when the cell itself empties. Thus this system is only a true batch system at the end phase, when the cell is emptying. The filtrate volume is measured in one second intervals and the flux calculated from this.
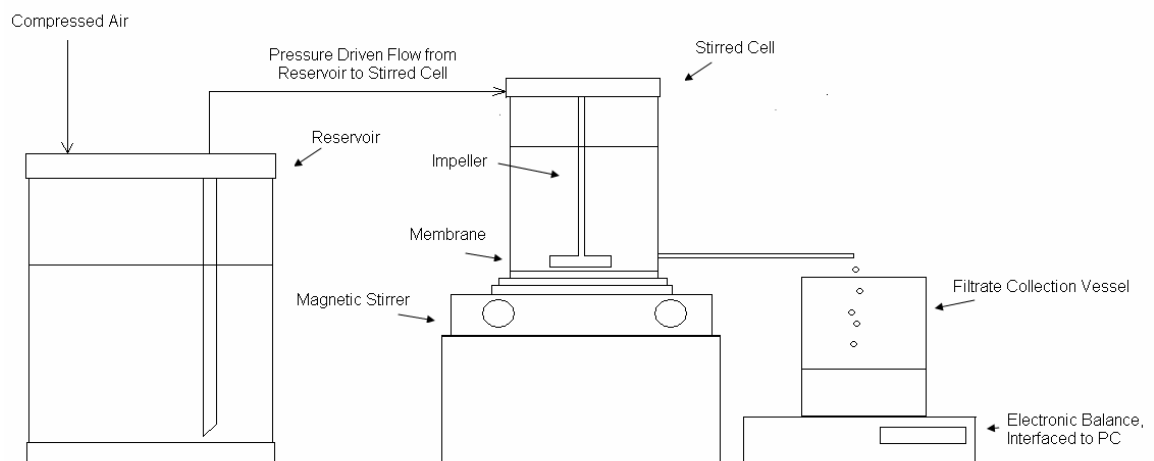
Figure 3-2: Stirred Cell Apparatus Incorporating Feed Reservoir

3.1.2 Membranes

Two different types of membranes were used, a glass fibre membrane of pore size 1μm (Pall), and a hydrophilic polyethersulfone membrane of pore size 0.45 μm (Pall). The membranes were of diameter 63 mm but the o-ring used in the cell

83

reduced the area available to flow, rendering the effective membrane area equal to 29.2 cm^2. PES membranes were not available in a suitable diameter for this particular apparatus. Therefore, membranes with 90 mm diameter were purchased and cut to size. This was done using a template manufactured specifically for this purpose in DCU. Membranes were held inside the template and cut with a sharp scalpel to the required size.

3.1.2.1   Membrane Resistance R_m

The hydraulic permeability or membrane resistance of each fresh membrane is measured by filtering pure water through the membrane and determining the resistance to flow in dead-end mode as described in Chapter 2.

Membrane compression effects, or the dependence of the hydraulic permeability of the membrane on pressure, have been seen in many cases to affect flux decline characteristics in all types of filtration. Compression of the membrane with applied pressure has been found to be linear in some cases and non linear in others, and has proven to be a membrane specific phenomenon. In the case of microfiltration, flux decline in crossflow mode has been attributed previously to membrane compression effects (Dharmappa and Hagare 1999). Non-linear membrane compression effects were seen to contribute to flux decline in the stirred microfiltration of cutinase and *E. Coli* cell fragments by Sousa *et al.* (2002). Flux decline was also found to be affected by membrane compression by Kelly *et al.* (1993) for the stirred microfiltration of proteins. A linear relationship between applied pressure and R_m calculated from pure water flux was observed by Lu *et al.* (2007) for ultrafiltration membranes. Membrane compression prior to filtration of proteins in a UF membrane was performed by Li *et al.* (2005).

Membrane compression effects were shown to affect the ultrasonic technique being investigated and pre-compression of the membrane allowed the ultrasonic signals from the membrane to stabilise. An increase in hydraulic permeability of nanofiltration membranes with increasing pressure was noted by Drews *et al.* (2003). Sjöman *et al.* (2007) also noted that membrane compression may have an effect on the nanofiltration of monosaccharide solutions. Membrane compression of membranes for reverse osmosis was examined in detail by Ermakova *et al.* (1998). Flux decline due to membrane compression at long times in crossflow RO of extracellular polymeric substances was observed by Tansel *et al.* (2006).

It is clear that it is necessary to quantify membrane compressibility and compression effects in order to accurately investigate the flux decline characteristics of the filtration system. As such, membrane compressibility for all membranes used was investigated for each experimental run, and the membranes were pressurised to the highest pressure used experimentally prior to investigation of the pressure dependence of the hydraulic permeability in order to account for effects related to non-relaxation of the membrane after compression, or hysteresis effects.

3.1.2.1.1 Glass Fibre Membranes

The resistance of the glass fibre membrane was found to be pressure dependent (Figure 3-3). A linear relationship between R_m and ΔP is evident. The variation in resistance from membrane to membrane was less than 1 % for all membranes investigated. The R_m for the glass fibre membranes ranged from 2.5 to 5.5 x 10^{10} m^{-1}.
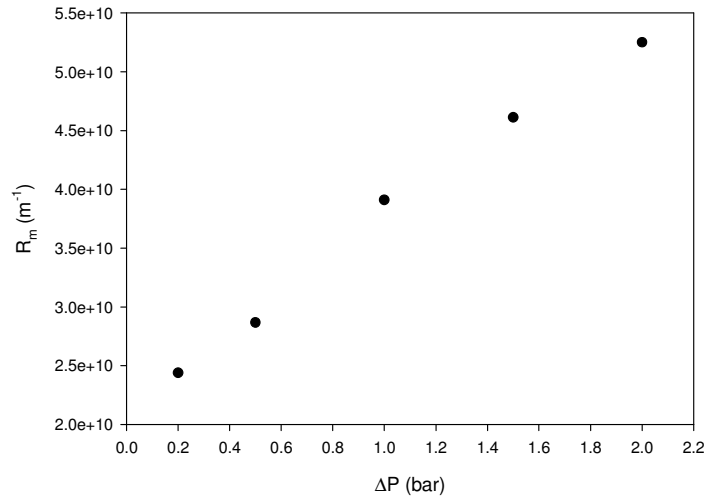
Figure 3-3: Effect of pressure on glass fibre membrane resistance

3.1.2.1.2 Hydrophilic Polyethersulphone Membranes

The resistance to flow of the PES (polyethersulphone) membranes was also found to be pressure dependent; however, the variability from membrane to membrane was greater for this type than for the glass fibre membranes. Figure 3-4 shows the pressure dependence of the membranes where the error bars represent the standard error for the data set.
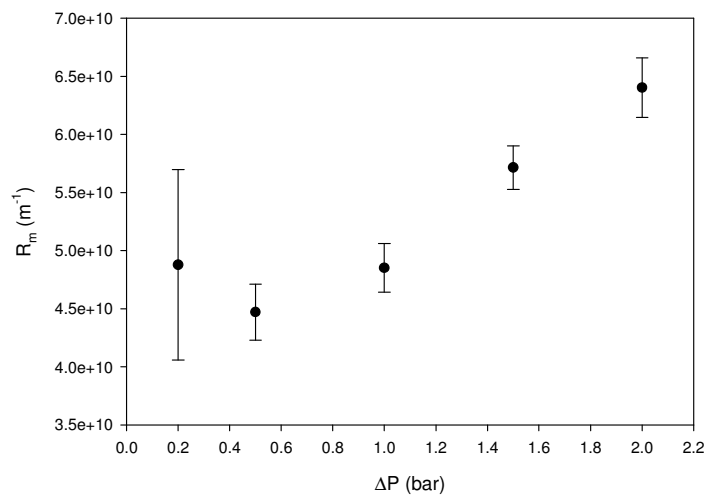
Figure 3-4: Effect of pressure on R_m for PES membranes with pore size 0.45μm

The standard error is calculated for a set of data with a single mean as the standard deviation of the data divided by the square root of the number of data points, i.e.,

$$\text{Standard Error} = \frac{\sigma}{\sqrt{N}} \qquad\qquad [3\text{-}2]$$

It appears that the pressure dependence of the R_m for these membranes is more complex than that of the glass fibre membranes, displaying a non-linear pressure dependency. However given the magnitude of the standard error associated with the membrane resistance at 0.2 bar, it is possible that this is not the case. The large standard error associated with the values obtained for R_m may be due to the cutting of the membranes prior to their use. Slight variations in the edges may have affected the value obtained. However, as the measured membrane resistance is used as an input to the neural network later, the variation between runs is of no consequence. The R_m is slightly higher than that for the glass fibre membranes, of the order of 4.5 to 6.5 $\times 10^{10}$ m^{-1}.

3.1.2.2 Impeller

The impeller speed was controlled using two magnetic stirring tables. The stirring tables had a number of speed settings numbered from 1 to 10. The stirring speeds corresponding to each setting when used with the stirred cell were found using a stroboscope (Radionics Ltd.).

A stroboscope consists of a strobe light, the frequency of which may be adjusted. The impeller was marked and for each stirring table setting, the frequency of the stroboscope was adjusted until the impeller appeared stationary, i.e. the frequency of the strobe light was equal to the frequency of rotation of the impeller.

3.1.3 Stirrer Table

The impeller speed was dependent on the type of stirrer table used and the setting. Two different stirring tables were used over the course of collecting the experimental data as one of the stirring tables malfunctioned. For the first stirring table used (Stuart Scientific) settings were adjusted between 4 and 8 as the stroboscope could not be used to determine impeller rotational speeds at setting lower than 4, and the amount of liquid in the stirrer cell could be entirely suspended causing the impeller to stop stirring at settings greater than 8. For the second stirring table used (IKA Labortechnik) the settings were adjusted between 2 and 8. The stirrer rotational speed N was calculated in RPM using the stroboscope and this was converted to an equivalent impeller tip speed by multiplying by the impeller radius which was 23.5 mm. Stirring speeds were in the range 0.07 to 0.31 m/s.

3.1.4 CaCO$_3$ and Bentonite Suspensions

Suspensions were made up by measuring out the appropriate mass of either CaCO$_3$ or bentonite and adding to ultra pure (RO) water to achieve the desired concentration. For bentonite suspensions, the pH was adjusted by addition of 0.5M NaOH or H$_2$SO$_4$ solutions. Suspensions were mixed for 24 hours before use to ensure complete suspension of bentonite. Filtration temperature was kept constant with the use of a water bath at the required temperature after pre-heating or cooling of the suspension.

3.2 Results and Discussion

3.2.1 Stirred Microfiltration of CaCO$_3$

Preliminary experiments were carried out using CaCO$_3$ in order to establish operating procedures for the cell. Glass fibre filters with pore size 1 μm were used for all CaCO$_3$ experiments. The parameters investigated were the initial CaCO$_3$ concentration, C_0; the applied transmembrane pressure, ΔP; the stirrer tip speed u; the membrane resistance R_m, and the temperature T which affects the filtrate viscosity μ. Filtration is faster at lower initial concentrations and higher pressures, and as such the feed is used up more quickly. This explains the different lengths of the curves in Figure 3-5 and Figure 3-6.

As mentioned previously, filtrate volume is measured at one second intervals; hence the flux is also calculated at one second intervals. This necessitates the use of continuous curves for data representation rather than individual symbols.
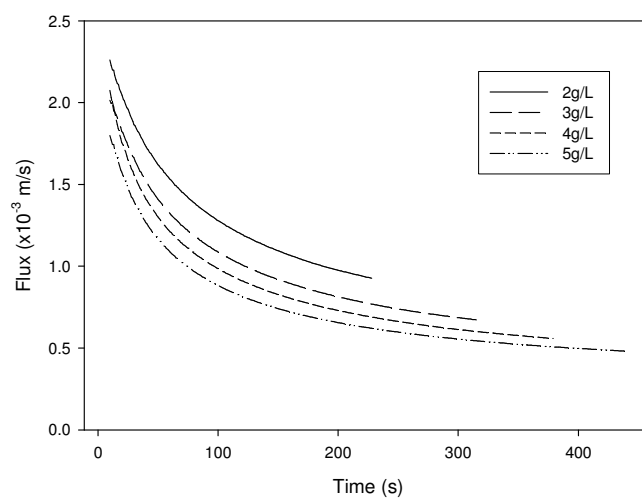
Figure 3-5: Effect of Increasing Initial CaCO$_3$ Concentration on Flux Decline

Filtration experiments were carried out between 2 and 5 g/L. The effect of increasing the concentration was to decrease the filtrate flux as can been seen from Figure 3-5, where the transmembrane pressure is 1 bar, stirrer tip speed is 0.08 m/s and the suspension temperature is 6 $^{\circ}$C.

It should be noted that the calculated values for fluxes at very low times is subject to a certain amount of experimental error. This is due to the fact that the experimenter must open the filtrate valve and start the timer simultaneously, a process that is currently performed by hand without the use of a control system. Error in the measurements at low filtration times is magnified by the differentiation of the filtrate mass in order to calculate the flux.

Although it would appear from Figure 3-5 that increasing suspension concentration decreases the initial filtrate flux, it would be expected that concentration would have no effect on initial fluxes and as such this phenomenon is attributed to the difficulties in accurately measuring the flux at low times.
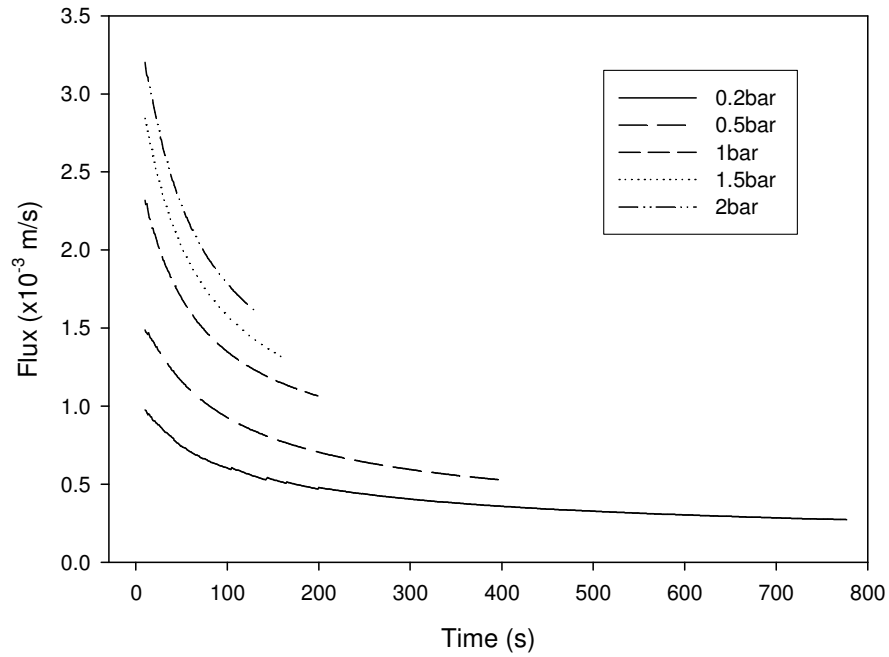
Figure 3-6: Effect of Increasing Pressure on Flux Decline

Figure 3-6 shows the effect of increasing transmembrane pressure is to increase the filtrate flux for an initial $CaCO_3$ concentration of 3g/L, stirrer tip speed 0.1 m/s and suspension temperature of 23 ^{o}C.

It is to be expected that the initial flux would increase with increased pressure, as the flux at low filtration times should be approximately equal to the flux through the clean membrane.
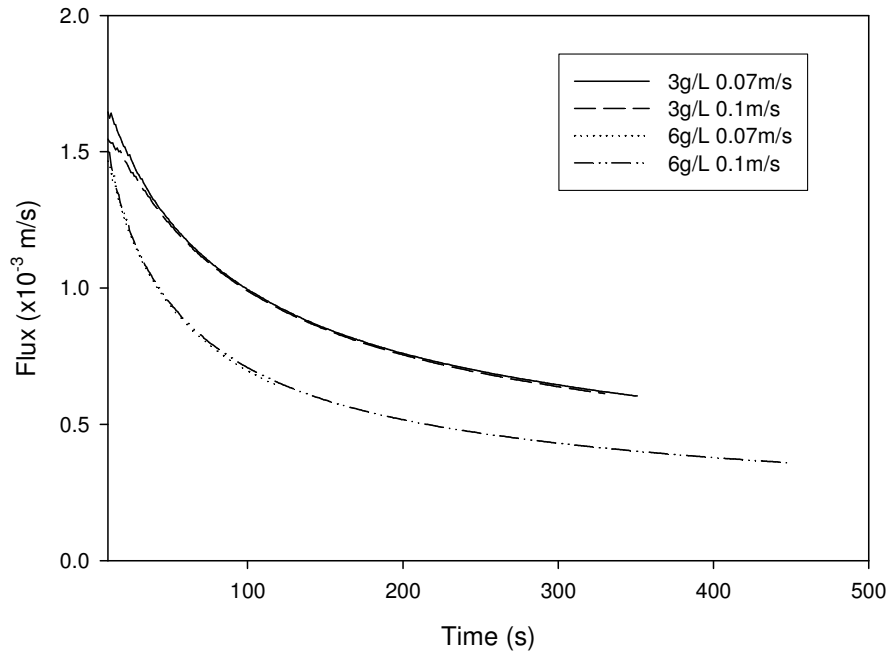
Figure 3-7: Effect of Increasing Stirrer Speed on Flux Decline

Figure 3-7 shows the effect of changing the stirrer speed at initial $CaCO_3$ concentrations of 3 g/L and 6 g/L, ΔP of 0.5bar and suspension temperature of 23 °C. It may be seen from Figure 3-7 that the stirrer speed has virtually no effect on the filtrate flux in the filtration of $CaCO_3$.

This phenomenon was also seen in the work of Kang & Choo (2003) where the fluxes were almost independent of stirring conditions. This may be due to the fact that the cake resistance is comparable to the membrane resistance, so that the dislodging of the cake layer at higher shear rates may not show any perceptible change of flux. Specific resistances for cakes of $CaCO_3$ determined using the stirred cell in dead-end mode (i.e. without the use of the stirrer) using the methods outlined in Chapter 2 are to the order of 10^{11} m/kg and, from this, cake resistances for the suspension concentrations achievable using this apparatus are calculated to be of the order of 10^{10} m^{-1} which is of the same order of magnitude as the

resistance to flow of the membrane itself. For example, supposing the cake resistance is 1.9×10^{10} m^{-1} and the membrane resistance is 2.9×10^{10} m^{-1}, and an increase in the shear causes a decrease in the cake resistance of 20 %. Thus the cake resistance is reduced to 1.5×10^{10} m^{-1} which corresponds to a drop in the total resistance to flow $(R_c + R_m)$ of just 6 %.

A fresh membrane is used for each run and the resistance to flow of each fresh membrane is measured as described in Section 3.1.2.1. Identical membranes are used for each run and the membrane resistance varies only slightly from membrane to membrane. As the resistance of a cake of $CaCO_3$ is comparable to that of the membranes used as discussed above, an increase in R_m has been shown to lead to a decrease in the filtrate flux as would be expected as it is the membrane resistance that is the limiting resistance in this case. This phenomenon may be observed in Figure 3-8 in which the $CaCO_3$ concentration is 3 g/L, ΔP is 0.5 bar, the stirrer speed is 0.1 m/s and the suspension temperature is 23 $^\circ$C. Two curves at the same membrane resistance are included to demonstrate the reproducibility of the flux decline experiments.
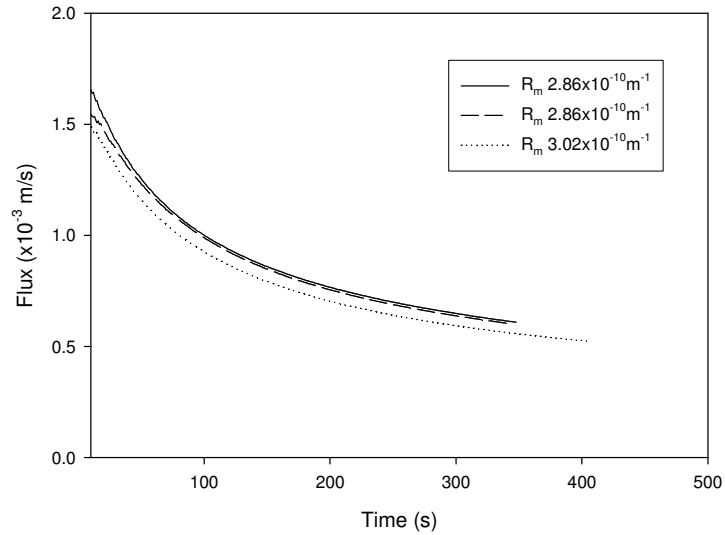
Figure 3-8: Effect of Increasing Membrane Resistance on Flux Decline

The filtrate in the case of filtration of $CaCO_3$ suspensions is pure water. An increase in suspension temperature decreases the filtrate viscosity. This leads to an increase in the filtrate flux as can be seen in Figure 3-9 where the initial $CaCO_3$ concentration C_0 is 3 g/L, the stirrer speed is 0.13 m/s and the transmembrane pressure ΔP is 1 bar.
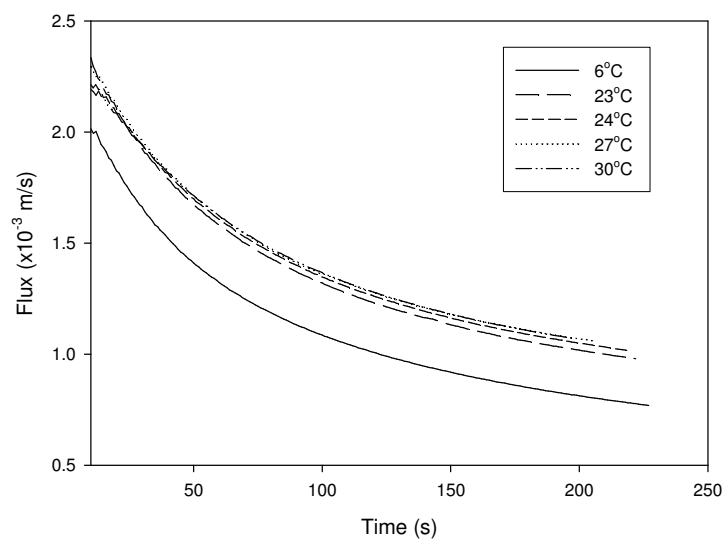
Figure 3-9: Effect of Increasing Temperature on Flux Decline

3.2.2   Stirred Microfiltration of Bentonite

Following on from preliminary investigations with the simpler Newtonian $CaCO_3$ suspensions, bentonite was used in order to collect data for a complex non-Newtonian system. Bentonite characteristics are discussed in detail in Chapter 1.

Three initial bentonite suspension concentrations were investigated, 0.5, 1 and 2 g/L. As expected, the effect of increasing the bentonite concentration was to decrease the quasi-steady state flux achieved at long filtration times. Little effect was apparent on the initial steep flux decline (Figure 3-10, where ΔP is 0.2 bar, u is 0.07 m/s, pH is 8 and filtrate temperature is 21 ^{o}C). It is worth noting however, that there is an extremely rapid decline in flux.
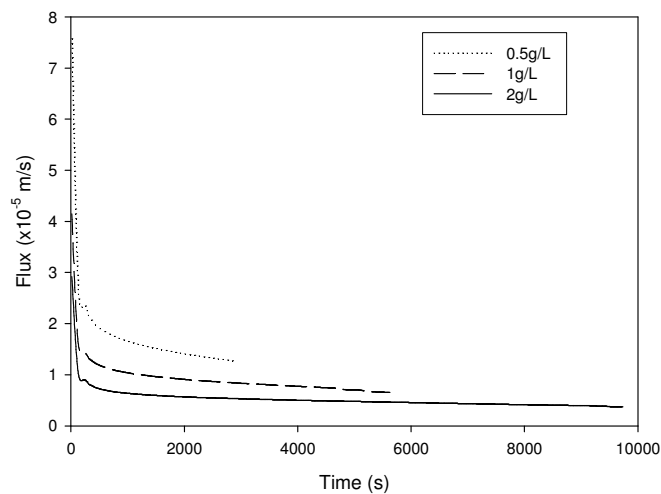
Figure 3-10: Effect of C_0 on Flux Decline for Stirred MF of Bentonite

Plotting the flux against the natural log of time enables the initial flux decline to be seen more clearly (Figure 3-11). As the flux reaches a quasi steady state rapidly, as mentioned previously, the effects of the operating parameters on the flux will be shown in this manner from this point forward.

95
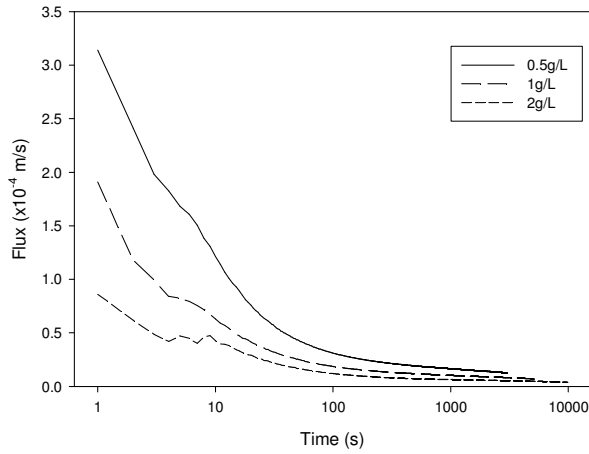
Figure 3-11: Semi-log Plot of the Effect of C_0 on Flux Decline

The effect of increasing the applied transmembrane pressure proves to be quite small as can be seen from Figure 3-12 (C_0 of 1 g/L, u of 0.07 m/s, pH of 8 and filtrate temperature of 21 ^{o}C), a phenomenon also observed by Ladva and Fordham (1989; 1992).
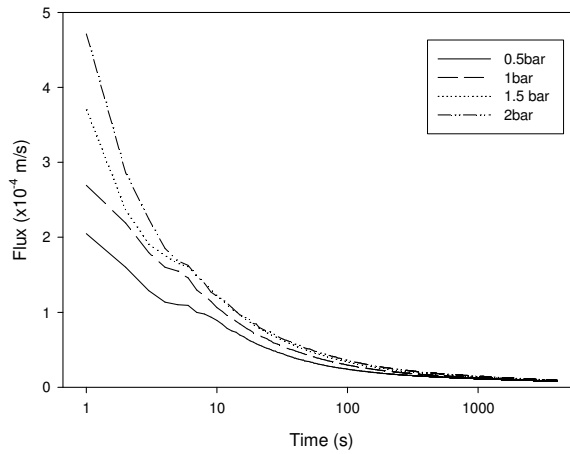
Figure 3-12: Semi-log Plot of the Effect of Pressure on Flux Decline

The stirring speed influences the shearing forces in the stirred cell and as such should affect the rheological properties of the suspension and also the deposition of bentonite on the membrane surface. It is clear from Figure 3-13 (C_0 of 1 g/L, ΔP of 0.5 bar, pH 8 and 22 ^{o}C), that an increase in the stirrer speed causes a corresponding increase in the filtrate flux.
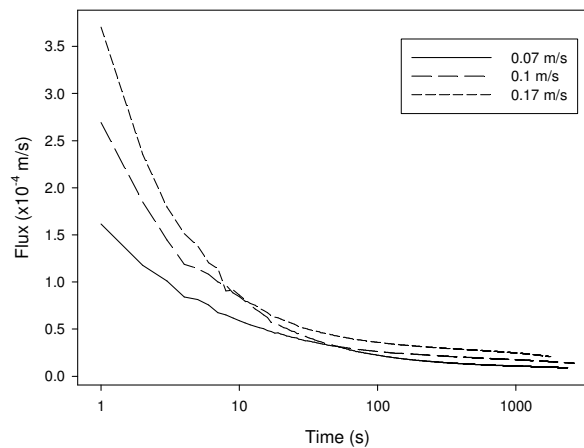
Figure 3-13: Semi-log Plot of the Effect of Stirrer Speed on Flux Decline

The resistance to flow provided by a cake of bentonite should be much higher than R_m which is of the order of 10^{10} m^{-1} as reported specific resistances for bentonite have been of the order of 10^{13} – 10^{14} m/kg. Based on a value of this magnitude, for the range of concentrations used in this study, the resistance of a cake of bentonite should be of the order of 10^{12} m^{-1}. It is clear from Figure 3-14 (C_0 of 2 g/L, ΔP of 0.2 bar, u of 0.07 m/s, pH 9 and 21 ^{o}C) that the membrane resistance has little or no effect on the flux time characteristics apart from at low filtration times when very little bentonite has deposited on the membrane, and that the flux versus time curves for specified operating parameters are very reproducible regardless of any variability in R_m.

97
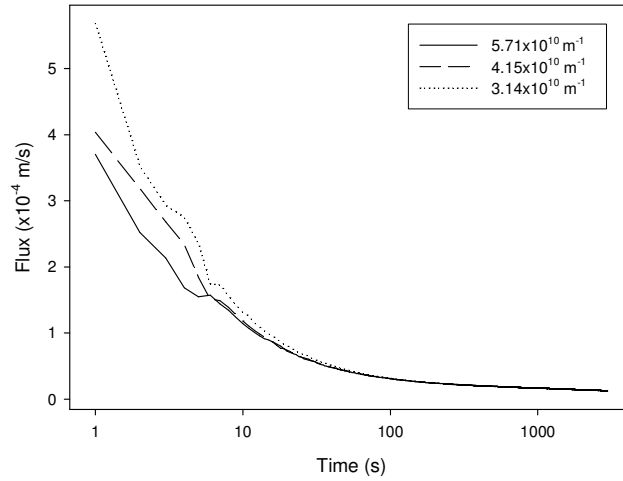
Figure 3-14: Semi-log Plot of the Effect of Membrane Resistance Flux Decline

It is clear from Figure 3-15 (C_0 of 1 g/L, ΔP of 0.5 bar, u of 0.07 m/s and 21 ^{o}C) that the filtration behaviour exhibits a complex dependence on the suspension pH, especially the period of initial flux decline where the more marked effect is observed.
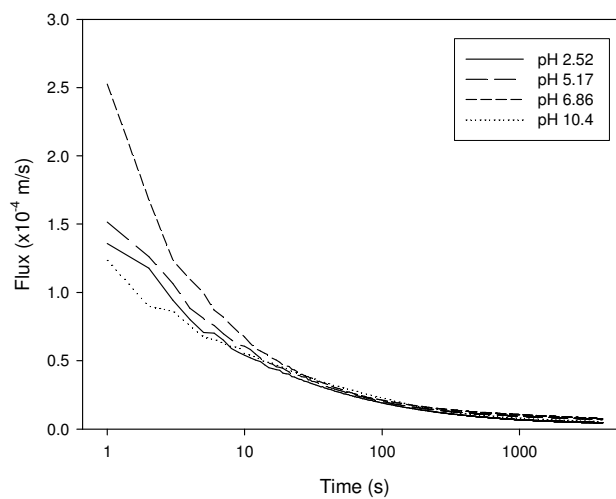
Figure 3-15: Semi-log Plot of the Effect of pH on Flux decline

Typical unadjusted pHs for the aqueous bentonite suspensions in this study are in the range 8 – 9. Lowering the suspension pH serves to decrease the filtrate flux. However, raising the pH to 10.4 decreases the filtrate flux to a value between that observed at pHs of 2.52 and 5.17. This may be explained in part by the complex dependency of the suspension rheology on the pH, as outlined in Chapter 1. Also, the specific resistance is well known to be a complex function of pH as outlined in Chapter 2.

3.2.3   Modelling of Filtration Data

In this section, the use of artificial neural networks in modelling the stirred cell filtration of calcium carbonate and bentonite suspensions is explored. Initially, the difficulties associated with using non-linear regression techniques for modelling such complex systems are demonstrated. For $CaCO_3$ and bentonite, experiments for each system are performed with various combinations of the operating parameters of interest and the flux-time curves generated for each experiment are the data used in modelling the system. $CaCO_3$ experiments are as presented previously in the Figures in Section 3.2.1 and the operating parameters for the Bentonite experiments are as outlined in Table 3-1. The experiments were selected in order to elucidate the effect of changing each parameter while holding all other parameters constant, for the range of operating parameters determined as important. The concentration range was chosen on the basis of the impeller – too high a concentration of bentonite and the stirrer was unable to turn. The pressure ranged up to 2 bar as low pressures are typically desirable industrially in order to retain economic viability (Mulder 1996; Keefe and Dubbin 2005). A relatively

small range of impeller tip speeds was attainable with this equipment, ranging

from 0.07 to 0.17 m/s.

Table 3-1: Bentonite Filtration Experiments

ΔP (bar)	C_0 (g/L)	u (m/s)	pH	T (^{o}C)	R_m ($\times 10^{10}$ m^{-1})
0.2	2.0	0.07	9.7	21	5.71
0.2	2.0	0.07	9.5	21	4.15
0.2	2.0	0.07	9.4	22	3.14
0.2	0.5	0.07	8.1	21	3.38
0.2	0.5	0.07	8.1	22	3.29
0.2	0.5	0.07	8.2	21	3.19
0.5	1.0	0.07	9.1	21	3.51
1.0	1.0	0.07	9.1	21	5.09
1.5	1.0	0.07	8.9	21	5.25
2.0	1.0	0.07	8.9	23	10.93
0.5	1.0	0.07	9.0	22	3.60
0.5	1.0	0.10	8.8	22	6.73
0.5	1.0	0.07	9.0	20	5.89
0.5	1.0	0.07	8.8	23	4.39
0.5	1.0	0.10	8.6	24	4.36
0.5	1.0	0.17	8.8	23	4.21
0.5	1.0	0.07	5.2	24	4.39
0.5	1.0	0.07	5.2	22	4.36
0.5	1.0	0.07	6.9	23	4.21
0.5	1.0	0.07	6.9	22	6.73
0.5	1.0	0.07	10.4	22	5.39
0.5	1.0	0.07	10.4	22	4.95
1.0	1.0	0.07	8.8	22	4.54
0.5	1.0	0.07	10.4	22	4.98
0.5	1.0	0.07	2.5	21	6.85
0.5	1.0	0.07	2.5	21	4.76
1.0	1.0	0.07	9.0	22	4.28
1.0	1.0	0.07	9.0	23	4.42
1.5	1.0	0.07	9.0	22	5.15
1.5	1.0	0.07	9.0	22	4.87
0.5	1.0	0.17	8.8	23	5.08

3.2.3.1 Non-Linear Regression

Non-linear regression is a traditionally used technique for quick correlation of

data, where regression equations may be used to gain some information about the

physical characteristics of a system. Preliminary analysis of data generated on stirred microfiltration of CaCO$_3$ indicated that the parameters that should be included in a model describing the process are the initial CaCO$_3$ concentration, C_0; the applied transmembrane pressure, ΔP; the membrane resistance R_m, and the temperature T, which affects the filtrate viscosity μ (Section 3.2.1). The stirrer speed is included as a parameter as this would be useful in the extension of this approach to systems in which the stirrer speed is important, and also to evaluate the models generated in terms of capturing the underlying physical phenomena of the system using the weight partitioning method described in Chapter 2. For Bentonite filtration, the parameters of interest are the initial bentonite concentration, C_0; the applied transmembrane pressure, ΔP; the membrane resistance R_m, the pH, the stirrer velocity u and the filtrate temperature (Section 3.2.2). The temperature was included as a parameter as the bentonite filtration experiments were performed at room temperature, (which varied between 20 ^{o}C and 24 ^{o}C depending on the day) and because bentonite filtration characteristics are found to be affected by the rheological properties of the fluid (Doneva *et al.* 1997).

Regression analysis examines the relationship of a dependent variable to specified independent variables. A regression equation used to fit data contains one or more unknown regression parameters (constants) which quantitatively link the dependent and independent variables and may be represented by

$$y = f(\theta) \hspace{4cm} \text{[3-3]}$$

where y is the dependent variable, and θ represents the variables upon which y depends. For a given system, the functional form for the regression model must be approximated and expressed as a mathematical function. Common equations used in biology and other fields of science include Gaussian distribution, sine wave, polynomial equations, exponential growth, Boltzmann sigmoid, power series and many others. Once a model is chosen that fits the data well, non-linear regression is used to give estimates of the regression equation parameters.

An initial value for each variable in the regression equation is estimated. The sum of squares of the vertical distances of the experimental data points from the points on the curve generated by employing the initial values of the regression parameters is calculated. This sum of squares is used as an indication of the goodness of fit of the curve to the data. The variables are adjusted to attempt to fit the curve to the data points. There are several algorithms that are commonly used for adjusting the variables, including Simulated Annealing, Gradient Descent, Conjugate Gradient, the Gauss-Newton Method and the Levenberg-Marqhardt Method (Krivý *et al.* 2000). The variables are adjusted many times according to the algorithm (each adjustment is called an iteration) until the sum of squares is virtually unaffected by adjustment of the variables.

Sigmaplot (© Systat Software Inc.) is used to perform non-linear regression on the experimental data in this research. The Sigmaplot Regression Wizard uses the Marquardt-Levenberg algorithm to find the coefficients (parameters) of the independent variable(s) that give the best fit between the equation and the data. This algorithm seeks the values of the parameters that minimize the sum of the squared differences between the values of the observed and predicted values of

the dependent variable. As previously mentioned, the process is iterative - the curve fitter begins with an initial guess at the parameters, checks to see how well the equation fits, then continues to make better guesses until the differences between the residual sum of squares no longer decreases significantly. This condition is known as convergence. With the SigmaPlot Regression Wizard, in order to speed up convergence, it is possible to specify values for the number of iterations; the step size, which is the limit of the initial change in parameter estimates between iterations; and the tolerance limits, being the absolute value of the difference between the square root of the sum of squares of the residuals from one iteration to the next.

In order to generate a regression model for a system, a functional form for the filtration characteristics must be approximated. A simple function that approximates flux decline data is the power law expression relating flux and time:

$$J = At^{-n} \qquad\qquad\qquad [3\text{-}4]$$

where J is the filtrate flux, t is the filtration time and A and n are constants. A log-log plot of flux decline data should give an indication as to whether this model may be used to approximate filtration data for the $CaCO_3$ system.

It should be noted that this type of analysis is questionable when the functional relationship used for the system does not have its basis in the physical characteristics of the system.
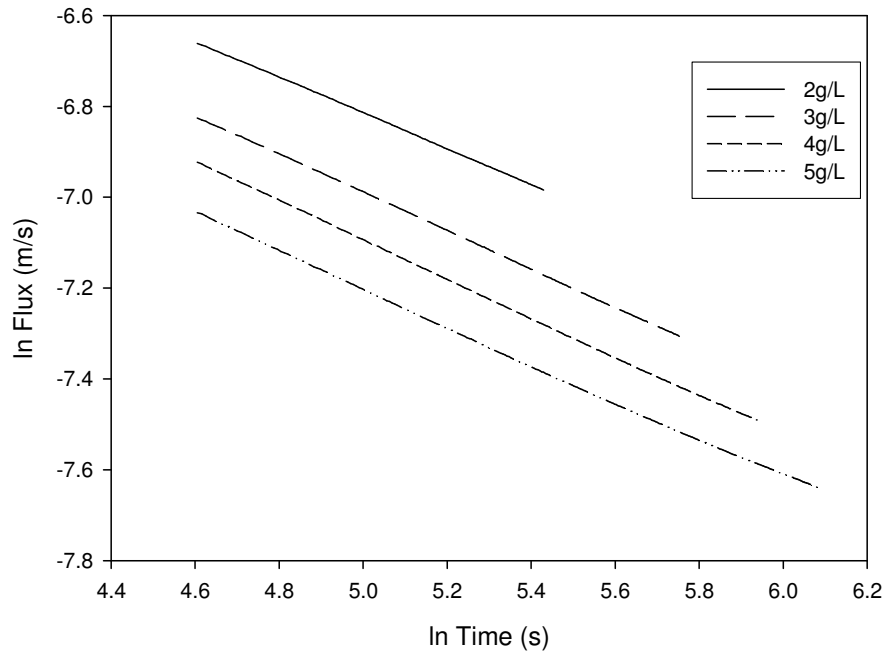
Figure 3-16: Log-log plot of flux decline for CaCO$_3$

It is clear from Figure 3-16 (Operating Conditions as Figure 3-5) that log-log plots of flux versus time are reasonably linear after initial low filtration times, and as such a power law approach may be justified. This type of expression is found to fit the flux versus time data well for CaCO$_3$, with R^2 values achieved for a power law fit for the data in Figure 3-6 ranging upwards from 0.97.

For the bentonite data, the power law fit does not have as good agreement as found for CaCO$_3$ as can be seen from Figure 3-17 (Operating Parameters as Figure 3-15), where a log-log plot of the flux versus time data is clearly non-linear.
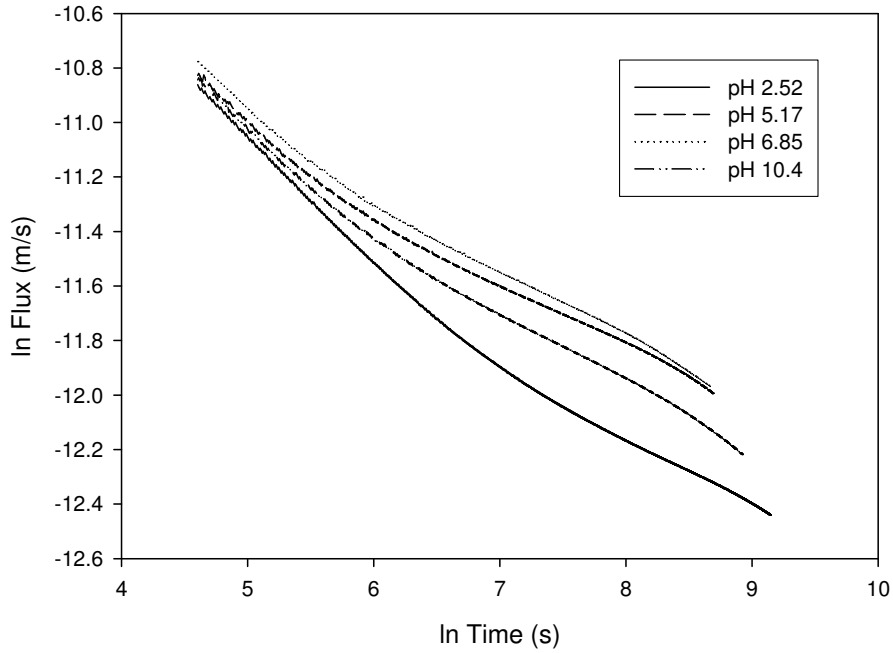
Figure 3-17: Log-Log Plot of Flux Decline for Bentonite

It is clear from this non-linearity that a power law fit is unsuitable for use in describing bentonite filtration data. It would be possible to explore the use of more complicated functions involving more than two empirical parameters, all of which might be related to the system parameters. However, such an approach would be time consuming and likely to lead to unwieldy correlations.

3.2.3.1.1 Regression Equations

A regression equation must be designed to relate the regression constants to the operating parameters. For the sake of simplicity, the constants in Equation 3-4 are assumed to be functions of the operating parameters as follows:

$$A = a\Delta P^b C_0^c u^d \mu^e R_m^f \qquad\qquad [3\text{-}5]$$

$$n = g\Delta P^h C_0^i u^j \mu^k R_m^l \qquad\qquad [3\text{-}6]$$

As outlined previously, this type of regression analysis would be suitable only for the $CaCO_3$ filtration data, due to the non-linearity of the log-log plots for the bentonite data. This difficulty in using non-linear regression techniques justifies the use of artificial neural networks, especially when attempting to model complex functions such as pH and ionic strength effects.

The constants in the regression equations were evaluated using non-linear regression in Sigmaplot 8.0 for Windows as described in Chapter 1. For each run, a power law model was applied to the flux-time data and regression analysis was used to find a value of A and n. Regression analysis was then performed on the values of A and n corresponding to the experimental conditions, to find the constants in Equations 3-5 and 3-6. Tolerance limits for convergence were set at 1×10^{-4} in all cases. When using Sigmaplot, the fit of regressions is shown using R^2 values and the norm (the sum of the squares of the residuals). R^2 values were between 0.8 and 1 in all cases, and norms to the order of 10^{-5} were achieved, indicating a successful convergence to a solution for the values of A and n.

3.2.3.1.2 Non-Linear Regression Model

The constants found for $CaCO_3$ are outlined in Table 3-2. It is important to note that these are dimensional constants, with units particular to the analysis used in this study. These constants would only be suitable for use with the correct units for the operating parameters and flux.

Table 3-2: Stirred MF of CaCO3 Regression Constants

Constant	Value	Constant	Value
a	3.2×10^{-7}	g	3.2×10^{-7}
b	0.23	h	-0.43
c	-0.02	i	0.22
d	0.41	j	0.44
e	0.47	k	1.39
f	0.44	l	1.18

Thus the regression equation to describe stirred microfiltration of $CaCO_3$ is

$$J = \left(3.2 \times 10^{-7}\, \Delta P^{0.24} C_0^{-0.02} u^{0.41} \mu^{0.47} R_m^{0.44}\right) \times t^{-\left(3.2 \times 10^{-7}\, \Delta P^{-0.43} C_0^{0.22} u^{0.44} \mu^{1.39} R_m^{1.18}\right)} \qquad [3\text{-}7]$$

The power law regression model for $CaCO_3$ is seen in Figure 3-18 to fit the data quite well, where the linear regression equation for the correlation is y = 0.96x + 5×10^{-5}, with an R^2 value of 0.97. Confidence intervals for the slope and the intercept are found to be [0.96, 0.97] and [4.07×10^{-5}, 5.26×10^{-5}] respectively. The power law model does not quite fit the data at low filtration times. The low filtration times correspond with the highest fluxes on the plot, i.e. to the right hand side. It is to be expected that a simple power law model would fit filtration data badly at low times as it predicts that the flux goes to infinity at t=0. This highlights a drawback of the non-linear regression technique, in that a functional relationship for the system must be approximated.
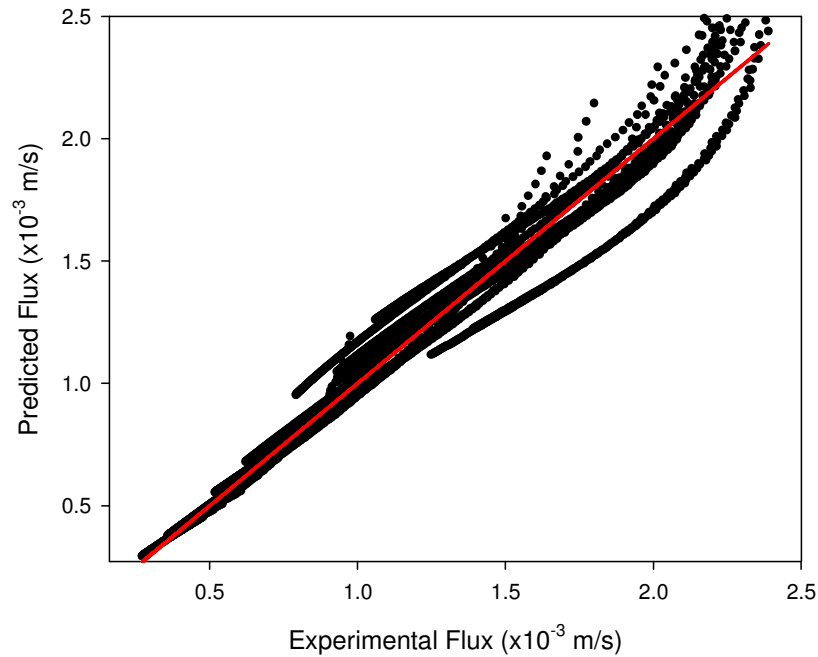
Figure 3-18: Fit of Power Law Model to CaCO$_3$ Filtration Data

Each experimental run is plotted in Figure 3-18, and it is possible to identify specific experimental runs from this Figure. In particular, a single experimental run lies below and to the right of the y=x line. It is clear that this particular experiment is not correlated well using the power law approach.

It is interesting to note that regression constants *a* and *g* are equal. Also the exponent for C_0 for the multiplier of the power law model is close to zero, implying an insignificant effect.

It is probably that this correlation could be improved by the use of other regression functions that would fit the system better. A technique known as symbolic regression may be used to generate functions to fit experimental data using evolutionary algorithms. This technique focuses on the fit of a functional set, consisting of user defined mathematical relationships, to a terminal set,

consisting of the constants and parameters of the problem (Cai *et al.* 2006). More simply, symbolic regression may be used to search a database of all possible regression equations to find the equation that fits the dataset, a process which would be exhaustive if attempted by hand. This may be an area for future work. Another approach that might simplify the conventional regression approach is dimensional analysis. Foley (2006) has shown that a dimensionless equation of the form $\dfrac{J}{u} = f\left(\dfrac{\Delta P}{cu^2}, \dfrac{\Delta P}{\mu u R_m}\right)$ fits steady state flux data for yeast suspensions with moderate accuracy. However, extension of this approach to time-dependent problems as we have here, would lead to an additional dimensionless group (involving time) that would still leave a challenging regression problem.

Although this approach generates a reasonable correlation for $CaCO_3$ filtration data after initial filtration times, it is questionable whether using this approach is scientifically sound and is included here simply as a comparison between traditional non-linear regression and the application of ANNs, which are regarded by many as simply a complex regression.

3.2.3.2   Artificial Neural Networks

The aim of this section is to design an ANN that can be used to model the $CaCO_3$ and bentonite filtration data and to develop a network for the bentonite data that can be used as a predictive tool. For modelling purposes alone, all of the available data is used in training the network, and for modelling and predictive purposes the data is divided into training, validation and testing sets as described in Chapter 2.

3.2.3.2.1 Calcium Carbonate

As outlined previously (Chapter 2) Matlab software was used in the development of the ANN for modelling of $CaCO_3$ data. The network inputs and output are normalised between 0 and 1 prior to being used with the network. The inputs to the network for $CaCO_3$ are ΔP, C_0, u, μ, R_m and t, the time, and the network output is the flux at each time step. All of the time data was used, leading to an input matrix with 26436 elements, and an output vector with 4406 elements. It is desirable to use the simplest network possible when using an ANN as a modelling tool as this gives the fastest processing time and makes the underlying model as simple as possible. The appropriate network architecture is found using a trial and error procedure as outlined in Chapter 2.

For the $CaCO_3$ system, it is found that a 6-6-1 backpropagation network using a sigmoidal transfer function models the system with an excellent degree of accuracy (Figure 3-19, where the red line indicates the y=x line)
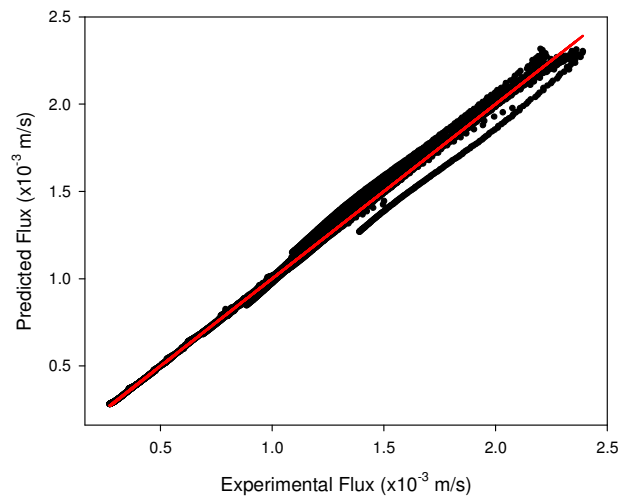
Figure 3-19: Fit of 6-6-1 ANN to CaCO$_3$ Filtration Data

110

This network architecture, which has the same number of neurons in the hidden layer as there are inputs to the system, is the simplest possible network architecture with the lowest number of neurons. This highlights the advantages of using an ANN rather than attempting to find a suitable regression function.

The regression equation for the data is $y = 0.995x + 5 \times 10^{-6}$, with an R^2 value of 0.99. 95 % confidence intervals for the slope and intercept are [0.993, 0.997] and [2.94×10^{-6}, 7.11×10^{-6}] respectively.

3.2.3.2.2 Bentonite

For the bentonite data, Trajan neural network software (StatSoft) is used. While Matlab is an excellent tool for design of ANNs (and provides an in-depth understanding of the functionality of ANNs due to the necessity for the user to construct the code required for training, validation and testing of a network) Trajan software proves to be more user friendly and eliminates the need for data pre-processing.

As mentioned previously, bentonite filtration characteristics have proved to be more complex than that of $CaCO_3$. This may be due to the non-Newtonian behaviour and the fact that more operating parameters are examined, particularly complex pH effects. Another point to note is that the filtration times with Bentonite are much longer than those for $CaCO_3$. This leads to longer processing times and it is much more difficult to achieve an accurate regression for an input matrix with 180,000 elements (this number is obtained from the number of experiments multiplied by the number of time points) – the larger the data set and the more complex the network, the longer the processing times and the computational power required. Using a laptop computer (Intel ® Core™ 2 CPU

T5500, 1.66GHz, 512MB of RAM), processing times were close to 30 minutes with the simplest possible network. An advantage of using ANNS for such a complex system is that the architecture of the ANN can be made more complicated in order to reflect the complexity of the data - the number of hidden layers can be increased, and the number of neurons in each hidden layer can be increased, until such a time as the network gives an acceptable approximation to the system behaviour. However, a disadvantage associated with this is that the more complex the network, the longer the processing time and the more memory required for processing the data. This proves to be a problem when dealing with such a large dataset.

3.2.3.3   Novel ANN Design for Modelling Microfiltration Dynamics

In this study, a novel approach was developed in which the number of data points was reduced by examining only particular time points along the flux-time curve, and, more importantly, the time was not included explicitly in the network. Although simply reduced the number of data points would be effective in reducing the amount of memory required for processing of the neural net, a more computationally efficient method is proposed which also allows easy access to the evolution of the weights along the time series. Previous work on time-series filtration data has always included time either as an input to the network, or a recurrent network has been used in which the output of the previous time point is used as an input to the next time point.

Table 3-3 gives a summary of previous work on application of ANNs to time series filtration data. The amount of published work on modelling of time series data using ANNs is quite small, however, it appears that time has been included

112

explicitly in all cases. The application of ANNs to time series data occurs across the spectrum of filtration processes, with CFMF representing crossflow microfiltration, CFUF crossflow ultrafiltration and CFNF nanofiltration, and where BP represents a standard backpropagation network and RB represents a radial basis ANN.

Table 3-3: Application of ANNs to Time Series Filtration

Study	Type of Filtration	Time Use
Aydiner *et al.* (2005)	CFMF	time as input to BP network
Bowen *et al.* (1998a)	CFUF	time as input to BP network
Bowen *et al.* (1998b)	CFUF	time as input to BP network
Cabassud *et al.* (2002)	CFUF	time as input to BP network
Chellam (2005)	CFMF	time as input to BP network
Chen and Kim (2006)	CFMF	time as input to BP and RB networks
Cheng *et al.* (2008)	CFMF	time as input to BP and RB networks
Curcio *et al* (2006)	CFUF	time as input to BP network
Curcio *et al.* (2005)	CFUF	time as input to BP network
da Silva and Flauzino (2007)	CFMF	time as input to BP network
Delgrange-Vincent *et al.* (2000)	CFUF	2 Recurrent Networks
Dornier *et al.* (1995a)	CFMF	time as input to BP network
Dornier *et al.* (1995b)	CFMF	time as input to BP network
Dornier *et al.* (1998)	CFMF	time as input to Simplex network
Hamachi *et al.* (1999)	CFMF	Recurrent Network
Piron *et al.* (1997)	CFMF	Recurrent Network
Rai *et al.* (2005)	Stirred UF	time as input to BP network
Razavi *et al.* (2003a)	CFUF	time as input to BP network
Razavi *et al.* (2003b)	CFUF	time as input to BP network
Razavi *et al.* (2004)	CFUF	time as input to BP network
Sahoo and Ray (2006)	CFMF	time as input to BP and RB networks
Shetty and Chellam (2003)	CFNF	time as input to BP network
Teodisiu *et al.* (2000)	CFUF	time as input to BP network

With time included explicitly, the number of outputs from the network for each experimental run corresponds to the number of time points taken from each run.

In order to reduce processing times and network complexity, a novel approach is developed here in which time is not included explicitly in the network. The network architecture used and the difference between the previous architectures and this novel configuration may be seen in Figure 3-20.
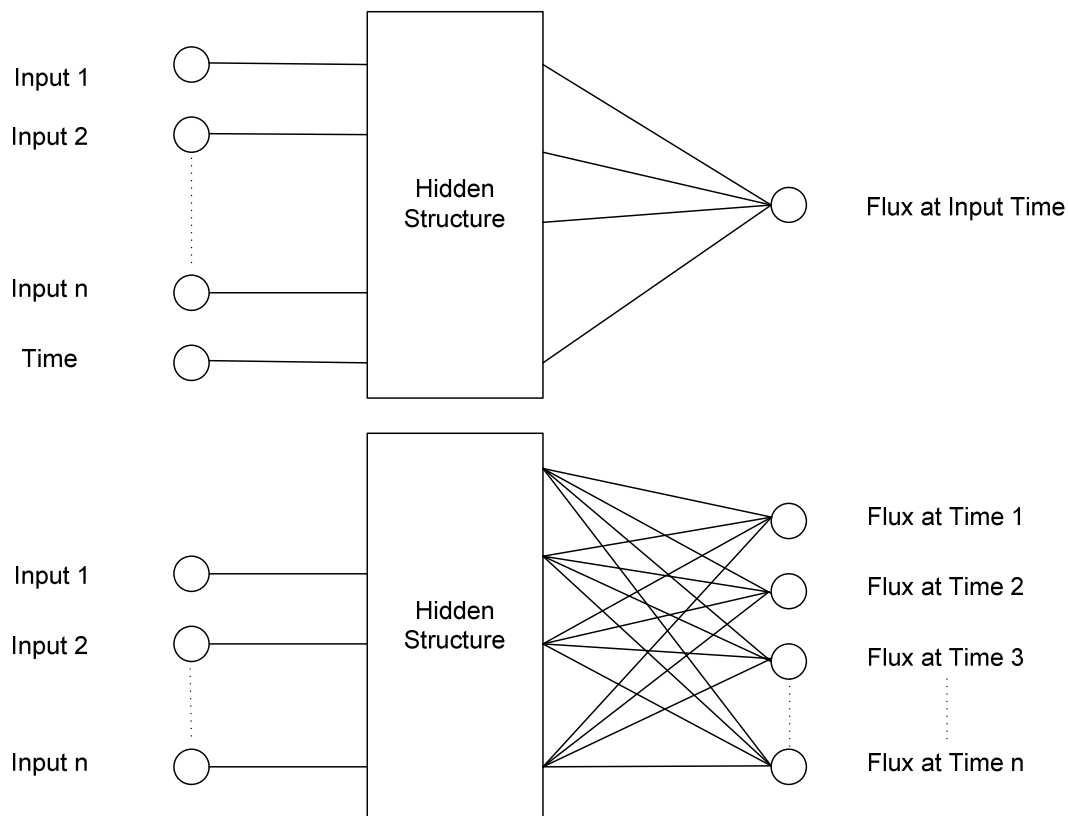
Figure 3-20: Comparison of Network Architectures for Time Series Data

The first architecture is that used in previous work on modelling of time series data and the second is the approach developed in this work.

As mentioned previously, the number of data points required for a network designed using time as an input will be as many times greater than the number of data points required for the architecture developed here as the number of time points used.

For these experiments, the time series data is found to be regular over the course of the filtration experiments in all cases. As such, it is justified to take a selection of data points along the flux – time curve to accurately represent the data. The use of fewer data points should not lead to any loss of information about the relationship between flux and time as no apparent anomalies occur across the time scale used to date. Data points here are chosen arbitrarily at 10 seconds, 50 seconds, 100 seconds and thereafter every 100 seconds until 1300 seconds, a total of 15 time points. Successive time points in smaller increments were chosen at low times as the shape of the flux-time curve dictates that greater changes occur at low times, with the significant initial flux decline, and as such extra data points at low times are necessary to represent the characteristics. Accurate measurement of fluxes at very low filtration times proves to be susceptible to experimental error, and as such the first time point included was at 10 seconds.

The flux at each of the chosen time points forms the output matrix for the network. This means that rather than 1 output at each time point (the technique employed in previous work) there are 15 outputs for each experimental run. For a network with 6 operating parameters and 31 experimental runs as in this case, taking 15 time points over the course of a run, the previously used approach requires an input matrix with 3255 elements, and an output vector with 465 elements. With the approach developed here, the input matrix consists of 186 elements, and the output matrix consists of 465 elements.

The differences in the input and output matrices are represented in Table 3-4. For the previous approaches used in modelling this dataset, the input matrix is a 465 x

7 matrix, whereas in the novel approach developed in this work, the input matrix

is a 31 x 6 matrix.

**Table 3-4: Input and Output Matrices for Modelling of Dynamic Filtration using ANNs –
Previous Approaches**

	Input Matrix		Output Matrix
	$\leftarrow$ *# Operating Parameters + 1* $\rightarrow$		$\leftarrow 1 \rightarrow$
	Operating Parameters Run 1	Time 1	Flux $_{1,1}$
$\uparrow$	Operating Parameters Run 1	Time 2	Flux $_{1,2}$
# Experiments(n)	$\vdots$	$\vdots$	$\vdots$
x	Operating Parameters Run 1	Time m	Flux $_{1,m}$
# Time Points (m)	$\vdots$	$\vdots$	$\vdots$
$\downarrow$			
	Operating Parameters Run n	Time 1	Flux $_{n,1}$
	$\vdots$	$\vdots$	$\vdots$
	Operating Parameters Run n	Time m	Flux $_{n,m}$

**Table 3-5: Input and Output Matrices for Modelling of Dynamic Filtration using ANNs –
Current Approach**

	Input Matrix	Output Matrix
	$\leftarrow$ *# Operating Parameters* $\rightarrow$	$\leftarrow$ *# Time Points (m)* $\rightarrow$
	Operating Parameters 1	Flux $_{1,1}$, Flux $_{1,2}$…Flux $_{1,m}$
$\uparrow$	Operating Parameters 2	Flux $_{2,1}$, Flux $_{2,2}$…Flux $_{2,m}$
# Experiments(n)	$\vdots$	$\vdots$
$\downarrow$	Operating Parameters n	Flux $_{n,1}$, Flux $_{n,2}$…Flux $_{n,m}$

This approach leads to shorter processing times and greater flexibility with

regards to increasing the network complexity. Another advantage of this approach

is that the evolution of the relative contribution of the input parameters to the flux

along the time series can be investigated, as will be discussed in Section 3.2.3.3.1.

For prediction purposes, the data is divided into three datasets for training, validation and testing as described in Chapter 2. The division consists of 10 runs for training, 10 for validation and 11 for testing, dividing the available data almost evenly but retaining the larger proportion of unseen data for testing purposes. Division of available data is performed randomly by using a function in Trajan that allows the user to input the number of experiments required in each set and then shuffles the data, assigning experiments to training validation and testing randomly. Random selection of training data for ANNs is desirable as it requires no *a priori* knowledge of the system. The division of data is summarised in Table 3-6. The size of the training set necessary for setting the network weights may be found by increasing the size of the dataset by a trial and error procedure until the prediction of the test data is sufficiently accurate. 30 % of the data for training was found to be sufficient in this case.

Table 3-6: Division of Data for Bentonite Network

Run	ΔP (bar)	C_0 (g/L)	u (m/s)	pH	T (^{o}C)	R_m ($\times 10^{10}$ m^{-1})
Training						
1	0.2	2.0	0.04	9.7	21	5.71
4	0.2	0.5	0.04	8.1	21	3.38
12	0.5	1.0	0.08	8.8	22	6.73
13	0.5	1.0	0.04	9.0	20	5.89
17	0.5	1.0	0.04	5.2	24	4.39
19	0.5	1.0	0.04	6.9	23	4.21
20	0.5	1.0	0.04	6.9	22	6.73
25	0.5	1.0	0.04	2.5	21	6.85
27	1.0	1.0	0.04	9.0	22	4.28
31	0.5	1.0	0.17	8.8	23	5.08
Validation						
6	0.2	0.5	0.04	8.1	21	3.19
8	1.0	1.0	0.04	9.1	21	5.09
9	1.5	1.0	0.04	8.9	21	5.25
14	0.5	1.0	0.04	8.8	23	4.39
15	0.5	1.0	0.08	8.6	24	4.36
16	0.5	1.0	0.17	8.8	23	4.21
18	0.5	1.0	0.04	5.2	22	4.36
21	0.5	1.0	0.04	10.4	22	5.39
22	0.5	1.0	0.04	10.4	22	4.95
26	0.5	1.0	0.04	2.5	21	4.76
Test						
2	0.2	2.0	0.04	9.5	21	4.15
3	0.2	2.0	0.04	9.4	22	3.14
5	0.2	0.5	0.04	8.1	22	3.29
7	0.5	1.0	0.04	9.1	21	3.51
10	2.0	1.0	0.04	8.9	23	1.09
11	0.5	1.0	0.04	9.0	22	3.60
23	1.0	1.0	0.04	8.8	22	4.54
24	0.5	1.0	0.04	10.4	22	4.98
28	1.0	1.0	0.04	9.0	23	4.42
29	1.5	1.0	0.04	9.0	22	5.15
30	1.5	1.0	0.04	9.0	22	4.87

A network architecture consisting of 1 hidden layer with 8 hidden neurons using a sigmoidal transfer function was found to be the most suitable configuration for this system using a trial and error method as outlined in Chapter 2, where the most

suitable architecture is the one which gives the lowest MSE for the dataset (Figure 3-21).
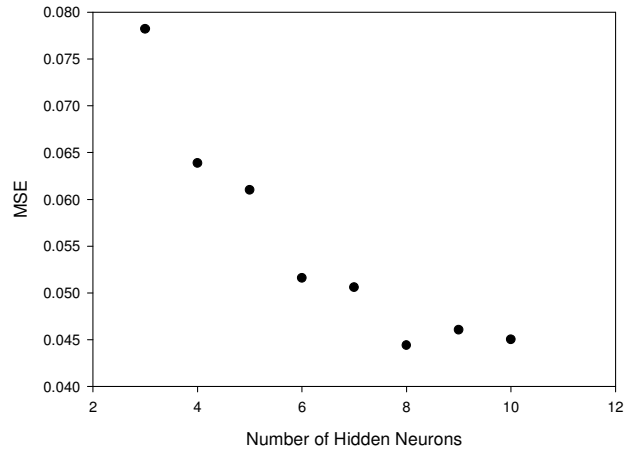
Figure 3-21: Optimisation of Bentonite Network

Comparison of the network predictions and targets for the training data set is presented in Figure 3-22, where the solid line indicates the y=x line. The regression equation for the data is $y = x - 0.03$ with an R^2 value of 0.99 and the 95 % confidence intervals for the intercept and slope are [-0.07, -0.001] and [0.99, 1.01].
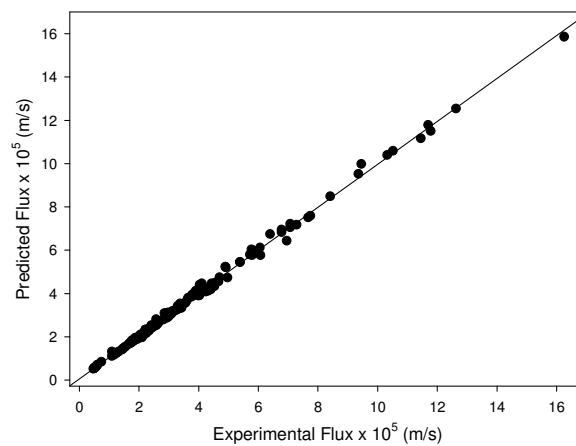
Figure 3-22: Fit of Network to Bentonite Training Dataset

As discussed in Chapter 2, the validation dataset is used in training the network in conjunction with the training dataset, serving as a method for the prevention of overtraining. The correlation of the validation dataset is presented in Figure 3-23. The regression equation for the validation dataset is $y = 1.08x - 0.08$ with an R^2 value of 0.92. The 95 % confidence intervals for the intercept and slope are [-0.33, 0.17] and [1.02, 1.12].
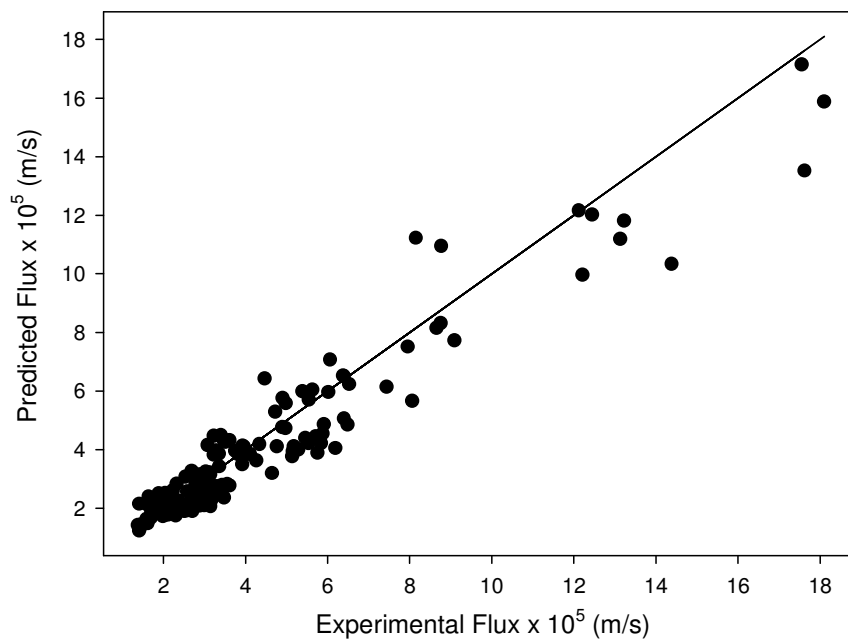
Figure 3-23: Fit of Network to Bentonite Validation Dataset

In this case the test dataset is made larger than either the training or validation datasets as it is desirable to use the smallest possible dataset in setting up the network, especially industrially where it may not be possible for economical reasons to generate a large databank prior to validation of a process (Maier and Dandy 2000).

The test data is made up of experimental data previously unseen by the network and it is this dataset that tests the prediction capabilities of the network. In this case the network predictions are correlated with the target values with a regression equation of y = 0.93x – 0.1105 with an R^2 value of 0.92 (Figure 3-24, where the solid line indicates the y=x line). 95 % confidence intervals for the slope and intercept are [0.88, 0.97] and [-0.3, 0.1] respectively.
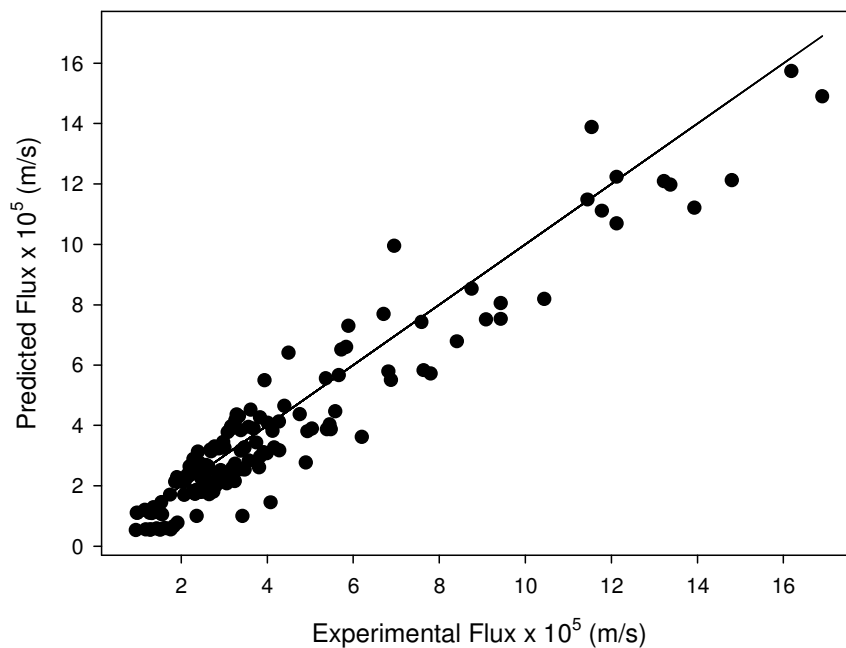
Figure 3-24: Fit of Network to Bentonite Test Dataset

3.2.3.3.1 Evaluating the relative contributions of inputs

It has been argued that the use of ANNs is akin to a 'black box' model, incapable of giving any insight into the physical characteristics of a system (Piron *et al.* 1997; Olden and Jackson 2002). However, it was shown in Chapter 2 that it is possible to give a qualitative insight into the characteristics of a dead-end microfiltration system using a weight partitioning method first proposed by Garson (1991) and later modified by Goh (1994). This approach may be used to

elucidate the relative contributions of the input parameters on the outputs from the network and has been used for transient crossflow filtration of polydispersed suspensions (Chellam 2005). For dynamic filtration, Chellam (2005) report a 20-40 % contribution of time to the fouling characteristics. Aydiner *et al.* (2005) also discussed the percentage contributions of the input variables to the flux for time series data (it was not stated how these contributions were calculated) reporting a 40-50 % effect of time, 15-20 % effect of concentration and of pressure and 4 % effect of membrane type. However, this analysis gives very little insight into the actual characteristics of the system – it is reasonable to assume that time will have a large effect on the flux as time series data is being analysed. Thus an investigation of this type on a network that uses time explicitly as an input cannot offer much significant benefit.

An approach used in Chapter 2 is further developed here to elucidate the relative contribution of the operating parameters along the time series using the novel network architecture proposed previously. The Garson Equation is used to evaluate the contribution to the flux of each input parameter at each point along the time series. Previous work using this approach, discussed in Chapter 1, focus on networks having only one output (O_j being the weight from each hidden neuron to the single output). However, in this case there are many outputs along the time series, as described in Section 3.2.3.3. Thus, it is possible to quantify the importance of the inputs at each time point. This should give a better insight into the physical characteristics of the system changing with time. Network weights are easily accessed using Trajan software using an option to display the weight distributions for each layer.

Using this approach it is shown that the relative contributions of applied pressure and initial concentration are approximately constant along the filtration runs with concentration accounting for approximately 35 % and pressure accounting for approximately 7 %. The slopes of plots of percentage contribution of applied pressure and initial concentration against time were insignificantly different from zero at the 95 % confidence level and thus it can be concluded that they are essentially constant (Figure 3-25).
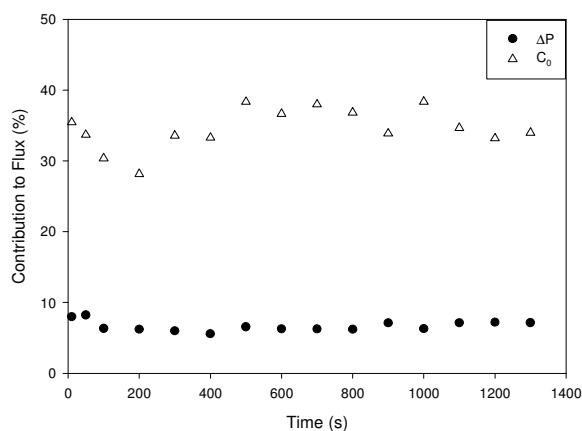
Figure 3-25 Contributions of Pressure and Initial Concentration along Time Series

The size of the importance of these parameters is reflected in the experimental investigations outlined in Section 3.2.2, where the initial concentration was seen to have a large effect on the flux-time curve, whereas the applied pressure was seen to have very little effect.

In the case of the membrane resistance and stirrer speed, the contribution of R_m is found to decrease overall while the contribution of the stirrer speed is found to increase along the flux-time curve (Figure 3-26).
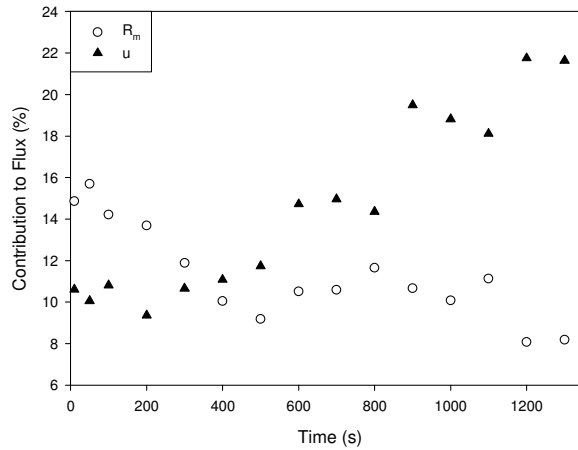
Figure 3-26: Contribution of Membrane Resistance and Stirring Speed along Time Series

This result would seem to be sensible given the mechanisms of stirred microfiltration. In the case of R_m, at the beginning of filtration there are few particles deposited on the membrane surface and so the membrane resistance governs filtrate flux, whereas towards the end of filtration the membrane is essentially covered by particles and ceases to be the limiting resistance and becomes less important. Cake resistance dominates at long times and is a function of the stirring speed - thus the effect of u should be strongest at long times.
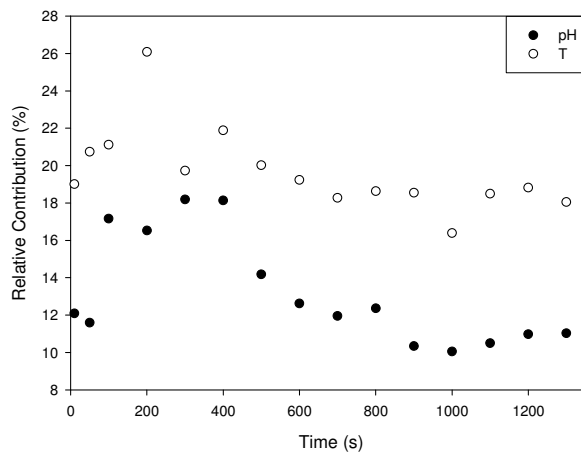
Figure 3-27: Contribution of pH and Temperature along Time Series

There is no constant increase or decrease in the effects of pH and temperature along the course of the filtration run, however it appears that both parameters decrease in relative importance with time, after an initial increase.

The case of stirred microfiltration is a relatively simple system however it is clear that this approach could be extended for use with systems in which the mechanisms would not be as easily understood.

3.3   Conclusions and Further Work

Correlation and prediction of complex non-Newtonian dynamic filtration data is shown to be possible using simple artificial neural network techniques incorporating a novel approach to modelling time series filtration data of Bentonite, a clay that forms a non-Newtonian aqueous suspension. The approach outlined in this study eliminates the use of time as an explicit input to the network, resulting in a massive reduction in the size of the input matrix to the network in comparison to previously published work on application of ANNs to dynamic filtration data (Table 3-3). Correspondingly, computation times are reduced and the network complexity may be increased as much as is necessary in order to accurately capture the complexities of the system in question. This network architecture has many outputs consisting of the time series data for the system of interest, rather than having one output from the network corresponding to many time series inputs. Using a weight partitioning method (Garson 1991), qualitative insight into the physical characteristics and the time dependence of the system mechanics may be assessed. The relative importance of input parameters along the time series is calculated and it is shown for the case of stirred microfiltration of bentonite, that the membrane resistance is very important at the start of filtration

becoming less important as filtration continues, whereas the stirrer speed is shown to be less important at the start of filtration (when the membrane is the dominating resistance to filtrate flux) and becomes more important as more particles are deposited on the membrane surface forming a cake. It is proposed that this approach could be used for systems which are little understood in order to gain some insight into the characteristics - gaining information that would be useful, for example, in the design of pilot plant studies, without the need to perform a full spectrum of experiments investigating system behaviour.

While the stirred cell set-up is a simple lab scale system for the collection of dynamic batch filtration data, the next logical step is extension of the method developed in this chapter to a system more similar to established industrial processes. Thus, Chapter 4 will focus on batch crossflow microfiltration.

In order to elucidate more information about the specific resistance of cakes formed in a stirred cell, the specific resistance will be evaluated from the end points of each filtration run. At this stage, the cell and reservoir have been emptied and the cake mass is easily quantifiable. Assuming no membrane fouling, the specific resistance may be easily calculated. It is proposed to determine whether the specific resistance values are dependent on stirrer speed. This data may prove useful in providing insight into the underlying physics of the system, and may give some idea as the effect of crossflow velocity in CFMF especially since so many difficulties surround the measurement of specific resistance in crossflow microfiltration (McCarthy 2001). This will be further discussed in Chapter 5.

As mentioned previously (Section 3.1.1), the stirred cell set-up in this study is not a true batch system in that it acts as a continuous system initially and then as a batch system when the feed reservoir has emptied. However, this system may approximate the situation industrially of the shut-down phase of filtration operations and as such provides an interesting system for analysis. While the ANN model presented is empirical in nature, and it has been shown that the use of the weight partitioning method can give some qualitative insight into the physical characteristics, semi-empirical modelling would be a more fundamental chemical engineering approach to the problem. Chapter 5 will focus on the developments of models to describe this system.

CHAPTER 4: BATCH CROSSFLOW MICROFILTRATION OF BENTONITE SUSPENSIONS USING TUBULAR CERAMIC MEMBRANES: DYNAMIC MODELLING WITH ARTIFICIAL NEURAL NETWORKS

4.1   Introduction

In crossflow microfiltration the flow is tangential to the membrane surface. The shearing action provided by the crossflow keeps solids suspended and limits deposition of particles on the membrane, similar to the shearing action of the stirrer in Chapter 3. This is discussed in detail in Chapter 1. Batch filtration systems present an interesting problem for modelling, as the concentration in the system is changing continuously. Chapter 3 examined the ANN modelling of semi-batch stirred microfiltration of bentonite, and this approach is extended here to batch crossflow microfiltration in a tubular ceramic system.

Filtrate flux in batch crossflow systems has been shown to exhibit an initial steep decline at low filtration times followed by a slower flux decline period for different suspension types from latex (Doneva *et al.* 1998) to gluten (Thompson *et al.* 2006). Higher initial suspension concentrations produce greater flux declines. Transmembrane pressure has been shown to have little effect on the filtrate flux of compressible cakes (Fordham and Ladva 1989), while increased crossflow velocity has been shown to increase the filtrate flux of lactic acid fermentation broths (Carrère and Blaszkow 2001), spleen extract (Li *et al.* 2008) and bentonite (Fordham and Ladva 1989).

There have been few reported studies of application of ANNs to batch crossflow filtration data. Chellam (2005) fitted flux decline data in batch crossflow filtration of incompressible glass and silica particles and used the Garson Equation used in Chapters 2 and 3 to elucidate the relative importance of the input parameters.

4.2   Materials and Methods

4.2.1   Crossflow Filtration Rig

The filtration module consists of a ceramic (Carbosepharose) tubular membrane (obtained from Techsep, France) encased in a stainless steel housing.
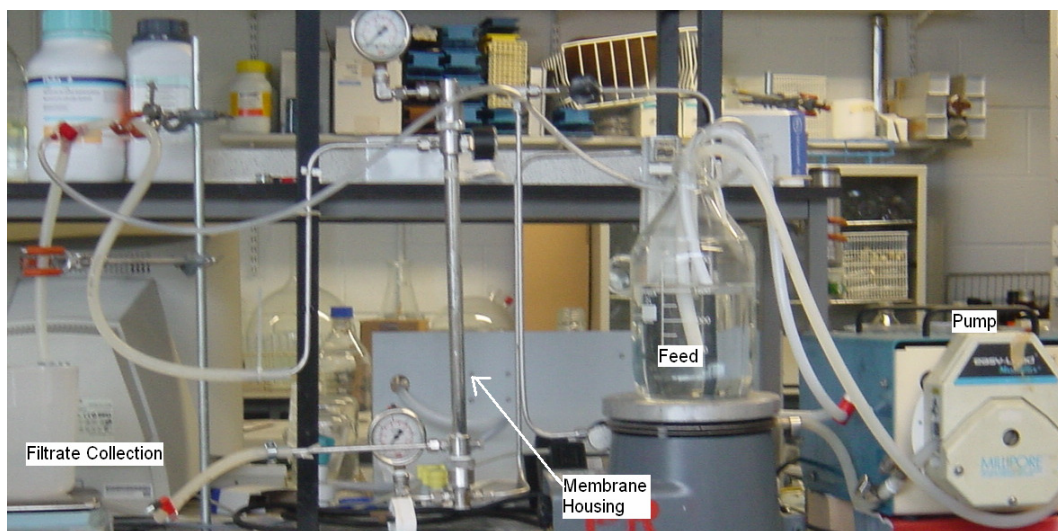
Figure 4-1: Crossflow Filtration Rig

The membrane is 0.4m in length with an inner diameter of 6mm and an outer diameter of 9mm. The membrane pore size is 0.12μm.
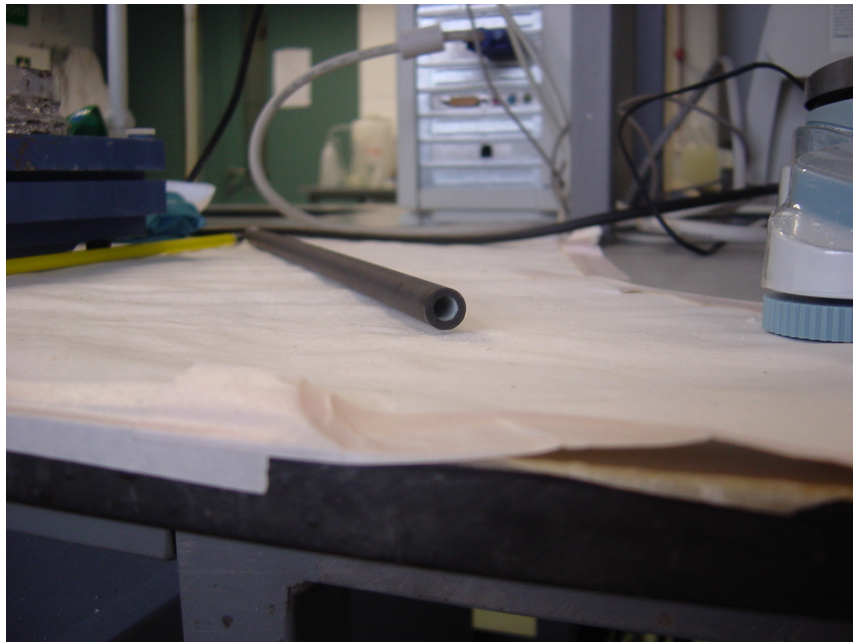
Figure 4-2: Ceramic Membrane

The crossflow filtration rig may be used for batch or continuous crossflow filtration. A schematic of the equipment used may be seen in Figure 4-3 and Table 4-1. A variable speed Millipore Easyload peristaltic pump (Millipore, Bedford, MA) is used to pump fluid through the system. Using this setup, the pressure and crossflow velocity may be varied independently of each other, due to the inclusion of a bypass line. The crossflow is set up by activating the pump (B), which pumps feed from the feed reservoir (A). Volumetric feed flow rate through the module is controlled by adjusting the speed setting on the pump and then using the valve on the feed line (V1) and the valve on the retentate line (V3), the pressure and crossflow may be adjusted to the desired levels. The feed is split in two, with a portion of the feed going through the bypass line, back into the feed reservoir, and the rest going through the flow meter to the membrane. Valve V3 is used to

increase or decrease the transmembrane pressure, while valve V1 controls the feed flowrate that passes into the membrane tube by controlling how much feed goes through the bypass line. By controlling the flowrate of the feed flowing through the bypass line, oscillations produced in the fluid flow by the pump could be dampened, and for the filtration run an essentially steady flow could be achieved. Feed pressure (P1), retentate pressure (P3) and filtrate pressure (P2) are monitored by pressure gauges on the relevant line as seen in Figure 4-3. The ΔP reported is the mean transmembrane pressure drop, ΔP_{tm} (referred to henceforth as ΔP), which is defined as:

$$\Delta P_{tm} = \frac{\left(P_{feed} - P_{retentate}\right)}{2} - P_{filtrate} \qquad\qquad [4\text{-}1]$$

where P_{feed} is the feed pressure measured using P1, $P_{retentate}$ is the retentate pressure measured using P3 and $P_{filtrate}$ is the filtrate pressure measured using P2.
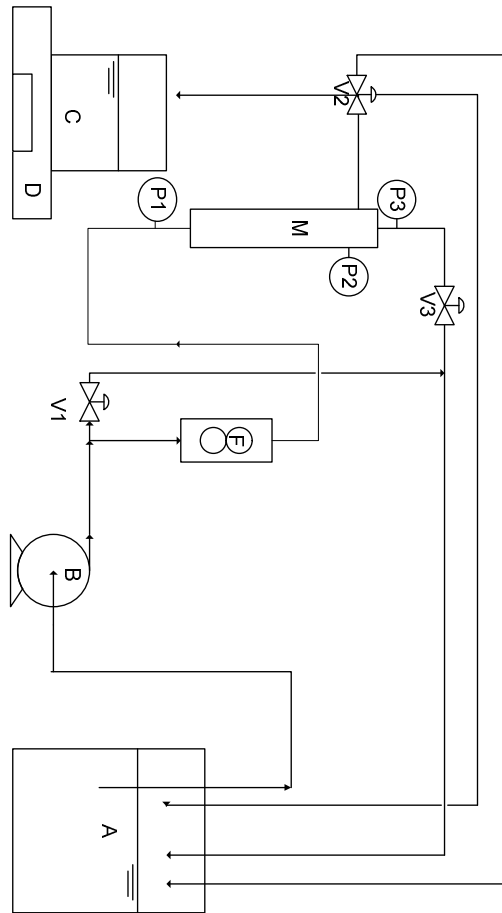
Figure 4-3: Crossflow Filtration Rig

Table 4-1: Key to Figure 4-3

Symbol	Key	Symbol	Key
A	Feed Reservoir	V_1	Needle valve on bypass line; controls flowrate to filtration module
B	Pump	V_2	3 way valve to allow collection of filtrate samples
C	Permeate Collection	V_3	Needle valve; controls transmembrane pressure
D	Balance	$P_{1,2,3}$	Pressure gauges as described
F	Flowmeter		

4.2.2 Preparation of Filtration Module

Previous work using this equipment indicated that membrane fouling was an important factor depending on the water source used for suspensions (McCarthy 2001), a phenomenon which may be due to the small membrane pore size. Extensive investigations were performed to elucidate the percentage increase in the 'clean' membrane resistance with filtration of 1 L of source waters including distilled water, deionised water (including deionised water pre-filtered to 0.8 μm and 0.45 μm) and ultrapure water (distilled water, purified using a Millipore water purification system by reverse osmosis and 0.2 μm ultrafiltration). It was found that the percentage increase using ultrapure water was less than 10 %, whereas in the worst case scenario, using deionised water, the percentage increase was more than 100 %. Thus only ultrapure water was allowed to contact the membrane for cleaning and for preparation of bentonite suspensions.

The resistance of the clean membrane, R_m, was measured prior to each filtration run using ultrapure water. The transmembrane pressure drop $\varDelta P$ was 100 kPa and the volumetric flowrate through the module was 0.8 L/min (an inlet crossflow velocity of 0.47 m/s). The clean membrane resistance was $7.4 \text{x} 10^{11}$ m^{-1} and experiments were conducted only when the measured value was within 10 % of this value.

Prior to conducting the crossflow experiments the membrane required chemical cleaning to restore the clean R_m. This cleaning schedule was established in previous work using this experimental rig (McCarthy 2001). The membrane was cleaned with 1 % NaOH followed by 2 % sodium hypochlorite (bleach), followed

by 2 % nitric acid and finally 1 % NaOH. 2 L of washing suspension at 70 – 80 $^{\circ}$C was used in each case. Approximately 0.5 L of the washing solution was allowed to pass through the membrane at a ΔP of 100 kPa, and then the filtrate line was closed and the cleaning solution was circulated through the module for 15 minutes at ΔP of zero. After use of each cleaning agent, the membrane was flushed with ultrapure water. The membrane resistance was measured at the end of the cleaning process and the protocol repeated if the membrane resistance was not within the desired limits. The pH of the water used to measure the membrane resistance after cleaning was checked to ensure that there was no change before and after contact with the module, to ensure that no residual acid/base remained in the system that could alter the pH of the bentonite suspensions.

Bentonite suspensions were made up using ultrapure water to the desired concentration as described in Chapter 3. Fresh suspensions were used for each experiment and suspensions were stirred for exactly 24 hours prior to use, and were used immediately, as bentonite has been reported as having thixotropic properties (Kelessidis and Maglione 2008). Suspension temperature was adjusted to the desired level by pre-heating/cooling and kept constant during filtration runs using a water/ice bath. Suspensions were stirred at constant shear throughout filtration runs by placing on a magnetic stirring table.

4.2.3 Batch Crossflow Operation

A known volume of suspension (4 L $\pm$ 0.05 L) was placed in reservoir A and placed on a stirring table. The filtrate valve V2 was closed and the pressure control valve V3 was fully opened to establish a ΔP of zero. The suspension was

allowed to circulate in the system for approximately 2 minutes to ensure thorough mixing of suspension with any residual ultrapure water trapped in the system.

Filtration runs were performed over two hours, with filtrate collected in vessel C. No filtrate was recycled to the feed vessel. Filtrate flux was measured by recording the mass of filtrate collected over time. Filtrate mass was measured at 1 minute intervals and the flux over each successive minute was calculated on the basis of the permeate volume collected over 60 seconds.

$$J = \frac{1}{A}\frac{dV}{dt}$$
[4-2]

The transmembrane pressure was controlled using valve V3 and the flowrate of suspension through the module was controlled by adjusting valve V1.

4.3 Results and Discussion

4.3.1 Experimental Observations

A small dataset was designed using a simple experimental design examining the effects of changing each operating parameter in turn on batch crossflow microfiltration. Operating parameters of interest are as outlined in Chapter 3: ΔP, pH, C_0, T, u and R_m. The dataset was kept as small as possible in order to mimic industrial practice, where economics dictate the use of the smallest dataset possible in design/validation of a process. It is expected that filtration characteristics for the crossflow system should be qualitatively similar to those found in the stirred cell setup in Chapter 3. The experiments performed may be seen in Table 4-2.

Table 4-2: Experimental Design for Batch Crossflow of Bentonite

Run	C_0 (g/L)	pH	u (m/s)	T (oC)	ΔP (kPa)	R_m (x10^{11}m^{-1})
1	0.5	7	0.24	21.0	100	7.43
2	0.5	7	0.47	21.0	100	7.36
3	0.5	7	0.59	21.0	100	7.44
4	1.0	7	0.47	21.5	100	7.85
5	5.0	7	0.47	21.5	100	7.62
6	0.5	3	0.47	20.5	100	7.45
7	0.5	7	0.47	20.5	100	7.36
8	0.5	9	0.47	20.5	100	7.30
9	0.5	11	0.47	20.5	100	7.30
10	0.5	7	0.47	21.0	60	7.46
11	0.5	7	0.47	21.0	80	7.46
12	0.5	7	0.47	21.0	120	7.29
13	0.5	7	0.47	10.0	100	7.32
14	0.5	7	0.47	20.0	100	7.36
15	0.5	7	0.47	32.0	100	7.25

Experimental fluxes were found to be very reproducible with careful cleaning of the membrane and precision in suspension preparation. Fluxes used are averaged over three experimental runs, with average errors of just over 1 %. Differences in experimental values were greatest at initial filtration times, with maximum differences from the average flux reaching up to 15 % in some cases, however the errors were reduced to less than 2 % by the second time point in all cases and as such it is reasonable to conclude that the experiments are easily reproducible (Figure 4-4). As observed in Chapter 3, the initial flux decline for microfiltration of bentonite suspensions is very rapid, and flux-time curves will be represented on a semi-log scale in order to see the initial flux decline more clearly.
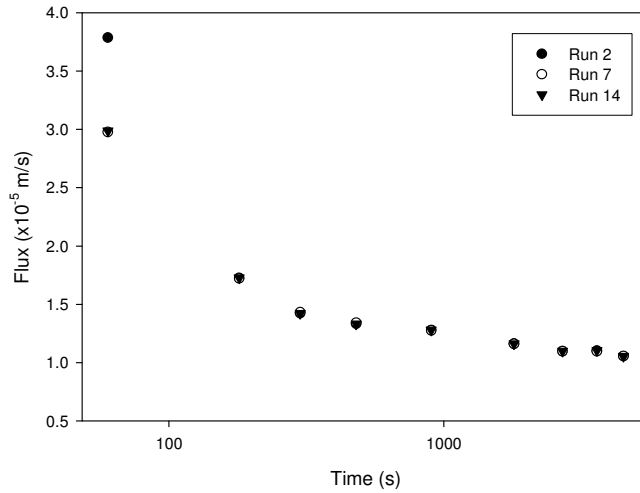
Figure 4-4: Reproducibility of Microfiltration Experiments

Filtration experiments were carried out for initial concentrations of between 0.5 and 2 g/L. The effect of increasing the initial concentration is to decrease the quasi-steady state flux achieved (Figure 4-5).
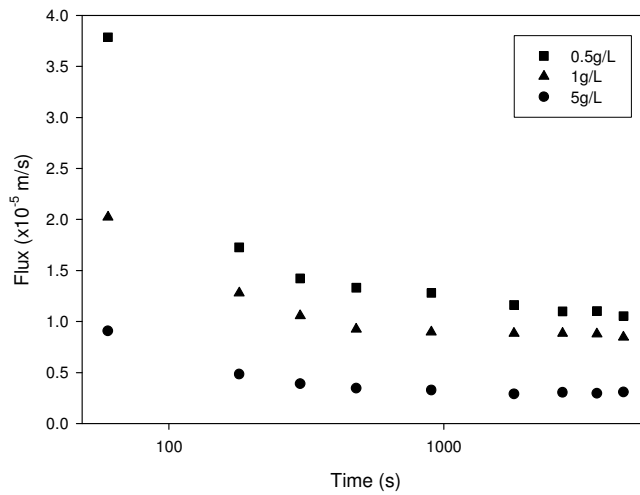
Figure 4-5: Effect of Initial Concentration on Flux Decline

As found in the stirred batch filtration of bentonite, applied pressure ΔP shows very little effect on the flux at longer processing times. Higher applied pressure

leads to higher initial fluxes (Figure 4-6) however little effect is seen after initial deposition of particles on the membrane. This phenomenon was also observed by Fordham and Ladva (1989; 1992).
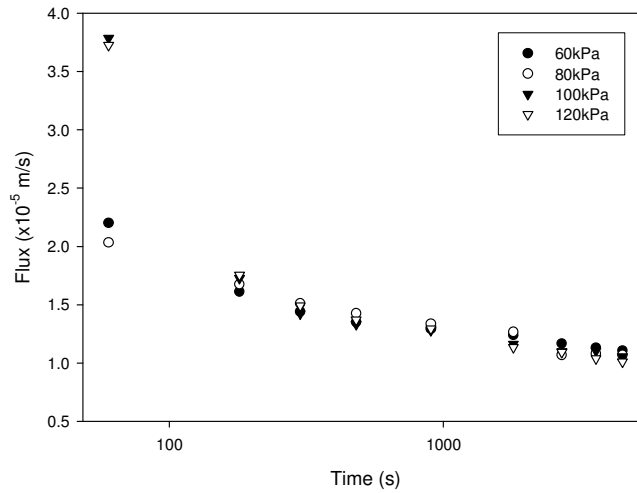
Figure 4-6: Effect of Pressure on Flux Decline

Increasing the crossflow velocity causes a corresponding increase in the permeate flux (Figure 4-7). This is as expected as the higher the crossflow the more the limitation of deposition on the membrane surface (Belfort *et al.* 1994).
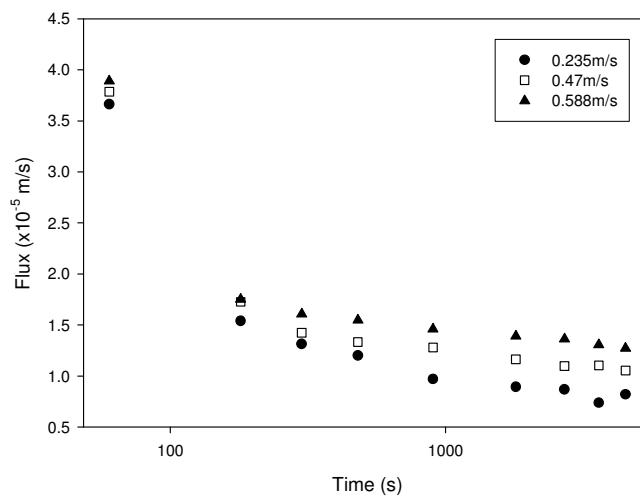
Figure 4-7: Effect of Crossflow Velocity on Flux Decline

The membrane resistance R_m is seen to have little or no effect on the filtrate flux in stirred microfiltration of bentonite in Chapter 3. The membrane resistance in this case is essentially constant, varying by less than 6 % across all experiments performed due to the chemical cleaning of the membrane until the original clean pure water flux is achieved. Thus examination of the effect of R_m on the filtrate flux is not possible for this system.

The flux characteristics are seen to exhibit a complex dependence on the pH (Figure 4-8). Little effect is observed at mid-range pHs (7, 9) whereas extremes of pH (3, 11) are seen to lower the flux considerably. This complexity is to be expected as a similar result was seen in batch stirred microfiltration of bentonite, where the lowest fluxes were at pHs of 11.4 and 2.52
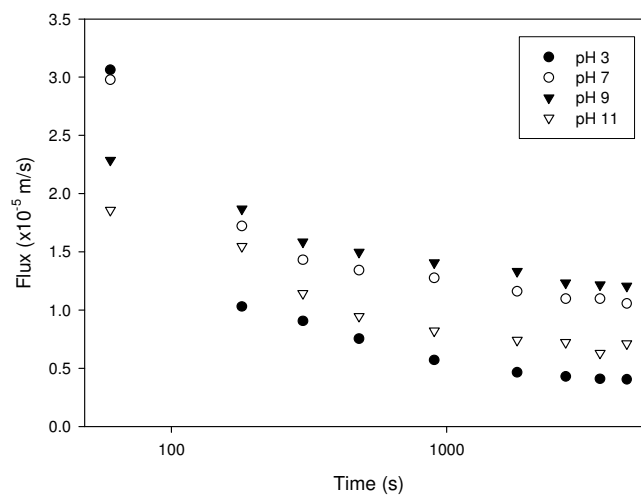
Figure 4-8: Effect of pH on Flux Decline

The effect of increasing or lowering the suspension temperature is to increase or decrease the flux (Figure 4-9). This is due to the temperature dependence of the viscosity of aqueous bentonite suspensions (Reineke and Varnado 1978) and the temperature dependence of the filtrate viscosity. The filtrate viscosity affects the

139

flux directly according to standard filtration theory. Increasing the suspension viscosity causes a corresponding increase in the wall shear stress which should decrease the cake mass, leading to increased fluxes. As the flux increases with increasing temperature for this system, it is clear that the effect of the increasing temperature decreasing the filtrate viscosity is the dominant effect in this case.
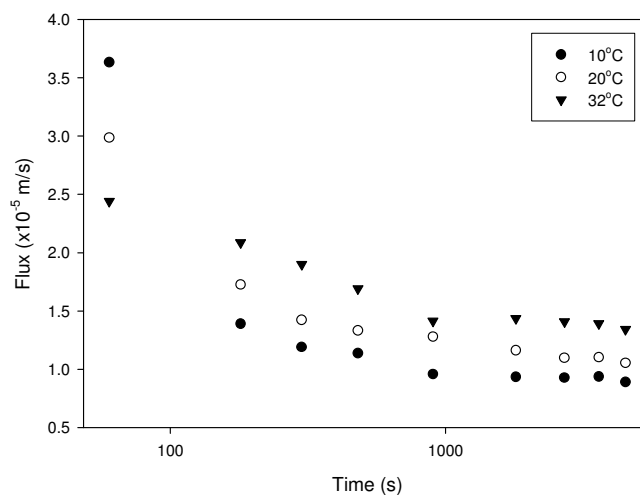
Figure 4-9: Effect of Temperature on Flux Decline

4.3.2 Artificial Neural Network Modelling

This section outlines the use of the novel approach developed in Chapter 3 for correlation and prediction of dynamic filtration data using ANNs. As described in Chapters 2 and 3, the entire data set is used for optimisation of the network architecture, and the dataset is then divided into training, validation and test sets in order to develop a network for prediction of previously unseen dynamic batch filtration data. As described in Chapter 3, Trajan Neural Network Software is used in all ANNs in this chapter.

A network with a single hidden layer with seven neurons is found to be the optimum network architecture for this dataset using the trial and error approach outlined in Chapter 2, with an MSE of 3.6×10^{-7}. No appreciable benefit is seen upon addition of a second hidden layer (Figure 4-10). The optimum architecture is the least complicated configuration which achieves the lowest possible error.
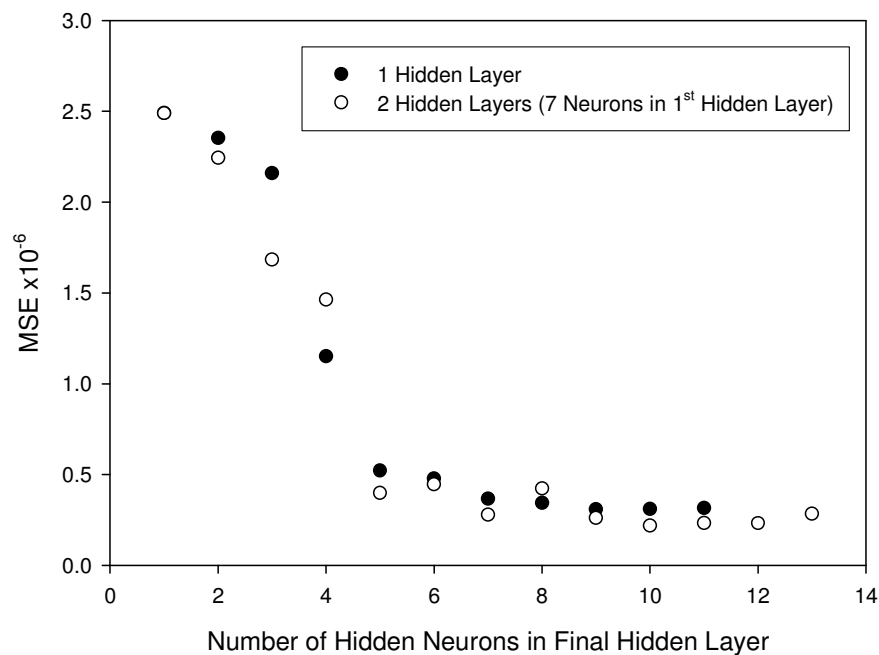
Figure 4-10: Network Optimisation

This network correlates the entire dataset with a regression equation of $y = 0.99\,x + 1 \times 10^{-7}$, with an R^2 value of 0.99 (Figure 4-11). 95 % confidence intervals for the slope and intercept are found to be [0.97, 1.004] and [-9.5×10^{-8}, 3.67×10^{-7}] This network has the architecture 6-7-9, where 6 is the number of inputs, 7 is the number of hidden neurons and 9 is the number of outputs (fluxes at specified time points). The number of data points used along the flux - time curve is minimised in order to allow for a simpler network; as the flux-time curves are regular in all cases it is reasonable to surmise that no loss of information about the shape of the

curves would result from omission of time points. Extra data points are used at low filtration times, where the initial flux decline is of interest. The times used are at 60, 180, 300, 480, 900, 1800, 2700, 3600 and 4500 seconds.
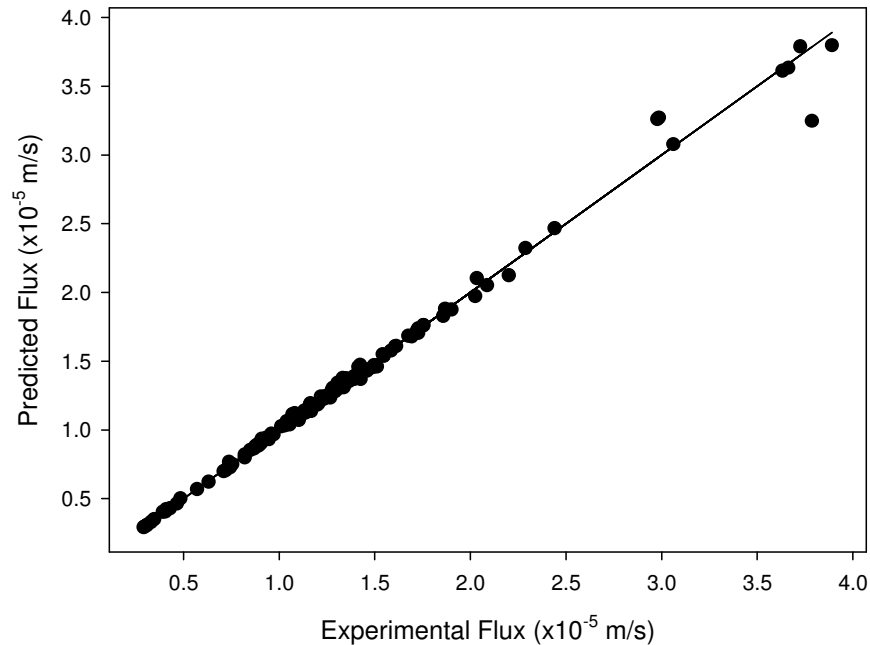
Figure 4-11: Correlation of Entire Dataset using 6-7-9 Network

4.3.2.1 Weight Partitioning Method

The weight partitioning method described in Chapter 3 (Garson 1991) is applied to examine the relative contribution of the inputs along the flux-time curve, incorporating the entire dataset,. This should give some insight into the mechanisms of batch crossflow filtration of bentonite.

The effects of the parameters seem to mimic the flux development, with changes observed in the input contributions at low filtration time, the relative contributions becoming essentially constant at longer filtration times (Figure 4-12).
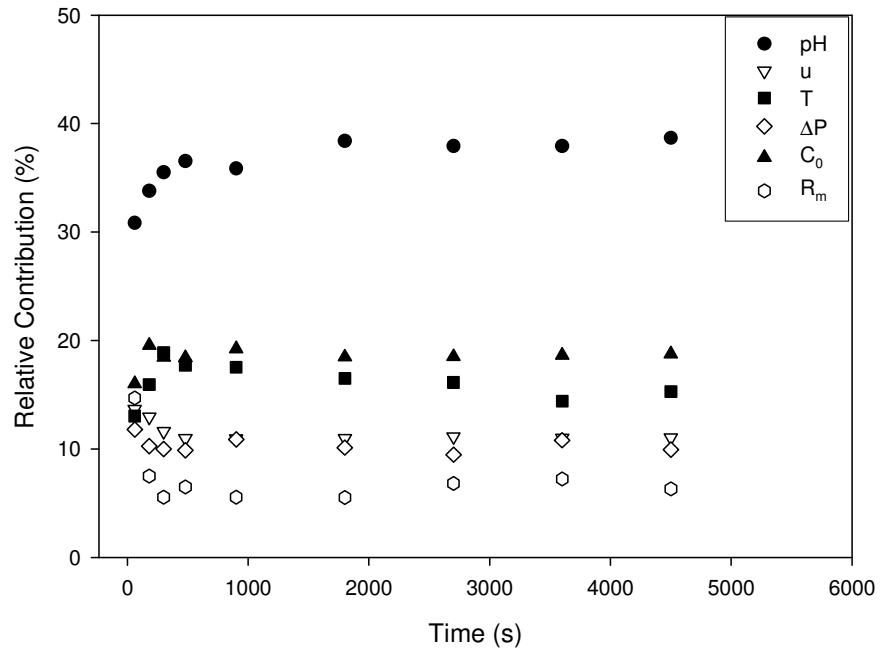
Figure 4-12: Evolution of Relative Input Contributions for Batch Crossflow
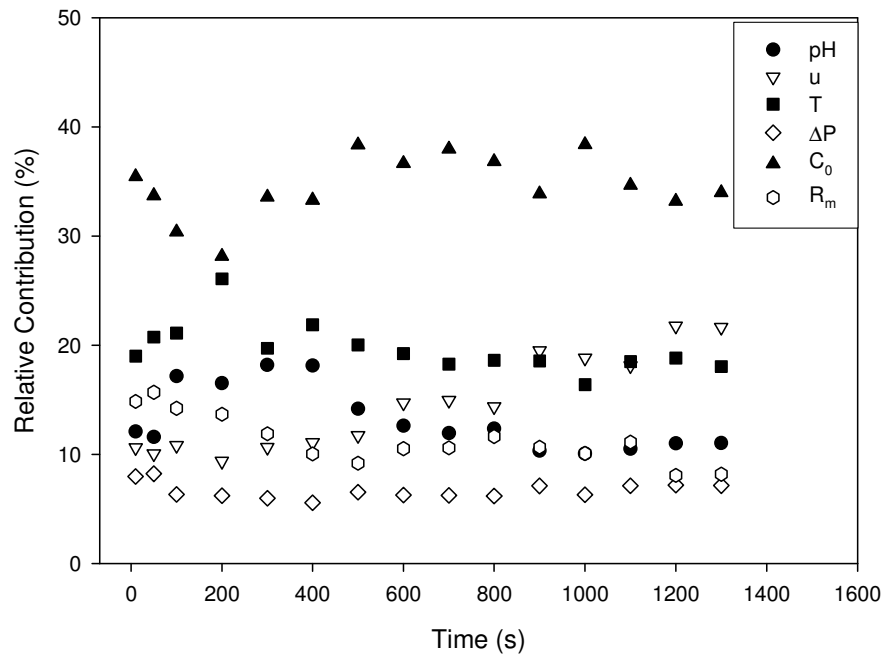
Figure 4-13: Evolution of Relative Input Contributions for Stirred Cell System

143

Overall, it is worth noting that the evolution of the inputs is quite different to that found for the stirred cell system. In particular, the effect of pH is much less significant for the stirred cell system.

It is also questionable whether the contributions found at the earliest time points are reliable, as the network prediction has been shown to be least accurate at these times.

Looking at the data more closely, Figure 4-14 shows that the effects of the initial concentration and the membrane resistance for this system seem to be interlinked, where both act together at initial filtration times, being of similar importance (15-16 %), and after initial deposition of particles on the membrane, the initial concentration becomes of greater importance (at approximately 19 %) than the membrane resistance (at approximately 9 %), both remaining essentially constant at longer filtration times.
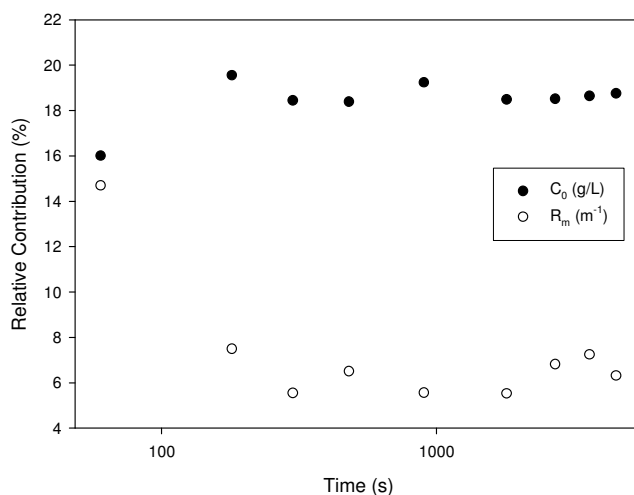
Figure 4-14: Evolution of Contribution of C_0 and R_m

This would seem to be a sensible result, given the mechanisms of crossflow microfiltration. However, this depends on whether the initial data point is reliable – the fit of the network is not as good at low filtration times as it is at longer times so this is questionable (see Figure 4-11, where data points on the right hand side correspond to initial filtrate fluxes).

The crossflow velocity is seen to be of greater importance at low filtration times at 13 %, decreasing to 11 % with time (Figure 4-15). This is the opposite effect to that found in the stirred cell experiments, where crossflow velocity was found to be of greater importance at later times. The decrease in the importance of crossflow velocity with time may indicate the formation of a partly irreversible cake after early filtration times. This is further supported by the chemical cleaning required to re-establish the pure water flux through the membrane prior to use. This will be discussed in further detail in Chapter 6.
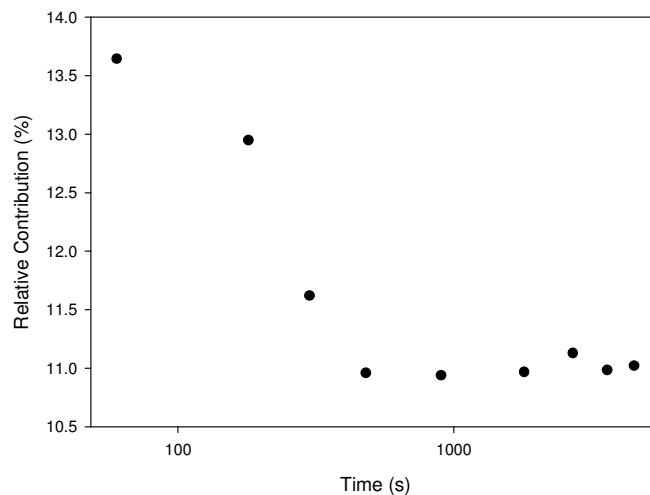
Figure 4-15: Evolution of Contribution of u

The pH effect is by far the most significant for the system, accounting for 30 - 40% (Figure 4-16).
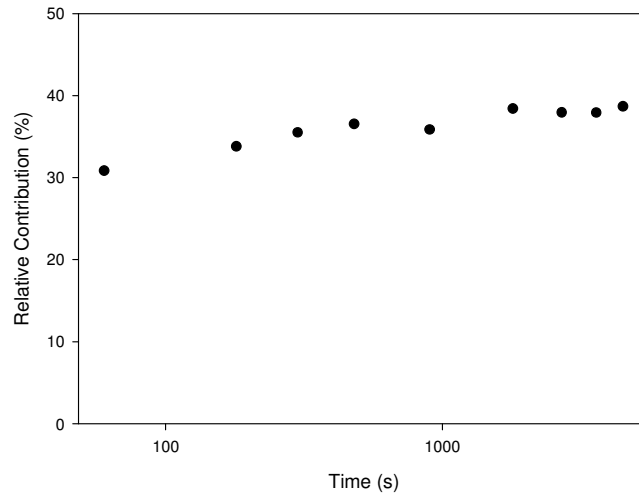
Figure 4-16: Evolution of Contribution of pH

The suspension temperature exhibits a sharp increase in importance from 13% to 19% over initial filtration times, subsequently declining along the course of flux-time curve to approximately 16% (Figure 4-17).
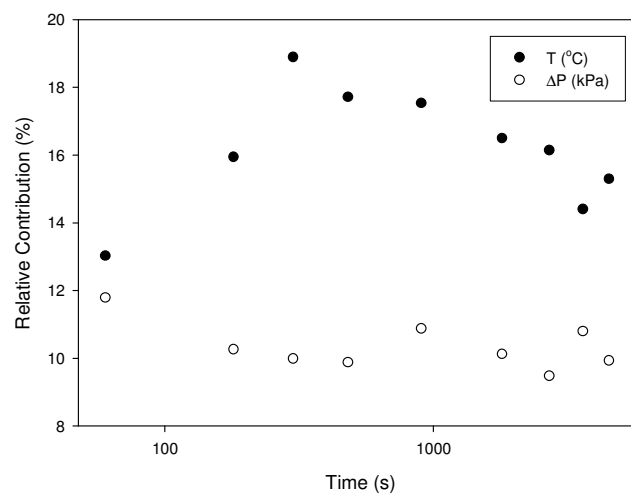
Figure 4-17: Evolution of Contribution of Temperature and Pressure

It is difficult to say if these changes are significant statistically without the availability of percentage contributions generated from another comparable dataset. However, it would be expected that temperature would be a stronger effect at the start of a filtration run whereas at the end of the run the cake is dominant. The applied pressure is of slightly greater importance at initial filtration times (12 %) declining to a steady 10 % at longer filtration times (Figure 4-17). This is in keeping with the simple cake formation model as discussed where the cake is dominant after initial filtration times.

The effect of pH is the greatest observed for the system and it has been established that the relationship between pH and filtrate flux of bentonite is a complex one (Chapter 3, Section 4.3.1) Further work could include the development of a network for bentonite batch crossflow filtration data at constant pH, allowing the examination of the other system parameters in greater detail.

Although it appears that the Garson Equation can be used to obtain some information about the physical phenomena occurring in the system, it is important to realise that the contributions are relative to each other. It is possible that physical arguments based on a single parameter may not be suitable for describing the system – if the relative contribution of one parameter changes it automatically affects the contribution of one or more of the other parameters. For example, if the effect of crossflow velocity becomes less important with time due to irreversible cake formation, then some other parameter must as a consequence become more important with time.

4.3.2.2 Training, Validation and Testing

The entire dataset was used initially in order to elucidate the relative importance of the operating parameters, as the larger the dataset, the less likely for noise in the data to affect the results. In this section, the ANN is trained with a portion of the available data in order to investigate the use of the ANN in predictive mode. The dataset is divided randomly into training, validation and test subsets as described in Chapter 3. Of the 15 experimental runs, 5 are used for training, 9 for testing and 1 for validation in order to prevent overfitting and loss of generalisation ability, as described in Chapters 2 and 3. It is desirable to use as few experiments as possible in training the network in order to reflect the industrial situation where minimisation of experimentation makes more economic sense. The dataset is divided up randomly into these subsets using the shuffle function in Trajan, as described in Chapter 3.The division of data is as outlined in Table 4-3.

T

	Run	C_0 (g/L)	pH	u (m/s)	T (°C)	ΔP (kPa)	R_m ($\times 10^{11}$ m^{-1})
Train	1	0.5	7	0.24	21.0	100	7.43
Test	2	0.5	7	0.47	21.0	100	7.36
Test	3	0.5	7	0.59	21.0	100	7.44
Train	4	1.0	7	0.47	21.5	100	7.85
Train	5	5.0	7	0.47	21.5	100	7.62
Test	6	0.5	3	0.47	20.5	100	7.45
Test	7	0.5	7	0.47	20.5	100	7.36
Train	8	0.5	9	0.47	20.5	100	7.30
Test	9	0.5	11	0.47	20.5	100	7.30
Test	10	0.5	7	0.47	21.0	60	7.46
Train	11	0.5	7	0.47	21.0	80	7.46
Val	12	0.5	7	0.47	21.0	120	7.29
Test	13	0.5	7	0.47	10.0	100	7.32
Test	14	0.5	7	0.47	20.0	100	7.36
Test	15	0.5	7	0.47	32.0	100	7.25

The fit of the predictions to the test flux data may be seen in Figure 4-18, where the dashed lines indicate the ANN prediction and the symbols represent experimental data. It is clear from Figure 4-18 that the network is capable of being used in predictive mode with great accuracy, with an R^2 value of 0.9874 for the fit of the network predictions to the test data.
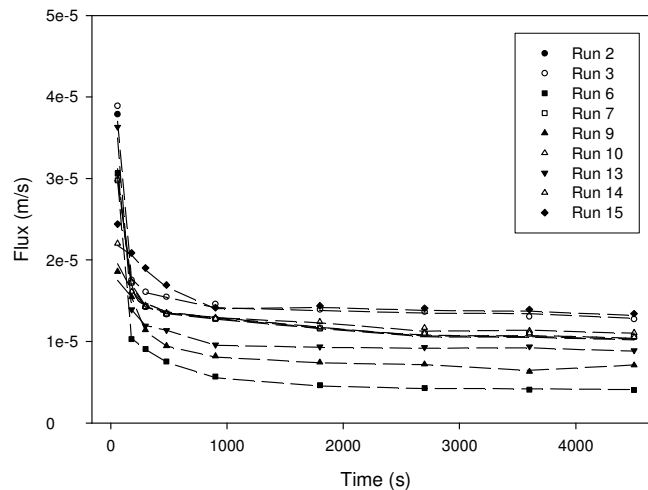
Figure 4-18: Fit of ANN Predictions to Test Dataset

The fit of the network predictions to the training and test datasets may be seen in Figure 4-19, where the solid line denotes the y=x line.
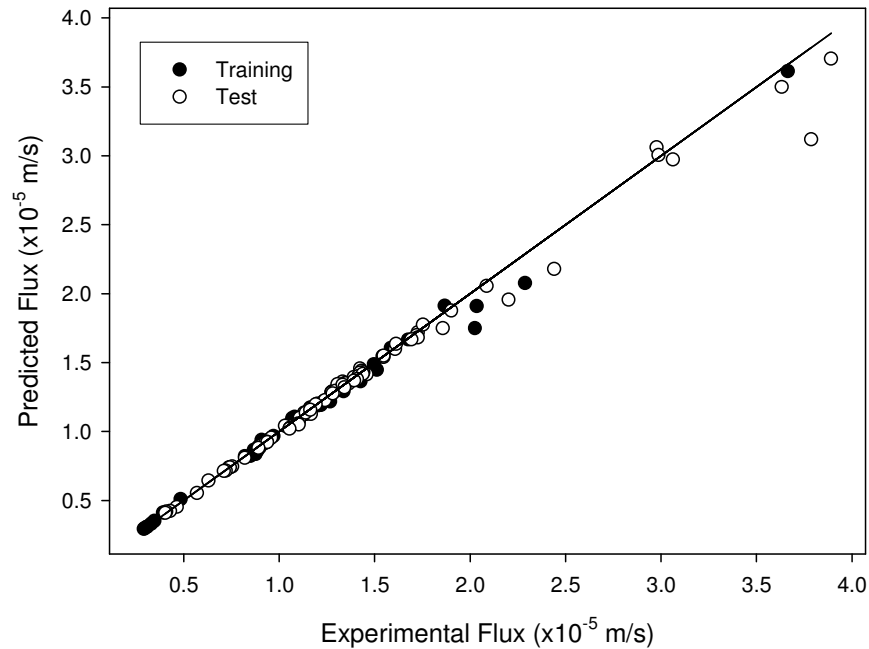
Figure 4-19: Correlation of Training and Test Datasets

For the training dataset, the regression equation is $y = 0.96x + 3 \times 10^{-7}$, with an R^2 of 0.99. 95 % confidence intervals for the slope and intercept are found to be [0.93, 0.97] and [-1.2×10^{-8}, 6.28×10^{-7}] respectively. For the test data, the regression equation is $y = 0.93x + 7 \times 10^{-7}$ with an R^2 value of 0.99. 95 % confidence intervals for the slope and intercept are found to be [0.9, 0.95] and [3.7×10^{-7}, 1.1×10^{-6}] respectively.

4.4   Conclusions and Further Work

In this chapter, batch crossflow microfiltration of bentonite was investigated and the effect of operating parameters on the flux-time curves was examined. The

results were as to be expected, with increasing initial suspension concentration and decreasing crossflow velocity and suspension temperature contributing to decline in quasi steady state fluxes achieved at long filtration times. Applied pressure was shown to have little effect on the flux, while the flux was shown to exhibit a complex dependence on the suspension pH. The filtrate flux was shown to achieve a quasi-steady state value at longer filtration times.

A feed-forward backpropagation ANN with one hidden layer containing 7 neurons was developed for correlation and prediction of the batch filtration data. The novel method outlined in Chapter 3 was used in designing of the network, with time not included explicitly in the network. The network consisted of 6 inputs and 9 outputs, composed of the fluxes at 9 times along the flux-time curve. Analysis of the network weights using the weight partitioning method proposed by Garson (1991) was used to gain some insight into the relative importance of the input parameters along the flux-time curve. It was found that the great effect by far was the pH effect, at 30 - 40 %. All of the other parameters showed initial change followed by a quasi-steady state, mimicking the action of the flux-time curve itself. The concentration was observed to increase in importance from an initial 15-16 % to 19 %, the membrane resistance was seen to decrease in importance from 15-16 % to 9 %, ΔP and u exhibited decreases in importance from 12 and 13 % to 10 and 11 % respectively, while the temperature displayed a sharp increase in importance initially from 13 % to 19 % and then declined to 16 % thereafter. As the pH effect is so large in comparison to the other effects, it is proposed that an area for further work could include the development of a dataset at constant pH in order to examine the effects of the other parameters in greater detail.

The dataset was divided into training, validation and test subsets as described in Chapters 2 and 3. A total of 5 experiments were used in training the network, while 1 was used for validation (prevention of overfitting and loss of generalisation ability). The network was tested using 9 experiments. Excellent correlation and prediction was achieved, with R^2 values of 0.99 for the entire dataset, 0.99 for the training subset, 0.99 for the validation set and 0.99 for the test set.

While the neural network approach is capable of giving an excellent result in terms of correlation and prediction of dynamic filtration data, and the weight partitioning method has been shown to be of use in gaining some qualitative insight into the mechanisms of the system, it has been argued that ANNs are technically a complicated non-linear regression approach to modelling a system with a regression structure that is extremely complicated due to the number of connections in the network, and useful only as a "brute force" or "black-box model" approach to modelling a system (Piron *et al.* 1997; Olden and Jackson 2002). While the weight partitioning method has shown results here that seem sensible in light of the mechanisms of crossflow microfiltration, it may be argued that a true chemical engineering approach to the problem must give some quantitative insight into the mechanisms of the system. Chapters 5 and 6 will thus focus on semi-empirical modelling of the semi-batch stirred, batch crossflow and continuous crossflow microfiltration of bentonite suspensions.

CHAPTER 5: SEMI-EMPIRICAL MODELLING OF STIRRED CELL AND CERAMIC CROSSFLOW MICROFILTRATION

5.1   Introduction

The neural network models presented so far in this research are empirical in nature. Although a legitimate approach especially in the modelling of complex systems, the development of physical models to describe the systems used in this research would be a more fundamental chemical engineering approach to the problem. The use of physical modelling especially in batch systems where the concentration in the system is changing as a function of time is an interesting problem and should give more qualitative insight into the underlying physical phenomena determining flux behaviour.

Mathematical modelling of filtration has been the subject of much research, as discussed in Chapter 1. Models have been developed based on different theories, including those based on resistance models (Hermia 1982), particle back-transport models including shear induced diffusion (Zydney and Colton 1986; Romero and Davis 1990) and inertial lift (Green and Belfort 1980; Altena and Belfort 1984), flowing cake and surface transport models (Davis and Leighton 1987) and force balance models (Lu and Ju 1989; Dharmappa *et al.* 1992; Foley *et al.* 1995b).

Bentonite filtration has been a subject of interest in research due to its applicability in oil and petroleum industries as mud used in drilling oil wells. Two regimes have been observed in the crossflow filtration of concentrated bentonite suspensions (Fordham and Ladva 1989; 1992) - an early regime in which the filtration was unaffected by shear and in which filtrate flux was indicative of

153

dead-end filtration and a later regime in which the flux was essentially constant. Weak pressure dependence was found during the initial flux decline at low filtration times, and negligible pressure dependence was found in the constant flux regime due to the reduction in cake permeability with filtration pressure (Ferguson and Klotz 1954; Bezemer and Havenaar 1966). Filtrate flux of colloids such as bentonite is shown to be controlled by cake properties (thickness and permeability) and significantly influenced by the shear rate and colloidal state of the suspension (Jiao and Sharma 1992).

Models have been developed to describe crossflow filtration of bentonite based on a number of the theories outlined above. The convective model or flowing cake model is one theory that has been applied to crossflow filtration of bentonite (Vassilieff *et al.* 1996; Doneva *et al.* 1997; Vassilieff and Doneva 1997). Analysis of model parameters and experimental data have shown that the initial transient flux decline observed in filtration of bentonite at low concentrations was achieved by accumulation of particles on the surface of the membrane rather than by plugging of the pores of the membrane.

Models balancing the forces acting on a particle have been proposed with varying mechanisms based on the method of removal of a particle from a surface. Removal may by assumed to occur by sliding with the use of a friction factor as the constant of proportionality between normal drag and tangential forces (Outmans 1963). If removal is assumed to take place by rolling, a torque balance may be performed (Jiao and Sharma 1994).

Experimental investigations into the crossflow filtration of colloids have shown that the cakes formed during crossflow microfiltration of bentonite are

inhomogeneous with smaller particles deposited as filtration proceeds. When no particles small enough to be deposited are available in the suspension, an equilibrium cake thickness is achieved (Jiao and Sharma 1994). This is in agreement with models developed on the basis of force balances taking polydispersity into account (Foley *et al.* 1995b).

Cakes formed during filtration of bentonite have been shown to be compressible (n = 0.83) with a power law relationship between specific cake resistance and filtration pressure fitting well to experimental data measured using dead-end ultrafilters (Choe *et al.* 1986; Gourgues *et al.* 1992). Specific cake resistances of the order of 10^{14} m/kg for bentonite concentrations of 0.1 g/L were found for pressures in the range 20-70 kPa by Kim and DiGiano (2006) using a flat sheet membrane with pore size 1 μm (membrane resistance was not reported). Pressure dependence of the specific cake resistance was correlated using the standard power law relationship and cakes of bentonite were found to be highly compressible, with *n* values of 0.97.

The aim of this chapter is to investigate the stirred and crossflow microfiltration of aqueous bentonite suspensions and to generate models to describe the systems based on semi-empirical modelling techniques incorporating mass and force balances for the systems. Theoretical models developed will be fit to experimental data in order to obtain values for parameters incorporated into the models, including specific cake resistance and parameters governing particle removal from the cake/membrane surface.

5.2   Model Development and Solution - Stirred Cell System

The stirred cell system is described in detail in Chapter 3. This set-up provides an interesting system for modelling purposes due to the essentially two-compartment configuration, i.e. the equipment may not be considered a single well-mixed system. A simple schematic for the system is presented in Figure 5-1 where V_R is the feed reservoir volume, C_0 is the initial feed concentration, J is the filtrate flux, A is the membrane area, V is the volume in the stirred cell, and C is the suspension concentration in the stirred cell.
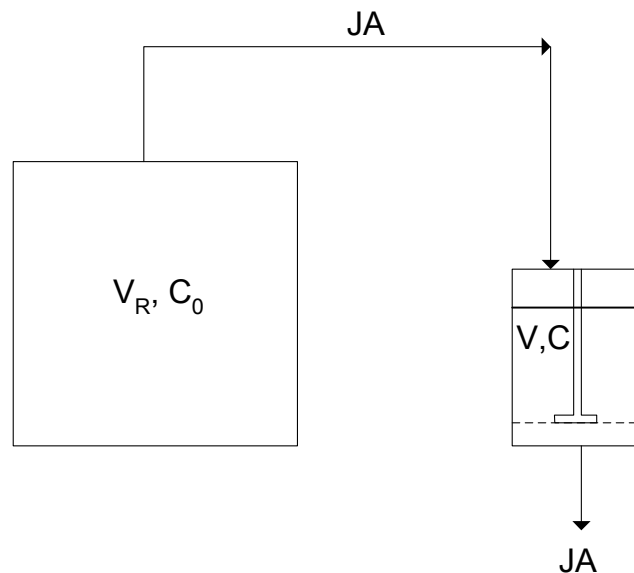
Figure 5-1: Stirred Cell Set-up for Modelling Purposes

Mass balances for the system are combined with the use of a simple equation used to describe the cake build-up in a stirred cell system in order to generate a functional model of the system behaviour.

5.2.1 Mass Balances

5.2.1.1 Feed Reservoir

As described in Chapter 3, the feed reservoir is initially filled with 700ml of feed. When the reservoir is pressurised (but before the filtrate line is opened), the application of pressure forces some of the feed into the stirred cell (the amount depends on the applied pressure). When the filtrate line is opened, the amount of feed in the stirred cell is kept constant by flux of feed from the reservoir to the stirred cell equalling the filtrate flux from the stirred cell. This setup is not unlike continuous diafiltration (constant volume diafiltration) where fresh water is fed from a reservoir and causes low molecular weight impurities to be flushed from the solution in the cell. Thus the rate of depletion of feed in the reservoir is equal to the filtrate flux.

Mathematically this may be represented by the following equations:

$$\frac{dV_R}{dt} = -AJ \text{ when } V_R > 0 \qquad\qquad\qquad \text{[5-1a]}$$

$$\frac{dV_R}{dt} = 0 \text{ when } V_R = 0 \qquad\qquad\qquad \text{[5-1b]}$$

Where V_R is the reservoir volume, A is the membrane area and J is the filtrate flux. The filtrate flux is defined using the classic equation for flux based on Darcy's Law as mentioned previously:

$$J = \frac{\Delta P}{\mu(R_m + \alpha m)} \qquad\qquad\qquad \text{[5-2]}$$

5.2.1.2 Stirred Cell

Once the stirred cell is filled with feed from the reservoir and filtration is started, the amount of feed in the cell is kept constant by flux of feed from the reservoir, i.e. the rate of depletion is zero. When the reservoir is emptied, the amount of feed in the stirred cell depletes at a rate equal to the flowrate of filtrate from the cell.

Mathematically the mass balance for the stirred cell may be represented by:

$$\frac{dV}{dt} = 0 \text{ when } V_R > 0 \qquad\qquad\qquad\qquad [5\text{-}3a]$$

$$\frac{dV}{dt} = -AJ \text{ when } V_R = 0 \qquad\qquad\qquad\qquad [5\text{-}3b]$$

where V is the volume of feed in the stirred cell.

5.2.1.3 Particle Balance for the Stirred Cell

While the reservoir is not empty and is transferring feed to the stirred cell, the rate of accumulation of particles in suspension in the stirred cell is equal to the influx of particles from the reservoir minus the rate of accumulation of particles on the surface of the membrane or on the cake. When the reservoir has emptied, the change in the amount of particles in the cell is equal to the cake formation rate.

A key assumption throughout the modelling work presented in this chapter is that the rate of cake formation is equal to the rate of deposition of particles on the membrane surface minus the rate of removal where the rate of removal is assumed to be proportional to the mass of particles per membrane area. This type of model owes its origins to early theories of heat exchanger fouling proposed by Kern and Seaton (1959). Those authors modelled surface fouling with a removal rate that

was proportional to the mass of deposited material and a rate constant that was proportional to the wall shear stress (Kern and Seaton 1959). This system is analogous to the situation in crossflow and stirred cell filtration systems where this modelling approach may be represented mathematically as follows:

$$\frac{dm}{dt} = CJ - km \qquad\qquad\qquad\text{[5-4]}$$

where C is the concentration of particles in the stirred cell and CJ is the deposition rate. The rate constant, k, will likely depend on the particle size and size distribution, and also on other characteristics of the particles such as the potential for adhesion on the membrane surface (McCarthy *et al.* 1996; Silva *et al.* 2000). As in heat exchanger cleaning theory, it would be expected to be a shear-dependent constant.

A particle balance for the stirred cell will take the following form

$$\frac{d(VC)}{dt} = C_0 AJ - A\frac{dm}{dt} \text{ when } V_R > 0 \qquad\qquad\text{[5-5a]}$$

$$\frac{d(VC)}{dt} = -A\frac{dm}{dt} \text{ when } V_R = 0 \qquad\qquad\text{[5-5b]}$$

Where C_0 is the initial feed concentration and *dm/dt* is defined as in Equation 5-4.

Expanding the first part of Equation 5-5a

$$V\frac{dC}{dt} + C\frac{dV}{dt} = C_0 AJ - A\frac{dm}{dt} \qquad\qquad\text{[5-6]}$$

When $V_R > 0$, $\frac{dV}{dt} = 0$ and $V = V_0$. Combining these and using Equation 5-4 for $\frac{dm}{dt}$, this may be written as

159

$$\frac{dC}{dt} = \frac{1}{V_0}\left(C_0 AJ - CAJ + kAm\right) \qquad\qquad \text{[5-7]}$$

with $C = C_0$ at t = 0.

Now, when the reservoir is empty (i.e. $V_R = 0$)

$$V\frac{dC}{dt} + C\frac{dV}{dt} = -A\frac{dm}{dt} \qquad\qquad \text{[5-8]}$$

However when the reservoir is empty $\frac{dV}{dt} = -AJ$, therefore

$$V\frac{dC}{dt} = CAJ - A\left(CJ - km\right) \qquad\qquad \text{[5-9]}$$

Giving

$$\frac{dC}{dt} = \frac{Akm}{V} \qquad\qquad \text{[5-10]}$$

Equations 5-1 and 5-3 describe the rate of change of the feed reservoir and stirred cell volume over time, Equation 5-2 describes the filtrate flux, Equation 5-4 describes the change in cake mass with time, and the change in concentration with time is given by Equations 5-7 and 5-10. These equations complete the model for cake formation and flux decline in the stirred cell system. It should be noted that in all cases, membrane fouling is assumed to be negligible, i.e., R_m is assumed constant.

5.2.2 Solution of Model Equations using Berkeley Madonna Software

5.2.2.1 Model Development

Berkeley Madonna 8.0.1 (© 1997-2001 Robert I. Macey and George F. Oster) is a fast and convenient general purpose differential equation solver. It can be used to solve ODEs (Ordinary Differential Equations) and difference equations – both initial value and boundary value problems. It is easy to use in that the equations describing the problem can be typed in ordinary mathematical notation, in any order. The equations are then compiled easily and plots of the model are generated automatically, without the need for coding. It is also possible to create models visually with icons using a flowchart editor function, which generates the equations automatically. A key advantage of Berkeley Madonna and the main reason for why this software was employed in the work for this thesis is the fact that experimental data may be imported and a curve fitter tool can be used to estimate parameters by fitting the model solution to one or more data sets (Macey *et al.* 2000). The relevant equations for the stirred cell system are coded as in Model 5-1 shown below.

Model 5-1: Stirred Cell with Reservoir

```
METHOD RK4
STARTTIME = 0
STOPTIME=9500
DT = 0.02
DTOUT = 10

K=0.0002
RM=3E10
ALPHA=3e13
MU=0.001
DP=1E5
C0 = 1
A = .002971


J=DP/MU/(RM+ALPHA*M)


VR0=7E-4
INIT(VR)=VR0
D/DT(VR) = IF(VR>0) THEN -A*J ELSE 0

V0=1.2E-4
INIT(V)=V0
D/DT(V) = IF(VR>0) THEN 0 ELSE -A*J

INIT(C)=C0
D/DT(C) = IF(VR>0) THEN 1/V0*(C0*A*J-C*A*J+K*A*M) ELSE
1/V*K*A*M

INIT(M)=0
D/DT(M)=C*J-K*M

VP = IF(VR>0) THEN VR0-VR ELSE V0-V+VR0
```

It is possible to specify an integration method for the model, the options being

Euler, 2nd order Runge-Kutta (RK2), 4th order Runge-Kutta (RK4), along with a

stiff integration method. The integration method chosen is Runge-Kutta 4, due to

its enhanced convergence capabilities and greater accuracy compared to Euler or

RK2 methods. Euler's method is not generally used in scientific computation as

the truncation error per step is larger than that associated with more advanced

methods, and the Runge-Kutta methods eliminate lower order errors (i.e. for the

RK4 method, only 4th order errors are present) (Press *et al.* 1988). The integration method chosen is specified in the model (METHOD RK4).

The terms STARTTIME and STOPTIME refer to the times between which the model is compiled. The start time is zero and the stop time is the time it takes for a filtration run to take place for the specified operating parameters set.

DT is the fixed stepsize for the integration. It is possible to ascertain whether the stepsize used is sufficiently small for accuracy using the Check DT function in Madonna. The check is performed by running the model twice – once with the stepsize specified, and then with the stepsize reduced by a factor of 10. After both runs have been completed, a report is generated where the maximum and minimum root mean square deviation between the two runs for each stored variable may be examined. A difference between the two runs may indicate that a smaller stepsize should be specified in the model code. The stepsize in this case is set to 0.02, which is small enough to give sufficient accuracy in all cases.

DTOUT is the interval at which results are stored in memory. In this case 10 seconds is chosen. Usually Berkeley Madonna would store an output point for each time step; however with a small stepsize (0.02 in this case) this would result in a large output dataset. The use of DTOUT enables storage of output data independently of the stepsize used to produce it.

The model parameters used are initialised in the code either to a fixed value or to an initial value if the parameter is involved in a differential equation. Boundary value problems are also possible using Berkeley Madonna however this is not necessary in this case. The model is initialised using parameter values however

163

these values may be tailored for each individual experiment using the Parameter Window in Madonna prior to each run. This window allows changes to be made to the parameters in the model as well as to the integration method used without recompiling the model.

To illustrate the behaviour predicted by this model the model parameters were chosen as described below. The cake removal constant k, [K] is given a value here of 2×10^{-4} s^{-1}; the membrane resistance R_m, [RM] which is given a value in the model code of 3×10^{10} m^{-1}; the specific cake resistance α, [ALPHA] initialized to a value of 3×10^{13} m/kg; the filtrate viscosity μ, [MU], set at 0.001 kg/ms; and the transmembrane pressure ΔP [DP] set at 1×10^5 kg/ms^2. The initial concentration C_0 [C0] is set at 1 g/L and the membrane area A is set at 0.002971 m^2.

The flux J is defined using Equation 5-2. The flux is dependent on the mass of cake per unit membrane area [M], while all other parameters are fixed.

The mass balance for the reservoir is outlined in Equation 5-1. The initial reservoir volume V_{R0} [VR0] is set at 7×10^{-4} m^3. The reservoir volume is initialised to this value [INIT(VR)=VR0] and the equation describing the change in the reservoir volume V_R with time is written [D/DT(VR) = IF(VR>0) THEN –A*J ELSE 0].

The change in concentration over time is incorporated into the model using Equations 5-7 and 5-10 where Equation 5-7 describes dC/dt when the reservoir is not empty, and Equation 5-10 describes dC/dt when the reservoir is empty. The concentration is initialised to C_0 [INIT(C) = C0]. Equations 5-7 and 5-10 are

164

written as [D/DT(C) = IF(VR>0) THEN 1/V0*(C0*A*J - C*A*J + K*A*M) ELSE 1/V*K*A*M]

The change in cake mass per unit membrane area with time is included with the mass being initialised to zero, i.e. no particles on the membrane [INIT(M)=0]. Then the cake formation rate is written as [D/DT(M)=C*J-K*M].

The permeate (filtrate) volume V_P is included in the model for completeness. While the feed reservoir has liquid in it, the filtrate volume at any point in time will be the initial reservoir volume minus the reservoir volume at that point in time (as the stirred cell volume is constant until the reservoir has emptied). When the feed reservoir is emptied, the filtrate volume will be the initial volume of the reservoir plus the initial volume in the stirred cell minus the volume in the stirred cell at that time point [VP = IF(VR>0) THEN VR0-VR ELSE V0-V+VR0].

The model is compiled by pressing the Run button on the Equations Window, as indicated below.

Figure 5-2: Screenshot of Equations Window in Berkeley Madonna

This generates plots automatically of each parameter against time (Figure 5-3). It is possible to view all of the parameters together, separately, or in different combinations.
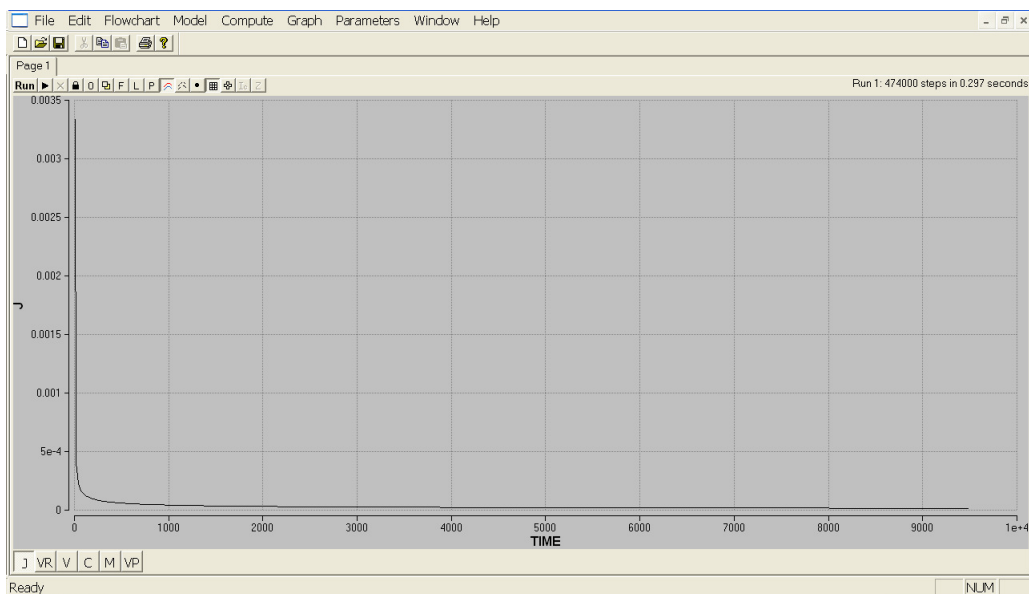
Figure 5-3: Screenshot of Predicted Flux versus Time

The initial flux decline is very rapid as is expected, followed by a period of slow flux decline. This is similar to the experimental results presented in Chapter 4. The reservoir volume decreases with time as filtration continues, until the point where the reservoir is empty (Figure 5-4). From this point onwards, the filter cell is operating in true batch mode.
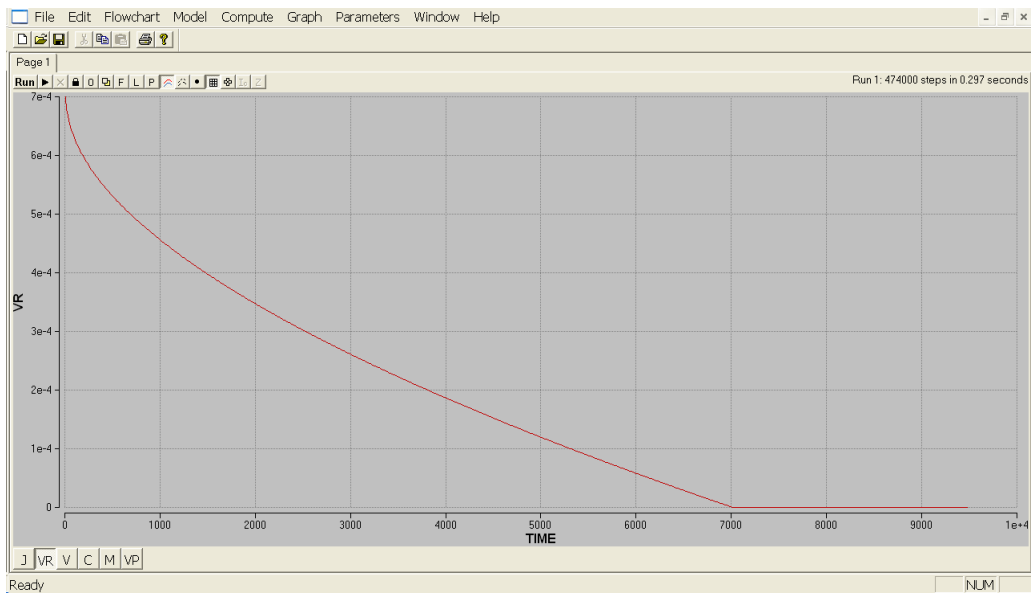
Figure 5-4: Predicted Reservoir Volume versus Time

When the reservoir has emptied, the filter cell starts to empty, operating in true batch mode as mentioned previously (Figure 5-5).
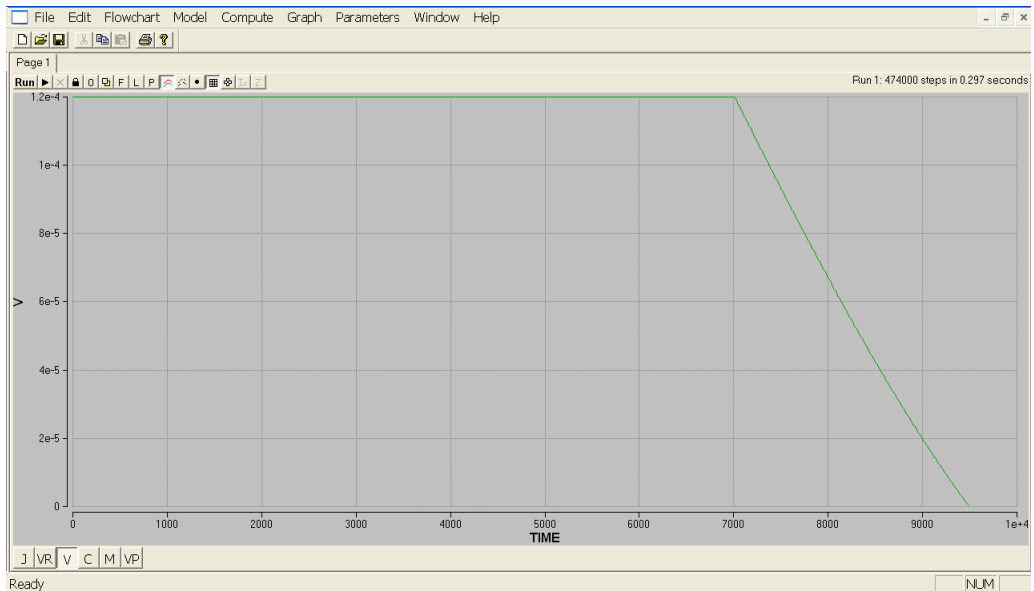
Figure 5-5: Predicted Filter Cell Volume versus Time

The concentration in the filter cell increases slowly over the course of filtration while the reservoir volume is greater than zero. When the reservoir volume has emptied and the cell is operating in true batch mode, there is a rapid increase in concentration, going to infinity as the volume of liquid in the cell goes to zero (Figure 5-6).
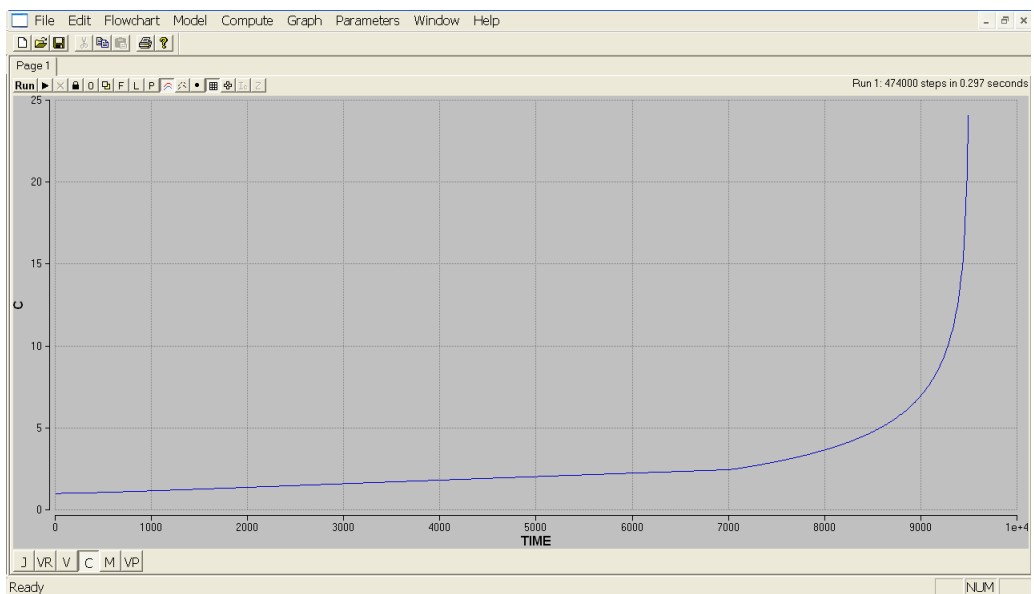
Figure 5-6: Predicted Concentration in Filter Cell versus Time

168

The mass of particles per unit membrane area increases over the course of the filtration as expected. The increase is faster as the filter cell itself is emptying in batch mode (Figure 5-7).
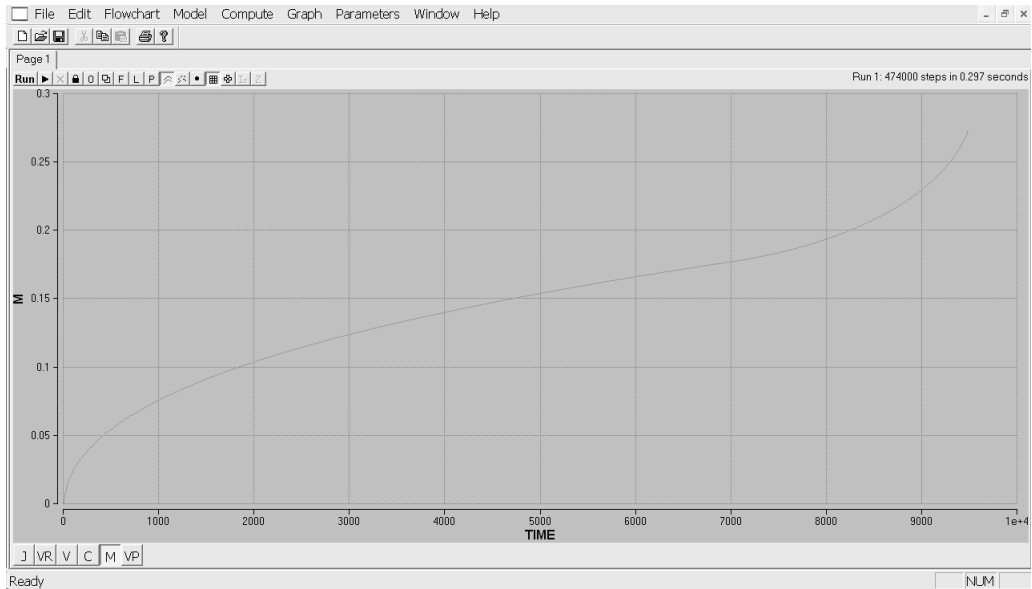
Figure 5-7: Predicted Mass of Particles per Unit Area of Membrane versus Time

The filtrate volume increases as filtration continues as expected, until all of the initial feed in the reservoir and stirred cell has been collected (Figure 5-8).
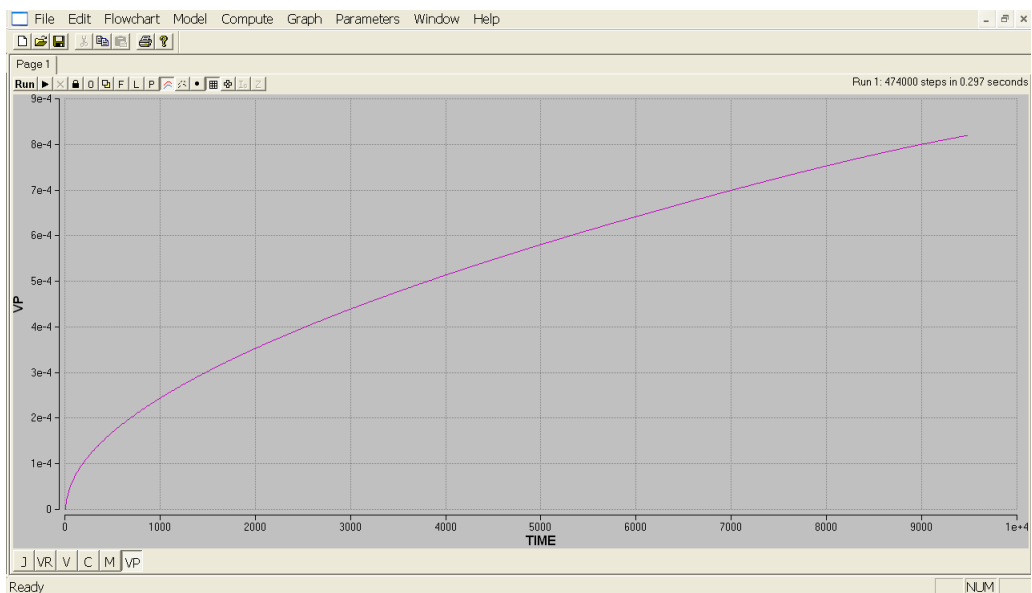
Figure 5-8: Predicted Filtrate Volume versus Time

169

5.2.2.2 Curve Fitting to Experimental Data

As mentioned previously, after the model has been compiled it is possible to set individual parameters for each experiment using the Parameter Window, and then run the model using these parameters without having to recompile the model completely. The parameter window may be seen in Figure 5-9.
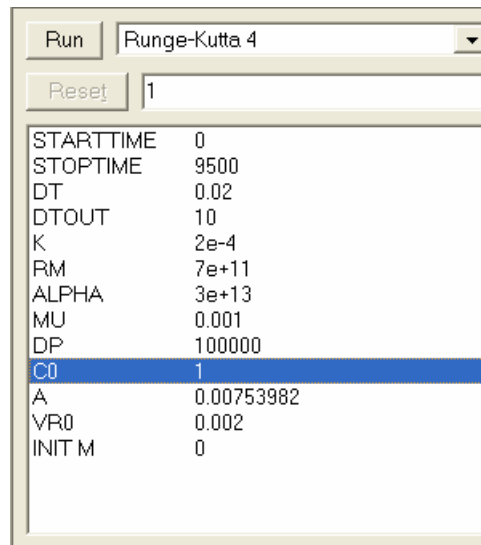
Figure 5-9: Parameter Window

Each parameter outlined in the model is shown, and it is possible to set a value relating to each experimental run. The experiments investigated here are the same as those outlined in Chapter 4. A star is shown beside each parameter that has been altered from the value used initially in the model development.

Once the appropriate parameters have been set in the Parameter Window, the model is run. The curve fitting function may then be used to fit the model to experimental data.

In this study, the parameters of interest are the cake removal constant, k, and the specific cake resistance, α.

Using the curve fit function, the parameters that are to be changed to fit the model to the experimental data may be selected, and a dataset to be modelled may be imported (Figure 5-10).
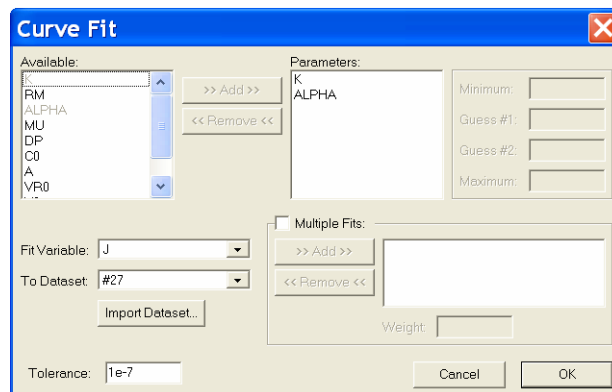
Figure 5-10: Selection of Model Parameters for Curve Fitting

All constants in the model except for k and α are fixed. The variable to be fitted to experiment is chosen as the flux. The experimental data to be imported is in the form of a text file with a column for time and a column for flux. A tolerance for convergence is set to 1e-7, which implies that the parameters are computed to 7 significant figures.

The model is then fit to the experimental data by automatically varying the values of k and α. The output from the curve fitting is a plot of both the model and the experimental data. The data may be viewed in table form. This may be copied and pasted into an Excel spreadsheet and R^2 values and confidence intervals for the slope and intercept of the regression equation of the model fit to the experimental data can then be found using the Data Analysis toolkit.

171

After the model has been fit to the experimental data, the Parameter Window displays the values of k and α that optimise the fit (Figure 5-9).

5.2.3 Experimental Values of Specific Cake Resistance

Measurement of the specific cake resistance in crossflow systems is generally problematic as it involves a direct measurement of the cake mass (McCarthy *et al.* 2002b). This is unlike dead-end filtration where cake mass can be inferred from the filtrate volume. In Chapter 3, experimental runs were performed in which the flux was measured as a function of time until such time as the reservoir and stirred cell were emptied. A useful consequence of this experimental set-up is that the cake mass at the end of the run is equal to the total amount of solids in the initial suspension.

The specific resistance, α is then calculated for each set of operating conditions by rearranging the classic equation describing filtration processes (Equation 1-2) to give

$$\alpha = \frac{1}{m}\left(\frac{\Delta P}{\mu J} - R_m\right)$$ [5-11]

where

$$m = \frac{V_0 C_0}{A}$$ [5-12]

and V_0 is the initial suspension volume.

This experimental value of α may then be compared with the value for α found using the curve fitting function in Berkeley Madonna. Trends in the values of α for varying experimental parameters may also be investigated.

5.3 Results and Discussion - Stirred Cell System

5.3.1 Curve Fitting of Model to Experimental Data and Comparison with Experimental Values for α

The model development and the curve fitting using Berkeley Madonna are described in Section 5.2. The model is fit to the experimental data collected as outlined in Chapter 3. The cake removal constant k and the specific cake resistance α are optimised to ensure a good fit of the model to the experimental data. In this section, the resulting values of k and α are analysed and the α values found are compared with specific cake resistances measured directly from the experimental data.

The model was found to fit the data well in all cases with the lowest R^2 value 0.7 and the highest 0.97. The lower R^2 values are due to noise in the data and to the model over-predicting the flux at the earliest time points. The lower R^2 values are mostly at high pH (10.4), where a faster flux decline is predicted by the model than exhibited by the experimental data.

The α and k values are determined by fitting the model to the experimental flux data and are analysed to ascertain whether there is good agreement with experimental α values and whether there are trends in k that may lend some

insight into the physical characteristics of the system. Values reported are for the most part the average of three experimental runs except where stated and the variability reported is the standard deviation expressed as a percentage of the average.

Increasing the initial concentration from 0.5 to 2 g/L (at ΔP of 0.2 bar and u of 0.09 m/s) leads to a decrease in the cake removal constant k from $3.4\text{x}10^{-3} \pm 38$ % to $1.26\text{x}10^{-3} \pm 10$ % s^{-1}. For a crossflow system, the increased suspension concentration leads to a more viscous suspension, which should lead to increased shear stress at the cake or membrane surface, which should lead to increased removal (i.e. a higher k). However in the stirred system, the increased viscosity may mean that the fluid flow is slower at higher concentrations at this rotational speed, leading to a decrease in k. The increase in initial concentration is seen to lead to a small increase in specific cake resistance, from $5.4\text{x}10^{13} \pm 14$ % to $6.2\text{x}10^{13} \pm 14$ % m/kg. Traditional filtration theory indicates that specific cake resistance is not dependent on suspension concentration and it is found experimentally that α is essentially constant at $1.8\text{x}10^{13}$ m/kg. Since the difference between the two α values determined using the model prediction is small (10 %) which is less than the variability in the values (14 %) it is reasonable to conclude that the model predicts that the specific resistance is independent of suspension concentration.

Both experiment and model exhibit a power law relationship for the specific cake resistance with applied pressure (Figure 5-11 - $C_0 = 0.5$ g/L, $u = 0.09$ m/s, pH 9), in agreement with conventional filtration theory for non-microbial suspensions (McCarthy *et al.* 1998a; McCarthy 2001).

174
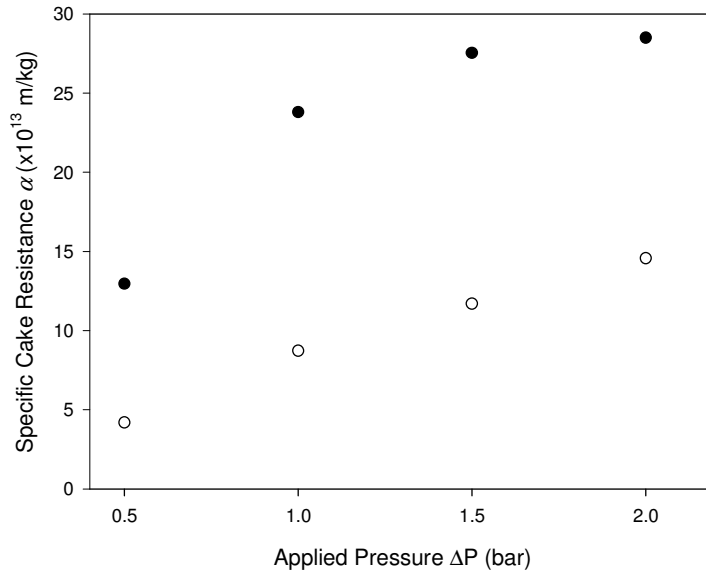
Figure 5-11: Effect of *ΔP* on *α* ○ Experiment; ● Model

The magnitude of the specific resistance is over-estimated by the model in all cases and the exponents of the power law models are different for the model prediction and experiment, the model prediction being to the power of 0.59 (with an R^2 value of 0.92) and the experimental value for the exponent being 0.90 with an R^2 value of 0.99. This is in good agreement with the exponent of 0.83 found previously (Choe *et al.* 1986; Gourgues *et al.* 1992).

The cake removal constant *k* was found to be essentially independent of pressure with a mean value of $2.75 \times 10^{-3} \pm 20 \%$ s^{-1} (The slope of a plot of *k* versus *ΔP* was insignificantly different from zero at the 95 % confidence level).

The increase of stirring speed has shown to lead to a decrease in the experimental specific cake resistance. Some theory suggests that the specific cake resistance should increase with increasing shear in the system due to the preferential deposition of small particles (Baker *et al.* 1985; Lu and Ju 1989). A possible

explanation for the findings of this study is that as the crossflow is increased, thinner cakes of bentonite are formed. Thus it might be expected that the pressure drop across the cake decreases as the crossflow velocity is increased. For a compressible cake, this could result in the specific cake resistance decreasing with crossflow velocity. It is difficult to say if this effect is significant in these experiments as to work out cake pressure drop accurately, it is necessary to know the membrane resistance at the end of the run (recalling that $\Delta P_c = \Delta P - \mu R_m J$). To do this, fouling of the membrane must be quantified which was not the case in these experiments.

Another possible reason for this decrease in the specific cake resistance is shear-induced agglomeration of bentonite. Shear induced agglomeration is a phenomenon that has been investigated for many types of suspension, from particulate non-colloidal suspensions (Chimmili *et al.* 1998), aqueous polymeric suspensions (Banerjee 2005), thixotropic alumina (where the shear induced agglomeration is shown to account for time-dependent changes in the apparent viscosity (Lemke *et al.* 1999) and for aqueous bentonite suspensions (Bekkour *et al.* 2005). An increase in shear in the system could lead to increased particle/agglomerate size and a resulting decrease in specific cake resistance.

Further work could include investigation into the structure of cakes of bentonite formed under different shear conditions in order to elucidate the mechanism of specific cake resistance reduction with stirring speed. SEM (scanning electron microscopy) or other in-situ methods of observation of the cake structure have been used with success for many different types of cakes and would be a useful tool in understanding the mechanisms of cake formation with bentonite (Flynn *et*

176

al. 1990; Wakeman 1994; Tarleton and Hancock 1996; Li *et al.* 1998; Mores and Davis 2001; Li *et al.* 2005).

In contrast to the consistent effect of stirrer speed on the experimental specific cake resistance, the model-derived values of α show no discernible dependence on stirrer speed (Figure 5-12 - C_0 = 0.5 g/L, ΔP = 0.5 bar, pH 9), and were also over-estimated.

Similarly, while one would have expected to cake removal constant to increase with increasing stirrer speed, curve fitting shows that k increases initially from $2.6 \times 10^{-3} \pm 30 \%$ s^{-1} to $1.7 \times 10^{-2} \pm 33 \%$ s^{-1} and then remains essentially constant as the stirring speed is increased from 0.09 to 0.18 and 0.31 s^{-1} (Figure 5-12).
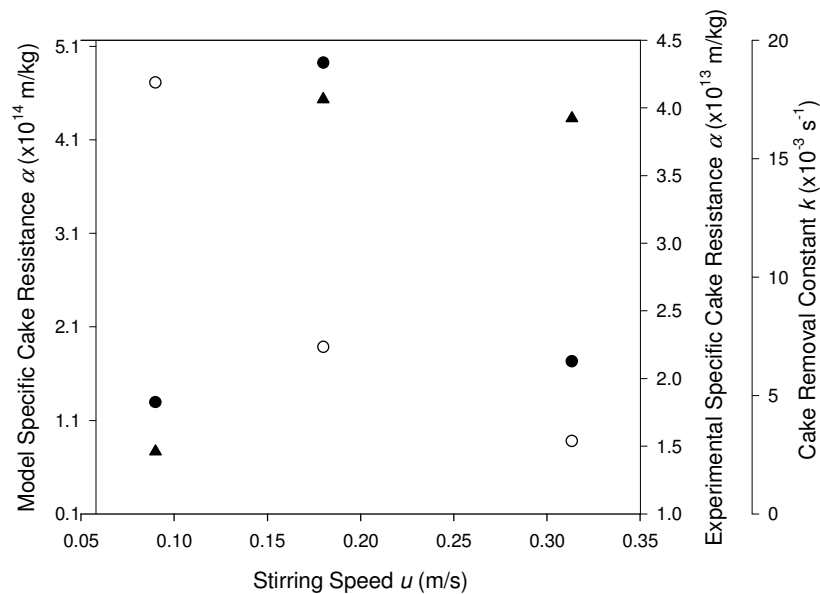
Figure 5-12: Effect of Stirring Speed on α (○ Experimental; ● Model); and k (▲)

The effect of pH is, as expected, a complex one. The specific cake resistance is seen to be at a minimum for pH 7 and a maximum for pH 10, mimicking the trend exhibited in the experimental data (Figure 5-13 - C_0 = 0.5 g/L, ΔP = 0.5 bar, u =

0.09 m/s). Again, however, the specific cake resistance is over-estimated by an order of magnitude ($\times 10^{14}$ instead of $\times 10^{13}$ m/kg). A similar trend is seen in the cake removal constant k (s^{-1}).
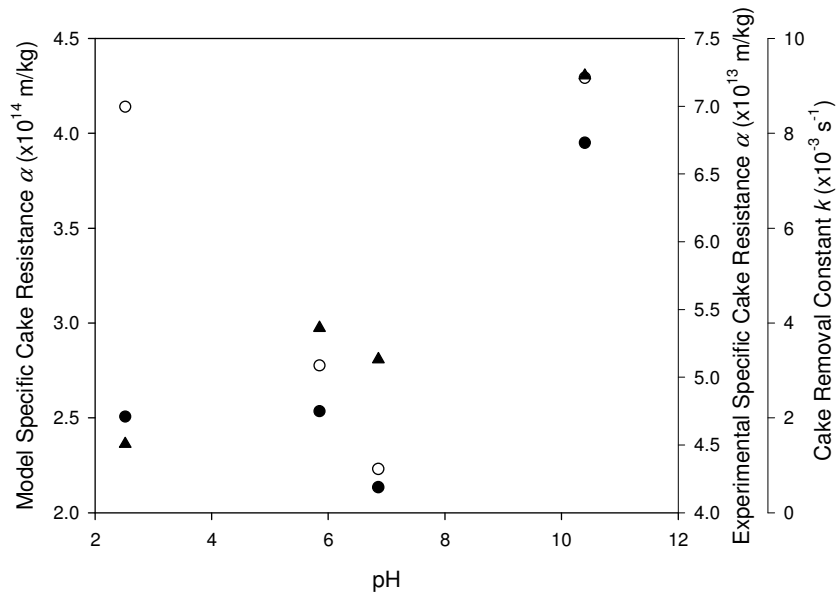
Figure 5-13: Effect of pH on α ($\circ$ Experimental; $\bullet$ Model); and k ($\blacktriangle$)

5.3.1.1 Variability in the Fitted Value for α

In general, the ability of the model to yield realistic values of the specific cake resistance is poor and this begs the question as to whether the model itself is fundamentally flawed. It is worth noting, however, that the computed value of α proves to be extremely dependent on the initial flux measured experimentally, leading to a lack of reproducibility in the values of specific resistance determined from the Berkeley Madonna model - the higher the initial flux, the lower the value of alpha that is computed. This may be observed in the case of two duplicate

experiments, each performed at 0.5 bar, 1 g/L, stirrer speed of 0.09 m/s, pH of 10.4 and R_m of 5.1×10^{10} m^{-1} (Figure 5-14). The flux data is very reproducible however for one experiment a slightly higher initial flux is measured. This may be due to experimental differences as the valve to start the permeate flow is opened by hand. The fitted α value for the first run is 5×10^{14} m/kg whereas the fitted value for the other run is 1.5×10^{14} m/kg. This discrepancy would imply that fitted alpha values are highly dependent on the initial rapid flux decline and especially the flux value for the 10 s reading. As this is quite subject to experimental error and general noise in the data, it is questionable whether the computed values for alpha are reliable.
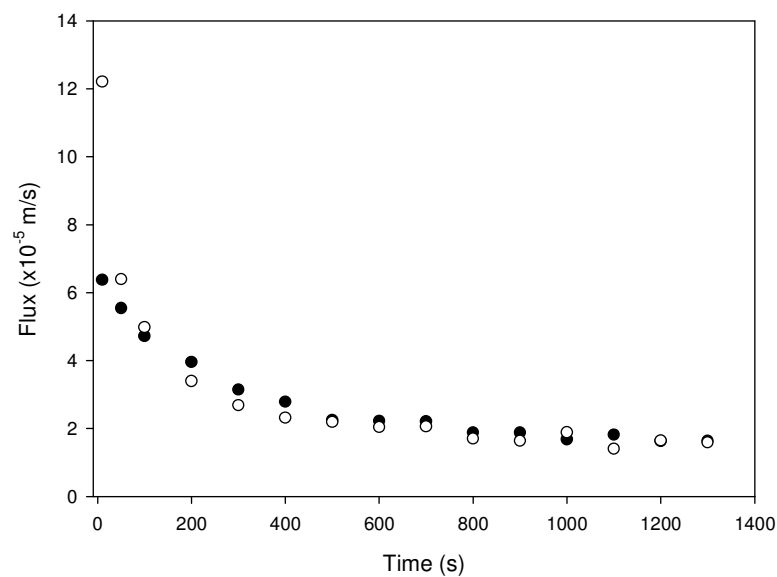
Figure 5-14: Duplicate run comparison:
● α is computed to be 5×10^{14} m/kg; ○ α is computed to be 1.5×10^{14} m/kg

5.3.2 Modifications to Model

Despite the inherent difficulties in evaluating consistent model parameters, the lack of clear trends in model parameters (except in the case of the pressure dependence of α), and the tendency of the model to overestimate the specific resistance, the ability of the model to capture the time dependence of the flux for a given run suggests that further investigation of this basic modelling approach, albeit with some modification, might be useful. In this section an attempt is made to modify the original, essentially empirical, model to take account of physical phenomena that are well known to be relevant in crossflow systems.

Firstly, it is proposed that filtration takes place in dead-end mode until the flux drops below a critical value, at which point cake removal begins, similar to previous experimental findings (Fordham and Ladva 1989; 1992). This concept is described in the next section. The second phenomenon to be incorporated into the model is membrane fouling and this is discussed later.

5.3.2.1 Critical Flux J^*

The model developed in this section contains a critical flux J^*, which is the flux below which cake removal takes place. Consider an isolated particle on the cake or membrane (Figure 5-15):

$$F_f = \eta_f F_N \qquad\qquad F_t = \tau_w \pi d^2$$

$$F_N = 3\pi\mu Jd$$
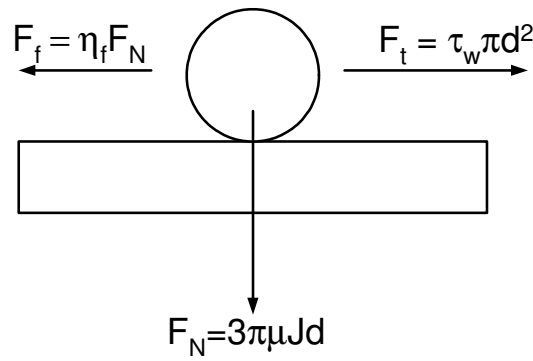
Figure 5-15: Force Balance for J^*

F_t is the tangential hydrodynamic force sweeping the particle off the cake or membrane; where d is the particle diameter and τ_w is the wall shear stress (assumed constant here, i.e. channel narrowing is assumed negligible).

F_N is defined as the normal force dragging the particle onto the membrane/cake, and F_f is the frictional force opposing the tangential force. All other possible forces are neglected.

For the case of a particle in contact with a membrane/cake whose thickness is much larger than the diameter of the particle, the normal drag force has been defined as (Sherwood 1988; Foley *et al.* 1995b)

$$F_N = k\mu Jd\beta^{-2/5} \qquad\qquad\qquad [5\text{-}13]$$

where k is a numerical constant, μ is the filtrate viscosity, J is the filtrate flux, d is the particle diameter and β is a constant defined as

$$\beta = \kappa d^2 \qquad\qquad\qquad\qquad [5\text{-}14]$$

The membrane permeability, κ, is defined by the equation

$$\kappa = \frac{L_m}{R_m}\left(\frac{1 + \delta/L_m}{1 + \alpha m/R_m}\right) \tag{5-15}$$

where L_m is the membrane thickness and δ is the cake thickness.

For a particle to stay on the membrane/cake, the frictional force must be greater than the tangential force ($F_f > F_t$), i.e.

$$3\eta_f J \kappa^{-2/5} > \tau_w d^{1/5} \tag{5-16}$$

where η_f is the coefficient of friction between the particle and the surface beneath it.

Thus a particle will not be removed as long as the flux exceeds the value J^* where

$$J^* = \frac{\tau_w d^{1/5}}{3\mu\eta_f}\kappa^{2/5} \tag{5-17}$$

When the cake resistance is dominant, Equation 5-15 may be written

$$\kappa = \frac{\delta}{\alpha m} = \frac{\delta}{\alpha\rho_p\phi_p\delta} = \frac{1}{\alpha\rho_p\phi_p} \tag{5-18}$$

Where ρ_p is the particle density and ϕ_p is the particle volume fraction in the cake.
Thus

$$J^* = \frac{\tau_w d^{1/5}}{3\mu\eta_f}\left(\frac{1}{\alpha\rho_p\phi_p}\right)^{2/5}$$
[5-19]

Thus J^* would be expected to increase with increasing τ_w, i.e. with increasing crossflow velocity, and to decrease with increasing pressure (as both α and ϕ_p increase with increasing pressure).

5.3.2.2   Modified Model incorporating J^*

As mentioned in the previous section, cake removal by the crossflow will only be effective if the flux is below J^*, the critical flux. Thus the differential equations developed in Section 5.2.1 must be modified to reflect this.

The rate of change of the specific cake mass will be

$$\frac{dm}{dt} = CJ \text{ if } J > J^*$$
$$\frac{dm}{dt} = CJ - km \text{ if } J \leq J^*$$
[5-20]

One of the features of this modified model is that it predicts that cake formation is at least partly irreversible, i.e., if the system is flushed with clean water ($C_0 = 0$) after cake formation, the flux will return to J^* and not J_0. This phenomenon is studied in more detail in Chapter 6.

Using the particle balance for the stirred cell (Equation 5-5) for the change in particle concentration with time depending on whether the reservoir is empty or not and whether cake removal is taking place or not, the relevant mass balances

lead to:

$$\text{When } V_R > 0 \text{ and } J > J^* \text{ then } \frac{dC}{dt} = \frac{AJ}{V}(C - C_0) \qquad [5\text{-}21a]$$

$$\text{when } V_R > 0 \text{ and } J \leq J^* \text{ then } \frac{dC}{dt} = \frac{1}{V}(C_0 AJ - CAJ + kAm) \quad [5\text{-}21b]$$

$$\text{when } V_R = 0 \text{ and } J > J^* \text{ then } \frac{dC}{dt} = 0 \qquad [5\text{-}21c]$$

$$\text{when } V_R = 0 \text{ and } J \leq J^* \text{ then } \frac{dC}{ct} = \frac{kAm}{V} \qquad [5\text{-}21d]$$

5.3.2.3 Membrane Fouling

Fouling is an almost universal feature of the flux decline in microfiltration systems (Belfort *et al.* 1994) and as such, any realistic model should take it into account. Very few models of membrane fouling exist and most simply assume some empirical relationship between membrane resistance and filtrate volume or cake mass (Hermia 1982). In this work, rapid instantaneous fouling is assumed, as more complicated approaches would lead to many model parameters which would be problematic from the point of view of fitting the model to experimental data. Instantaneous fouling would be consistent with surface blocking of the membrane pores by the initially deposited layers of particles.

Instantaneous membrane fouling may be represented by

184

$$R_m = R_{m_0} b \qquad\qquad\qquad\qquad\qquad\qquad\qquad\qquad [5\text{-}22]$$

Where R_m is the membrane resistance after time zero, i.e. the instantaneously fouled membrane resistance; and R_{m0} is the initial clean membrane resistance and b is a constant that will be fitted to the experimental data.

When membrane fouling occurs, the experimentally measured specific resistance is actually an *apparent* specific resistance, measured at the end of a run when all particles have deposited (Foley 1994). This may be related to the true specific resistance, α, by manipulation of the basic flux equation. The flux measured at the end of the run may be represented by the apparent specific resistance α_{app} and the true specific cake resistance α as follows:

$$\frac{\Delta P}{\mu\left(R_{m0} + \alpha_{app}m\right)} = J = \frac{\Delta P}{\mu\left(R_m + \alpha m\right)}$$

Thus $R_{m0} + \alpha_{app}m = R_m + \alpha m$

Rearranging

$$\alpha_{app} = \alpha + \frac{R_m - R_{m0}}{m}$$

Using Equation 5-22:

$$\alpha_{app} = \alpha + (b-1)\frac{R_{m_0}}{m} \qquad\qquad [5\text{-}23]$$

The parameters to be computed from the experimental data are the critical flux J^* (m/s), the cake removal rate, k (s^{-1}), the true specific cake resistance α (m/kg) and the instantaneous membrane fouling constant b. From these, the model apparent specific resistance, α_{app}, can be determined and compared with the experimental value.

The modified model equations may finally be coded in Berkeley Madonna as follows (Model 5-2):

$$\alpha_{app} = \alpha + (b-1)\frac{R_{m_0}}{m}$$

Model 5-2: Modified Model for Stirred Cell with Reservoir

```
METHOD RK4
STARTTIME = 10
STOPTIME=9500
DT = 0.02
DTOUT = 10

K=0.0002
RM0=3E10
B=1.01
RM=RM0*B
ALPHA=3E13
MU=0.001
DP=1E5

JSTAR=5E-5
J=DP/MU/(RM+ALPHA*M)

C0 = 1
A = .002971

VR0=7E-4
INIT(VR)=VR0
D/DT(VR) = IF(VR>0) THEN -A*J ELSE 0

V0=1.2E-4
INIT(V)=V0
D/DT(V) = IF(VR>0) THEN 0 ELSE -A*J

C0=1
INIT(C)=C0
D/DT(C) = IF(VR>0) AND(J>JSTAR) THEN (1/V)*(A*J*(C0-C))
ELSE IF(VR>0) AND(J<=JSTAR) THEN (1/V)*(C0*A*J-C*A*J+K*A*M)
ELSE IF(VR<=0) AND (J>JSTAR) THEN 0
ELSE (A*K*M)/V

INIT(M)=0
D/DT(M)=IF(J>JSTAR) THEN C*J ELSE C*J-K*M

VP = IF(VR>0) THEN VR0-VR ELSE V0-V+VR0

ALPHAAPP = IF(M>0) THEN ALPHA+(B-1)*(RM0/M) ELSE ALPHA
```

The modifications to the original model should give rise to improved insight into the physical characteristics of the trends in the system, and more accurate

approximations to the specific cake resistance measured experimentally.

5.3.2.4 Curve Fitting of Modified Model to Experimental Data

The model development and the curve fitting using Berkeley Madonna are as described previously. The model is fit to the experimental data collected as outlined in Chapter 3. The cake removal constant k, the specific cake resistance α, the instantaneous membrane fouling constant b and the critical flux, J^* are optimised to ensure a good fit of the model to the experimental data. In this section, the resulting values of k, b, J^* and α are analysed and the α values found are compared with specific cake resistances measured directly from the experimental data. Unlike the previous section where the model was fit to the flux data, here it is fit to the original filtrate volume data. Using the volume data eliminates the need for differentiating the data to get the flux, a process that magnifies errors.

The model is seen to be capable of being fitted to the data well in all cases with R^2 values close to 1 and 95 % confidence intervals for the slope and intercepts of a regression line relating the experimental and predicted data spanning 1 and 0 in all cases.

An example of the fit of the model to experimental data is shown in Figure 5-16, where the experimental conditions are: initial concentration 2 g/L, 0.2 bar, 0.09 m/s, pH 9.7 and 21 $^{\circ}$C. The experiments are the same as those outlined in the previous section.
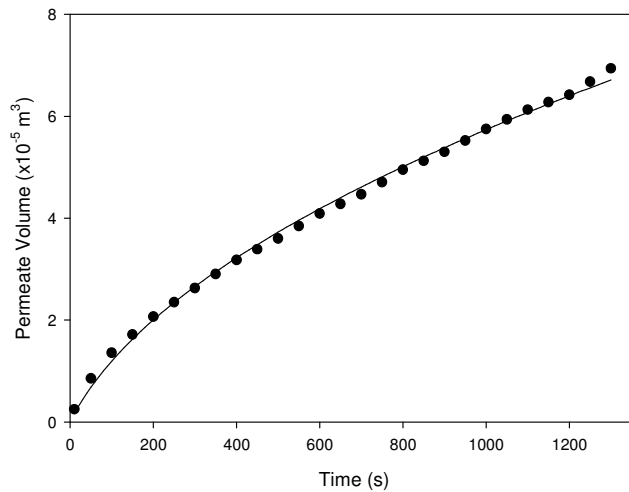
Figure 5-16 – Fit of Model (—) to Experiment (●)

As mentioned previously, the experimentally determined apparent specific resistance α_{app} is essentially constant at 1.8×10^{13} ($\pm$ 6 %) m/kg for an increase in C_0 of 0.5 g/L to 2 g/L. As discussed previously, the value for α computed from the model may be converted to an apparent specific resistance for comparison using Equation 5-23. The apparent specific resistance calculated from the computed value for α, the instantaneous membrane fouling constant b, and the initial membrane resistance, is seen to increase slightly from 2×10^{13} ($\pm$ 20 %) to 3.9×10^{13} ($\pm$ 13 %) m/kg. This computed increase in the specific cake resistance

with concentration clearly does not agree with experiment.

The cake removal constant k was found to be concentration dependent, increasing from 9.15×10^{-6} ($\pm$ 12 %) to 1.68×10^{-5} ($\pm$ 58 %) s^{-1} over the range studied. It is difficult to ascertain whether this is a true trend for the data or not due to the high level of variability in the computed values for k. However an increase with concentration would be in agreement with an increase in τ_w due to increased suspension viscosity, which would make removal more efficient.

The instantaneous membrane fouling constant b increases from 5.86 ($\pm$ 15 %) to 10.88 ($\pm$ 45 %) indicating a greater degree of instantaneous membrane fouling with increasing initial concentration. Variability in the values of b computed is high, again making it difficult to say that this represents a trend in the data.

The critical flux, J^*, shows a slight increase from 6.26×10^{-6} ($\pm$ 22 %) at a concentration of 0.5 g/L to 6.85×10^{-6} ($\pm$ 67 %) m/s at a concentration of 2 g/L. The variability found in the fitted values for J^* are high and as such it is difficult to say whether this represents a trend.

The effect of pressure on the computed value of the apparent specific cake resistance correlates well with the experimentally measured α values, where a regression on the experimentally measured and model values gives an R^2 value of 0.88 (Figure 5-17).

The experimentally determined α_{app} values obtained in this study lead to a

relationship of $\alpha_{app} = 8\text{x}10^{13}\Delta P^{0.9}$ while the fitted model relationship is $\alpha_{app} = 1\text{x}10^{14}\Delta P^{0.61}$ (ΔP in bar, Figure 5-17 - $C_0 = 0.5$ g/L, $u = 0.09$ m/s, pH = 9). This is in reasonable agreement with previous studies on bentonite filtration where the exponent found was 0.83 (Choe *et al.* 1986; Gourgues *et al.* 1992). Variability in the fitted values of α are higher than the unmodified model when averaged over 4 experimental runs, ranging from 17 % for 1.5 bar to 37 % for 1 bar, in contrast with variability ranging from 10 % - 26 % with the unmodified model. The exponent for the power law relationship is slightly closer to the experimentally determined value with the modified model at 0.61 in contrast to the original model which gave an exponent of 0.59. It is worth noting that the magnitudes of the specific resistances obtained by fitting the modified model are much closer to experiment than with the previous, unmodified model.
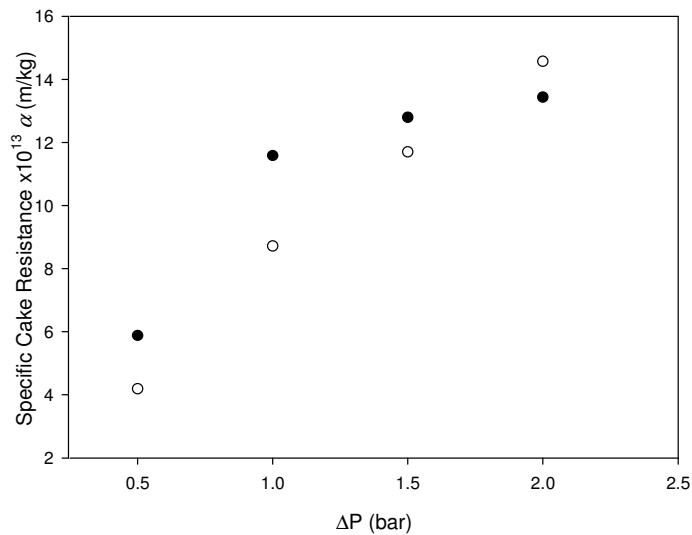
Figure 5-17: Effect of *ΔP* on *α*ₐₚₚ ○ Experiment; ● Model

The fitted values of the cake removal constant k, instantaneous membrane fouling constant b and critical flux, J^*, all increase with applied pressure up to 1.5 bar (Figure 5-18 - $C_0 = 0.5$ g/L, $u = 0.09$ m/s, pH = 9). A decrease is then seen for the 2 bar experiment. This may be an experimental discrepancy, however, as the experiment at 2 bar was performed only once. Variability in the values fitted averaged over up to 4 experimental runs are high in all cases, at up to 33 % for the cake removal constant k, 36 % for the instantaneous membrane fouling constant b, and 93 % for the flux below which cake removal occurs, J^*.
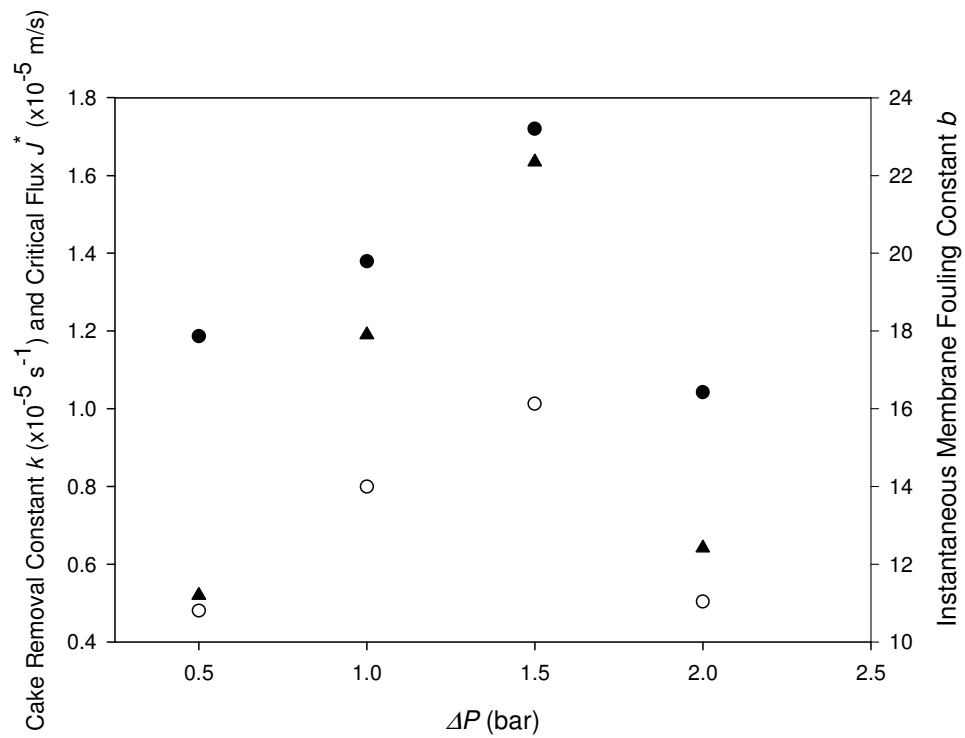
Figure 5-18: Effect of ΔP on k (●) J^* (○) and b (▲)

The decrease in the specific cake resistance with increasing stirring speed found experimentally is predicted well by the model (Figure 5-19 - C_0 = 0.5 g/L, ΔP = 0.5 bar, pH = 9).
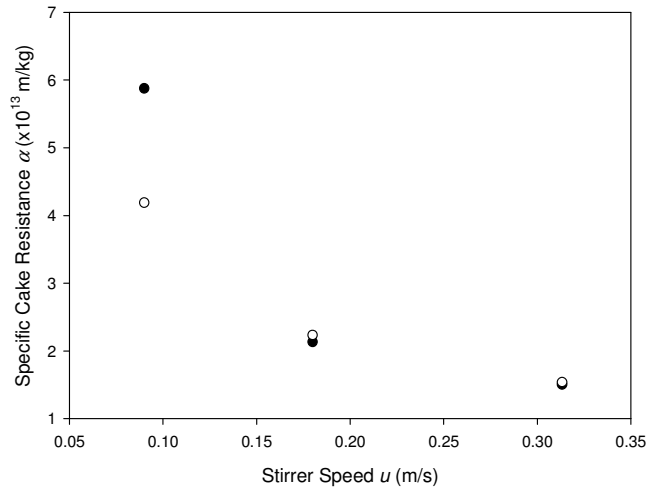
Figure 5-19: Effect of u on α_{app} ○ Experiment; ● Model

The model performs better at high stirring speeds. Variability in the computed values of α_{app} ranges between 3 and 24 %. The original model did not predict the decline in specific cake resistance with stirring speed.

It would be expected that the cake removal constant k would increase with stirring speed however this trend is not apparent in the computed values, with k initially decreasing from 1.2×10^{-5} ($\pm$ 33 %) to 1.1×10^{-5} ($\pm$ 17 %) s^{-1} as the speed is increased from 0.09 m/s to 0.18 m/s, and then increasing to 1.5×10^{-5} ($\pm$ 64 %) s^{-1} as the speed is increased further to 0.31 m/s.

The instantaneous membrane fouling constant b does not exhibit a clear trend with increasing stirring speed, increasing from 11 ($\pm$ 36 %) to 21 ($\pm$ 21 %) and then decreasing to 18 ($\pm$ 11 %) as the speed is increased, however there is no reason to suppose that instantaneous fouling would be dependent on stirrer speed.

The critical flux, J^* is seen to exhibit an increase from 4.8×10^{-6} ($\pm$ 93 %) to 8.54×10-6 ($\pm$ 48 %) and to 8.64×10^{-6} ($\pm$ 32 %) m/s with stirring speed, however variability is so high that it is difficult to say if this is a significant trend. However, an increase in J^* would be consistent with the force balance model (Equation 5-19) as J^* is proportional to the wall shear stress, which should increase with stirring speed.

The trends in α with pH are approximated well by the model, although the specific cake resistance is over-estimated for all pHs, most notably at pH of 2.5. However the trend of a decrease in α with pH from 2.5 to 7 followed by a sharp increase for a pH of 10 is captured well by the model (Figure 5-20 – C_0 = 0.5 g/L, ΔP = 0.5 bar, u = 0.09 m/s). Variability in the computed value of α_{app} is as much as 35 % and up to 17 % for the experimentally determined values, averaged over up to 3 experimental runs. No discernible trends are seen in the other fitted model parameters.
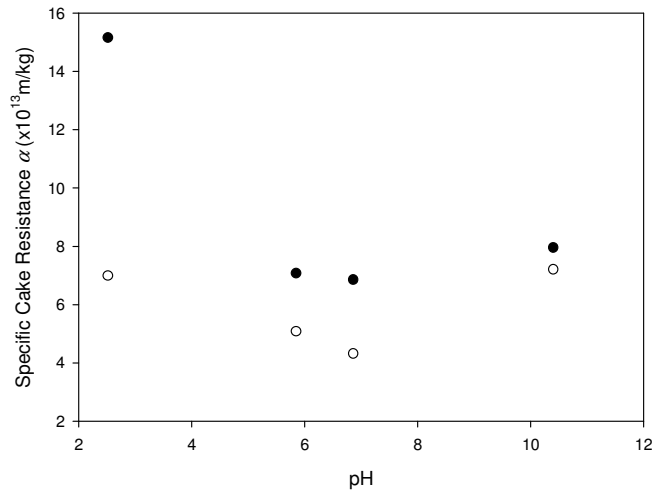
Figure 5-20: Effect of pH on α_{app} ○ Experiment; ● Model

To conclude this section, it can be said that the modified model is capable of fitting experimental data with greater accuracy than the original model presented, with R^2 values of close to 1 in all cases. Experimental trends in the specific cake resistance with transmembrane pressure, stirring speed and pH are found to be predicted well by the modified model, although the magnitude of the specific resistance is still over-predicted in many cases.

There is a general lack of expected trends in the other model parameters (k, b and J^*) and the run-to-run variability in the predicted values of these parameters is high in many cases. However, the predicted values rely heavily on initial fluxes measured which may be subject to high experimental variability due to the experimental set-up.

As described previously the batch crossflow system used in Chapter 4 is a more

widely used configuration industrially. As the ceramic membrane used in the batch system is re-used for each experimental run and is more robust than the membranes used in the stirred cell, it is hoped that the experimental data in the batch crossflow system may be more reliable, especially at early times. In the next section, the modified model developed here is applied to the batch ceramic crossflow filtration data first presented in Chapter 4.

5.4   Model Development and Solution - Batch Crossflow System

The batch crossflow filtration system is described in detail in Chapter 4. As the permeate is collected, the volume of feed in the tank decreases, while the concentration of particles, which are retained by the membrane, increases (Figure 5-21).
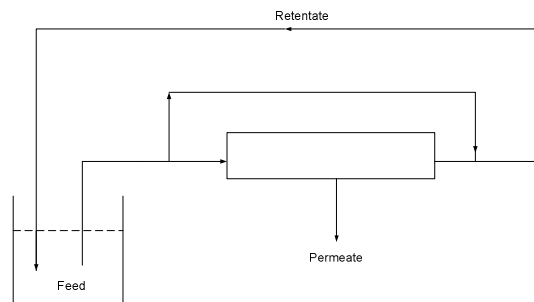
Figure 5-21: Schematic of Batch Crossflow Filtration Setup for Modelling Purposes

Mass balances for the system are combined with the use of the simple equation used to describe the cake build-up previously for the stirred cell system, in order to generate a functional model of the system behaviour. This system is very

similar to the stirred cell system; however, it does not have the added complication of a two-compartment setup. The modified analysis developed in the previous section is also employed here.

5.4.1 Mass Balances

The particle balance for the system may be represented mathematically by

$$\frac{d}{dt}(VC) = -A\frac{dm}{dt} \qquad\qquad [5\text{-}24]$$

where C is the solids concentration in the feed tank and V is the volume in the feed tank at time, t,

Similarly the rate of depletion of volume from the feed tank should equal the permeate flowrate through the membrane

$$\frac{dV}{dt} = -AJ \qquad\qquad [5\text{-}25]$$

It is assumed that the cake forms in the manner outlined in Section 5.2.1.

$$\text{For } J > J^* \text{ then } \frac{dm}{dt} = CJ$$
$$\text{For } J \leq J^* \text{ then } \frac{dm}{dt} = CJ - km \qquad [5\text{-}26]$$

These equations can then be combined to give

$$\text{For } J > J^* \text{ then } \frac{dC}{dt} = 0$$

$$\text{For } J \leq J^* \text{ then } \frac{dC}{dt} = \frac{Akm}{V}$$

[5-27]

5.4.2 Modelling using Berkeley Madonna

The mass balances are coded in Madonna as described previously (Model 5-3) where it should be noted that instantaneous membrane fouling is again included.

Model 5-3: Batch Crossflow

```
METHOD RK4
STARTTIME = 0
STOPTIME=9500
DT = 0.02
DTOUT = 10


K=0.0002
RM0=7e11
B=1.01
RM=RM0*B
ALPHA=3e13
MU=0.001
DP=1E5


JSTAR=5e-5
J=DP/MU/(RM+ALPHA*M)

C0 = 1
A = 7.539822e-3

VR0=2e-3
INIT(VR)=VR0
D/DT(VR) = -A*J

INIT(C)=C0
D/DT(C) = IF(J>JSTAR) THEN 0 ELSE A*K*M/VR

INIT(M)=0
D/DT(M)=IF(J>JSTAR) THEN C*J ELSE C*J-K*M

VP = VR0-VR

ALPHAAPP = IF(M>0) THEN ALPHA+(B-1)*(RM0/M) ELSE ALPHA
```

The model is fit to the batch filtration data outlined in Chapter 4 in the manner discussed in Section 5.2.2.2.

5.5   Results and Discussion - Batch Crossflow System

The model is found to fit experimental permeate volume data well, with R^2 values close to 1 in all cases. A typical fit is depicted in Figure 5-22 where this figure shows permeate flux data with experimental conditions C_0 of 0.5 g/L, ΔP of 100 kPa, u of 0.235 m/s, pH 7 and 21°C.
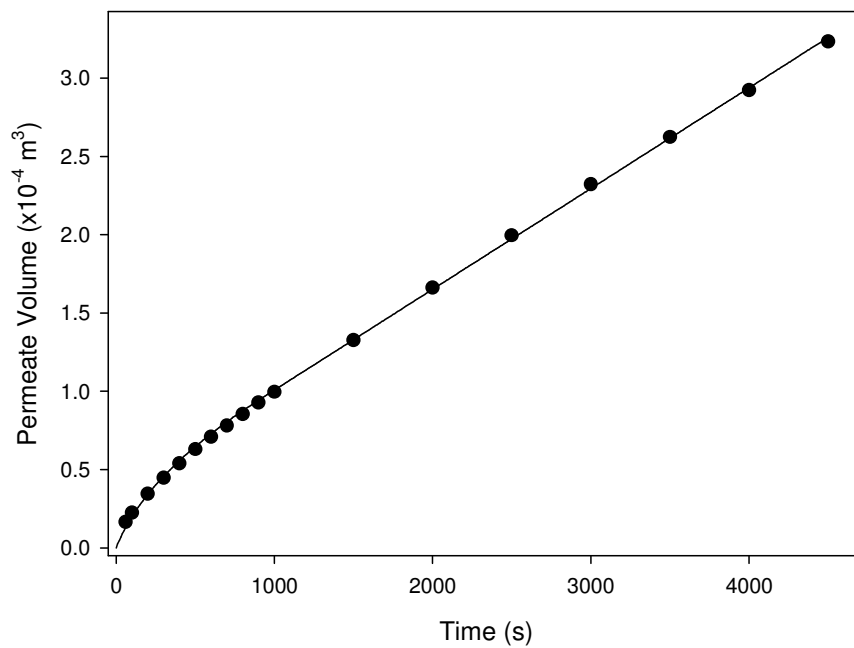
Figure 5-22: Fit of Model (──) to Experiment (●)

By differentiation of the permeate fluxes predicted by the model, flux decline

patterns in the data are found to be approximated well by the model, matching the behaviour discussed in Chapter 4. However, fitting of the model to experimental data does not give much insight qualitatively or quantitatively into the mechanisms of the system. The computed model parameters are as outlined in Table 5-1.

Table 5-1: Model Parameters

Run	C_0 (g/L)	pH	u (m/s)	T (°C)	ΔP (kPa)	R_m (x10^{11} m^{-1})	α (x10^{14} m/kg)	k (x10^{-3} s^{-1})	b	J^* (x10^{-4} m/s)
1	0.5	7	0.24	21.0	100	7.43	10.9	4.25	5.12	0.06
2	0.5	7	0.47	21.0	100	7.36	18.1	1.64	2.89	5.20
3	0.5	7	0.59	21.0	100	7.44	7.10	3.10	5.67	0.09
4	1.0	7	0.47	21.5	100	7.85	18.8	2.00	5.67	2.71
5	5.0	7	0.47	21.5	100	7.62	26.0	1.51	9.50	23.0
6	0.5	3	0.47	20.5	100	7.45	54.8	0.48	1.00	15.3
7	0.5	7	0.47	20.5	100	7.36	8.75	1.83	5.38	1.99
8	0.5	9	0.47	20.5	100	7.30	6.62	1.28	6.11	1.03
9	0.5	11	0.47	20.5	100	7.30	9.07	1.13	9.42	1.64
10	0.5	7	0.47	21.0	60	7.46	2.85	0.77	4.42	0.10
11	0.5	7	0.47	21.0	80	7.46	2.46	0.38	6.09	0.27
12	0.5	7	0.47	21.0	120	7.29	11.0	1.77	5.82	0.59
13	0.5	7	0.47	10.0	100	7.32	31.3	7.87	2.17	3.93
14	0.5	7	0.47	20.0	100	7.36	7.38	1.34	6.16	0.78
15	0.5	7	0.47	32.0	100	7.25	1.03	0.34	7.49	0.14

The magnitude of the specific cake resistance values is such that it is likely that they are overestimated, as was found in the stirred cell analysis. The trends in the alpha values are also not as expected. In particular, the pressure dependence of the

specific resistance does not follow power law behaviour. Furthermore, there is no clear effect of crossflow velocity on specific resistance.

The other model parameters do not fare any better, with cake removal constants showing a clear trend only for temperature (decreasing k with increasing temperature). Instantaneous membrane fouling constants b are shown to increase with initial feed concentration and applied pressure, show no trend with increase in crossflow velocity (decreasing and then increasing) and increase with pH and temperature. The critical flux, J^* exhibits a decrease with initial feed concentration, increases with applied transmembrane pressure, and shows no clear trend with crossflow velocity, pH or temperature. In contrast, the force balance model, summarised in Equation 5-19, would predict that J^* decreases with increasing pressure (as it is inversely proportional to α and ϕ_p, the particle volume fraction in the cake) and increases with u, as J^* is proportional to τ_w, and be inversely proportional to μ. The prediction of the effect of concentration on J^* is difficult as this depends on the viscosity of the suspension. Increased concentration leads to a higher suspension viscosity, and increased viscosity leads to a higher wall shear stress – however greater shear in the system leads to a decreased suspension viscosity for a shear-thinning fluid. More in-depth rheological studies would be necessary to quantify the effect of increasing suspension concentration on J^*, however a decrease in J^* with concentration indicates that the increased suspension viscosity due to concentration is the

dominant effect, with the changes in τ_w playing a lesser part.

There may be several possible explanations as to why the model works better for the stirred cell experiments than for the ceramic membrane experiments. However the most likely explanation is that of changing flow regimes in the crossflow system.

Reynolds numbers for the ceramic system, (based on an approximation of the dilute bentonite suspension as having Newtonian water-like characteristics) range from 1400 – 3500. For the ceramic system, the seeming lack of trends in the model parameters may be due to the transition between flow regimes as the crossflow is increased. Most experiments are performed at a crossflow velocity of 0.47 m/s which corresponds to a Reynolds number of 2820. Most researchers would agree that the onset of laminar flow in a circular pipe occurs at a Reynolds number of approximately $2.3x10^3$ however this number would of course be affected by the wall conditions in the circular pipe – in the case of the ceramic membrane, the build-up of cake on the walls of the membrane and the changing surface of the cake may lead to differences between experimental runs in the flow regime established, since the crossflow velocity yields a Reynolds number so close to the theoretical transitional value.

However, treating the bentonite suspension as a Newtonian fluid may be a gross over-simplification – as the fluid is Non-Newtonian its viscosity within the membrane system will depend on the shear conditions specific to the membrane

configuration.

Previous investigations into the rheological characteristics of aqueous bentonite suspensions have shown pseudoplasticity (Khandal and Tadros 1988; Sohm and Tadros 1989) and experimental studies have confirmed that aqueous bentonite suspensions in the concentration range used in this study exhibit pseudoplastic behaviour, with the flow behaviour index of approximately 0.83 which is independent of bentonite concentration for the range of concentrations investigated. (Previous studies for concentrated bentonite suspensions have indicated n values of 0.3 (Jiao and Sharma 1994) however this value is found for suspensions to the order of 40 g/L). The fluid consistency index K increases with concentration, the relationship being characterised well (with an R^2 value of 0.9989 for the range of concentrations in this study) by the equation

$$K = 0.0112 C^{0.6515}$$
[5-28]

A method of determining the Reynolds number for thixotropic pseudoplastic flow in straight pipes (Honey and Pretorius 2000) may be used to give some idea as to whether the flow is laminar or turbulent (Frost 1982)

$$\mathrm{Re} = \frac{\rho u D}{K \left[\dfrac{3n+1}{4n} \right]^{n} \left(\dfrac{8u}{D} \right)^{n-1}}$$
[5-29]

where D is the pipe diameter. The critical Reynolds number beyond which

turbulent flow is established may be determined using

$$\text{Re}_{crit} = \frac{6464n}{(1+3n)^2 \left[\dfrac{1}{2+n}\right]^{\left(\frac{2+n}{1+n}\right)}}$$
[5-30]

The critical Reynolds number is calculated to be 2200. Using the experimentally determined values for n and K outlined previously, and using a density for aqueous bentonite suspensions of between 2000 and 3000 g/L (Brunton 1988; Doneva *et al.* 1997) it may be shown that the flow is laminar for the lower crossflow velocity used, 0.235 m/s and turbulent for the 0.47 and 0.5875 m/s crossflows for 0.5 g/L. In the case of concentration, where it is to be expected that the density would increase with suspension concentration, the more concentrated the suspension the lower the Reynolds number. Thus by approximating a suspension density between 2000 and 3000 g/L the flow regime for 0.47 m/s will be turbulent for 0.5 g/L and laminar for 5 g/L, whereas it is uncertain whether the flow will be laminar or turbulent for 1 g/L. This transition from turbulent to laminar flow for 5 g/L may explain the model prediction of a constant specific resistance for 0.5 and 1 g/L but a much higher specific resistance for 5 g/L.

The Reynolds number for flow of a pseudoplastic fluid in a stirred tank may be calculated using

$$\text{Re} = \frac{N^{2-n}d^2\rho}{K}$$
[5-31]

Where N is the stirring speed (s^{-1}), and d is the impeller diameter (m). This leads to Reynolds numbers in the range 3400 – 15000, indicating turbulent flow in all cases for the stirred cell. Laminar flow in a stirred vessel would only be achieved at very slow impeller rotational speeds.

Changing flow regime would be expected to affect the predicted values of the model parameters. Laminar flow would be expected to have a lower cake removal constant than turbulent and this effect may be seen for example in the case of increased initial concentration in the ceramic system (Figure 5-23), where the flow is laminar for an initial concentration of 5 g/L and turbulent for concentrations of 0.5 and 1 g/L at $\Delta P = 100$ kPa, $u = 0.47$ m/s, T = 21°C and pH of 7.
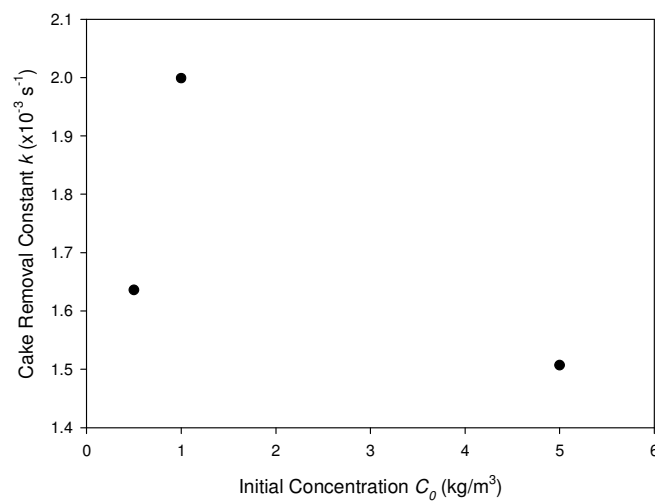
Figure 5-23: Effect of Flow Regime on Cake Removal Constant

Further work may include the investigation of the effect of rheological properties

of bentonite suspension on crossflow filtration characteristics and development of a mathematical model taking the flow regime into account, incorporating more detailed experimental rheological studies.

5.6 Conclusions and Further Work

In this chapter, a number of mathematical models for stirred and ceramic membrane crossflow microfiltration of bentonite were developed. The models combine classical filtration theory with mass and particle balances for the specific systems in question, incorporating a simple equation for calculation of the change in specific cake mass with time. Solving of the differential equations generated for each system allow the evolution of the flux (or permeate volume) with time to be assessed.

A basic model developed for stirred filtration is found to over-estimate the specific cake resistance when compared to experimentally determined values. A modified model is developed in which the idea of a critical flux above which cake removal (by stirring or crossflow) does not take place. This model also takes into account instantaneous membrane fouling, where the membrane is assumed to be irreversibly fouled by contacting with the bentonite suspension.

This modified model is found to give reasonable approximations to the experimentally determined values of the specific resistance. The most notable trend in the specific cake resistance is that of a decrease with increasing crossflow

velocity. It is proposed that this phenomenon, which is contrary to traditional filtration theory which would predict the opposite behaviour, is due to shear-induced agglomeration of the bentonite particles, and increased crossflow velocity leading to thinner cakes. The model parameters (cake removal constant k, instantaneous membrane fouling constant b and critical flux J^*) are also fitted by the model and are found to exhibit expected trends in some cases, however run-to-run variability makes it difficult to say if these are true trends or not.

This same model is applied to batch crossflow filtration data. It would be expected that similar results would be obtained, however although the model fits flux decline data well, the specific cake resistance is largely overestimated and this and other model parameters were not found to follow consistent trends. This finding may be at least partly due to the changing flow regimes in the system due to increasing suspension concentration and crossflow velocity.

This modelling approach has been shown to be somewhat useful in the estimation of the specific cake resistance for the stirred system and in the prediction of sensible trends in some cases for model parameters that give some insight into the physical characteristics of the stirred and ceramic systems. The modified model has also incorporated irreversibility and it is proposed that this may be used to give some idea as to the fouling mechanisms in the ceramic system.

Further work may include the investigation of the effect of rheological properties of bentonite suspension on crossflow filtration characteristics and development of

207

a mathematical model taking the flow regime into account, incorporating more detailed experimental rheological studies.

This chapter has suggested that incorporating irreversibility, either in terms of cake formation and/or membrane fouling is a necessary part of a model to describe crossflow microfiltration. The goal of Chapter 6 is to provide further insight into irreversibility during ceramic membrane crossflow microfiltration of bentonite suspensions.

CHAPTER 6: Studies on Irreversibility in Cake Formation and Flux Decline in Continuous Crossflow Microfiltration of Bentonite

6.1 Introduction

The models presented in this research have encompassed neural network models and semi-empirical models based on simultaneous cake deposition and removal for stirred and ceramic membrane crossflow microfiltration of bentonite. While the empirical models are only partly successful in fitting to experimental data, they did raise the issues of membrane fouling and irreversible cake formation. The latter phenomenon, in particular, has not been addressed previously in the literature. The objective of this chapter was to carry out further studies on irreversibilities in crossflow microfiltration using continuous ceramic membrane filtration of bentonite as a model system. In particular, the aim was to design experiments that will test whether the models developed in the previous chapter do in fact represent reality.

A continuous crossflow filtration set-up is utilised in this chapter in order to eliminate the modelling complications arising from the changing bulk suspension concentration that characterises the batch system in the previous chapter. The continuous crossflow set-up is thus simpler in nature and should allow attention to

be more focused on addressing the various phenomena contributing to flux decline in the system.

Theoretical studies in continuous crossflow microfiltration and associated fouling mechanisms have been the subject of considerable research. Crossflow microfiltration systems have been found in general to be susceptible to fouling (Tarleton and Wakeman 1993; 1994) that may be reversible or irreversible. Reversible fouling may be composed of particle build-up on the cake/membrane surface which may be removed by flushing with clean water whereas irreversible fouling must be removed by some other method, chemical cleaning being the most widely used (Scott 1995; Mulder 1996). Application of CFMF to industrial processes can be limited by fouling, as cleaning of the membrane module may render a process unviable economically – cleaning is costly in terms of downtime and loss of product. Much research has focused on the development of methods to eliminate fouling such as the critical flux concept (Field *et al.* 1995). This is defined slightly differently to the critical flux used in this thesis as it represents the initial flux below which no particle deposition occurs. Other methods include periodic reversal of the direction of the tangential flow (Howell *et al.* 1993), reversal of the direction of filtrate flow, i.e., backflushing (Tanaka *et al.* 1995; Redkar *et al.* 1996), pulsation of the feed stream (Czekaj *et al.* 2000b; Mores and Davis 2002) and production of centrifugal instabilities such as Dean and Taylor vortices (Moulin *et al.* 1996; Czekaj *et al.* 2000b; Moll *et al.* 2007).

This chapter will again focus on the development of a semi-empirical balance to

describe continuous crossflow microfiltration of bentonite. However, the key aim here is to shed light on irreversibilities caused by irreversible cake formation and membrane fouling. Experiments involving the flushing of module with pure water are designed and interpreted in light of the model developed.

6.2   Model Development and Solution

A schematic of the experimental configuration for modelling purposes is presented in Figure 6-1. This configuration, known as total recycle mode, is an excellent approximation to a true continuous system. Mass balances for the system are combined with a simple expression for cake build-up in order to develop a model describing the system in a manner similar to that outlined in Chapter 5.
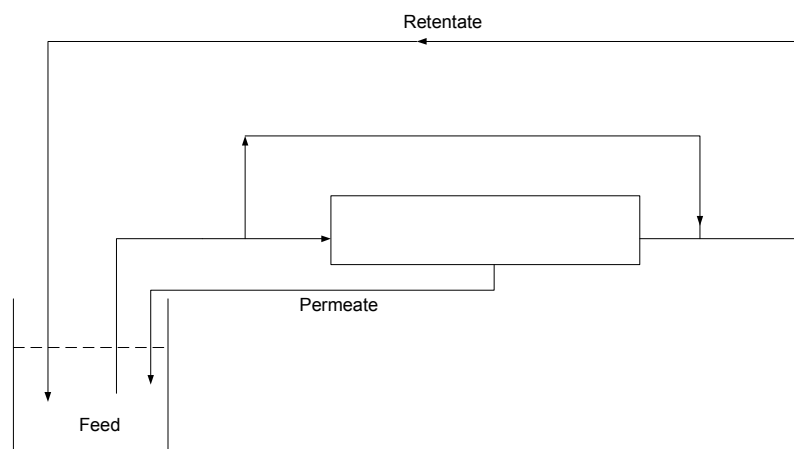
Figure 6-1: Schematic of Continuous Crossflow Filtration Operation

The filtrate flux is defined using the classic equation for flux based on Darcy's

211

Law as mentioned previously:

$$J = \frac{\Delta P}{\mu(R_m + \alpha m)}$$

[6-1]

The cake formation rate (or, rate of accumulation of particles on the membrane surface) may be assumed to be equal to the rate of deposition of particles on the membrane surface minus the mass of particles per membrane area multiplied by some cake removal rate, k, where this depends on the crossflow velocity. As described in Chapter 5, the cake is assumed to be removed only when the flux drops below a certain critical level, J^*. This may be represented mathematically as follows:

$$\frac{dm}{dt} = CJ \text{ if } J > J^*$$
$$\frac{dm}{dt} = CJ - km \text{ if } J \leq J^*$$

[6-2]

where C is the constant bulk concentration of particles in the feed stream.

Membrane fouling is a common feature in flux decline in filtration systems. This is taken into account here in a similar manner to that employed in Chapter 5, using the idea of instantaneous membrane fouling where the membrane is subject to initial deposition of layers of particles on the surface of the membrane blocking the membrane pores. This may be described by

$$R_m = R_{m_0} b \qquad\qquad\qquad\qquad [6\text{-}3]$$

where b is the instantaneous fouling constant, R_m is the instantaneously fouled membrane resistance and R_{m0} is the original clean membrane resistance.

Assuming that at steady state in continuous filtration (t_{ss}), the cake mass is m_{ss} and the feed is replaced with an infinite reservoir of pure water (i.e. no increase in feed concentration as the cake is flushed off the membrane). In this case the model becomes

$$\text{For } J < J^* \qquad \frac{dm}{dt} = -km \qquad\qquad\qquad [6\text{-}4a]$$

$$\text{For } J > J^* \qquad \frac{dm}{dt} = 0 \qquad\qquad\qquad [6\text{-}4b]$$

Thus the model predicts that the cake mass will decrease exponentially with respect to time during flushing. If membrane fouling is irreversible and $J^* < bJ_0$, the model predicts that some of the cake will remain on the membrane and the flux will recover to J^*. Likewise if $J^* > bJ_0$, all of the cake (bar the initial layer bound to the membrane and causing blockage of the pores) will be removed and the flux will recover to bR_{m0}.

In reality, the feed reservoir used in this study is not infinite, and the concentration in the feed tank increases during the course of the flushing process. The concentration is constant for the filtration phase, zero at the start of the

flushing phase, and then increases by the amount of bentonite that is flushed off

the membrane surface.

If $t < t_{flush}$ $C = C_0$ [6-5a]

If $t = t_{flush}$ $C = 0$ [6-5b]

If $t > t_{flush}$ $\dfrac{dC}{dt} = \dfrac{Akm}{V_R}$ [6-5c]

Where t_{flush} is the time at which the flushing phase is started, C_0 is the initial

(constant) concentration at the start of the filtration phase, A is the membrane

area, k is the cake removal rate, m is the mass of particles per unit membrane area

and V_R is the volume of the feed reservoir.

The parameters to be computed from the experimental data are the critical flux, J^*,

the cake removal rate, k, the specific cake resistance α and the instantaneous

membrane fouling constant b. The equations may be coded and fit to the

experimental data using Berkeley Madonna as described previously and the model

code may be seen in Model 6-1. This code models both the filtration and flushing

phases.

Model 6-1

```
METHOD RK4
STARTTIME = 0
STOPTIME=70000
DT = 0.02
DTOUT = 10


K=0.0002
RM0=7E11
B=1.01
RM=RM0*B
ALPHA=3E13
MU=0.001
DP=1E5
C0=5
TFLUSH=7200


JSTAR=5E-5
J=DP/MU/(RM+ALPHA*M)


C= IF (TIME<TFLUSH) THEN C0
ELSE IF (TIME=TFLUSH) THEN 0
ELSE X

INIT(X)=0

D/DT(X)=IF (TIME>TFLUSH) THEN (A*K*M)/VR
ELSE 0

A = 7.539822E-3
VR=2E-3



INIT(M)=0
D/DT(M)=if (J>JSTAR) THEN C*J ELSE C*J-K*M
```

6.3 Materials and Methods

6.3.1 Crossflow Filtration Rig

The crossflow rig is as described in Chapters 4 and 5. Here the operation is in continuous mode, i.e. the permeate and retentate streams are both recycled to the feed reservoir, keeping the feed volume constant (Figure 6-1).

6.3.2 Continuous Crossflow Experiments

Experiments are chosen to encompass the effects of feed concentration, crossflow velocity and transmembrane pressure on the filtrate flux. Experiments are duplicated at least once in order to ensure reproducibility.

As it was found in the previous chapter that the flow regime changed from laminar to turbulent during the course of the filtration experiments, the concentration of the feed suspension here is increased in order to assure laminar flow in all cases, with Reynolds numbers of less than 1000 for all experiments (the critical Reynolds number for the system being approximately 2200).

All experiments are performed at pH 3 as this pH is found to give the most marked flux decline in the batch filtration data in Chapter 5, thus producing more interesting data for analysis. The experiments performed are summarised in Table

216

6-1.

Table 6-1: Continuous Crossflow Experimental Runs

Run	C_0 (g/L)	ΔP (kPa)	u (m/s)	T (^{o}C)	R_m ($\times 10^{11}$ m^{-1})
1	5	100	0.47	19.1	6.30
2	5	100	0.47	19.2	6.54
3	5	100	0.47	19.7	6.33
4	5	60	0.47	20.4	8.43
5	5	60	0.47	20.6	7.10
6	5	140	0.47	20.6	6.62
7	5	140	0.47	20.9	6.12
8	5	100	0.47	20.2	8.40
9	5	100	0.24	19.7	6.08
10	5	100	0.24	20.9	7.99
11	5	100	0.71	19.3	6.33
12	5	100	0.71	19.1	7.06
13	10	100	0.47	19.9	7.07
14	3	100	0.47	19.3	7.26

6.3.3 Experimental Procedure

The experimental procedure is similar to that described in Chapter 5 for batch crossflow filtration, the only difference being that the permeate is recycled to the feed vessel.

As mentioned previously (Chapters 4 and 5) ultrapure water is used in cleaning and suspension of the bentonite in order to avoid water fouling of the membrane

(McCarthy 2001). Membrane cleaning is as outlined in Chapter 4. The clean membrane resistance is measured prior to each filtration run and the cleaning schedule is repeated if the clean membrane resistance is not acceptable. The clean membrane resistance is approximately 7×10^{11} m^{-1}.

Bentonite suspensions were made up as described previously. Suspension pH was adjusted to pH 3 in all cases.

6.3.3.1 Crossflow Filtration Operation

A known volume of suspension (2L $\pm$ 0.05L) was placed in reservoir A and set on the stirring table. The filtrate valve V2 was closed and the pressure control valve V3 was fully opened to establish a ΔP of zero. The suspension was allowed to circulate in the system for approximately 2 minutes to ensure thorough mixing of suspension with any residual ultrapure water trapped in the system.

Filtration experiments were carried out for 2 hours in total recycle mode, i.e. with permeate and retentate streams recycled to the feed reservoir. However the first 25 ml of filtrate was collected in batch mode in order to capture more data points during the period of rapid initial flux decline. The volume collected during the initial batch period is sufficiently small so as not to impact on filtration performance. After the initial sample was collected it was returned to reservoir A, and the permeate was directed into Feed Reservoir A using valve V2 (See Figure 4-1). Valve V2 was used to collect filtrate samples throughout the filtration

period. After each sample was collected it was returned to Reservoir A. Flux values were determined by recording the length of time taken to collect a known volume of filtrate (typically sample sizes of 5 – 10 ml).

The transmembrane pressure was controlled using valve V3 and the flowrate of suspension through the module was controlled by adjusting valve V1.

6.3.3.2   Flushing with Pure Water

Prior to flushing, it was ensured that the permeate flux had reached steady state. Steady state flux was established in all cases for the experimental conditions in this study after two hours of filtration.

The hold-up in the system (liquid retained in piping etc) was determined to be approximately 180 ml by allowing the system to drain completely after filtration runs were completed. After each filtration run, the hold-up of bentonite suspension in the system was replaced with ultrapure water by closing the permeate valve and pumping clean water at zero transmembrane pressure and a very low crossflow velocity (approximately 0.05 m/s) into the system until 180 ml of bentonite suspension had been collected and the fluid in the system appeared clear as viewed through the glass on the flowmeter.

The feed was then switched to a 2 L reservoir of clean ultrapure water. The ultrapure water flushing phase for each experiment was carried out at the same transmembrane pressure and crossflow velocity as the filtration phase. Permeate

flux during the flushing phase was measured in the same manner as during the filtration phase, described previously.

6.4　Results and Discussion

6.4.1　Experimental Observations and Fit of Model to Experiment

6.4.1.1　Filtration Phase

As described previously, the effects of feed concentration, applied pressure and crossflow velocity on the permeate flux are assessed. All runs are very reproducible and the averages of at least 2 experimental runs with the same operating parameters are displayed in this section.

The cake removal constant k, the specific cake resistance α, the instantaneous membrane fouling constant b and the critical flux, J^* are optimised to ensure a good fit of the model to the experimental data. The fit of the model to experiment and the resulting values and trends in the parameters of k, b, J^* and α are analysed. The model was found to fit to the flux decline data with excellent accuracy, with R^2 values of close to 1 in all cases.

The effect of increasing feed concentration is to decrease the permeate flux as expected (Figure 6-2 – 100 kPa, 0.47 m/s, pH 3, 20 ^{o}C).
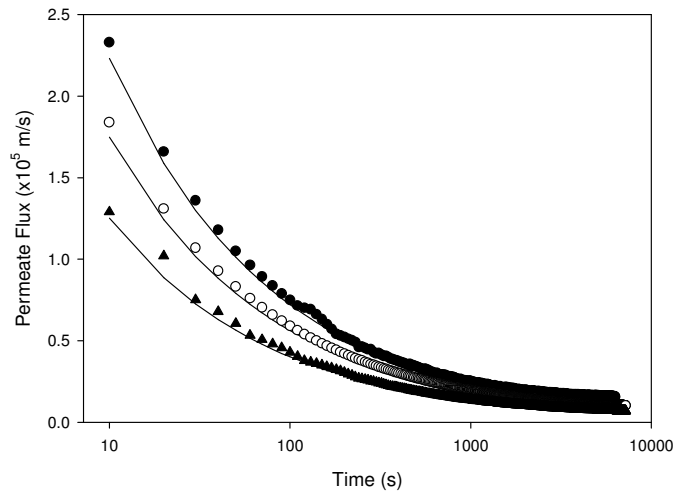
Figure 6-2: Effect of Concentration on Flux Decline
(● 3 g/L, ○ 5 g/L, ▲ 10 g/L, — Model)

An increase in mean transmembrane pressure leads to a corresponding decrease in the filtrate flux (Figure 6-3 – 5 g/L, 0.47 m/s, pH 3, 20 ^{o}C). However the effect of pressure on the filtrate flux is very small due to the compressibility of cakes of bentonite, as found previously in batch crossflow microfiltration of bentonite (Chapters 4 and 5). This phenomenon was also observed by Fordham and Ladva (1989; 1992).
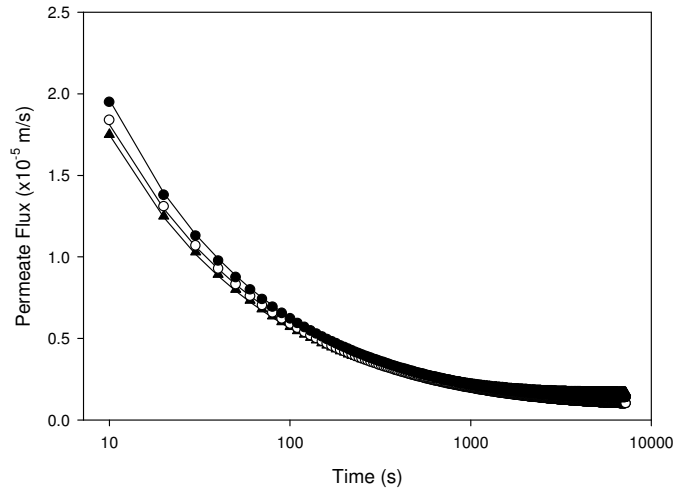
Figure 6-3: Effect of Pressure on Flux Decline
(● 140 kPa, ○ 100 kPa, ▲ 60 kPa, — Model)

The effect of increasing the crossflow velocity is to increase the filtrate flux as expected (Figure 6-4 – 5 g/L, 100 kPa, pH 3, 20 $^{\circ}$C).
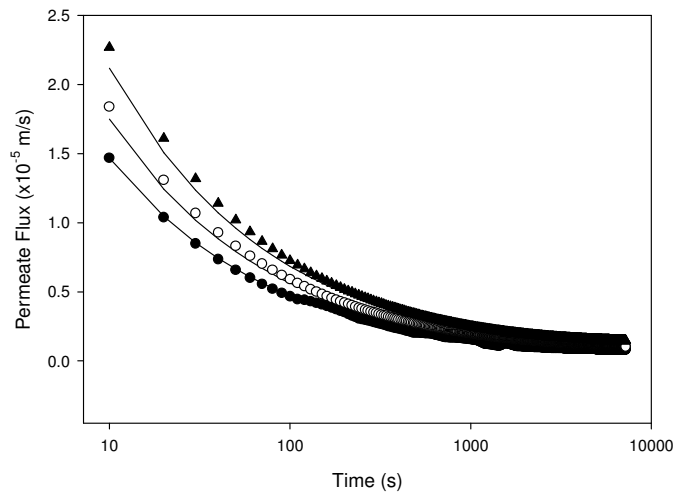

Figure 6-4: Effect of Crossflow Velocity on Flux Decline
(● 0.235 m/s, ○ 0.47 m/s, ▲ 0.705 m/s, — Model)

222

6.4.1.2   Flushing Phase

The model is found to fit poorly to the flushing phase, with low R^2 values. The model predicts that the flux should initially increase during the flushing phase. However, the removable portion of the cake flushed off the membrane is predicted to increase the concentration of the feed stream, thus causing a subsequent decline in flux as particles are re-deposited on the cake (Figure 6-5 – 100 kPa, 0.47 m/s, 20 ^{o}C, pH 3). However, the experimental data is clearly in qualitative disagreement with this as is shown in Figures 6-5, 6-6 and 6-7.
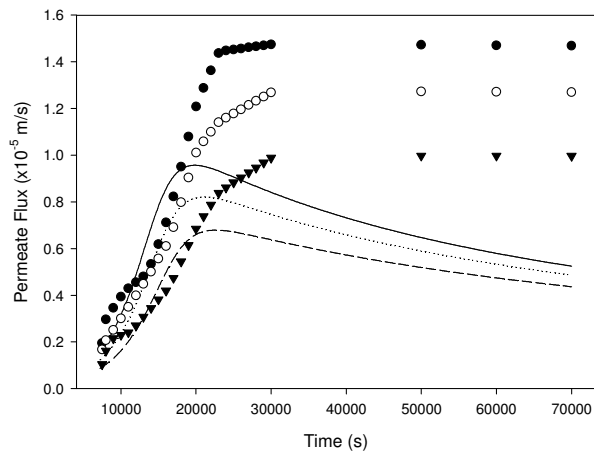
Figure 6-5: Fit of Model to Flushing Phase for Various Values of C$_{0}$

(Lines – Model, Symbols – Experimental)

— ● 3 g/L – – – ○ 5 g/L ⋯ ▼ 10 g/L

Similar disagreement is shown in Figure 6-6 (5 g/L, 0.47 m/s, pH 3, 20 ^{o}C), where the effect of pressure on the flushing phase is shown.
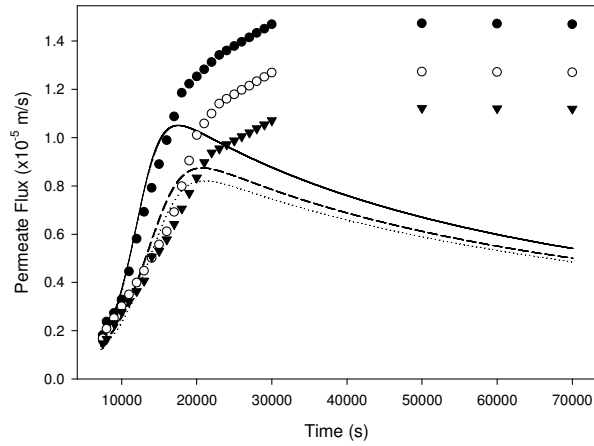
Figure 6-6: Fit of Model to Flushing Phase at Various Pressures
(Lines – Model, Symbols – Experimental)
— ● 60 kPa – – – ○ 100 kPa ⋯ ▼ 140 kPa

Increasing the crossflow velocity causes a corresponding increase in the recovery efficiency (Figure 6-7 – 5 g/L, 100 kPa, pH 3, 20 ^{o}C). Clean membrane fluxes are generally of the order of 10^{-4} m/s, while recovered fluxes are of the order of 10^{-5} m/s.
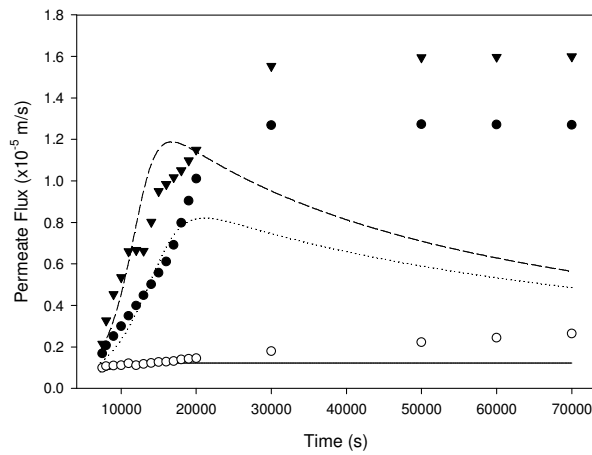

Figure 6-7: Fit of Model to Flushing at Various Crossflow Velocities
(Lines – Model, Symbols – Experimental)
— ○ 0.235 m/s ⋯ ● 0.47 m/s – – – ▼ 0.705 m/s

6.4.2 Trends in Model Parameters

In the last two sections, it was shown that the model fits flux decline data very well but when extrapolated to the flushing phase it gives poor results. For completeness, this section summarises the trends in model parameters as determined from the fits to the filtration phase data. In theory, we would expect more consistent behaviour in the trends as the flow is consistently laminar in these experiments.

The fitted values of the specific cake resistance are found to be essentially independent of concentration for the range of concentrations investigated at $3.21 \times 10^{15} \pm 1.5$ % m/kg. This result is in agreement with established filtration theory and also with experimental measurements of specific cake resistances of bentonite using a stirred cell (Chapter 5). However the order of magnitude of the specific cake resistances predicted by the model is 10^{15} m/kg rather than 10^{13} m/kg as measured experimentally in the stirred cell. Specific cake resistances found by fitting the model in Chapter 5 to batch microfiltration data led to specific cake resistances to the order of 10^{13} m/kg which increased with suspension concentration, however, as discussed previously, flow in the system was turbulent in some cases and laminar in others, and trends in the model parameters may be unreliable.

The cake removal constant k decreased with increasing suspension concentration (Figure 6-8, 100 kPa, 0.47 m/s, pH 3, 20 $^{\mathrm{o}}$C). This is contrary to the result

obtained with the stirred cell, where the cake removal constant was seen to increase with increasing suspension concentration. This result is unexpected as it would be easy to assume that higher concentrations would create a higher viscosity which increases the wall shear stress and thus makes particle removal more efficient.

The critical flux, J^* is also seen to decrease with increasing suspension concentration, which ties in with the experimental finding that flux recovery is more efficient at lower initial feed concentrations (Figure 6-8).

The decrease in k and J^* with suspension concentration may be due to adhesive forces between the membrane and particles which will be discussed in more detail later.
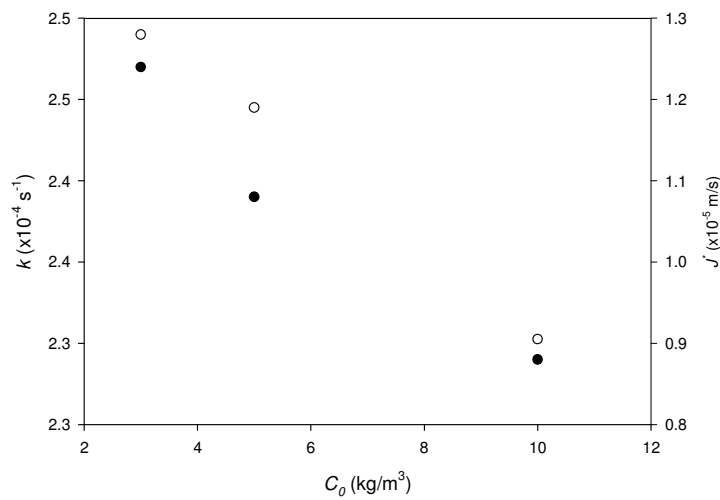
Figure 6-8: Effect of Feed Concentration on k (●) and J^* (○)

The fitted specific cake resistance is found to exhibit a power law type dependence on pressure (Figure 6-9, 5 g/L, 0.47 m/s, pH 3, 20 $^{\circ}$C; R^2 = 0.94):

$$\alpha = 5 \times 10^{13} \Delta P^{0.89} \qquad\qquad\qquad [6\text{-}6]$$

where ΔP is measured in kPa. The exponent is in good agreement with previous studies where an exponent of 0.83 was found (Choe *et al.* 1986; Gourgues *et al.* 1992). However the magnitude of the specific cake resistance is again higher than that found experimentally in the stirred cell and in previous studies.
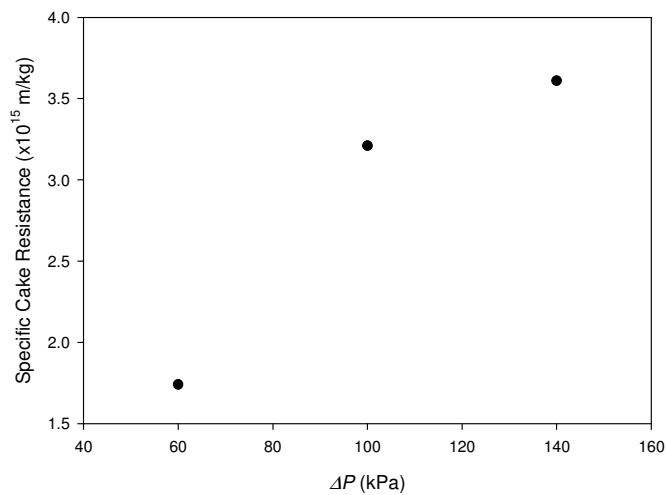
Figure 6-9: Effect of Pressure on Fitted α

Increasing the transmembrane pressure is seen to lead to a decrease in the cake removal constant when the pressure is increased from 60 kPa to 100 kPa and to remain essentially constant when the pressure is further increased to 140 kPa

(Figure 6-10, 5 g/L, 0.47 m/s, pH 3, 20 $^{\circ}$C).

The increase in transmembrane pressure serves to increase J^*, however it would be expected that J^* would decrease with increased pressure according to the force balance analysis outlined in Chapter 5. A reason for this trend may be that the parameters are solved for on the basis of the entire experimental run, incorporating both filtration and flushing phases. As the flux recovers to a higher level during the flushing phase due to the higher driving force for filtration at increased pressure, (Figure 6-6), the solved-for values of J^* may reflect the recovered flux, rather than reflecting a true trend for the filtration phase.
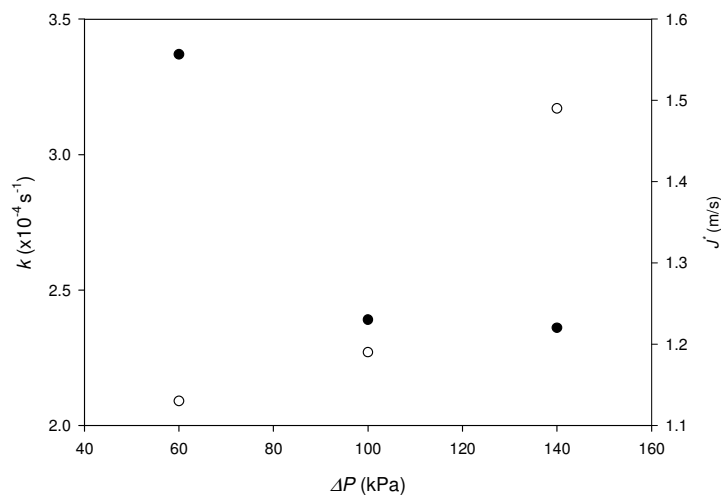
Figure 6-10 – Effect of Pressure on k (●) and J^* (○)

The specific cake resistance is seen to decrease with increasing crossflow velocity (Figure 6-11, 5 g/L, 100 kPa, pH 3, 20°C). This is as found experimentally using the stirred cell set-up in Chapter 5. Traditional filtration theory would indicate that

at higher shear rates, preferential deposition of small particles leads to an increase in specific cake resistance. A number of possible reasons for this discrepancy were raised in Chapter 5, where it was proposed that increased crossflow velocity led to thinner cakes with a corresponding decrease in pressure drop across the cakes, and as the cakes of bentonite are highly compressible (Fordham and Ladva 1989; 1992), this leads to a decrease in α with increased crossflow velocity. It was also proposed that shear-induced agglomeration could contribute to this phenomenon where an increase in shear in the system can lead to an increased particle size and hence a reduced specific cake resistance.
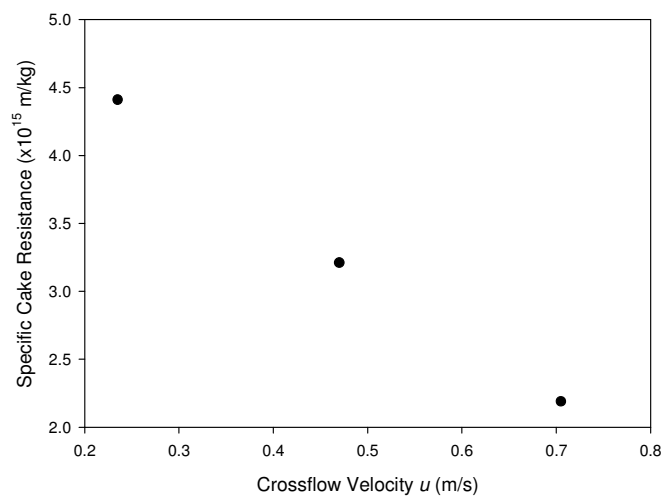
Figure 6-11: Effect of Crossflow Velocity on Fitted α

The cake removal constant k and J^* are seen to increase with increasing crossflow velocity (Figure 6-12). These trends are as expected.
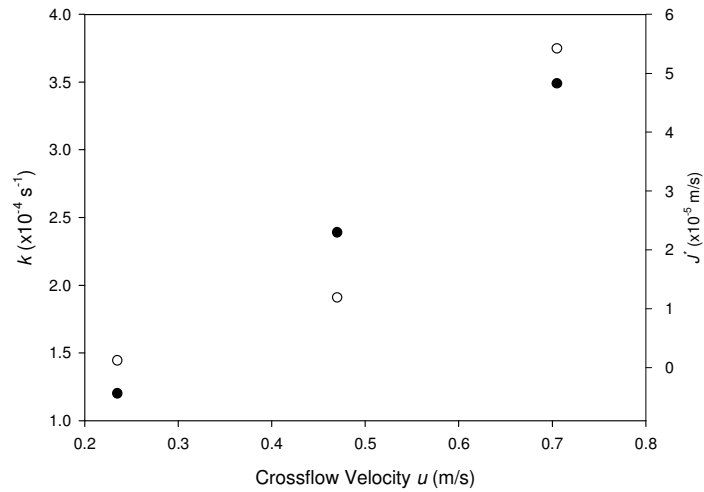
Figure 6-12: Effect of Crossflow Velocity on k (●) and J^* (○)

6.4.3 Membrane Fouling and Irreversible Cake Formation

The model presented in this chapter is capable of representing flux decline in continuous crossflow microfiltration of bentonite well, with sensible trends in the model parameters observed for the most part. In contrast, the ability of the model to fit the flushing phase was found to be poor. However, this poor fit is probably due to experimental error. The transmembrane pressure for the system is controlled manually by manipulation of the valves on the rig. As the flushing portion of the experiments was run overnight, the transmembrane pressure increased in the absence of correction during the flushing portion of the experiment and was re-set to the correct pressure when the rig was manned again. This would explain why the flux did not decline at later times during the flushing phase due to re-deposition of flushed cake.

Irreversibility, either in terms of cake formation or membrane fouling, is a necessary part of a comprehensive model exploring CFMF and an attempt has been made to incorporate this into the model by using the parameter J^* to account for irreversible cake formation. The model developed in this study predicts qualitatively the formation of irreversible cakes however quantitative and qualitative agreement with experimental data for hydraulic cleaning by filtration of ultrapure water is poor.

Although the data for the flushing portions of the experiments is unreliable, the flushing did confirm the irreversibility of cake formation in the system, leading to the consideration of irreversibility phenomena for the system.

Further work should include the development of a control system for the crossflow rig to ensure that operating parameters for the system are kept at the correct levels. Further experimental investigations may include flushing at zero filtrate flux and assessment of irreversibility and model performance under these conditions, in order to provide more information about irreversibilities in the system.

It is interesting to note that for continuous crossflow, the instantaneous membrane fouling constant, b, is found to be equal to approximately 1 in all cases except at a crossflow velocity of 0.235 m/s where $b = 2.1$, for the range of concentrations, pressures and crossflows studied at pH 3 and 20°C. This result is contrary to that found for the batch stirred and crossflow systems investigated in Chapter 5, where

considerable membrane fouling was found to occur. Instantaneous membrane fouling constants were found to be greater than 1 in all cases in fitting of the model to batch crossflow and stirred microfiltration in Chapter 5. Suspension concentration was shown to lead to an increase in the instantaneous membrane fouling constant b for batch crossflow filtration in Chapter 5. For the batch crossflow set-up, filtration of a suspension with concentration 5 g/L at a transmembrane pressure of 100 kPa and crossflow velocity of 0.47 m/s yields a b value of 9.5. A continuous crossflow filtration run for the same experimental conditions yields a b value of 1. The only difference in experimental conditions is the pH – batch crossflow experiments were performed at pH 7 whereas continuous crossflow experiments were performed at pH 3.

Comparing the batch and continuous crossflow experiments mentioned above, the specific cake resistance at pH 3 in continuous crossflow is 3.2×10^{15} m/kg, whereas the batch experiment at pH 7 yields a lower α of 2.6×10^{15} m/kg. Stirred cell experiments at pH 8.5 – 9 showed even lower specific cake resistances, to the order of magnitude of 10^{13} m/kg although there was no experiment performed at exactly the same process conditions for comparison. This lower specific cake resistance would suggest larger particles/aggregates, or higher cake voidage. It is possible that the attractive forces discussed previously at low pH lead to a lower cake voidage, with smaller aggregates, which would lead to a decrease in specific cake resistance. It has been shown previously that under acidic conditions, attractive forces between bentonite particles are dominant, whereas in basic

media, inter-particle interactions lead to a card-house-like structure based on edge to edge, edge to face, and face to face repulsion, instead of attraction (Benna *et al.* 1999).

On the basis of this, it is proposed that the irreversible cake formation of bentonite seen in continuous crossflow filtration of bentonite at pH 3 investigated in this chapter may be due to adhesive or electrostatic forces acting to bind the deposited particles together, a common feature in microfiltration of colloids (Chen *et al.* 2005). Bentonite has been reported to develop opposite charges on the lateral and basal surfaces of the particles leading to attraction at low pHs which would support this theory (Cadene *et al.* 2005). The low pH used for continuous experiments was chosen on the basis of a faster flux decline leading to what was deemed more interesting data for analysis. It is possible that this choice of pH led also to a change in the flux decline mechanism, as the fouling of the membrane by blocking of the membrane pores found for batch crossflow filtration of bentonite at pH 7 (*b*>1) was not predicted for continuous crossflow filtration of bentonite at pH 3.

It is clear from these investigations into the influence of pH on the model parameters that the suspension conditions play a large part in the filtration characteristics and the fouling mechanisms of filtration on bentonite. Further work may include the development of a model incorporating inter-particle interactions that could take into account the effect of pH on the suspension characteristics,

thus reducing the degree of empiricism.

6.5   Conclusions

A mathematical model for continuous crossflow microfiltration of bentonite suspensions is developed based on the techniques outlined in Chapter 5. The model is found to fit flux decline data well for a range of operating parameters, with sensible trends in many cases in the model parameters (specific cake resistance α, cake removal constant k, instantaneous membrane fouling constant b and flux below which cake removal occurs J^*).

Crossflow experiments are extended to investigate the irreversibility of cake formation in the continuous system. Cake formation is found to be partly irreversible; with permeate flux of clean flushing water recovering to a plateau lower than the clean membrane flux. This irreversibility of cake formation is incorporated into the model by the inclusion of the parameter J^*.

The model is found to fit the data well in terms of the filtration phase; however, the cake removal by flushing phase is not well represented by the model. This is attributed to experimental error and the difficulties in maintaining operating conditions constant over long flushing times without the use of a control system for the equipment.

Comparison of fouling mechanisms for batch and continuous filtration show that fouling by surface blocking of membrane pores is predicted in the batch filtration

of bentonite at pH 7 ($b>1$), whereas this effect is not apparent for continuous filtration at identical operating conditions at pH 3, where only irreversible cake formation is observed ($b=1$).

Further work may include a more in-depth analysis of fouling mechanisms in continuous crossflow microfiltration of bentonite and the incorporation of interparticle interactions into the force balance model in order to reduce the degree of empiricism of the model, to work towards a general model for filtration. More information about the irreversibilities in the system may be gleaned from further flushing experiments at zero filtrate flux.

CHAPTER 7: SUMMARY AND FUTURE WORK

7.1   Summary

Development of models to describe characteristics of microfiltration has been the subject of significant research. However, limited applicability of theoretical and empirical models describing flux decline in filtration systems has meant that a general model to predict flux decline remains elusive. This thesis has focused on application of Artificial Neural Networks for empirical modelling of dead-end filtration of yeast, stirred and batch crossflow filtration of bentonite and on the development of semi-empirical models based on simultaneous cake deposition and removal to describe stirred, batch and continuous crossflow of bentonite.

In Chapter 2, a feedforward backpropagation ANN was developed for the correlation and prediction of specific resistance and steady state flux in dead-end filtration of washed yeast cells. Excellent agreement was achieved between the network predictions for specific cake resistance and steady state flux, where the network was trained using 70 % of the available data, and a previously unseen dataset consisting of approximately 25 % of the data. A weight partitioning method was introduced, and used to examine the relative importance of the input parameters on the specific cake resistance and the steady state flux.

In Chapter 3, a novel ANN architecture for dynamic filtration data was introduced, increasing the computational efficiency of the network by eliminating

time as a specific input parameter to the network. This approach allowed examination of the evolution of the relative importance of the input parameters with time in stirred microfiltration of bentonite. Chapter 4 focused on the application of the techniques developed in Chapter 3 to batch crossflow filtration of bentonite in ceramic tubular membranes. Excellent agreement was achieved for both datasets, with one third of the data being used for testing the stirred cell network, and almost two thirds being used in testing the network for the batch crossflow data.

In Chapters 5 and 6, a semi-empirical model to describe flux decline in stirred, batch and continuous crossflow filtration of bentonite based on simultaneous cake deposition and removal was developed, incorporating a cake removal constant based on the Kern-Seaton model for fouling in heat exchangers. Specific cake resistance for cakes formed during stirred microfiltration was measured by filtration of ultrapure water through the cakes. The effects of feed concentration and applied pressure on the specific resistance were as expected, the most interesting result being the decline in specific resistance with increasing stirring speed. The model developed reflected the trends in specific resistance with pressure and stirring speed, although in many cases the magnitude of the specific resistance was larger than that found experimentally. The basic model was extended to address the issues of fouling and irreversible cake formation in the system by inclusion of parameters to account for instantaneous fouling of the membrane and a critical flux below which cake removal takes place. Good

agreement was achieved in the generation of flux decline curves when the model parameters were fit to experimental flux decline data. Trends in the model parameters (k, α, b and J^*) were found to be sensible in most cases for stirred microfiltration, however for the most part no reasonable trends were found in batch crossflow filtration. This result was attributed to changing flow regimes in the system due to increasing concentration and crossflow velocity. Subsequent experimentation in continuous crossflow filtration was restricted to laminar flow at all times, and in general distinct trends in the model parameters were found. However, specific cake resistances found by fitting the model to flux decline data for the crossflow system were much larger than those found experimentally using the stirred cell, and the extension of the model to flushing of the membrane by filtration of ultrapure water proved to be incapable of capturing the flushing dynamics. This was attributed to experimental error due to the difficulties in maintaining constant operating parameters over the course of a long flushing phase, without the use of an automatic control system.

Due to the complex nature of filtration processes, it has proven difficult to quantify the interactions and relationships that exist between process parameters and how they affect filtration characteristics. The wealth of research addressing modelling of filtration systems can attest to this. Modelling of filtration processes has been the subject of much and varied research for half a century, and yet a unifying model or theory to describe or predict flux decline has yet to be developed.

Process models, where they exist, are often the result of lab and pilot scale work, and are generally based on experiments where many of the process parameters are held constant. Apart from the issue of categorising the effects of individual process parameters, identification of the importance of the interactions between process parameters also proves to be a difficult matter, with extensive experimentation required. Empirical models of this type tend to be system-specific, and unable to cope with simultaneous fluctuations in more than one or two key variables at a time, thus making them of little use in an industrial context.

The development of theoretical models requires an in-depth understanding of the physical phenomena associated with a given system. Filtration problems in particular are subject to numerous interactions affecting the characteristics, all of which must be incorporated into a theoretical model for it to be useful. Despite the many years of research into filtration, the factors affecting flux decline including fouling mechanisms, irreversible cake build-up, inter-particle and particle-membrane interactions, coupled with the effects of operator-controlled process parameters remain little understood. Also, existing models describing filtration of a particular system are difficult to extend to filtration of different suspension types due to the differences in interactions – for example, a theoretical model describing filtration of cells must include terms describing phenomena such as the cell morphology and cell wall properties, whereas these terms may be inapplicable to a model describing filtration of incompressible particles, or colloids.

The use of artificial neural networks as an alternative to traditional modelling

techniques has many advantages. From an industrial point of view, development of networks that can be used for process modelling and optimisation requires far less experimentation than that required for the development of traditional empirical models. It has also been shown that the use of weight partitioning methods such as that employed in this work can yield some information about the physical phenomena governing the system.

Dynamic simulations are becoming widely used industrially in training and in selection of potential employees (Jago 2008). Dynamic simulations are mathematical representations of actual plants that can accurately mimic the process conditions of the plant. These dynamic simulations can be based on theory; however development of theoretical models describing an entire plant would be subject to massive experimentation requirements and rigorous understanding of the interactions within the processing plant. It is easy to see that development of an ANN describing an entire plant would be far more cost effective, requiring relatively little experimentation. However, due the unsuitability of ANNs for extrapolation far outside of the parameters of the training data, the use of dynamic simulations based on ANNs in training personnel for major emergency situations in a virtual reality environment may be unreliable.

Although ANNs are a valuable tool for use in quick correlation of data, and have great potential for the design and optimisation of filtration systems, continuing research into the development of theoretical and semi-empirical models is

necessary in order to further understanding of the fundamental basis of filtration behaviour on a universal scale.

7.2   Recommendations for future work

While artificial neural networks have been used in correlation and prediction of specific resistance, steady state flux and flux decline data with excellent accuracy in this work, there remains much potential for extension of this approach.

The use of ANNs as an optimisation tool for a given system should be explored. Steady state permeate fluxes as high as possible would be of great importance industrially, where the main drawbacks to the use of membrane filtration as a separation technique is fouling and flux decline. The minimisation of these phenomena has been the subject of much research particularly in the areas incorporating the idea of critical flux. Much research has also focused on mechanical and chemical methods of reducing flux decline and fouling. It is proposed that an ANN could be developed in which the input to the network is the steady flux for an established process, and the outputs of the network the operating parameters. In this way, using a trained, validated and tested network, it should be possible to use the network to predict the process parameters that would give a desired permeate flux.

The use of a weight partitioning method has shown some success in elucidating the relative importance of the process parameters for the filtration systems

addressed in this study. However, this method does not allow for the analysis of interactions between process parameters. It is also questionable whether this approach is useful if the optimum network architecture is not used, and if the global minimum on the error surface is not achieved in the training of the network.

Genetic algorithms have been shown to be useful in the design of the optimum network structure (Sahoo and Ray 2006) for prediction of flux decline in crossflow filtration and this is an evolving area worthy of further study.

Development of hybrid models incorporating theory and ANNs (known as 'grey-box modelling') has also been shown recently to have great potential (Jones *et al.* 2007). This area should be considered for future work.

Non-linear regression was shown in Chapter 3 to be applicable to stirred microfiltration of $CaCO_3$ suspensions. One of the drawbacks of this approach was the requirement for choosing a suitable functional relationship for the system. The use of symbolic regression using evolutionary algorithms to generate functions to fit experimental data may be an area for further study. This approach may be simplified by the use of dimensional analysis to generate dimensionless groups describing the system.

In Chapters 5 and 6, models to describe flux decline in stirred, batch and continuous crossflow systems were developed. Changing flow regimes in the

batch system were found to affect model parameters, and inter-particle interactions were shown to possibly have an effect on fouling mechanisms and to greatly affect flux decline characteristics. Future research should focus on the development of more sophisticated models incorporating the flow regime and inter-particle interactions, in order to reduce the degree of empiricism. Further study on the formation of cakes of bentonite under crossflow conditions and the influence of suspension properties such as the pH on fouling mechanisms would be necessary in the development of a more accurate model.

BIBLIOGRAPHY

Al Akoum, O., M. Y. Jaffrin, L. Ding, P. Paullier and C. Vanhoutte (2002). "An hydrodynamic investigation of microfiltration and ultrafiltration in a vibrating membrane module." Journal of Membrane Science **197**: 37-52.

Alemdar, A., N. Öztekin, F. B. Erim, Ö. I. Ece and N. Güngör (2005). "Effects of polyethylenimine adsorption on rheology of bentonite suspensions." Bulletin of Materials Science **28**(3): 287-291.

Altena, F. W. and G. Belfort (1984). "Lateral migration of spherical particles in laminar porous tube flows: application to membrane filtration." Chemical Engineering Science **39**: 343-355.

Amari, S.-I., N. Murata, K.-R. Müller, M. Finke and H. H. Yang (1997). "Asymptotic statistical theory of overtraining and cross-validation." IEEE Transactions on Neural Networks **8**(5): 985-996.

Aydiner, C., I. Demir and E. Yildiz (2005). "Modeling of flux decline in crossflow microfiltration using neural networks: the case of phosphate removal." Journal of Membrane Science **248**: 53-62.

Bai, R. and H. F. Leow (2002). "Modeling and experimental study of microfiltration using a composite module." Journal of Membrane Science **204**: 359-377.

Baker, R. J., A. G. Fane, C. J. D. Fell and B. H. Yoo (1985). "Factors affecting flux in crossflow filtration." Desalination **53**: 81-93.

Banerjee, S. (2005). "Spark-induced agglomeration of aqueous polymeric suspensions." Journal of Colloid and Interface Science **292**(2): 595.

Bekkour, K., M. Leyama, A. Benchabane and O. Scrivener (2005). "Time-dependent rheological behavior of bentonite suspensions: An experimental study." Journal of Rheology **49**(6): 1329.

Belfort, G., R. H. Davis and A. L. Zydney (1994). "The behaviour of suspensions and macromolecular solutions in crossflow microfiltration." Journal of Membrane Science **96**: 1-58.

Benna, M., N. Kbir-Ariguib, C. Clinard and F. Bergaya (2001). "Static filtration of purified sodium bentonite clay suspensions. Effect of clay content." Applied Clay Science **19**: 103-120.

Benna, M., N. Kbir-Ariguib, A. Magnin and F. Bergaya (1999). "Effect of pH on rheological properties of purified sodium bentonite suspensions." Journal of Colloid and Interface Science **218**: 442-455.

Bezemer, C. and I. Havenaar (1966). "Filtration behaviour of circulating drilling fluids." Society of Petroleum Engineering Journal **6**(4): 292-298.

Blanpain, P., J. Hermia and M. Lenoel (1993). "Mechanisms governing permeate flux and protein rejection in the microfiltration of beer with a cyclopore membrane." Journal of Membrane Science **84**: 37-51.

Bowen, W. R. (1993). "Understanding flux pattern in membrane processing of protein solutions and suspensions." Trends in Biotechnology **11**: 451-460.

Bowen, W. R. and X. Cao (1998). "Electrokinetic effects in membrane pores and the determination of zeta-potential." Journal of Membrane Science **140**: 267-273.

Bowen, W. R. and F. Jenner (1995). "Theoretical descriptions of membrane filtration of colloids and fine particles: An assessment and review." Advances in Colloid and Interface Science **56**: 141-200.

Bowen, W. R., M. G. Jones, J. S. Welfoot and H. N. S. Yousef (2000). "Predicting salt rejections at nanofiltration membranes using artificial neural networks." Desalination **129**: 147-162.

Bowen, W. R., M. G. Jones and H. N. S. Yousef (1998a). "Dynamic ultrafiltration of proteins - A neural network approach." Journal of Membrane Science **146**: 225-235.

Bowen, W. R., M. G. Jones and H. N. S. Yousef (1998b). "Prediction of the rate of cross-flow membrane ultrafiltration of colloid - a neural network approach." Chemical Engineering Science **53**: 3793-3802.

Brosse, S., J.-F. Guégan, J. N. Tourenq and S. Lek (1999). "The use of artificial neural networks to assess fish abundance and spatial occupancy in the littoral zone of a mesotrophic lake." Ecological Modelling **120**(2-3): 299-311.

Brunton, G. D. (1988). "Density and compressibility of Wyoming bentonite particles." Clays and Clay Minerals **36**(1): 94-95.

Cabassud, M., N. Delgrange-Vincent, C. Cabassud, L. Durand-Bourlier and J. M. Lainé (2002). "Neural networks: a tool to improve UF plant productivity." Desalination **145**: 223-231.

Cadene, A., S. Durand-Vidal, P. Turq and J. Brendle (2005). "Study of individual Na-montmorillonite particles size, morphology, and apparent charge." Journal of Colloid and Interface Science **285**(2): 719.

Cai, W., A. Pachego-Vega, M. Sen and K. T. Yang (2006). "Heat transfer correlations by symbolic regression." International Journal of Heat and Mass Transfer **49**: 4352-4359.

Callan, R. (1999). The Essence of Neural Networks, Prentice Hall.

Carrère, H. and F. Blaszkow (2001). "Comparison of operating modes for clarifying lactic acid fermentation broths by batch cross-flow microfiltration." Process Biochemistry **36**(8-9): 751.

Chandler, M. and A. Zydney (2004). "High throuput screening for membrane process development." Journal of Membrane Science **237**: 181-188.

Chang, S. and A. G. Fane (2001). "The effect of fibre diameter on filtration and flux distribution -- relevance to submerged hollow fibre modules." Journal of Membrane Science **184**(2): 221.

Chellam, S. (2005). "Artificial neural network model for transient crossflow microfiltration of polydispersed suspensions." Journal of Membrane Science **258**: 35-42.

Chellam, S. and M. R. Weisner (1998). "Evaluation of crossflow filtration models based on shear-induced diffusion and particle adhesion: Complications induced by feed suspensions polydispersivity." Journal of Membrane Science **138**: 83-97.

Chen, H. and A. S. Kim (2006). "Prediction of permeate flux decline in crossflow membrane filtraton of colloidal suspension: a radial basis function neural network approach." Desalination **192**: 415-428.

Chen, J. C., M. Elimelech and A. S. Kim (2005). "Monte Carlo simulation of colloidal membrane filtration: Model development with application to characterization of colloid phase transition." Journal of Membrane Science **255**(1-2): 291.

Chen, V., A. G. Fane, S. S. Madaeni and I. G. Wenten (1997). "Particle deposition during membrane filtration of colloids: transition between concentration polarization and cake formation." Journal of Membrane Science **125**: 109-122.

Cheng, L.-H., Y.-F. Cheng and J. Chen (2008). "Predicting effect of interparticle interactions on permeate flux decline in CMF of colloidal suspensions: An overlapped type of local neural network." Journal of Membrane Science **308**(1-2): 54-65.

Cheryan, M. (1986). The Ultrafiltration Handbook, Technomic, USA.

Chimmili, S., D. Doraiswamy and R. K. Gupta (1998). "Shear-Induced Agglomeration of Particulate Suspensions." Ind. Eng. Chem. Res. **37**(6): 2073-2077.

Cho, M.-H., C.-H. Lee and S. Lee (2006). "Effect of flocculation conditions on membrane permeability in coagulation-microfiltration." Desalination **191**:

386-396.

Choe, T. B., P. Masse, A. Verdier and M. J. Clifton (1986). "Flux decline in batch ultrafiltration: concentration polarization and cake formation." Journal of Membrane Science **26**: 1-15.

Choo, K.-H. and C.-H. Lee (1998). "Hydrodynamic behavior of anaerobic biosolids during crossflow filtration in the membrane anaerobic bioreactor." Water Research **32**: 3387-3397.

Curcio, S., V. Calabrò and G. Iorio (2006). "Reduction and control of flux decline in cross-flow membrane processes modeled by artificial neural networks." Journal of Membrane Science **286**: 125-132.

Curcio, S., G. Scilingo, V. Calabrò and G. Iorio (2005). "Ultrafiltration of BSA in pulsating conditions: an artificial neural networks approach." Journal of Membrane Science **246**(2): 235-247.

Curry, B. and P. H. Morgan (2006). "Model selection in neural networks: some difficulties." European Journal of Operational Research **170**: 567-577.

Czekaj, P., F. López and C. Güell (2000a). "Membrane fouling during microfiltration of fermented beverages." Journal of Membrane Science **166**: 199-212.

Czekaj, P., F. López and C. Güell (2001). "Membrane fouling by turbidity constituents of beer and wine: characterization and prevention by means of infrasonic pulsing." Journal of Food Engineering **49**: 25-36.

Czekaj, P., W. Mores, R. H. Davis and C. Güell (2000b). "Infrasonic pulsing for foulant removal in crossflow microfiltration." Journal of Membrane Science **180**: 157-169.

da Silva, I. N. and R. A. Flauzino (2007). "An approach based on neural networks for estimation and generalization of crossflow filtration processes." Applied Soft Computing **8**(1): 590-598.

Davis, R. H. and S. A. Birdsell (1987). "Hydrodynamic model and experiments

for crossflow microfiltration." <u>Chemical Engineering Communications</u> **49**: 217-234.

Davis, R. H. and D. T. Leighton (1987). "Shear-induced transport of a particle layer along a porous wall." <u>Chemical Engineering Science</u> **49**: 217-234.

de Barros, S. T. D., C. M. G. Andrade, E. S. Mendes and L. Peres (2003). "Study of fouling mechanism in pineapple juice clarification by ultrafiltration." <u>Journal of Membrane Science</u> **215**(1-2): 213-224.

Delgrange-Vincent, N., C. Cabassud, M. Cabassud, L. Durand-Bourlier and J. M. Lainé (2000). "Neural networks for long term prediction of fouling and backwash efficiency in ultrafiltration for drinking water production." <u>Desalination</u> **131**: 353-362.

Delgrange, N., C. Cabassud, M. Cabassud, L. Durand-Bourlier and J. M. Lainé (1998). "Neural networks for prediction of ultrafiltration transmembrane pressure - application to drinking water production." <u>Journal of Membrane Science</u> **150**: 111-123.

Demuth, H. and M. Beale (2004). <u>Neural Network Toolbox for use with MATLAB®</u>, The Mathworks, Inc.

Dharmappa, H. B. and P. Hagare (1999). "Economic analysis and design of crossflow microfiltration for water treatment systems." <u>Desalination</u> **121**(1): 1-11.

Dharmappa, H. B., J. Verink, R. Ben Aim, K. Yamamoto and S. Vigneswaran (1992). "A comprehensive model for cross-flow filtration incorporating polydispersity of the influent." <u>Journal of Membrane Science</u> **65**(1-2): 173.

Doneva, T. A., C. S. Vassilieff and E. D. Krusteva (1998). "Cross-flow microfiltration of latex suspensions: test of different models." <u>Colloids and Surfaces A: Physicochemical and Engineering Aspects</u> **138**(2-3): 245.

Doneva, T. A., C. S. Vassilieff, E. D. Krusteva and I. B. Petkanchin (1997). "Cross-flow microfiltration of bentonite in water dispersions: effects of

suspension rheology." Journal of Dispersion Science and Technology **18**(6-7): 699-717.

Dornier, M., M. Decloux, G. Trystram and A. Lebert (1995a). "Dynamic modeling of crossflow microfiltration using neural networks." Journal of Membrane Science **98**: 263-273.

Dornier, M., M. Decloux, G. Trystram and A. Lebert (1995b). "Interest of neural networks for the optimization of the crossflow filtration process." LWT - Food Science and Technology **28**: 300-309.

Dornier, M., B. Heyd and M. Danzart (1998). "Evaluation of the simplex method for training simple multilayer neural networks." Neural Computing and Applications **7**(2): 107-114.

Drakos, N. and R. Moore (1993). Implementation of a fast artificial neural network library (FANN). Copenhagen, Department of Computer Science University of Copenhagen.

Drews, A., T. Klahm, B. Renk, M. Saygili, G. Baumgarten and M. Kraume (2003). "Nanofiltration of CIP waters from iodine X-ray contrast media production: process design and modelling." Desalination **159**(2): 119-129.

Einstein, A. (1956). Investigations of the Theory of the Brownian Movement. New York, Dover Publications Inc.

Ermakova, L., M. Sidorova, I. Savina and D. Aleksandrov (1998). "Structural and electrochemical parameters of asymmetric membranes for reverse osmosis." Colloids and Surfaces A: Physicochemical Engineering Aspects **142**(2-3): 265-274.

Fan, L., J. L. Harris, F. A. Roddick and N. A. Booker (2001). "Influence of the characteristics of natural organic matter on the fouling of microfiltration membranes." Water Research **35**(18): 4455-4463.

Ferguson, C. F. and J. A. Klotz (1954). "Filtration from mud during drilling."

AIME Transactions **201**: 29-42.

Field, R. W., D. Wu, J. A. Howell and B. B. Gupta (1995). "Critical flux concept for microfiltration fouling." Journal of Membrane Science **100**: 259-272.

Flynn, C., P. Geoffroy and G. Foley (1990). "A novel technique for the study of cake formation during cross-flow microfiltration of microbial cells." Biotechnology Techniques **5**: 325-328.

Foley, G. (1994). "Membrane fouling in crossflow filtration: Implications for measurement of the steady state specific cake resistance." Biotechnology Techniques **8**(10): 743-746.

Foley, G. (2006). "A review of factors affecting filter cake properties in dead-end microfiltration of microbial suspensions." Journal of Membrane Science **274**(1-2): 38-46.

Foley, G., P. F. MacLoughlin and D. M. Malone (1995a). "Membrane fouling during constant flux crossflow microfiltration of dilute suspensions of active dry yeast." Separation Science and Technology **30**: 383-398.

Foley, G., D. M. Malone and P. F. MacLoughlin (1995b). "Modelling the effects of particle polydispersity in crossflow filtration." Journal of Membrane Science **99**: 77-88.

Fordham, E. J. and H. K. J. Ladva (1989). "Cross-flow filtration of bentonite suspensions." PhysicoChemical Hydrodynamics **11**(4): 411-439.

Fordham, E. J. and H. K. J. Ladva (1992). "Cross-flow filtration of bentonite suspensions II." Journal of Colloid and Interface Science **148**(1): 29-34.

Forstrom, R., K. Bartelt, P. Blackshear and T. Wood (1975). "Formed element deposition onto filtering walls." Transactions - American Society for Artificial Internal Organs **21**: 602-608.

Free, M. L., J. S. Zhu and B. M. Moudgil (1998). "Use of a new particle contact probability filtration rate model to determine effect of particle size

distribution in filtration." <u>Separation Science and Technology</u> **33**: 57-66.

Frost, R. C. (1982). Prediction of friction losses for the flow of sewage sludge through straight pipes. Stevenage, UK, Water Research Centre.

Fu, R.-Q., T.-W. Xu and Z.-X. Pan (2005). "Modelling of the adsorption of bovine serum albumin on porous polyethylene membrane by back-propagation artificial neural network." <u>Journal of Membrane Science</u> **251**: 137-144.

Garson, G. D. (1991). "Interpreting neural network connection weights." <u>AI Expert</u> **6**: 47-51.

Goh, A. T. C. (1994). "Seismic Liquefaction Potential Assessed by Neural Networks." <u>Journal of Geotechnical Engineering</u> **120**(9): 1467-1480.

Gourgues, C., P. Aimar and V. Sanchez (1992). "Ultrafiltration of bentonite suspensions with hollow fibre membranes." <u>Journal of Membrane Science</u> **74**: 51-69.

Gozlan, R. E., S. Mastrorillo, G. H. Copp and S. Lek (1999). "Predicting the structure and diversity of young-of-the-year fish assemblages in large rivers." <u>Freshwater Biology</u> **41**(4): 809–820.

Green, G. and G. Belfort (1980). "Fouling of ultrafiltration membranes: lateral migration and the particle trajectory model." <u>Desalination</u> **35**: 129-147.

Güngör, N. (2000). "Effect of the Adsorption of surfactants on the rheology of Na-Bentonite slurries." <u>Journal of Applied Polymer Science</u> **75**: 107-110.

Hajmeer, M., I. A. Basheer and Y. M. Najjar (1997). "Computational neural networks for predictive microbiology II. Application to microbial growth." <u>International Journal of Food Microbiology</u> **34**: 51-66.

Hamachi, M., M. Cabassud, A. Davin and M. Mietton Peuchot (1999). "Dynamic modelling of crossflow microfiltration of bentonite suspension using recurrent neural networks." <u>Chemical Engineering and Processing</u> **38**: 203-

210.

Hamachi, M. and M. Mietton Peuchot (1996). Dynamic measurement of deposit thickness on inorganic membrane. 4th International Congress on Inorganic Membranes, Gatlinburg, Tennessee, U.S.A.

Hamachi, M. and M. Mietton Peuchot (1999). "Experimental investigations of cake characteristis in crossflow microfiltration." Chemical Engineering Science **54**: 4023-4030.

Hamachi, M. and M. Mietton Peuchot (2002). "Analysis of deposit behaviour in crossflow microfiltraiton by means of thickness measurement." Chemical Engineering Journal **86**: 251-257.

Hermia, J. (1982). "Constant pressure blocking filtration laws - Application to power-law non-Newtonian fluids." Transactions of the Institution of Chemical Engineers **60**: 183-187.

Ho, C.-C. and A. L. Zydney (2000). "A combined pore blockage and cake filtration model for protein fouling during microfiltration." Journal of Colloid and Interface Science **232**: 389-399.

Hodgson, P. H., G. L. Leslie, S. R.P., A. G. Fane, C. J. D. Fell and K. C. Marshall (1993). "Cake resistance and solute rejection in bacterial microfiltration: the role of the extracellular matrix." Journal of Membrane Science **79**: 35-53.

Honey, H. C. and W. A. Pretorius (2000). "Laminar flow pipe hydraulics of pseudoplastic thixotropic sewage sludges." Water S.A. **26**(1): 19-26.

Hong, S., R. S. Faibish and M. Elimelech (1997). "Kinetics of permeate flux decline in crossflow membrane filtration of colloidal suspensions." Journal of Colloid and Interface Science **196**: 267-277.

Howell, J. A., R. W. Field and D. Wu (1993). "Yeast cell microfiltration: Flux enhancement in baffled and pulsatile flow systems." Journal of Membrane Science **80**: 59-71.

Hughes, D. and R. W. Field (2006). "Crossflow filtration of washed and unwashed yeast suspensions at constant shear under nominally sub-critical conditions." Journal of Membrane Science **280**(1-2): 89.

Jago, S. (2008). Even better than the real thing. The Chemical Engineer. **804:** 42-43.

Jiao, D. and M. M. Sharma (1992). Formation damage due to static and dynamic filtration of water based muds. SPE Formation Damage Control Symposium, Lafeyette, L.A.

Jiao, D. and M. M. Sharma (1994). "Mechanism of Cake Buildup in Crossflow Filtration of Colloidal Suspensions." Journal of Colloid and Interface Science **162**(2): 454.

Jones, D. M., J. Watton and J. K. Brown (2007). "Comparison of black-, white-, and grey-box models to predict ultimate tensile strength of high-strength hot rolled coils at the Port Talbot hot strip mill." Proceedings of the Institution of Mechanical Engineers, Part L: Journal of Materials: Design and Applications **221**(1): 1-9.

Kang, S.-K. and K.-H. Choo (2003). "Use of MF and UF membranes for reclamation of glass industry wastewater containing colloidal clay and glass particles." Journal of Membrane Science **223**: 89-103.

Keefe, R. J. and D. M. Dubbin (2005). Specifying Microfiltration Systems. Chemical Engineering.

Kelessidis, V. C. and R. Maglione (2008). "Yield stress of water-bentonite dispersions." Colloids and Surfaces A: Physicochemical and Engineering Aspects **318**(1-3): 217.

Kelly, S. T., W. S. Opong and A. Zydney (1993). "The influence of protein aggregates on the fouling of microfiltration membranes during stirred cell filtration." Journal of Membrane Science **80**: 49-57.

Kern, D. and R. Seaton (1959). "A theoretical analysis of thermal surface

fouling." <u>British Chemical Engineering</u> **4**: 256-262.

Khandal, R. K. and T. F. Tadros (1988). "Application of viscoelastic measurements to the investigation of the swelling of sodium montmorillonite suspensions." <u>Journal of Colloid and Interface Science</u> **125**(1): 122.

Kim, A. S., A. G. Fane and C. J. D. Fell (1988). "The performance of ultrafiltration membranes pretreated by polymers." <u>Desalination</u> **70**: 229-249.

Kim, J.-S., C.-H. Lee and I.-S. Chang (2001). "Effect of pump shear on the performance of a crossflow membrane bioreactor." <u>Water Research</u> **35**(9): 2137.

Kim, J. and F. A. DiGiano (2006). "Defining critical flux in submerged membranes: Influence of length-distributed flux." <u>Journal of Membrane Science</u> **280**: 752-761.

Kluge, T., C. Rezende, D. Wood and G. Belfort (1999). "Protein transmission during dean vortex microfiltration of yeast suspensions." <u>Biotechnology and Bioengineering</u> **65**: 649-658.

Knoell, T., J. Safarik, T. Cormack, R. Riley, S. W. Lin and H. Ridgeway (1999). "Biofouling potentials of microporous polysulfone membranes containing a sulfonated polyether-ethersulfone/polyethersulfone block copolymer: correlation of membrane surface properties with bacterial attachment." <u>Journal of Membrane Science</u> **157**(1): 117-138.

Kramer, P. W., Y. S. Yeh and H. Yasuda (1989). "Low temperature plasma for the preparation of separation membranes." <u>Journal of Membrane Science</u> **46**: 1-28.

Krivý, I., J. Tvrdík and R. Krpec (2000). "Stochastic algorithms in nonlinear regression." <u>Computational Statistics & Data Analysis</u> **33**(3): 277.

Leighton, D. T. and A. Acrivos (1987). "The shear-induced migration of particles

in concentrated suspensions." <u>Journal of Fluid Mechanics</u> **181**: 415-439.

Lemke, T., F. Bagusat, K. Köhnke, K. Husemann and H. J. Mögel (1999). "Time dependent viscosity of concentrated alumina suspensions." <u>Colloids and Surfaces A: Physicochemical and Engineering Aspects</u> **150**(1-3): 283.

Leonard, E. P. and C. S. Vassilieff (1984). "The deposition of rejected matter in membrane separation processes." <u>Chemical Engineering Communications</u> **30**(3): 209-217.

Li, H., A. G. Fane, H. G. L. Coster and S. Vigneswaran (1998). "Direct observation of particle deposition on the membrane surface during crossflow microfiltration." <u>Journal of Chemical Technology and Biotechnology</u> **149**: 83-97.

Li, J., R. D. Sanderson, G. Y. Chai and D. K. Hallbauer (2005). "Development of an ultrasonic technique for in situ investigating the properties of deposited protein during crossflow ultrafiltration." <u>Journal of Colloid and Interface Science</u> **284**(1): 228-238.

Li, S. L., K. S. Chou, J. Y. Lin, H. W. Yen and I. M. Chu (1996). "Study of the microfiltration of Escherichia coli containing fermentation broth by a ceramic membrane filter." <u>Journal of Membrane Science</u> **110**: 203-210.

Li, Z., A. H-Kittikun and W. Youravong (2008). "Removal of suspended solids from tuna spleen extract by microfiltration: A batch process design and improvement." <u>Biochemical Engineering Journal</u> **38**(2): 226.

Lim, Y., Y.-S. Moon and T. W. Kim (2007). "Artificial neural network approach for prediction of ammonia emission from field-applied manure and relative significance assessment of ammonia emission factors." <u>European Journal of Agronomy</u> **26**(4): 425-434.

Lu, R. R., S. Y. Xu, Z. Wang and R. J. Yang (2007). "Isolation of lactoferrin from bovine colostrum by ultrafiltration coupled with strong cation exchange chromatography on a production scale." <u>Journal of Membrane Science</u>

13

297(1-2): 152-161.

Lu, W.-M. and S. C. Ju (1989). "Selective particle deposition in crossflow filtration." Separation Science and Technology **24**: 517-540.

Macey, R., G. Oster and T. Zahnley (2000). Berkeley Madonna User's Guide Version 8.0. California, University of California

Department of Molecular and Cellular Biology.

Mackley, M. R. and N. E. Sherman (1992). "Cross-flow cake filtration mechanisms and kinetics." Chemical Engineering Science **47**(12): 3067.

Madaeni, S. S., A. G. Fane and G. S. Grohmann (1995). "Virus removal from water and wastewater using membranes." Journal of Membrane Science **102**: 65.

Mahto, V. and V. P. Sharma (2004). "Rheological study of a water based oil well drilling fluid." Journal of Petroleum Science and Engineering **45**(1-2): 123.

Maier, H. R. and G. C. Dandy (2000). "Neural networks for the prediction and forecasting of water resources variables: a review of modelling issues and applications." Environmental Modelling and Software **15**: 101-124.

Maiorella, B., G. Dorin, A. Carion and H. Harano (1991). "Crossflow microfiltration of animal cells." Biotechnology and Bioengineering **37**: 121-126.

Mastrorillo, S., S. Lek and F. Dauba (1997). "Predicting the abundance of minnow *Phoxinus phoxinus* (Cyprinidae) in the River Ariège (France) using artificial neural networks." Aquatic Living Resources **10**: 169-176.

McCarthy, A. (2001). The Filtration Properties of a Dimorphic Yeast. School of Biotechnology. Dublin, Dublin City University. **Ph.D.:** 212.

McCarthy, A., H. Conroy, P. K. Walsh and G. Foley (1998a). "The effect of pressure on the specific resistance of yeast filter cakes during dead-end

filtration in the range 30-500kPa." <u>Biotechnology Techniques</u> **12**: 909-912.

McCarthy, A., P. K. Walsh and G. Foley (1996). "On the relation between filtrate flux and particle concentration in batch crossflow microfiltration." <u>Separation Science and Technology</u> **31**(11): 1615-1627.

McCarthy, A., P. K. Walsh and G. Foley (2002a). "Characterising the packing and dead-end filter cake compressibility of the polymorphic yeast Kluyveromyces Marxianus var. marxianus NRRLy2415." <u>Journal of Membrane Science</u> **198**: 87-94.

McCarthy, A. A., P. Gilboy, P. K. Walsh and G. Foley (1999). "Characterisation of cake compressibility in dead-end microfiltration of microbial suspensions." <u>Chemical Engineering Communications</u> **173**: 79-90.

McCarthy, A. A., D. G. O'Shea, N. T. Murray, P. K. Walsh and G. Foley (1998b). "Effect of cell morphology on dead-end filtration of the dimorphic yeast *Kluyveromyces marxianus* Var. *marxianus* NRRLy2415." <u>Biotechnology Progress</u> **14**: 279-285.

McCarthy, A. A., P. K. Walsh and G. Foley (2002b). "Experimental techniques for quantifying the cake mass, the cake and membrane resistances and the specific cake resistance during crossflow filtration of microbial suspensions." <u>Journal of Membrane Science</u> **201**: 31-45.

Meireles, M., E. Lavoute and P. Bacchin (2003). "Filtration of a bacterial fermentation broth: harvest conditions effects on cake hydraulic resistance." <u>Bioprocess and Biosystems Engineering</u> **25**: 309-314.

Mishra, G. C., N. K. Pandey and P. K. Pandey (1985). "Greases from Indian Bentonite." <u>Indian Journal of Chemical Technology</u> **23**: 190-194.

Moll, R., D. Veyret, F. Charbit and P. Moulin (2007). "Dean vortices applied to membrane process: Part I. Experimental approach." <u>Journal of Membrane Science</u> **288**(1-2): 307.

Mores, W. D. and R. H. Davis (2001). "Direct visual observation of yeast deposition and removal during microfiltration." Journal of Membrane Science **189**: 217-230.

Mores, W. D. and R. H. Davis (2002). "Yeast foulant removal by backpulses in crossflow microfiltration." Journal of Membrane Science **208**: 389-404.

Mota, M., J. A. Teixeira and A. Yelshin (2004). Dependence of *Saccharomyces cerevisiae* filtration through membrane on yeast concentration. 9th World Filtration Congress, New Orleans.

Moulin, P., C. Serra, J. C. Rouch, M. J. Clifton and P. Aptel (1996). "Dean vortices in coiled tubular membranes." Journal of Membrane Science **114**: 235-244.

Mulder, M. (1996). Basic Principles of Membrane Technology, Springer.

Nagata, K., K. J. Herouvis, D. M. Dziewulski and G. Belfort (1989). "Cross-flow membrane microfiltration of a bacterial fermentation broth." Biotechnology and Bioengineering **34**: 447-466.

Nakanishi, K., T. Tadokoro and R. Matsuno (1987). "On the specific resistance of cakes of microorganisms." chemical Engineering Communications **62**: 187-201.

Nuengjamnong, C., J. H. Kweon, J. Cho, C. Polprasert and K.-H. Ahn (2005). "Membrane fouling caused by extracellular polymeric substances during microfiltration processes." Desalination **179**(1-3): 117.

Nyström, M. and P. Jarvinen (1991). "Modification of polysulfone ultrafiltration membranes with UV irradiation and hydrophilicity increasing agents." Journal of Membrane Science **60**: 275-296.

Ogden, G. E. and R. H. Davis (1990). "Experimental determination of the permeability and relative viscosity for fine latexes and yeast suspensions." Chemical Engineering Communications **91**: 11-28.

Ognier, S., C. Wisniewski and A. Grasmick (2002). "Characterisation and

modelling of fouling in membrane bioreactors." <u>Desalination</u> **146**: 141-147.

Ohmori, K. and C. E. Glatz (1999). "Effects of pH and ionic strength on microfiltration of *C. Glutamicum*." <u>Journal of Membrane Science</u> **153**: 23-32.

Ohmori, K. and C. E. Glatz (2000). "Effect of carbon source on microfiltration of Corynebacterium glutamicum." <u>Journal of Membrane Science</u> **171**: 263-271.

Ohmori, K., K. Hoshida and E. Iritani (2004). "Interactions between cells, proteins and salts in microfiltration of Corynebacterium glutamicum slurry." <u>Journal of Chemical Engineering of Japan</u> **37**(1497-1503).

Ohmori, K. and E. Iritani (2004a). "Effect of addition of amino acids on microfiltration behavior of a microorganism slurry." <u>Journal of Chemical Technology and Biotechnology</u> **79**: 1169-1173.

Ohmori, K. and E. Iritani (2004b). "Ultrafiltration behavior of Corynebacterium glutamicum slurry with and without bovine serum albumin." <u>Journal of Chemical Engineering of Japan</u> **37**: 842-849.

Okamoto, Y., K. Ohmori and C. E. Glatz (2001). "Harvest time effects on membrane cake resistance of *Escherichia coli* broth." <u>Journal of Membrane Science</u> **190**: 93-106.

Olden, J. D. and D. A. Jackson (2002). "Illuminating the "black box": a randomization approach for understanding variable contributions in artificial neural networks." <u>Ecological Modelling</u> **154**(1-2): 135-150.

Oolman, T. and T.-C. Liu (1991). "Filtration Properties of Mycelial Mocrobial Broths." <u>Biotechnology Progress</u> **7**: 534-539.

Outmans, H. D. (1963). "Mechanics of static and dynamic filtration in the borehole." <u>Society of Petroleum Engineering Journal</u> **3**(3): 236-344.

Park, H., K.-H. Choo and C.-H. Lee (1999). "Flux enhancement with powdered

activated carbon addition in the membrane anaerobic bioreactor." Separation Science and Technology **34**: 2781-2792.

Piron, E., E. Latrille and F. René (1997). "Application of artificial neural networks for crossflow microfiltration modelling: "black-box" and semi-physical approaches." Computers in Chemical Engineering **21**: 1021-1030.

Piron, E., F. Rene and E. Latrille (1995). "A crossflow-microfiltration model based on integration of the mass transport equation." Journal of Membrane Science **108**: 57-70.

Porter, M. C. (1990). Microfiltration. Handbook of Industrial Membrane Technology. M. C. Porter, William Andrew Publishing/Noyes**:** 61-.

Press, W. H., B. P. Flannery, S. A. Teukolsky and W. T. Vetterling (1988). Numerical Recipes in C - The Art of Scientific Computing, Cambridge University Press.

Pritchard, M., J. Howell and R. W. Field (1995). "The ultrafiltration of viscous fluids." Journal of Membrane Science **102**: 223-235.

Rai, P., G. C. Majumdar, S. DasGupta and S. De (2005). "Modelling the performance of batch ultrafiltration of synthetic fruit juice and mosambi juice using artificial neural network." Journal of Food Engineering **71**: 273-281.

Razavi, M. A., A. Mortazavi and M. Mousavi (2003a). "Dynamic modeling of milk ultrafiltration by artificial neural network." Journal of Membrane Science **220**: 47-58.

Razavi, M. A., A. Mortazavi and M. Mousavi (2004). "Application of neural networks for crossflow milk ultrafiltration simulation." International Dairy Journal **14**: 69-80.

Razavi, M. A., M. Mousavi and A. Mortazavi (2003b). "Dynamic prediction of milk ultrafiltration performance: A neural network approach." Chemical Engineering Science **58**: 4185-4195.

18

Redkar, S., V. T. Kuberkar and R. H. Davis (1996). "Modeling of concentration polarization and depolarization with high-frequency backpulsing." Journal of Membrane Science **121**: 229-242.

Reineke, R. C. and S. G. Varnado (1978). Portable high temperature, high pressure viscometer. Workshop on geothermal drilling fluids, Houston, TX, USA.

Reismeier, B., K. H. Kroner and M.-R. Kula (1989). "Tangential filtration of microbial suspensions: filtration resistances and model development." Journal of Biotechnology **12**: 153-172.

Riesmeier, B., K. H. Kroner and M. R. Kula (1989). "Tangential filtration of microbial suspensions: filtration resistances and model development." Journal of Biotechnology **12**(2): 153.

Romero, C. A. and R. H. Davis (1990). "Transient model of crossflow microfiltration." Chemical Engineering Science **45**(1): 13-25.

Rumelhart, D. E., G. E. Hinton and R. J. Williams (1986). "Learning representations by back-propagating errors." Nature **323**: 533-536.

Rushton, A. and H. E. Khoo (1977). "Filtration characteristics of yeast." Journal of Applied Chemistry and Biotechnology **27**: 99-109.

Rushton, A., A. S. Ward and R. Holdich (1995). Introduction to Solid-Liquid Filtration and Separation Technology, Wiley-VCH.

Rushton, A., A. S. Ward and R. G. Holdich (1996). Solid-Liquid Filtration and Separation Technology. New York, Weinheim: VCH, 1996.

Sahoo, G. B. and C. Ray (2006). "Predicting flux decline in crossflow membranes using artificial neural networks and genetic algorithms." Journal of Membrane Science **283**: 147-157.

Sakai, K., K. Ozawa, K. Ohashi, R. Yoshida and H. Sakurai (1989). "Low-temperature plasma separation by crossflow filtration with microporous

glass membranes." Ind. Eng. Chem. Res. **28**(1): 57-64.

Sarle, W. S. (1997, 23rd June 2000). "How to measure importance of inputs?"

Scott, K. (1995). Handbook of Industrial Membranes. Oxford, Elsevier Advanced Technology.

Sherwood, J. D. (1988). "The force on a sphere pulled away from a permeable half space." PhysicoChemical Hydrodynamics **10**: 3-12.

Shetty, G. R. and S. Chellam (2003). "Predicting membrane fouling during municipal drinking water nanofiltration using artificial neural networks." Journal of Membrane Science **217**: 69-86.

Shetty, G. R., H. Malki and S. Chellam (2003). "Predicting contaminant removal during municipal drinking water nanofiltration using artificial neural networks." Journal of Membrane Science **212**: 99-112.

Shimuzu, Y., K. Matsushita and A. Watanabe (1994). "Influence of shear breakage of microbial cells on cross-flow microfiltration flux." Journal of Fermentation and Bioengineering **78**: 170-174.

Shimuzu, Y., K.-I. Shimodera and A. Watanabe (1993). "Cross-flow microfiltration of bacterial cells." Journal of Fermentation and Bioengineering **76**(6): 493-500.

Shirato, S. and S. Esumi (1963). "Filtration of the cultured broth of *Streptomyces griseus*." Journal of Fermentation Technology **41**: 87-92.

Silva, C. M., D. W. Reeve, H. Husain, H. R. Rabie and K. A. Woodhouse (2000). "Model for flux prediction in high-shear microfiltration systems." Journal of Membrane Science **173**(1): 87.

Sjöman, E., M. Mänttäri, M. Nyström, H. Koivikko and H. Heikkilä (2007). "Separation of xylose from glucose by nanofiltration from concentrated monosaccharide solutions." Journal of Membrane Science **292**(1-2): 106-115.

Sohm, R. and T. F. Tadros (1989). "Viscoelastic properties of sodium montmorillonite (Gelwhite H) suspensions." Journal of Colloid and Interface Science **132**(1): 62.

Sousa, A. C., J. M. S. Cabral and M. Mateus (2002). "Microfiltration of cutinase and *Escherichia coli* cell fragment suspensions: The role of the electrolyte environment on the development of dynamic cake layers." Journal of Membrane Science **207**: 171-187.

Sridang, P. C., A. Pottier, C. Wisniewski and A. Grasmick (2008). "Performance and microbial surveying in submerged membrane bioreactor for seafood processing wastewater treatment." Journal of Membrane Science **317**(1-2): 43.

Tanaka, T., H. Itoh, K. Nakanishi, T. Kume and R. Matsuno (1995). "Crossflow filtration of bakers yeast with periodical stopping of permeation flow and bubbling." Biotechnology and Bioengineering **47**: 401-404.

Tanaka, T., R. Kamimura, R. Fujiwara and K. Nakanishi (1994). "Crossflow filtration of yeast cultivated in molasses." Biotechnology and Bioengineering **43**: 1094-1101.

Tanaka, T., R. Kamimura, K. Itoh, K. Nakanishi and R. Matsuno (1993). "Factors affecting the performance of crossflow filtration of yeast cell suspension." Biotechnology and Bioengineering **41**: 617-624.

Tanaka, T., T.-S. Tsuneyoshi, W. Kitazawa and K. Nakanishi (1997). "Characteristics in crossflow filtration using yeast suspensions." Separation Science and Technology **32**: 1885-1898.

Tansel, B., J. Sager, J. Garland, S. Xu, L. Levine and P. Bisbee (2006). "Deposition of extracellular polymeric substances (EPS) and microtopographical changes on membrane surfaces during intermittent filtration conditions." Journal of Membrane Science **85**(1-2): 225-231.

Tarleton, E. S. and D. L. Hancock (1996). "Imaging of filter cakes through

electrical impedance tomography." <u>Filtration and Separation</u> **33**(6): 491-494.

Tarleton, E. S. and R. J. Wakeman (1993). "Understanding flux decline in crossflow microfiltration: Part I - Effects of particle and pore size." <u>Chemical Engineering Research and Design</u> **71**(A4): 399-410.

Tarleton, E. S. and R. J. Wakeman (1994). "Understanding flux decline in crossflow microfiltration: Part II - Effects of process parameters." <u>Chemical Engineering Research and Design</u> **72**(A3): 431-440.

Teodisiu, C., O. Pastravanu and M. Macoveanu (2000). "Neural network models for ulrafiltration and backwashing." <u>Water Research</u> **34**(18): 4371-4380.

Thompson, C. I., K. D. Rausch, R. L. Belyea and M. E. Tumbleson (2006). "Microfiltration of gluten processing streams from corn wet milling." <u>Bioresource Technology</u> **97**(2): 348.

Tien, C. and B. V. Ramarao (2008). "On the analysis of dead-end filtration of microbial suspensions." <u>Journal of Membrane Science</u> **319**(1-2): 10.

Tracey, E. M. and R. H. Davis (1994). "Protein fouling of track-etched polycarbonate microfiltration membranes." <u>Journal of Colloid and Interface Science</u> **167**: 104-116.

Vassilieff, C. S. and T. A. Doneva (1997). "The convective model of cross-flow microfiltration is not inconsistent." <u>Journal of Membrane Science</u> **133**(2): 275.

Vassilieff, C. S., T. A. Doneva and L. G. Ljutov (1996). "Cross-flow microfiltration of bentonite-in-water dispersions: initial transient effects at low concentration." <u>Journal of Membrane Science</u> **119**: 65-80.

Vyas, H. K., R. J. Bennett and A. D. Marshall (2001). "Cake resistance and force balance mechanism in the crossflow microfiltration of lactalbumin particles." <u>Journal of Membrane Science</u> **192**(1-2): 165.

Wakeman, R. J. (1975). "Packing densities of particles with log normal size

distributions." Powder Technology **11**: 297-299.

Wakeman, R. J. (1994). "Visualisation of cake formation in crossflow microfiltration." Transactions of the Institution of Chemical Engineers **72A**: 530-540.

Wang, W., X. Jia and G. A. Davies (1995). "A theoretical study of transient cross-flow filtration using force balance analysis." The Chemical Engineering Journal and the Biochemical Engineering Journal **60**(1-3): 55.

Wickramasinghe, S. R., Y. Wu and B. Han (2002). "Enhanced microfiltration of yeast by flocculation." Desalination **147**: 25-30.

Youn, K.-S., J.-H. Hong, D.-H. Bae, S.-J. Kim and S.-D. Kim (2004). "Effective clarifying process of reconsituted apple juice using membrane filtration with filter aid pretreatment." Journal of Membrane Science **228**: 179-186.

Zaidi, S. K. and A. Kumar (2005). "Experimental analysis of a gel layer in dead-end ultrafiltration of a silica suspension." Desalination **172**: 107-117.

Zoecklein, B. (1988). Bentonite Fining of Juice and Wine. Virginia, Virginia Polytechnic Institute and State University**:** 8.

Zokaee, F., T. Kaghazchi and A. Zare (1999). "Cell harvesting by microfiltration in a dead-end system." Process Biochemistry **34**: 803-810.

Zydney, A. L. and C. K. Colton (1986). "A concentration polatization model for the filtrate flux in cross-flow microfiltration of particulate suspensions." Chemical Engineering Science **47**: 1-21.